AC RELAXATION IN THE Fe_8 MOLECULAR MAGNET

By

Geordie Rose

B. Eng. (Engineering Physics), McMaster University, 1994

A THESIS SUBMITTED IN PARTIAL FULFILLMENT OF

THE REQUIREMENTS FOR THE DEGREE OF

DOCTOR OF PHILOSOPHY

in

THE FACULTY OF GRADUATE STUDIES

DEPARTMENT OF PHYSICS AND ASTRONOMY

We accept this thesis as conforming

to the required standard

THE UNIVERSITY OF BRITISH COLUMBIA

January 2000

In presenting this thesis in partial fulfilment of the requirements for an advanced degree at the University of British Columbia, I agree that the Library shall make it freely available for reference and study. I further agree that permission for extensive copying of this thesis for scholarly purposes may be granted by the head of my department or by his or her representatives. It is understood that copying or publication of this thesis for financial gain shall not be allowed without my written permission.

Department of Physics and Astronomy
The University of British Columbia
6224 Agricultural Road
Vancouver, B.C., Canada
V6T 1Z1

Date: APRIL 28 / 2000

Abstract

We investigate the low energy magnetic relaxation characteristics of the "iron eight" (Fe_8) molecular magnet. Each molecule in this material contains a cluster of eight Fe^{3+} ions surrounded by organic ligands. The molecules arrange themselves into a regular lattice with triclinic symmetry. At sufficiently low energies, the electronic spins of the Fe^{3+} ions lock together into a "quantum rotator" with spin $S = 10$.

We derive a low energy effective Hamiltonian for this system, valid for temperatures less than $T_c \sim 360\ mK$, where T_c is the temperature at which the Fe_8 system crosses over into a "quantum regime" where relaxation characteristics become temperature independent. We show that in this regime the dominant environmental coupling is to the environmental spin bath in the molecule. We show how to explicitly calculate these couplings, given crystallographic information about the molecule, and do this for Fe_8. We use this information to calculate the linewidth, topological decoherence and orthogonality blocking parameters. All of these quantities are shown to exhibit an isotope effect. We demonstrate that orthogonality blocking in Fe_8 is significant and suppresses coherent tunneling.

We then use our low energy effective Hamiltonian to calculate the single-molecule relaxation rate in the presence of an external magnetic field with both AC and DC components by solving the Landau-Zener problem in the presence of a nuclear spin bath. Both sawtooth and sinusoidal AC fields are analyzed. This single-molecule relaxation rate is then used as input into a master equation in order to take into account the many-molecule nature of the full system. Our results are then compared to quantum regime relaxation experiments performed on the Fe_8 system.

Table of Contents

List of Tables

List of Figures

Acknowledgements

There are many people who have provided support during the completion of this work. Firstly I would like to thank Philip Stamp, both for introducing me to the complex and important world of the nuclear spin bath and for allowing me significant leeway in my approach to the difficult problems treated in this document. The education I received from him in the area of quantitative treatments of decoherence will be absolutely invaluable to the success of my post-doctoral pursuits. I hope that we will be working together for many years to come.

I would also like to thank the other great teachers I have had the opportunity to learn from in my time at UBC, and in particular Ian Affleck, who has influenced my understanding of several aspects of condensed matter physics, and Haig Farris, who has become a good friend, mentor and business partner over the past year.

As well I would like to thank colleagues and collaborators Mehrdad Sharifzadeh-Amin, Tim Duty, Sebastian Jaimungal, Alexandre Zagoskin, Jonathan Oppenheim, Suresh Pillai, Michel Olivier, Martin Dube, Stephanie Curnoe, Igor Tupitsyn, Nikolai Prokofiev and Jeff Sonier. Also I would like to thank Wolfgang Wernsdorfer for his amazing Fe_8 data.

The completion of this document would not have been possible without the support of my parents Dr. George and (soon to be Dr.) Sarah Rose, who I would like to dedicate this thesis to–I finally did it!

I would like to thank Craig Thomas for trying to keep up with me on the beach volleyball circuit, RANDy for hours of revolting amusement, and Shawn Kenney, Don and Kamara Lucas and Camille Parent for putting up with me.

Finally I would like to thank my wife Valerie, for believing that someday the re-write I was doing would be the last one.

Chapter 1

Introduction and Overview

Component sizes in commercially available semiconductor structures have been halving rather steadily every eighteen months or so since the early 1950s. This decrease in size, know as Moore's Law (named for Gordon Moore, one of the founders of Intel), is tracked by concommitant halvings in price and energy consumption and doublings of processor speed (see figures 1.1, 1.2 and 1.3) [1, 2, 3].

This continued shrinkage is producing much excitement and consternation in the high-tech world, for a very simple reason–it is clearly not sustainable. Naively one could say that this is because device sizes are limited to be larger than atomic length scales,

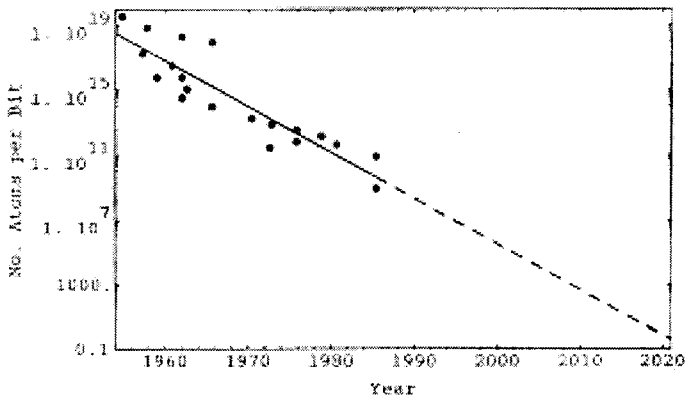

Figure 1.1: The number of atoms needed to represent one bit of information as a function of calendar year. Extrapolation of the trend suggests that the one atom per bit level is reached in about the year 2020. Adapted from [1].

which are on the order of Angstroms–at current shrinkage rates this barrier will be met in approximately 20 years. However it is not yet clear that the limitation on computing speed cannot be overcome in the near-term (10-30 years) with more efficient computer architecture–for example, stacking transistors horizontally [4], or even more exotic solutions such as the recent IBM SMASH proposal [5].

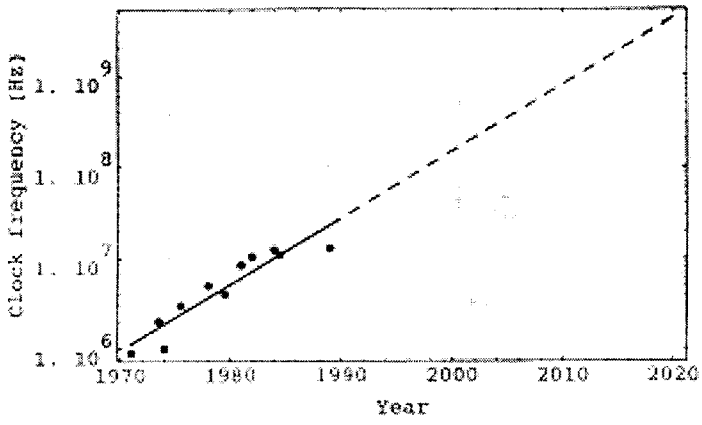

Figure 1.2: Clock speed (Hz) vs. calendar year. Adapted from [1].

Physicists have long been thinking about what will happen when component sizes become *mesoscopic*; that is, much larger than atomic length scales, but small enough so that at least in part they must be treated quantum mechanically [6, 7, 8, 9]. This line of thought has produced many extremely startling predictions. It is now well known that standard models of computation, based on the universal computing model or Turing model [10], contain an implicit assumption. This assumption is that the physical system which encodes and manipulates information evolves according to the classical laws of physics. This assumption can break down when components become "small enough". For example, quantum effects in mesoscopic normal metal rings [11], superconducting structures [12, 13] and in molecular magnets [14, 15, 16, 17] have been observed.

If one rewrites computer science with quantum mechanics implicitly included from the outset it turns out that the range of tasks that computing machines can perform is increased. The most famous example of this is the solution of the factoring problem [1, 19] using a "quantum computer" (which is a theoretical machine which has the capability of storing and manipulating coherent two level systems (quantum bits, or qubits)) in polynomial time, as opposed to superpolynomial time with classical computers. In addition to this, it is quite obvious that a quantum computer could in an analog fashion solve many important quantum mechanical problems, some of which are exceedingly important (such as pharmaceutical design), which are completely unsolvable using even the fastest imaginable classical supercomputers.

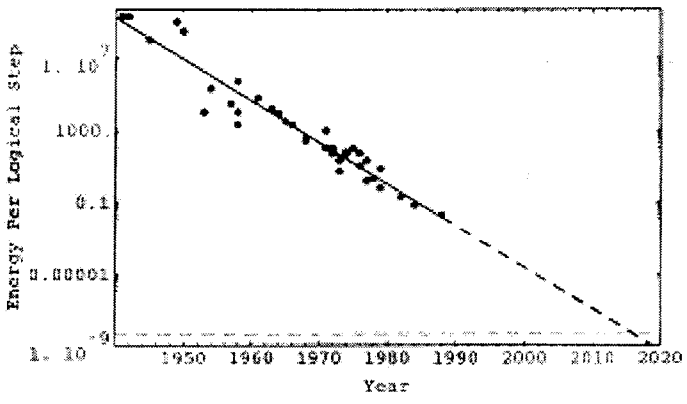

Figure 1.3: Energy (pico-Joules) dissipated per logical operation as a function of calendar year. The 1 kT level is indicated by a dashed line. Adapted from [1].

These theoretical musings are now coming face to face with some very real physical problems, as engineers undertake to build quantum devices. If one wants to construct a quantum computer, there are several aspects of mesoscale condensed matter physics that must be understood wholly and completely. The most important of these is the

process known as *decoherence*, which involves the transferral of phase information from a quantum bit into an *environment* (such as nuclear spins [20] or phonons [21, 22]). Decoherence is anathema to quantum computation (and interesting also from a purely theoretical perspective), and yet how it works in practice, quantitatively, is still not satisfactorily understood.

There exists a class of mesoscopic systems where an attempt can be made at a quantitative theory of decoherence. These are the so-called "molecular magnets". One of these materials, which we will refer to throughout as "iron-eight" (Fe_8), is particularly well suited to a quantitative study of decoherence due to localized environmental modes, and in particular nuclear spins. The development of this quantitative theory as a tool to be used in future investigations of mesoscale systems in the context of developing solid state quantum bits provides the main motivation for the work presented in this thesis.

1.1 An Introduction to Fe_8

Fe_8 was first synthesized in 1984 by Wieghardt et.al. [23]. This material, with the rather imposing chemical formula

$$\{[(tacn)_6Fe_8(\mu_3 - O)_2(\mu_2 - OH)_{12}]Br_7 \cdot H_2O\}^{\oplus}[Br \cdot 8H_2O]^{\ominus} \tag{1.1}$$

where $tacn \equiv 1,4,7$ triazacyclonane, was the first oligomer with greater than three Fe^{3+} ions per unit cell ever characterized. X-ray crystallography studies performed on this material indicated that six of the Fe^{3+} ions were bonded to amine ligands FeN_3O_3 and the remaining two were surrounded by a distorted octahedral array of 6 O atoms. The iron ions are coupled via 12 μ_2- hydroxo bridges and two μ_3- oxo bridges. Three views of the unit cell are presented here, in figures 1.4, 1.5 and 1.6. The positions of the ions shown here were obtained from the Cambridge Crystallographic Database [24], which contains the original X-ray data obtained by Weighardt et.al. [23].

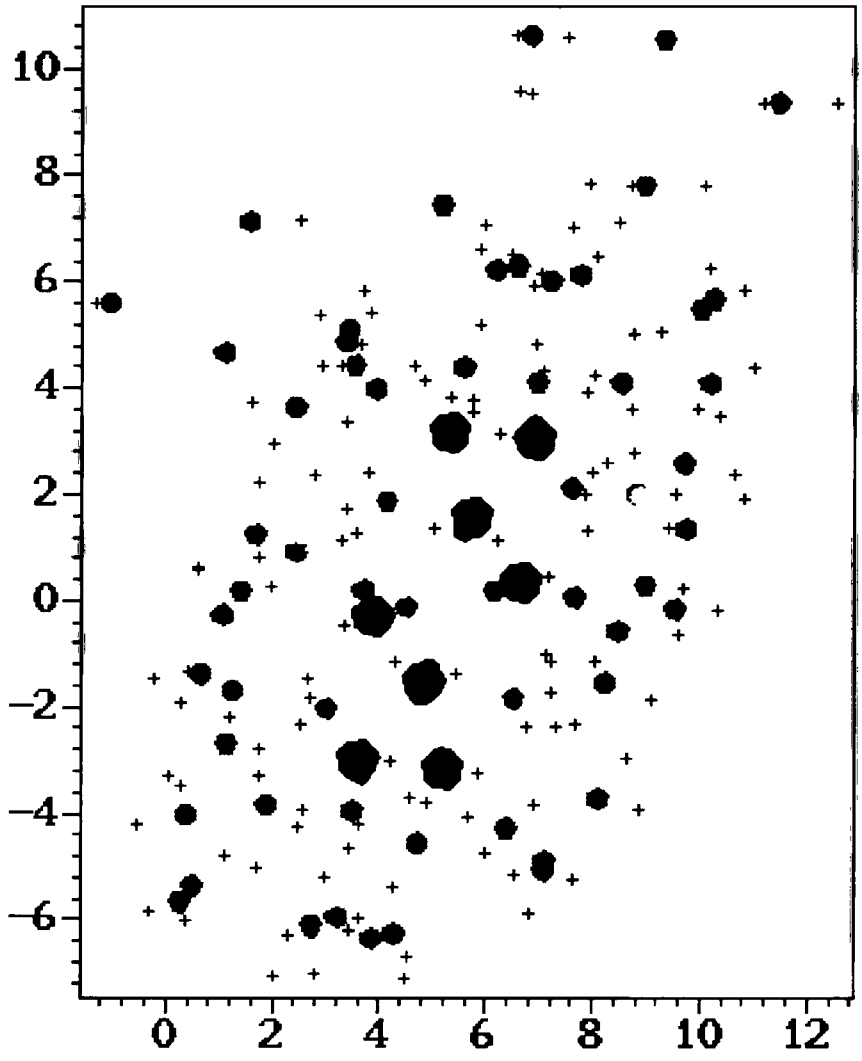

Figure 1.4: A 2-D projection view of the Fe_8 unit cell onto the $y - z$ plane. Distances shown are in Angstroms. Legend: Red, iron; Purple, bromine; Light Blue, oxygen; Green, nitrogen; Yellow, carbon; and Dark Blue Crosses, hydrogen. Note the central magnetic core, surrounded by a shield of organic species.

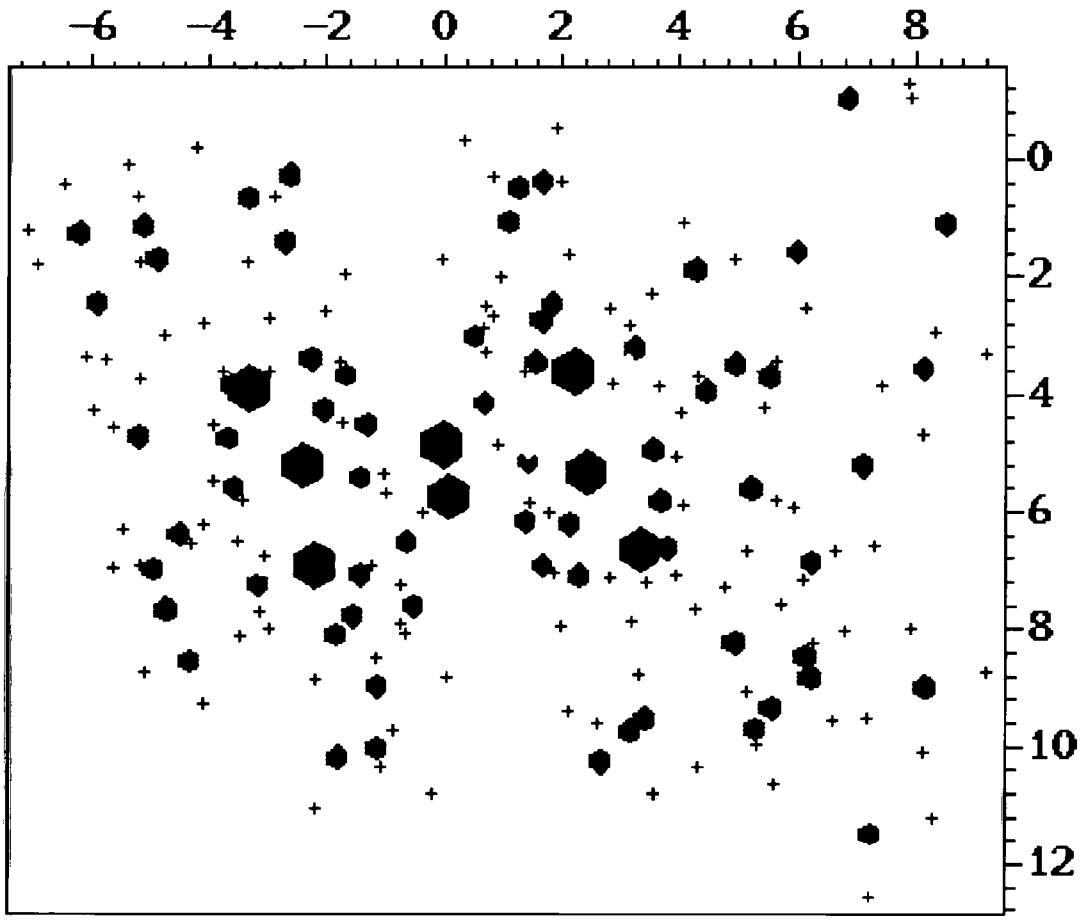

Figure 1.5: A view of the Fe_8 unit cell in the $x - z$ plane.

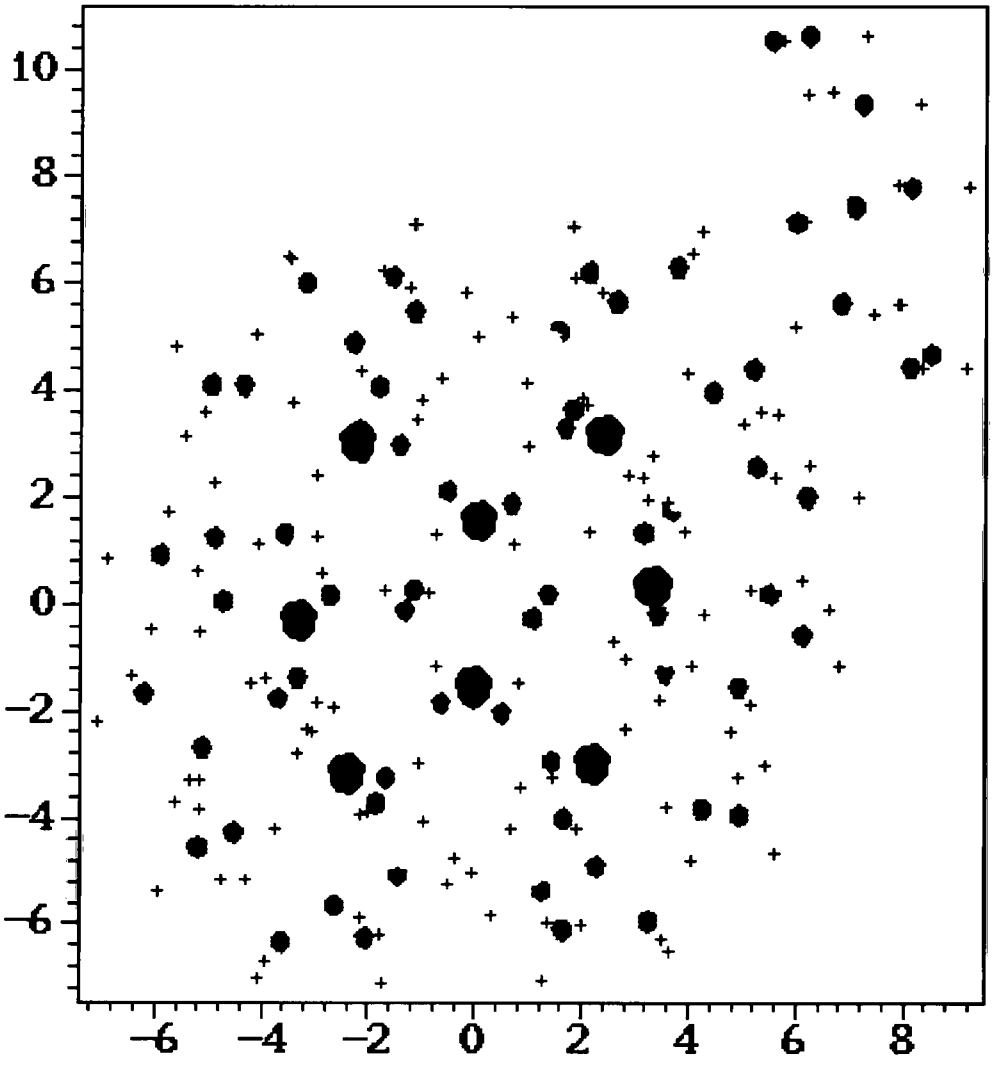

Figure 1.6: A view of the Fe_8 unit cell in the $x - y$ plane. Here we are looking right down the "easy axis" of the molecule (see chapter 2).

The amine groups are cyclic and hydrophobic. The Br atoms are bonded electrostatically to $NH^{\ominus}$ and $OH^{\ominus}$. The space group of the material is $P1$ (triclinic), with lattice parameters $a = 10.522$, $b = 14.05$ and $c = 15.00$ Angstroms with unit cell angles $\alpha = 89.90$, $\beta = 109.65$ and $\gamma = 109.27$ [23]. The molecular weight of the substance per unit cell is 2250. The lattice structure is of the AB type, with the cation and anion in (1.1) occupying the A and B sites respectively (this is simply a distorted NaCl structure).

1.1.1 Giant Spins and Quantum Environments

Experimental interest in the low temperature *magnetic* characterization of Fe_8 surprisingly did not arise until much later [18]. However in the experimental lull between 1984 and 1993 much theoretical work was being done that would lay the groundwork for understanding the low-energy magnetic nature of this substance.

There are two basic themes that needed to be developed to understand the experimental results that would later appear. The first of these is the understanding of the dynamics of "giant spins", that is systems that have large spin quantum number. One of the most obvious systems that can be thought of as a giant spin is a single isolated ferromagnetic grain, well below its Curie temperature. All the electronic spins lock together, and one could think of this object as a single degree of freedom, albeit with spin quantum number as large as $S = 10^8$. The interesting thing about these systems, and one of the main motivations for their early study, is that here we have an adjustable parameter (S) which as it is increased should cause the system to go from being quantum mechanical (say for $S = 1/2$) to being classical (say $S = 10^8$) in a way that we can study with some intimacy.

Two papers that would prove to be important in this respect were those of Van Hemmen and Suto [25] and Enz and Shilling [26], both in 1986. These discussed the dynamics of giant spins in the WKB approximation. In particular, the problem of how

large spin objects tunnel between energetic minima was treated.

The second basic theme that needed to be developed was an understanding of the effects of "environments" on the dynamics of the degrees of freedom to which they couple. It was shown by Feynman and Vernon [21] that if there exist environmental couplings that are weak, in the sense that their effect can be treated in second-order perturbation theory, one can model their effects by coupling the interesting degree of freedom to an oscillator bath. In a solid at low energies, it is usually the case that delocalized modes, such as phonons and photons, can be mapped to oscillator baths. This is because low energy modes have long wavelengths and therefore their overlap with the localized interesting degree of freedom is small.

Various aspects of the dynamics of a central degree of freedom coupled to oscillator baths have been investigated [22]. Perhaps the most famous of these is the treatment by Leggett et.al. of the so-called spin-boson problem [27]. In the spin-boson problem, the central degree of freedom is a two-state system (a spin). This is then coupled to an oscillator bath and the dynamics of the central spin are then extracted. It is possible to obtain analytic results for certain choices of parameters in the spin-boson Hamiltonian, but in general dynamical solutions are difficult to obtain.

1.1.2 A Related System is Characterized

In 1991 a substance that would turn out to be related to Fe_8 underwent low temperature magnetic characterization [28]. This substance is usually called Mn_{12}-acetate, or simply Mn_{12}, and has chemical formula

$$[Mn_{12}(CH_3COO)_{16}(H_2O)_4O_{12}] \cdot 2CH_3COOH \cdot 4H_2O \tag{1.2}$$

Crystals of this substance were known [29, 30] to have tetragonal symmetry of spatial group $I\bar{4}$ with unit cell parameters $a = 17.3$ Angstroms and $b = 12.39$ Angstroms. The

total molecular weight per unit cell is 2060. X-ray crystallography was performed [30] on this substance, and the atomic positions stored in the Cambridge Crystallographic Database. This data is presented in figures 1.7, 1.8 and 1.9. We see that there are two "rings" of manganese atoms. The inner ring consists of four Mn^{4+} ions with spin $S = 3/2$, while the outer ring consists of eight Mn^{3+} ions with spin $S = 2$. It was proposed that all these ions couple to each other primarily via superexchange through mediating oxo-bridges [30].

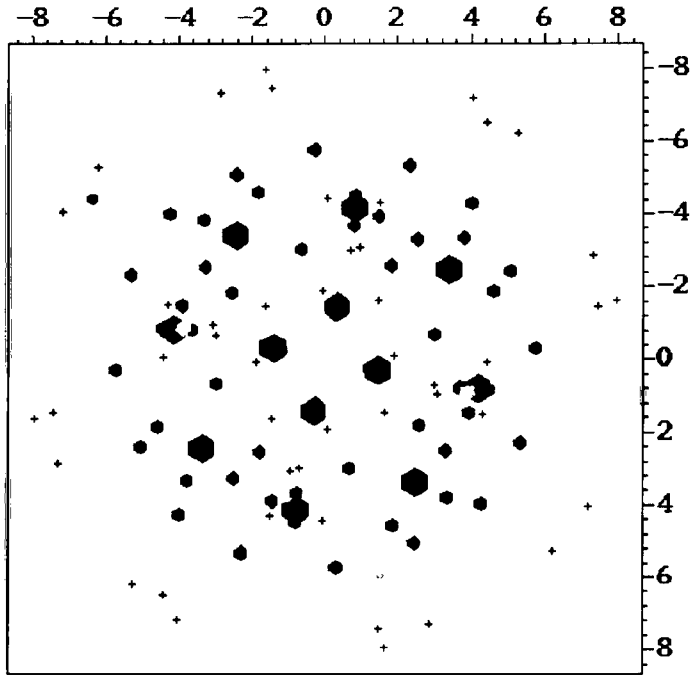

Figure 1.7: Projection of the Mn_{12} unit cell onto the $x - y$ plane. Here we are looking down the easy axis of the crystal. The axes scales are in Angstroms. Legend: Red, manganese; Purple, oxygen; Yellow, carbon; Dark Blue Crosses, hydrogen. Note the inner and outer "rings" of manganese ions.

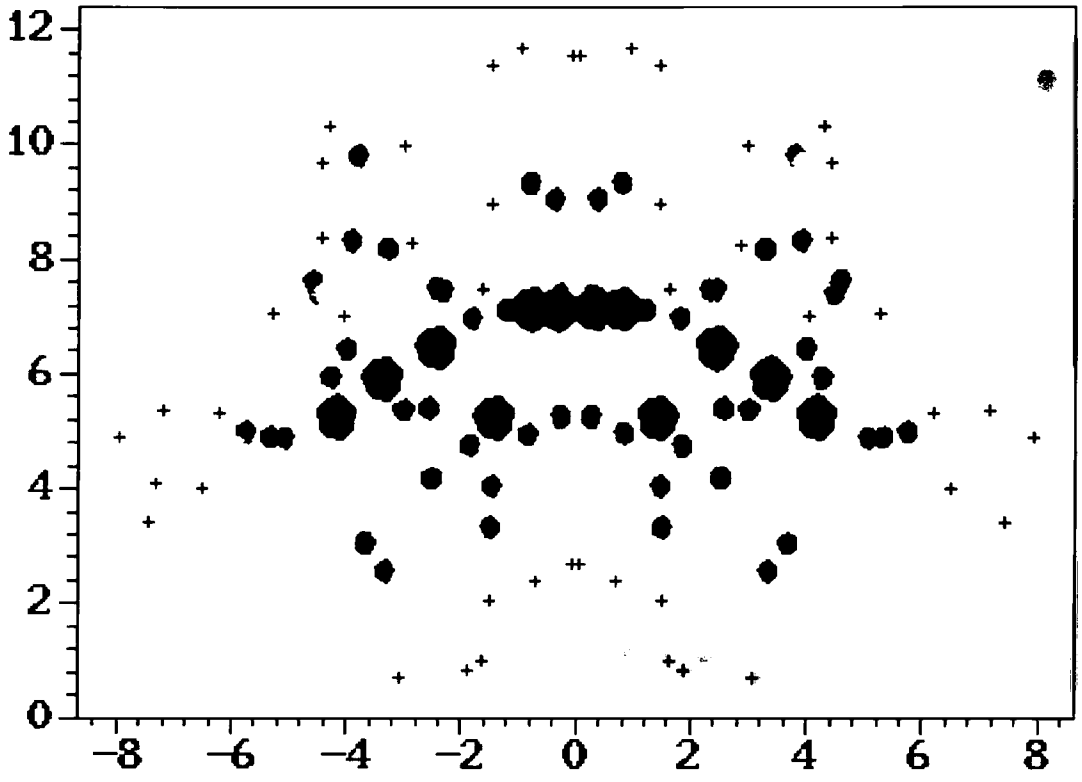

Figure 1.8: Projection of the Mn_{12} unit cell onto the $x - z$ plane.

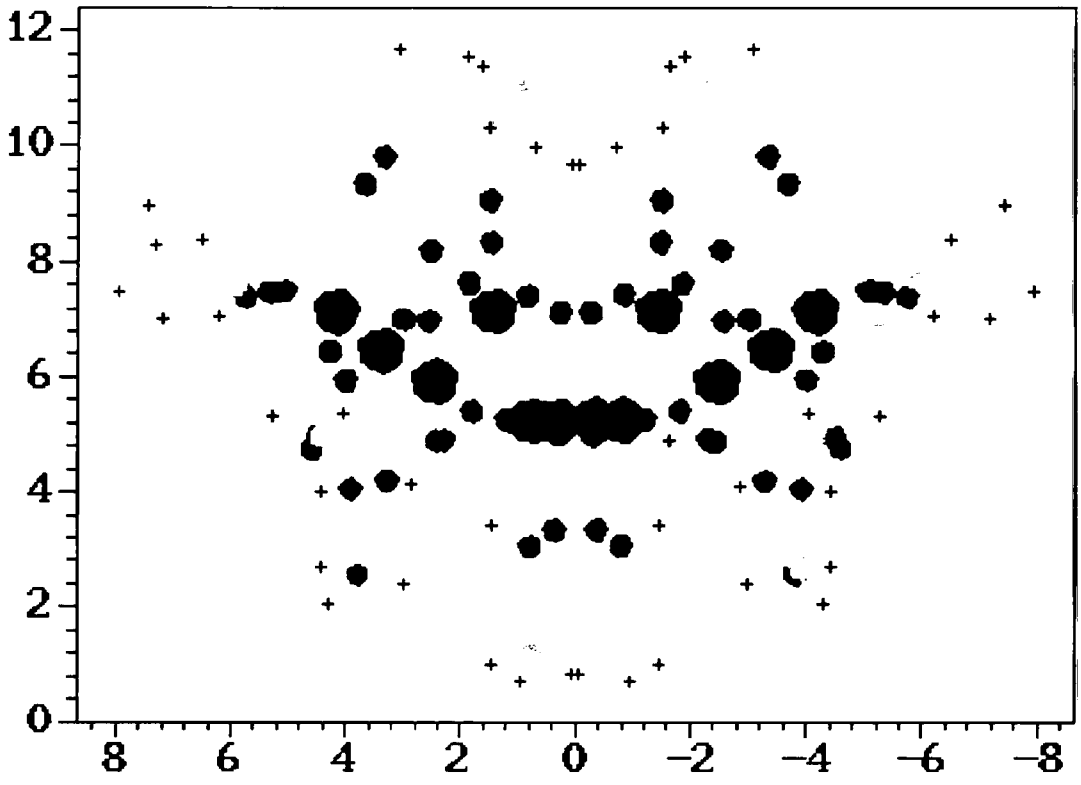

Figure 1.9: Projection of the Mn_{12} unit cell onto the $y-z$ plane.

The 1991 paper of Caneschi et.al. described results of AC susceptibility, high field magnetization and EPR measurements on crystals of Mn_{12} which indicated that each Mn_{12} molecule had an $S = 10$ groundstate. A mechanism was described whereby the twelve manganese ions in each unit cell lock together via superexchange at low temperatures into a giant spin. In this material an easy axis was observed, and was explained as being due to crystal anisotropy and/or spin-orbit coupling effects. These results produced much excitement, as here we have what seems to be (in zero external magnetic field and in a low-energy limit) a two state system ($|S = +10>$ and $|S = -10>$, correspondinging in a semi-classical picture to the giant spin pointing parallel/antiparallel to the easy axis respectively) whose dynamics should demonstrate quantum effects of some kind (as S is in the fuzzy mesoscale region). An analysis of what was known of Mn_{12} and some other molecular magnets was performed in 1993 by Sessoli et.al. [31] and provides an excellent review.

1.1.3 Magnetic Characterization of Fe_8

In 1993 a comprehensive characterization of the magnetic properties of Fe_8 at low temperatures was performed by Delfs et.al. [18]. In this study, AC and DC susceptibility, magnetization as a function of external field and EPR studies were performed which indicated that Fe_8 had, like Mn_{12}, a spin 10 groundstate.

This paper described its results in terms of a unit cell containing eight $S = 5/2$ Fe^{3+} ions which couple to each other via exchange and superexchange via oxygen and hydroxo bridges. At temperatures less than $T \sim 20\ K$ these lock together into a spin complex with $S = 10$. Because of spin-orbit couplings and crystal field anisotropies the spectrum of the spin 10 rotator is split into 10 doublets and one singlet, with $m_s = \pm 10$ being nearly degenerate lowest energy states corresponding in a semi-classical picture to the central spin object pointing "up" or "down" along the easy axis selected by the

anisotropy in the spin Hamiltonian (a rough first approximation to this spin Hamiltonian is given by $H = -DS_z^2$, where D is a measure of the strength of the various anisotropies in the crystal [32, 33, 34]–see chapter 2 for a comprehensive treatment of the low energy effective Hamiltonian for this system). The parameter D was reported to be on the order of $D \sim 0.3K$ [18].

1.1.4 Results in the Quantum Regime

The low temperature magnetic characterizations of Fe_8 and Mn_{12} led to a flood of important results, both from theorists and from the experimental community. Theorists were presented with a truly mesoscopic problem with a growing number of experimental results, and experimentalists had access to systems where they could directly measure macroscopic quantum effects. The study of Mn_{12} produced much work on the macroscopic quantum tunneling of the central spin of each molecule [35, 36, 37, 38]. Arguably the most important early experimental result was that of Thomas et.al. [17] in 1996, which presented clear-cut evidence for incoherent macroscopic tunneling of the magnetization in Mn_{12} (see figure 1.10). Even more astonishing were results obtained in 1997 on the Fe_8 system which clearly demonstrates the existence of a regime where magnetic relaxation rates become temperature independent–the so-called quantum regime (see figure 1.11) [14]. The authors attribute relaxation below $T \sim 360\ mK$ to be due to purely quantum mechanical tunneling between groundstates of the Fe_8 molecules in the crystals measured.

Results of magnetic relaxation measurements on these systems for the most part was amenable to analysis within existing theoretical frameworks [40-48]. In particular a framework had been constructed by Prokofiev and Stamp [41, 45, 46, 47] to explain the physics of relaxation in molecular magnets. In the models of Prokofiev and Stamp, each molecular magnet is treated as a giant spin which couples to various environments,

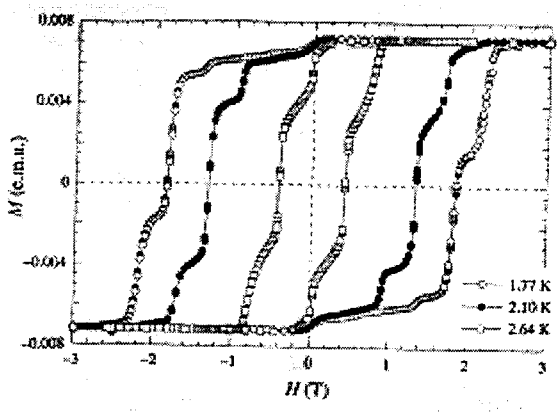

Figure 1.10: Magnetization steps in the hysteresis curve of Mn_{12}. From [17].

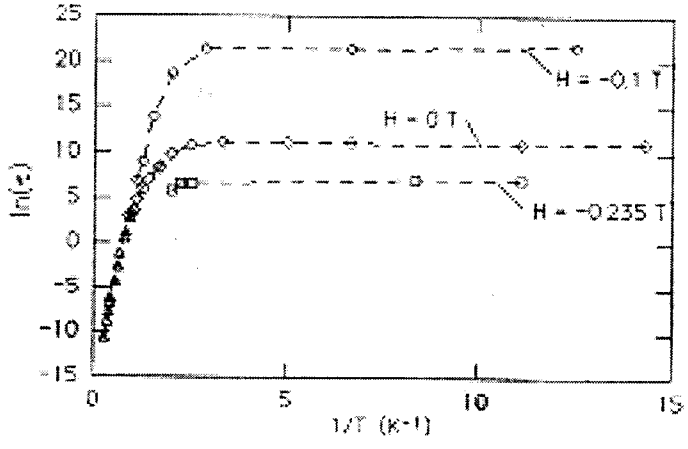

Figure 1.11: This data shows the log of the relaxation time vs. 1/T in Fe_8. At high temperatures thermal activation is observed, while for $T <\sim 360\ mK$ relaxation becomes temperature independent. Figure obtained from [14].

the most important of which it is argued are localized modes, such as nuclear spins and magnetic impurities. Note that localized modes such as these can not in general be mapped to oscillator baths as the coupling strengths are not in general small (for example, contact hyperfine couplings in rare earths can be as large as 1 K [48]). They show that the relaxation characteristics of giant spins in condensed matter systems should be strongly influenced by these localized modes, and hardly influenced at all by oscillator baths (such as phonons). In the quantum regime demonstrated to exist in Fe_8, the temperature independence is evidence that the phonon bath is not playing a significant role in relaxation.

But here was a curious thing. The fact that the Fe_8 crystals were relaxing at all in the quantum regime was quite strange, for the following reason. The bare tunneling amplitude between the groundstates of the Fe_8 molecules was estimated (by exactly diagonalizing phenomenological spin Hamiltonians whose parameters were extracted from various experiments) to be $\Delta \sim 10^{-8}\ K$ [45]; and yet the scale of the dipolar interaction between different molecules can quite easily be estimated to be of the order of $\sim 0.5\ K$. This means that in a crystal of molecules, only an extremely tiny fraction of molecules could ever be in resonance, and therefore their dynamics should be frozen.

A resolution of this difficulty was proposed in 1997 by Prokofiev and Stamp, and the proposed mechanism involved the nuclear spins present in the Fe_8 crystal [15]. At temperatures lower than $\sim 360\ mK$, there exists only one source of dynamics in the system, and that is the nuclear spin bath. These typically do not freeze out until μK temperatures and so at mK they are effectively in a high-temperature limit. The rate at which the nuclei in Fe_8 perform so-called T_2 flips [64, 65, 66], where the overall magnetization of a pair does not change, was estimated by these authors to be $\sim 1\ kHz - 1\ MHz$. The effect of these flips is to cause a time-varying magnetic field to be generated at each central spin, which was postulated to immensely increase the "resonance window"

and therefore allow the crystal to relax.

The mechanism works like this. At the beginning of relaxation, all molecules sit in a combination of the dipolar fields caused by all other molecules in the crystal and the time-varying magnetic fields caused by the nuclei present. There will be a small number of molecules that can be brought to resonance by the time-varying magnetic fields generated by the T_2 flipping nuclei. When one of these molecules tunnels, it rearranges the dipolar field configuration in the sample. This can bring other molecules to resonance, and so the crystal relaxes.

This theory contained certain testable predictions about the relaxation characteristics one should see if the hypotheses were correct. One of these was that the relaxation of Fe_8 in its quantum regime should be square root in time.

Although relaxation data existed up to this point that was taken as a function of time, the presence of the square root temporal dependence was not realized until after Stamp and Prokofiev looked for confirmation of their theory. At this point it was realized that earlier data did in fact follow a square root temporal relaxation. Subsequent measurements vindicated the idea, not only in Fe_8 but also in Mn_{12}.

The observation of the square root temporal dependence in Mn_{12} was not understood until quite recently [?]. The prediction of a square root relaxation rate depends quite clearly on the system that is relaxating being in a quantum regime–that is, the presence of thermally occupied higher levels destroys the square root. This seemed to contradict the fact that the relaxation characteristics in Mn_{12} were clearly temperature dependent down to at least 60 mK. The resolution of this difficulty is that Mn_{12} crystals contain "rogue" species of Mn_{12} that relax at different rates. Because of this it is possible that in certain temperature regimes one species of Mn_{12} is in its quantum regime and relaxes as a square root whereas the rest don't relax at all (see [63] for a discussion of this point).

In the next section we shall take a close look at relaxation experiments, as they

provide tantalizing glimpses of unresolved puzzles, some of which will be resolved in later chapters.

1.2 An Introduction to Relaxation Experiments

The general strategy for performing a relaxation experiment on a molecular magnetic crystal is quite straightforward [49]. One takes a sample of the material and cools it down to some temperature T in some static field $\vec{\mathcal{H}}$ over some time t_0. The initial magnetization of the sample is measured using a SQUID magnetometer array. The static field $\vec{\mathcal{H}}$ is then abruptly changed to some new field, which is in general time dependent $\vec{H}(t)$, and the magnetization of the sample (M) is then measured as a function of time. This gives us a quantity $M(T, t_0, \vec{\mathcal{H}}, \vec{H}(t), t)$ which tells us about how the crystal, initially prepared using $\{\vec{\mathcal{H}}, t_0\}$, relaxes in the presence of the field $\vec{H}(t)$ at the temperature T.

Several such experiments have been performed of late [49-63]. We shall focus our attention on those using the Fe_8 system, as this material has generated a wealth of excellent experimental data deep into the so-called "quantum regime"–the region where relaxation characteristics become completely independent of temperature (this happens in Fe_8 for temperatures lower than $T_c \sim 360\ mK$; see figure 1.11) [14]. The other heavily studied molecular magnet (Mn_{12}) is similar in many ways in its relaxation characteristics. However, there is an important difference–the relaxation characteristics of Mn_{12} show clear temperature dependence down to the lowest temperatures investigated ($T \sim 60\ mK$) [17]. In this thesis we have chosen to focus our efforts on understanding the physics of the quantum regime.

Now as we have described the experiment above, there are four basic parameters that we can play with in order to customize a particular relaxation experiment–the temperature at which it is performed (T), the static field in which it is cooled $\vec{\mathcal{H}}$, the time over

which it is cooled t_0 and the time-dependent field applied during relaxation $\vec{H}(t)$. Our strategy in this chapter will be to simply present the experimental situation in each particular case that we will review (that is, we will state what the parameters $\{T, t_0, \vec{\mathcal{H}}, \vec{H}(t)\}$ are) and then give the results. No theoretical justification or explanation will be presented here–we shall make this the task of the remainder of the thesis.

1.2.1 DC Field Relaxation in Polarized Fe_8

The first class of experiment that we will review was historically the first to be performed, perhaps because it is the simplest [18, 50]. In these experiments, the Fe_8 samples are cooled slowly from room temperature to the quantum regime in a large static bias field $\vec{\mathcal{H}}$, applied along the easy axis of the crystal (see chapter 2 for information about the crystal symmetry in Fe_8). This has the effect of preparing the crystal in an initially polarized state. Once the initial magnetization has been measured, the large static bias field is removed, and a smaller DC bias field $\vec{H}$ in applied to the crystal along its easy axis. The magnetization as a function of time is then measured. Shown in figures 1.12 and 1.13 are results for $M(t)$ for two different crystals in different experiments of this type. Note the unusual square-root relaxation characteristic. Also included here is a similar experiment performed on the Mn_{12} molecular magnet (figure 1.14) [58]. The relaxation for this material is also square-root in time, albeit with a strong temperature dependence.

1.2.2 DC Relaxation of Annealed Crystals

A second class of experiments involve a different method of preparation of the sample under study. Instead of slowly lowering the temperature down into the quantum regime we may instead rapidly quench the temperature over a time t_0 that is so small that the

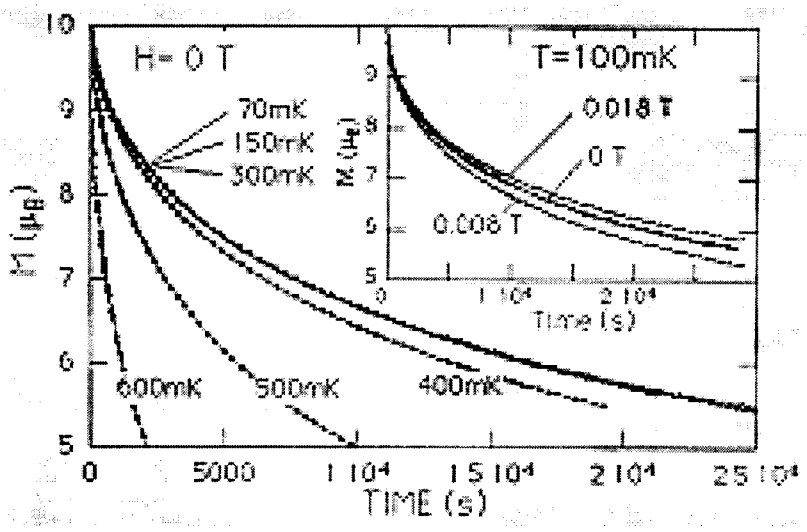

Figure 1.12: Relaxation of the magnetization measured at $\vec{H} = 0$ after first saturating in a field of $\vec{\mathcal{H}} = 3.5\ T\ \hat{z}$. As indicated in figure 1.11, the curves superimpose for $T < 360\ mK$. Shown in the inset are relaxation characteristics in the quantum regime for some $\vec{H} \neq 0$, applied along the easy ($\hat{z}$) axis. Figure from [50].

thermal distribution of molecular magnetization is frozen into the initial state of the crystal [49]. That is, the elevated temperature of the molecular ensemble before the quench enables a thermal distribution of the magnetic moments of the molecules. The state of the crystal after the quench retains this distribution initially, before it begins to relax. This procedure is called annealing. The initial magnetization of the sample can be arbitrarily chosen in this scenario, depending only on the pre-quench temperature and static field $\vec{\mathcal{H}}$. Note that the first type of experiment considered is a limiting case of this one.

After the sample is quenched and the initial magnetization is measured, a longitudinal DC field is applied either against or in the direction of the magnetization, and the function $M(t)$ is measured. Presented in figure 1.15 are results from this type of experiment.

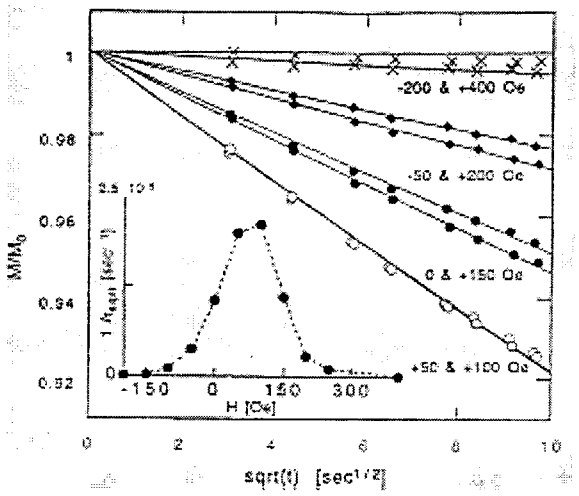

Figure 1.13: Short time relaxation of a single crystal of Fe_8, measured at $150mK$. Here several different DC bias fields $\vec{H}$ were applied along the easy axis of the crystal. Note that the data is plotted against square root t. The inset shows the slope of each of these lines as functions of the DC bias field. Figure from [55].

1.2.3 Hole Digging and the Time-Dependent Internal Longitudinal Bias Distribution

It has been proposed that the DC relaxation of the magnetization $M(\vec{H},t)$ can be related to the time-dependent distribution of internal bias fields in the sample [15, 51, 49]. In chapter 6 we shall review the current DC theory and supplant this with our AC results. The basic idea is that the relaxation characteristic $M(\vec{H},t)$ is seen experimentally to be square root in time for short times. The "relaxation rate" $\Gamma_{sqrt}(\vec{H})$, defined via $M(\vec{H},t) \sim 1 - \sqrt{\Gamma_{sqrt}(\vec{H})t}$ can then be measured. The assumption then is that the internal distribution of longitudinal biases $P(\xi,t)$ (where ξ is the longitudinal bias field) is proportional to the relaxation rate $P(\xi,t) \sim \Gamma_{sqrt}(\vec{H})$ where the field $\vec{H}$ is applied at time t.

Shown in figure 1.16 is the relaxation rate $\Gamma_{sqrt}(H_z)$ of a sample that was prepared in

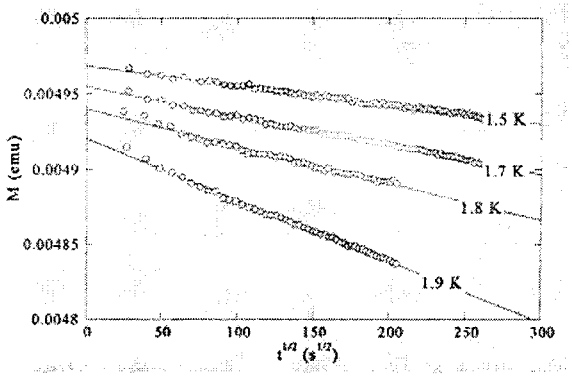

Figure 1.14: Here we include some data from a different kind of molecular magnet, the Mn_{12} system. Here we again see the clear square-root relaxation characteristic. However in this case the relaxation rates are temperature dependent. Figure from [57].

an initially polarized state. In figure 1.17 the evolution of these rates over time is shown. Note that as the sample evolves, there appears a "hole" in the relaxation rates near zero internal bias. Shown in figure 1.18 is the evolving relaxation rate spectrum of a sample that was initially annealed such that $M(0) \sim 0.2$. Again we see evidence of a hole being dug near zero bias in this distribution.

This hole in the annealed samples has an interesting feature. If samples are annealed to $|M(0) < 0.5|$ there is found an intrinsic hole width of approximately 0.8 mT (see figure 1.19). Stamp and Prokofiev suggested that this intrinsic linewidth was due to nuclear spins [20]. We present a framework in chapter 3 for calculating the linewidth due to the nuclei and demonstrate that our result agrees quantitatively with these experimental results, supporting the contention that nuclear broadening is responsible for this intrinsic hole.

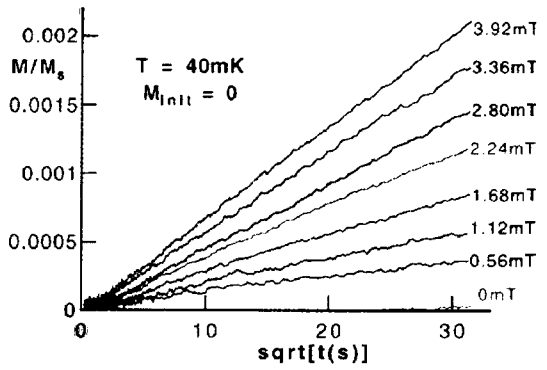

Figure 1.15: Here is data from an experiment on an Fe_8 sample that was annealed in zero field, giving it zero initial magnetization. The sample was then exposed to longitudinal DC fields of various magnitudes. We see here relaxation away from $M = 0$, in the direction of the applied field, with the same square root temporal dependence as in the initially polarized case. From [49].

1.2.4 AC Relaxation of Annealed Crystals

The final kind of relaxation experiment that we shall review differs from the previous type in that the field applied during relaxation contains a periodic time-dependent component, applied in the direction of the easy-axis of the crystal [51]. The beauty of this type of experiment is that it is possible to measure extremely small relaxation rates, which presents us with a useful probe of much of the physics of these systems. In addition, there now exists a quantitative theory of how molecular magnets respond to this kind of perturbation, which we shall develop in the later chapters.

1.2.5 Extraction of Tunneling Matrix Elements

Shown in figures 1.20 and 1.21 are quantities extracted from AC relaxation measurements, which are related to the tunneling matrix elements of the single-molecule effective Hamiltonian of Fe_8 (we shall show exactly how they are related in chapter 6). What is

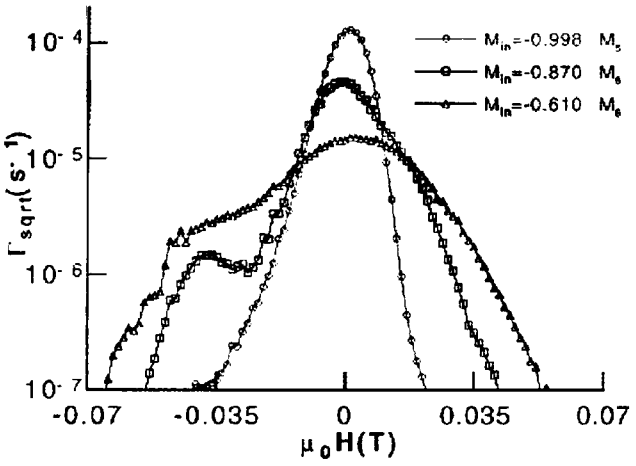

Figure 1.16: Field dependence of short time square root relaxation rates $\Gamma_{sqrt}(H_z)$. The initial distribution is labelled with $M_{in} = -0.998\ M_S$ whereas the others are distributions obtained by thermal annealing. The latter are distorted at higher fields by nearest neighbour lattice effects. Figure from [49].

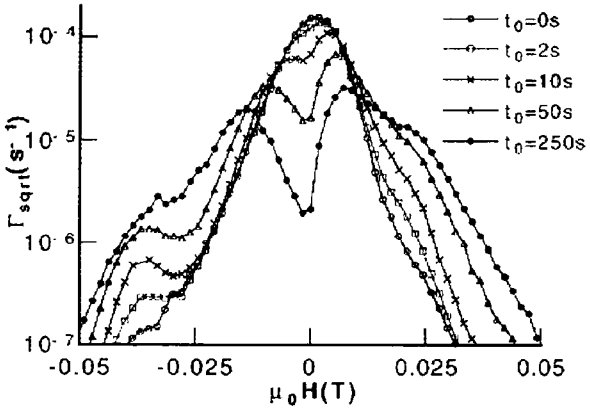

Figure 1.17: Quantum hole-digging. For each point, the sample was first saturated in a field of -1.4 T at a temperature of $T \sim 2\ K$ and then cooled to 40 mK. The sample was then allowed to relax for times t_0. After this time had elapsed, a DC field H_z was applied, and Γ_{sqrt} was measured. Note the rapid decrease in relaxation rate near $H_z = 0$. Figure from [49].

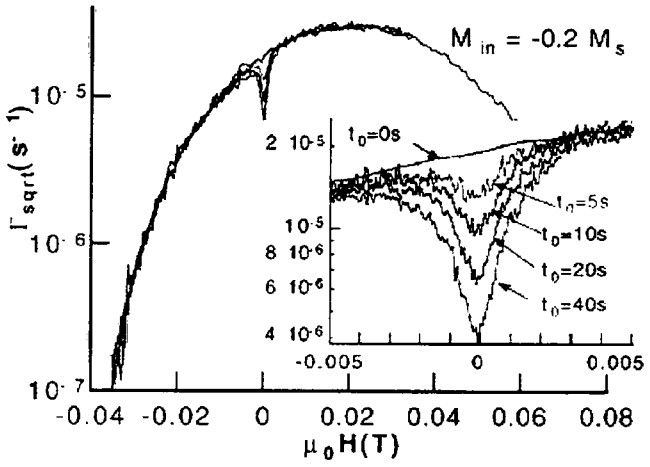

Figure 1.18: Quantum hole digging, as in figure 1.17, but now for a sample that has been annealed to $M_{in} = -0.2\ M_s$. The resulting evolution shows a very narrow hole (see inset). Near zero bias the hole develops very rapidly although the rest of the distribution hardly changes at all. Figure from [49].

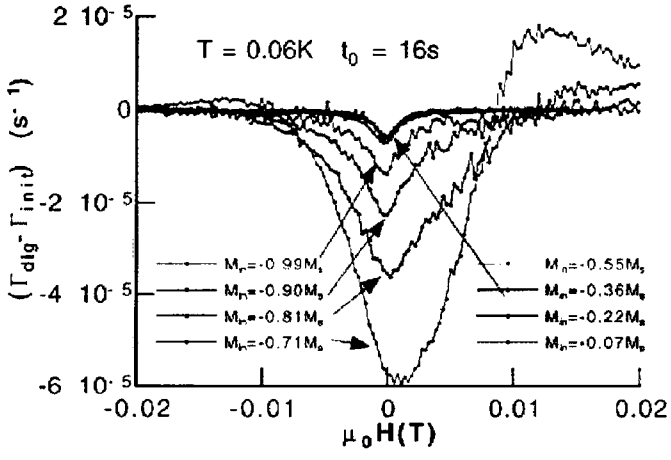

Figure 1.19: Here is plotted the difference between the relaxation rates at $t = 0$ (Γ_{init}) and at $t_0 = 16s$ (Γ_{dig}), for several different amounts of annealing. Note that for $|M_{in}| < 0.5$ the hole width becomes independent of $|M_{in}|$, with an intrinsic width of $\sim 0.8\ mT$. Figure from [49].

actually measured here is simply the magnetization as a function of time, $M(t)$ as per usual, in the presence of a longitudinal sawtooth AC field of amplitude A and frequency ω, a longitudinal DC bias field $H_z\hat{z}$, and a static transverse DC field $\vec{H} = H_x\hat{x} + H_y\hat{y}$. The authors find that $M(t) \sim \exp[-\Gamma t]$, ie. the relaxation is exponential, with a rate Γ that is a function of the applied longitudinal AC field, the transverse DC field and the longitudinal DC field. They then define their quantity Δ in the figures shown via the following relation;

$$\Delta^2 = \frac{\Gamma A \omega}{\pi} \tag{1.3}$$

Note that as advertised we are not going to try to justify this relation theoretically just yet–there will be much on this later.

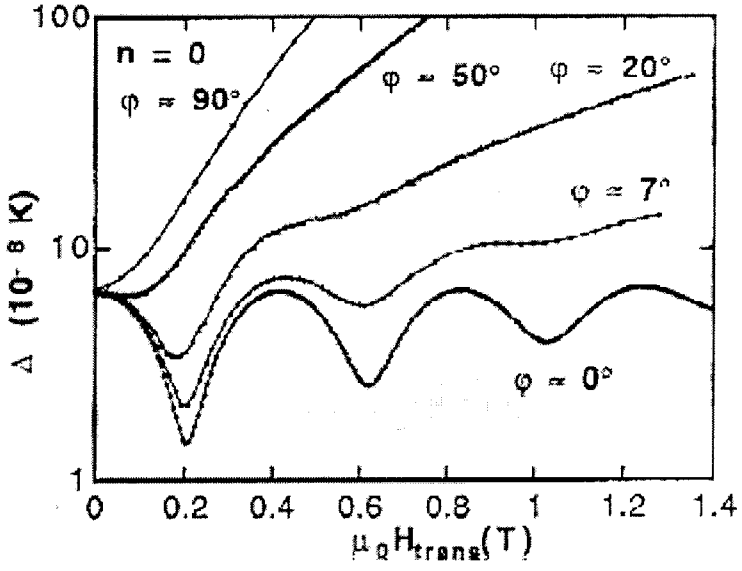

Figure 1.20: The quantity Δ here is related to the relaxation rate of the crystal's magnetization via (1.3). Here it is shown as a function of the magnitude of the transverse DC field $|\vec{H}| = \sqrt{H_x^2 + H_y^2}$ for several orientations of this field $\varphi = \tan^{-1}(H_y/H_x)$. In this case the longitudinal DC field was taken to be zero ($H_z = 0$). Figure from [51].

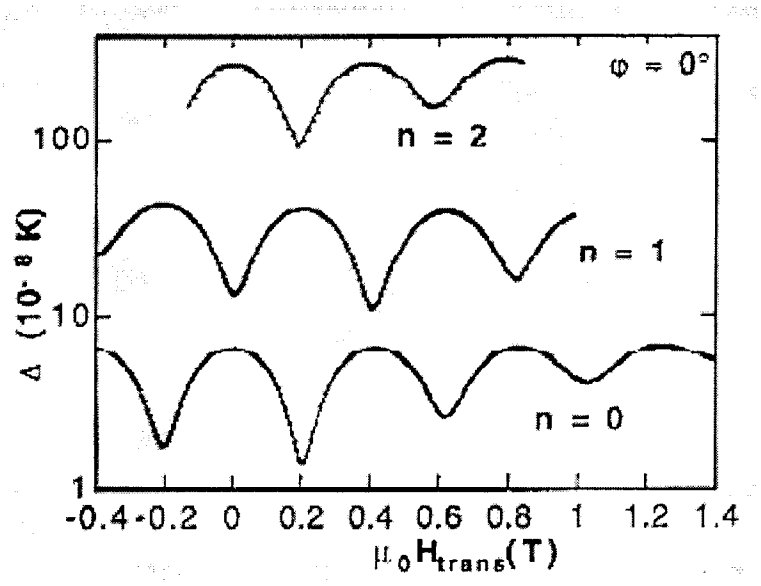

Figure 1.21: The quantity Δ shown for $\varphi = 0$, as a function of $|\vec{H}|$. Shown here are results for three different values of H_z. The lowest curve was obtained for $H_z = 0$; the middle curve for $H_z = 0.22T$, and the upper curve for $H_z = 0.44T$. In terms of the energy level structure of the Fe_8 molecule's spin Hamiltonian presented in chapter 1, these applied fields correspond to resonance situations between $|-S> \leftrightarrow |+S>$, $|-S> \leftrightarrow |+S-1>$ and $|-S> \leftrightarrow |+S-2>$ respectively. Notice that a parity effect is observed. Figure from [51].

1.3 Thesis Overview

Our goal will be to work up to a quantitative theory of AC relaxation in Fe_8 crystals. In order to do this we shall need to develop several key concepts.

We begin in chapter two with an analysis of the problem of deriving an effective Hamiltonian for a single Fe_8 molecule.

In chapter three we calculate the hyperfine couplings between a central spin object and all the nuclei in the molecule. Using this information we calculate all the decoherence parameters introduced by Prokofiev and Stamp in their theory of the spin bath. We show

that there should exist measurable isotope effects in Fe_8 and give quantitative predictions of the linewidth due to nuclear spins in an Fe_8 crystal with arbitrary isotopic content.

In chapter four we introduce and develop some of the machinery of the Landau-Zener problem. This involves using a time-dependent Hamiltonian to extract transition probabilities between states of the central object of interest.

Chapter five is the heart of the thesis, and contains an extension of the Landau-Zener problem in which nuclear spins are included. We use the results of this calculation to find a single-molecule relaxation rate in the presence of an external magnetic field with both AC and DC components.

Chapter six then uses this general single-molecule relaxation rate as the input to a master equation so as to model the temporal evolution of a crystal of Fe_8 molecules. We extract time-dependent relaxation characteristics from our theory and compare these to experimental results.

We conclude our analysis in chapter seven with a summary of results and the current outlook for our theory of AC relaxation.

Chapter 2

Effective Hamiltonians

In this chapter we derive a low energy effective Hamiltonian for a single isolated Fe_8 molecule. We begin by listing all terms found in the Hamiltonian of a single free Fe^{3+} ion. We then describe how these will be modified by placing the Fe^{3+} ions into a crystalline environment, following the treatment of Abragam and Pryce [67] (see also [68, 69]). This leads to a single ion "spin Hamiltonian". We then build up the Fe_8 Hamiltonian by introducing exchange/superexchange terms between the Fe^{3+} ions and terms coming from both the nuclear spin environment [20] and phonon [70] and photon [71] oscillator baths.

This "bare" description of the Fe_8 molecule, containing eight single ion Fe^{3+} terms, exchange/superexchange couplings between these and the various environments is then investigated. The exchange/superexchange coupling energies are much larger than all other energy scales [72, 73]. This suggests the hypothesis that at low energies these couplings lock the electronic spins together into a "giant spin" [20]. We assume that this is the case and write down a "giant spin Hamiltonian" that we postulate could in principle be derived from the bare Hamiltonian in a similar manner to how the single ion spin Hamiltonians were derived from their bare descriptions, ie. by finding the "giant spin" ground state of the system and performing perturbation theory around it to eliminate all the electronic spin degrees of freedom but one.

We then proceed to the investigation of the properties of general giant spin Hamiltonians in the absence of environmental couplings. We calculate tunneling matrix elements

for Hamiltonians with various symmetries using instanton [74, 75], WKB [25, 26], perturbation theory [70] and exact diagonalization methods.

We conclude by returning to the specific case of the Fe_8 giant spin Hamiltonian. The giant spin possesses two preferred directions due to crystal anisotropy which are identified, in zero external field, with the $\pm\hat{z}$ directions (states $|S = +10>$ and $|S = -10>$). At temperatures much lower than the difference in energies between $|+9>$ and $|+10>$ states ($\sim 5\ K$) only the $|\pm 10>$ states have significant thermal populations. This allows us to derive a final effective description where the central spin object is treated as a two level ($|\pm 10>$) system, following the treatment of Tupitsyn et.al. [74].

2.1 The Fe^{3+} Free Ion Hamiltonian

We shall begin our analysis of the complicated Fe_8 system (whose structure was shown in the introductory chapter) by concentrating our attention on the iron ions. We shall begin by studying a general Hamiltonian for a *free* Fe^{3+} ion. This treatment follows that of [69].

The dominant term in this description is the Coulomb interaction amongst the electrons (here there are N_e of them) and between the electrons and nuclear charge Ze

$$V_F = \sum_{j=1}^{N_e} \left(\frac{\vec{p}_j{}^2}{2m} - \frac{Ze^2}{r_j} \right) + \sum_{j<k=1}^{N_e} \frac{e^2}{r_{jk}} \tag{2.1}$$

The next most important term is the magnetic interaction between the orbital angular momentum $\vec{l}_j$ and the electronic spin $\vec{s}_k$

$$V_{LS} = \sum_{j,k} a_{jk} \vec{l}_j \cdot \vec{l}_k + b_{jk} \vec{l}_j \cdot \vec{s}_k + c_{jk} \vec{s}_j \cdot \vec{s}_k \tag{2.2}$$

where a_{jk}, b_{jk} and c_{jk} are constants. Next comes the direct interaction between spins

$$V_{SS} = \sum_{jk} \frac{\vec{s}_j \cdot \vec{s}_k}{r_{jk}^3} - \frac{3(\vec{r}_{jk} \cdot \vec{s}_j)(\vec{r}_{jk} \cdot \vec{s}_k)}{r_{jk}^5} \tag{2.3}$$

Weaker still are the terms

$$V_N = 2g_n\mu_B\mu_n\left[\sum_k\left\{\frac{(\vec{l}_k-\vec{s}_k)\cdot\vec{I}}{r_k^3}+\frac{3(\vec{r}_k\cdot\vec{s}_k)(\vec{r}_k\cdot\vec{I})}{r_k^5}\right\}+\frac{8\pi}{3}\delta(r_k)(\vec{s}_k\cdot\vec{I})\right] \tag{2.4}$$

where the term in curly brackets is the dipole-dipole interaction between the nuclear and electronic moments and the last term is the so-called anomalous hyperfine term which comes about from the overlap of the wavefunction of s electrons with the nucleus and

$$V_Q = \frac{e^2Q}{2I(2I-1)}\left[\sum_k\frac{I(I+1)}{r_k^3}-\frac{3(\vec{r}_k\cdot\vec{I})^2}{r_k^5}\right] \tag{2.5}$$

which represents the electrostatic interaction between the nuclear quadrupole moment Q and the gradient of the electric field due to the electrons. Interaction with an external magnetic field produces the terms

$$V_H = \sum_k \mu_B(\vec{l}_k+2\vec{s}_k)\cdot\vec{H} \tag{2.6}$$

and

$$V_h = -g_n\mu_n\vec{H}\cdot\vec{I} \tag{2.7}$$

corresponding to the interactions with the electrons and nucleus respectively. The total free ion Hamiltonian is now just the sum of these;

$$H = V_F + V_{LS} + V_{SS} + V_N + V_Q + V_H + V_h \tag{2.8}$$

Orders of magnitude of these may be obtained from optical spectra and are, for Fe^{3+}, $V_F \sim 5\cdot10^5\ K$, $V_{LS} \sim 100-300\ K$, $V_{SS} \sim 1-2\ K$, $V_N \sim 1-200\ mK$ and $V_Q \sim 1-2\ mK$ [76].

We see that V_F is by far the dominant term in this expression. If we neglect all terms but this one, then $\vec{L}$ and $\vec{S}$ (the total angular momentum and spin of the ion) commute with V_F. This means that we may in this approximation label the states of

the free ion with the quantum numbers L, L_z, S, S_z, J and J_z. Since the filled inner shells have $S = L = J = 0$ we may describe the ion by referring only to the state of the partially filled outer $3d$ shell. It is known that the V_F term in Fe^{3+} leads to a groundstate that is an orbital singlet ${}^6\mathcal{S}_{5/2}$ [77], where we use the standard notation that the superscript refers to the spin multiplicity $2S + 1$, the capital script letter refers to the total angular momentum of the ion ($\mathcal{S} \rightarrow 0$, $\mathcal{P} \rightarrow 1$, $\mathcal{D} \rightarrow 2$, etc.) and the subscript refers to the total angular momentum $\vec{J}$. This state may be obtained via the use of Hund's first two rules [78]–we first maximize the total spin by filling up five d orbitals with $s = +1/2$ electrons (giving total spin $5/2$) and then maximize the orbital angular momentum ($L = 2 + 1 + 0 + (-1) + (-2) = 0$). Note that for all half-filled shells (here we have 5 d electrons out of a possible 10) we get an orbital singlet for the groundstate.

2.2 The Effect of the Crystalline Environment

In general, when a transition metal ion is placed in a crystalline environment, the first question that must be resolved is the question of the nature of the bonding between the ion and the ligands. This is because the dominant new term that must be dealt with comes from the electrostatic interaction between the ion's d shell electrons and all the charged matter in the molecule. If this bonding is mostly ionic, then one can make the approximation that the ion sits in an electrostatic field coming predominantly from its nearest neighbours, which are treated as point charges. This is the so-called *crystal field* [79] approximation. Although it is crude, it is often a useful starting point for understanding the effect of the Coulombic interaction between the ion and its environment. A little more sophisticated is the *ligand field* [80] approximation. In this treatment allowance is made for the direct overlap of the ion's d shell electrons with the ligands, ie. an attempt to deal with covalency is presented. Better yet are *molecular orbital* [81]

methods, which use as their starting points the orbitals of each of the ligands and ions and the interactions between these.

Now in our specific case we are interested only in the low energy properties of the Fe^{3+} ion. The free ion groundstate is, as mentioned, an orbital singlet ${}^6\mathcal{S}_{5/2}$. What will be the effect of the inclusion of the Coulombic environment on this groundstate and the low-lying excited states? In order to answer this question we need only to know the relative strengths of the "on-site" Coulomb terms V_F and the "off-site" Coulomb terms V_C. The strength of this coupling in several materials containing Fe^{3+} ions has been determined, with these ranging from $V_C \sim 17000 - 23000\ K$ [82]; however V_C has not been measured in Fe_8. Fortunately there a way to know what the relative magnitude of these are without a direct measurement. If $V_F \gg V_C$ then the groundstate of the ion will remain ${}^6\mathcal{S}_{5/2}$, as the electric field cannot split a singlet. If we are in the opposite limit $V_C \gg V_F$ then the Fe^{3+} ions will go into a "spin-paired" state with spin $S = 1/2$ (ie. Hund's rules are modified). Since it is known experimentally that the Fe^{3+} ions are in fact in a $S = 5/2$ state we infer that we are in the limit $V_F \gg V_C$, which is in accord with the crystal field strengths reported for other materials with Fe^{3+} centers.

We see that the experimentally observed fact that the Fe^{3+} ions have spin $S = 5/2$ simplifies our task tremendously. This is because this is *prima facie* evidence that the groundstate of the Fe^{3+} ions, even in the molecular environment, is ${}^6\mathcal{S}_{5/2}$. More precisely, this is evidence that the groundstate of the Hamiltonian $H = V_F + V_C$, where V_C includes all Coulombic terms coming from the interaction of the ion with the ligand environment, is an orbital singlet ${}^6\mathcal{S}_{5/2}$.

Now the tack that we shall choose in what follows is this. Since the Coulombic environment does not split the groundstate here, but does affect the excited ionic states (the nearest state is a ${}^4\mathcal{G}$ state [165] in the free ion), and since we are not in the position to quantitatively account for its effects anyway (this would require a molecular orbital

approach, and even these do not always work [83]), we shall adopt the crystal field paradigm in dealing with charges external to the ion. In this picture the excited states of the Fe^{3+} free ion are split by the crystal field, with some orbitals being favoured above others because of their spatial dependence and relative positioning in the molecule. In our case the Fe^{3+} ions all have six nearest neighbours arranged in a distorted octahedral shape. This allows us in principle to calculate the splittings of the excited states. We shall not do this however–as we shall see, the magnitude of these will only quantitatively change the results of the arguments to come.

2.3 The Single Ion Effective Hamiltonian

We now want to consider the effect of the free ion terms $V_{LS} + V_{SS} + V_N + V_Q + V_H + V_h$. What we shall do is follow the treatment of Abragam and Pryce [67], calculating their effect perturbatively on the ${}^6\mathcal{S}_{5/2}$ groundstate of $H = V_F + V_C$. The first step in this treatment is to rewrite these perturbations in terms of total single ion spin and angular momentum operators $\vec{S}$ and $\vec{L}$. This will be permissible as long as there is no significant chemical bonding between the iron ions and their surroundings, which as we saw in the preceding is supported by the $S = 5/2$ nature of the ions. This has been done; we repeat this process here (for a detailed explanation of the steps outlined here, see [68]). Our terms transform as follows;

$$\begin{aligned} V_{LS} &\to \lambda\, \vec{L}\cdot\vec{S} \\ V_{SS} &\to \rho\left[(\vec{L}\cdot\vec{S})^2 + \frac{1}{2}\vec{L}\cdot\vec{S} - \frac{1}{3}L(L+1)S(S+1)\right] \\ &\to \rho\left[\frac{1}{2}(L^\alpha L^\beta + L^\beta L^\alpha)S_\alpha S_\beta - \frac{1}{3}L(L+1)S(S+1)\right] \end{aligned} \tag{2.9}$$

The effective spin-orbit coupling parameter λ for free Fe atoms is measured to be $138K$ [84] and is expected to be slightly smaller for Fe^{3+} ions. The parameter ρ is difficult to

calculate [85] but is expected to be much smaller than λ [86]. We also have

$$V_N \to g_n\mu_\beta\mu_n \left\langle \frac{1}{r^3} \right\rangle \left[(\vec{L}\cdot\vec{S}) + \xi L(L+1)(\vec{S}\cdot\vec{I}) - \frac{3}{2}\xi(\vec{L}\cdot\vec{S})(\vec{L}\cdot\vec{I}) \right.$$
$$\left. -\frac{3}{2}\xi(\vec{L}\cdot\vec{I})(\vec{L}\cdot\vec{S}) \right] - g_n\mu_\beta\mu_n\kappa \left\langle \frac{1}{r^3} \right\rangle (\vec{S}\cdot\vec{I})$$
$$V_Q \to \frac{\eta e^2 Q}{2I(2I-1)} \left\langle \frac{1}{r^3} \right\rangle \left[3(\vec{L}\cdot\vec{I})^2 + \frac{3}{2}(\vec{L}\cdot\vec{I}) - L(L+1)I(I+1) \right] \qquad (2.10)$$

where for the iron group

$$\xi = \frac{(2l-1)-4S}{S(2l-1)(2l+3)(2L-1)} \quad , \quad \eta = \pm 2S\xi \qquad (2.11)$$

(the sign of η depends on whether the d shell is less or more than half filled) and

$$\left\langle \frac{1}{r^3} \right\rangle = \int d^3\vec{r}\, \frac{|\psi(\vec{r})|^2}{r^3} \qquad (2.12)$$

where $\psi(\vec{r})$ is the spin density of the outer core d electrons. The factor κ comes from the polarization of the core s-electrons due to the d electrons and will lead to the contact hyperfine interaction in ^{57}Fe. The terms proportional to the external field are

$$V_H = \mu_\beta \vec{H}\cdot(\vec{L}+2\vec{S})$$
$$V_h = g_n\mu_n \vec{H}\cdot\vec{I} \qquad (2.13)$$

Putting all these together we get the perturbation term

$$H_1 = (\lambda - \frac{1}{2}\rho)\vec{L}\cdot\vec{S} - \rho(\vec{L}\cdot\vec{S})^2 + \mu_\beta\vec{H}\cdot(\vec{L}+2\vec{S})$$
$$+g_n\mu_n P\left[(\vec{L}\cdot\vec{I}) - \kappa\vec{S}\cdot\vec{I} - \frac{1}{7}(\vec{L}\cdot\vec{S})(\vec{L}\cdot\vec{I}) - \frac{1}{7}(\vec{L}\cdot\vec{I})(\vec{L}\cdot\vec{S}) \right] + g_n\mu_n\vec{H}\cdot\vec{I} \qquad (2.14)$$

where $P = 2\mu_\beta \left\langle \frac{1}{r^3} \right\rangle$.

2.3.1 First Order Perturbation Theory

We want to use (2.14) to perturb our groundstate out of the $^6S_{5/2}$ state. In the first order perturbation we find that the only terms that contribute are ones that don't contain L,

because $< 0|L|0 >= 0$ for an orbital singlet, except for the term $< 0|L_iL_j + L_jL_i|0 >= \frac{2}{3}L(L+1)\delta_{ij} + l_{ij}$ where $l_{ii} = 0$. As well, we have in this case that $\xi = 2/21$ and $\eta = 0$. Thus the terms we get from first order perturbation from ${}^6S_{5/2}$ are

$$H_2 = -g_n\mu_n P(\kappa\delta^{\alpha\beta} + \frac{2}{7}l^{\alpha\beta})S_\alpha I_\beta + 2\mu_\beta \vec{H}\cdot\vec{S} + g_n\mu_n\vec{H}\cdot\vec{I} \tag{2.15}$$

2.3.2 Second Order Perturbation Theory

In the second order we have to calculate all the terms coming from

$$\sum_{n\neq 0}\frac{< 0|H_1|n >< n|H_1|0 >}{E(n) - E(0)} \tag{2.16}$$

where n labels the excited orbital states. Where these excited states lie, ie. the exact values of $E(n)$, are functions of the details of the crystal field splitting and as such we shall not attempt to calculate them exactly. We may obtain order of magnitude estimates for these by comparing to existing materials that contain Fe^{3+} centers. In these cases the energy of the first excited state $E(1)$ is in the range $17000 - 23000\ K$ [82], which is extremely large compared to the scale in which we are interested. Defining the tensors

$$\begin{aligned}
\Lambda^{\alpha\beta} &= \sum_{n\neq 0}\frac{< 0|L^\alpha|n >< n|L^\beta|0 >}{E(n) - E(0)} \\
u^{\alpha\beta} &= -\frac{i\epsilon^{\alpha\gamma\delta}}{2}\sum_{n\neq 0}\frac{< 0|L_\delta|n >< n|L^\beta L_\gamma + L_\gamma L^\beta|0 >}{E(n) - E(0)} \quad , \quad u^{\alpha\alpha} = 0 \\
T^{\alpha\beta\gamma\delta} &= \frac{\rho^2}{4}\sum_{n\neq 0}\frac{< 0|L^\alpha L^\beta + L^\beta L^\alpha|n >< n|L^\gamma L^\delta + L^\delta L^\gamma|0 >}{E(n) - E(0)}
\end{aligned} \tag{2.17}$$

gives, upon collecting terms, an effective Hamiltonian

$$H_S = T^{\alpha\beta\gamma\delta}S_\alpha S_\beta S_\gamma S_\delta + \mu_\beta g^{\alpha\beta}H_\alpha S_\beta + D^{\alpha\beta}S_\alpha S_\beta + g_n\mu_n A^{\alpha\beta}S_\alpha I_\beta + g_n\mu_n R^{\alpha\beta}H_\alpha I_\beta \tag{2.18}$$

where we have defined

$$g^{\alpha\beta} = 2(\delta^{\alpha\beta} - \Lambda^{\alpha\beta}) \quad , \quad D^{\alpha\beta} = -\lambda^2\Lambda^{\alpha\beta} - \rho l^{\alpha\beta}$$
$$A^{\alpha\beta} = -P\left[\kappa\delta^{\alpha\beta} + \frac{2}{7}l^{\alpha\beta} + 2\lambda\Lambda^{\alpha\beta} - \frac{2}{7}\lambda u^{\alpha\beta}\right] \quad , \quad R^{\alpha\beta} = 1 - 2P\mu_\beta\Lambda^{\alpha\beta} \tag{2.19}$$

The meaning of these terms is as follows [87]. $g^{\alpha\beta}$ is the so-called "spectroscopic splitting factor". It is anisotropic in general, containing reference to the higher lying orbital states. $D^{\alpha\beta}$ is a measure of the splitting of the ground state and contains reference to both the spin orbit coupling and the spin-spin contribution in an asymmetrical crystal field. $A^{\alpha\beta}$ represents the hyperfine couplings between the nucleus and the electronic spin. This term is made up of contributions from overlap of s electrons with the nucleus (κ), an orbital contribution $l^{\alpha\beta}$ and a spin-orbit contribution $\lambda\Lambda^{\alpha\beta}$. In the expression for the coupling between the nuclear spin and an external field we see that there is an anisotropic component which can be of the same order of magnitude as the direct contribution.

2.3.3 Higher Orders Perturbation Theory

It is clear that performing third and higher order perturbation theory will produce terms of higher spin multiplicity in the spin Hamiltonian [25]. Terms in the spin Hamiltonian up to $2S^{th}$ order in the spin operators S_x, S_y and S_z are in general possible. In the case of the Fe^{3+} ion this means that all terms up to fifth order must be considered in a general treatment; we can write this general fifth order spin Hamiltonian in the form

$$\begin{aligned} H_{Fe^{3+}} &= G^{\alpha_1\alpha_2\alpha_3\alpha_4\alpha_5}(\vec{H})\ S_{\alpha_1}S_{\alpha_2}S_{\alpha_3}S_{\alpha_4}S_{\alpha_5} + g^{\alpha\beta}\mu_B S_\alpha H_\beta \\ &+ g_n\mu_n\left[A^{\alpha\beta}S_\alpha I_\beta + R^{\alpha\beta}H_\alpha I_\beta\right] \end{aligned} \tag{2.20}$$

where the $S_{\{\alpha_i\}}$ can be any of S_x, S_y, S_z or the identity 1, the prefactor G can be a function of magnetic field, and we have explicitly separated out the Zeeman term. We

only keep to first order in terms containing the nuclear spin $\vec{I}$.

The terms in the single ion spin Hamiltonian must inherit any symmetry that the crystalline electric field possesses, which reduces the total number of possible terms. Unfortunately in our case the Fe^{3+} ions do not sit in positions of high symmetry. However the symmetry is close to being cubic–the nearest neighbours of the Fe^{3+} are distributed in a distorted octahedral fashion. To give a concrete example of how the crystal field symmetry selects specific terms out of the general $2S^{th}$ order spin Hamiltonian, consider the case of an Fe^{3+} ion in a cubic crystal field. This case has been previously treated, with resulting spin Hamiltonian [77]

$$\begin{aligned} H_{Fe^{3+}}^{cubic} &= \frac{a}{6}\left(S_x^4+S_y^4+S_z^4\right)+g^{\alpha\beta}\mu_B S_\alpha I_\beta + g_1(S_x^3H_x+S_y^3H_y+S_z^3H_z) \\ &+ g_2(S_x^5+S_y^5H_y+S_z^5H_z)+g_n\mu_n\left[A^{\alpha\beta}S_\alpha I_\beta + R^{\alpha\beta}H_\alpha I_\beta\right] \\ &+ g_3\left[S_x(S_y^4+S_z^4)H_x+S_y(S_z^4+S_x^4)H_y+S_z(S_x^4+S_y^4)H_y\right] \end{aligned} \tag{2.21}$$

(compare to (2.20). It is found that the constants g_1, g_2 and g_3 are always very small and therefore the terms proportional to these are usually neglected [77]. Typical values for a range from 0.1 mK to 3 mK [88].

A Useful Approximation

Measurements of $g^{\alpha\beta}$ in other insulating materials containing Fe^{3+} support the following approximation [89]. We take the tensor $g^{\alpha\beta}$ to be isotropic and furthermore that $g^{\alpha\beta} = g = 2$, the spin-only value. The justification for doing this comes from the $L = 0$ nature of the groundstate–perturbations of the spin levels coming from crystal field and/or spin-orbit coupling will be very small and therefore a spin-only approximation for $g^{\alpha\beta}$ is justified.

2.4 The Single Molecule Effective Hamiltonian

We now want to consider the Hamiltonian of an entire Fe_8 molecule. We label the spin Hamiltonian (2.20) H_p for the p^{th} iron ion (there are eight of these). Now because each sits in a distinct crystal field, with different principle axes, it is very difficult (although in principle possible) to write down the specific terms for each ion. For example, if we were to make the approximation that the crystal field for each is exactly cubic and kept only the two dominant terms in (2.21), ie.

$$H^{cubic}_{Fe^{3+}} \sim \frac{a}{6}\left(S_x^4 + S_y^4 + S_z^4\right) + g\mu_B \vec{H}\cdot\vec{S} \tag{2.22}$$

then we immediately run into the following technical problem. The axes, as defined by the local crystal fields for each Fe^{3+}, are different. This means that if we fix the axes such that for one of the ions (2.22) is correct, then in writing down all the other single ion spin Hamiltonians we have to rotate the axes through some (albeit known) angles from the "natural" basis picked out by the crystal field. This has the effect of hiding the symmetry explicit in (2.22), and bringing us back to a general type of description like (2.20).

We shall therefore at this stage write the collection of eight iron single ion spin Hamiltonians as

$$\begin{aligned} H &= \sum_{p=1}^{8} H^p_{Fe^{3+}} = \sum_{p=1}^{8}\Big[G_p^{\alpha_1\alpha_1\alpha_1\alpha_1\alpha_1}(\vec{H})\ S^p_{\alpha_1}S^p_{\alpha_2}S^p_{\alpha_3}S^p_{\alpha_4}S^p_{\alpha_5} + g\mu_B\vec{S}_p\cdot\vec{H} + g_{n_p}\mu_n\Big[A^{p\alpha\beta}S^p_\alpha I^p_\beta \\ &+ R^{p\alpha\beta}H_\alpha I^p_\beta\Big]\Big] \end{aligned} \tag{2.23}$$

where for all quantities the label p points to the p^{th} iron ion.

2.4.1 Inclusion of Exchange and Superexchange Terms

It is known that there exist exchange and superexchange couplings between the iron ions. In general these couplings can be anisotropic, leading to a general expression of the form

$$H_{ex} = \sum_{p<q} J_{pq}^{\alpha\beta} S_{\alpha}^{p} S_{\beta}^{q} \tag{2.24}$$

where the sums over p, q are over the ions 1..8 and the labels α, β refer to spatial directions x, y, z. Exact diagonalization studies on this term have been performed, with results compared to EPR and susceptibility measurements performed on Fe_8 [18]. The model used in these calculations assumes that the couplings are isotropic, although it is not clear that this has to be the case (Dzyaloskinski-Morya interactions, for example, are excluded in the isotropic case [90]). The pathways, as well as the magnitude of the coupling strengths extracted from fits to experiment, are shown in figure 2.1. Note that the coupling energies extracted are far larger than the single-ion anisotropy terms–as we have seen, the terms in the single ion spin Hamiltonian are typically on the order of mK, while the energies extracted by Delfs et.al. [18] are in the tens to hundreds of Kelvin.

2.4.2 "Offsite" Dipolar and Quadrupolar Contributions

The electronic state of each Fe^{3+} ion will couple via dipole-dipole interactions with all the other dipoles present in the molecule. This includes the other Fe^{3+} electronic spins and all the nuclear spins in the molecule. As well, all nuclei in the system with spins $I > 1/2$ will have an electric quadrupole moment which couples to inhomogeneous electric fields in the molecule. It will turn out that these contributions will be quite important in the chapters that follow. As such we shall go over the derivation of these terms carefully.

The general interaction between the electronic and nuclear degrees of freedom may be split into two parts [64]. The first of these, the electrostatic interaction between nuclear and electronic charges, will be considered first. The second part, the magnetic coupling

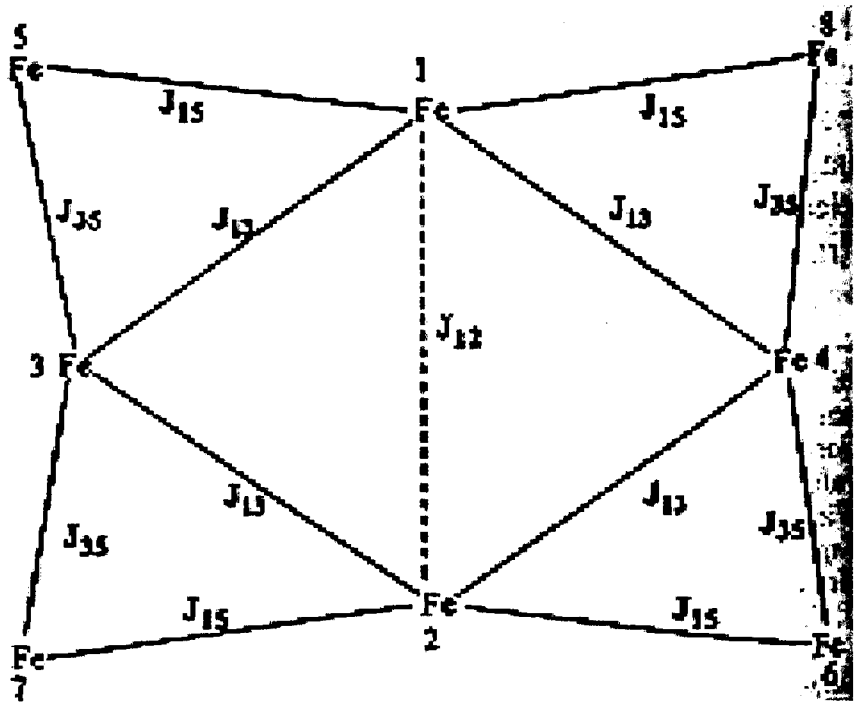

Figure 2.1: Exchange pathways in Fe_8 in the isotropic model of Delfs et.al. [18]. Fits to susceptibility data give $J_{12} \sim 35K$, $J_{13} \sim 180K$, $J_{15} \sim 22K$ and $J_{35} \sim 52K$, with all couplings antiferromagnetic.

between the moments of the nuclei and the magnetic fields generated by the spin and orbital currents of the electrons, will be dealt with later.

The standard derivation [64] of the form of the electrostatic couplings begins by describing the nuclei and electronic clouds as classical charge distributions $\rho_n(r_n)$ and $\rho_e(r_e)$ with mutual electrostatic energy

$$E = \int\int \frac{\rho_e(r_e)\rho_n(r_n)dr_e dr_n}{|\vec{r}_n - \vec{r}_e|} \tag{2.25}$$

This expression may be simplified by expanding the Coulomb potential in terms of spherical harmonics. After some algebra one can show that this energy is the expectation value

of the Hamiltonian

$$H_{elec} = \sum_{l,m} A_l^m B_l^{m*} \tag{2.26}$$

where

$$A_l^m = e\sqrt{\frac{4\pi}{2l+1}} \sum_{i=1}^{N_n} R_i^l Y_l^m(\Theta_i, \Phi_i) \tag{2.27}$$

$$B_l^m = -e\sqrt{\frac{4\pi}{2l+1}} \sum_{i=1}^{N_e} r_i^{-(l+1)} Y_l^m(\theta_i, \phi_i) \tag{2.28}$$

Here N_n and N_e are the number of protons per nucleus and electrons respectively, $\{R_i, \Theta_i, \Phi_i\}$ and $\{r_i, \theta_i, \phi_i\}$ are the polar coordinates of the i^{th} proton and i^{th} electron respectively and Y_l^m are the standard spherical harmonics.

The general expression (2.26) may be further simplified by the following observations. It is well-known that stationary nuclear states have well-defined parities, implying that the expectation values of terms A_l^m odd in l are zero. That this is in fact true has been confirmed experimentally to a high degree of precision with the $l = 1$ (electric dipole) term [64]. This leaves us with a sum over even l, which can be manipulated further. The $l = 0$ (monopole) term can be seen to be constant, and can therefore be omitted from consideration. As well, it is seen experimentally that the strength of the terms in the series decrease rapidly with increasing l. In fact, direct contributions from the $l = 4$ term are so weak that they have never been seen in NMR studies in solids. We may therefore omit all terms with $l > 2$, leaving only the electric quadrupolar term

$$H_Q = \sum_{m=-2}^{2} A_2^m B_2^{m*} \tag{2.29}$$

The tensors appearing in (2.29) can be recast in a more useful form. One can show [64, 91] that the Hamiltonian (2.29) produces the same matrix elements in the nuclear

spin subspace as the form

$$H_Q = \sum_{k=1}^{N} \frac{eQ_k}{6I_k(2I_k - 1)} V^{k\alpha\beta} I^k_{\alpha\beta} \tag{2.30}$$

where N is the total number of nuclei,

$$V^{k\alpha\beta} = \frac{\partial^2 V^k}{\partial x^\alpha \partial x^\beta} \tag{2.31}$$

where V^k is the potential at the k^{th} nucleus due to the charge distribution in the molecule,

$$I^k_{\alpha\beta} = \frac{3}{2}(I^k_\alpha I^k_\beta + I^k_\beta I^k_\alpha) - \vec{I}_k^{\,2}\delta_{\alpha\beta} \tag{2.32}$$

and Q_k is the electric quadrupole moment of the k^{th} nucleus, which is a measure of the nonspherical distribution of charge inside the nucleus. Q_k is zero for all nuclear spins with $I_k = 1/2$ and is typically on the order of $1 - 10 \cdot 10^{-24}\ cm^2$. In Fe_8, the nuclei that have non-zero electric quadrupole moments are the two species of bromine ^{79}Br and ^{81}Br, ^{14}N and ^{16}O.

The description (2.30) accounts for all electrostatic effects between electronic and nuclear charge distributions in the molecule. We now turn to the second part of the electron-nucleus interaction, the magnetic couplings. We have already used the fact that stationary nuclear states have a fixed parity to eliminate certain terms in the multipole expansion of the electrostatic coupling. We may perform a similar trick here by noting that the magnetic field feels the opposite parity effect of the electric field (since they are axial and polar vectors respectively). This means that all even orders of the multipole expansion of the magnetic structure of the nucleus have to be zero. Similarly to the electrostatic case, the strength of the contributions of higher order terms in the expansion fall off extremely rapidly with increasing l; as previously, no evidence of $l = 3$ (magnetic octopolar) terms has ever been directly seen by NMR in bulk matter.

This makes our job considerably easier from the start, as we can treat the general nucleus as a magnetic dipole without loss of generality, and the interaction of the magnetic

field generated by the electrons and any magnetic dipole can easily be dealt with. One finds an interaction Hamiltonian of the form [64]

$$H_{mag} = \frac{\mu_0 g \mu_\beta}{4\pi} \sum_{l=1}^{8} \sum_{k=1}^{N+8} \frac{g_{n_k} \mu_n}{r_{lk}^3} \left[\vec{S}_l \cdot \vec{I}_k - 3(\vec{S}_l \cdot \hat{r}_{lk})(\vec{I}_k \cdot \hat{r}_{lk}) \right] \tag{2.33}$$

where we have used our isotropic g approximation, the sum over electronic spins is over the eight Fe^{3+} sites and the sum over nuclear sites is over all possible nuclear sites (N is the number of spins in the ligand bath; accounting for the possibility of up to eight ^{57}Fe nuclei gives $k = 1..N+8$). We do not include the "self-coupling" term here where the electronic spin interacts with a ^{57}Fe nucleus on the same site, as this term is included in the single ion spin Hamiltonian derived earlier (it is a "contact" term). g_{n_k} and μ_n are the nuclear g-factor of the k^{th} nucleus and nuclear magneton respectively. It is possible to rewrite this term by defining a matrix

$$M_{lk}(\vec{r}_{lk}) = \frac{\mu_0 g \mu_B}{4\pi} \frac{1}{r_{lk}^3} \begin{bmatrix} 1 - 3\hat{r}_{lkx}^2 & -3\hat{r}_{lkx}\hat{r}_{lky} & -3\hat{r}_{lkx}\hat{r}_{lkz} \\ -3\hat{r}_{lkx}\hat{r}_{lky} & 1 - 3\hat{r}_{lky}^2 & -3\hat{r}_{lky}\hat{r}_{lkz} \\ -3\hat{r}_{lkx}\hat{r}_{lkz} & -3\hat{r}_{lky}\hat{r}_{lkz} & 1 - 3\hat{r}_{lkz}^2 \end{bmatrix} \tag{2.34}$$

This allows us to write (2.33) in the simple form

$$H_{mag} = \sum_{l=1}^{8} \sum_{k=1}^{N+8} g_{n_k} \mu_n M_{lk}^{\alpha\beta} S_\alpha^l I_\beta^k \tag{2.35}$$

where α and β are again spatial labels x, y or z. Note that one may calculate exactly the values of these terms, as they depend only on the relative locations of the nuclei and the iron ions which are known from crystallographic data (this will turn out to be quite important in later chapters, particularly chapters 3 and 5).

Together with the term derived earlier (2.30) we have a complete description of the "offsite" (ie. not including on-site contact hyperfine interactions) electromagnetic interaction of all the nuclei with all the electronic spins in the Fe_8 molecule. We may write

the final description of this nuclear-electronic coupling in the form

$$H = \sum_{k=1}^{N+8} \left[\frac{eQ_k}{6I_k(2I_k-1)} V^{k\alpha\beta} I^k_{\alpha\beta} + \sum_{l=1}^{8} g_{n_k} \mu_n M^{\alpha\beta}_{lk} S^l_\alpha I^k_\beta \right] \tag{2.36}$$

2.4.3 Intra-Nuclear Spin Couplings

A similar analysis may be performed on the electromagnetic couplings between the nuclei themselves. As was indicated in the previous section, by far the dominant contribution to this effect comes from dipole-dipole interactions of the form

$$H_{nn} = \frac{\mu_0 \mu_n^2}{4\pi} \sum_{l<k} \frac{g_{n_l} g_{n_k}}{r^3_{lk}} \left[\vec{I}_l \cdot \vec{I}_k - 3(\vec{I}_l \cdot \hat{r}_{lk})(\vec{I}_k \cdot \hat{r}_{lk}) \right] \tag{2.37}$$

where g_{n_l} and g_{n_k} are the nuclear g-factors for the l and k species of nuclei.

2.4.4 Couplings of the Nuclear Bath to External Magnetic Fields

We shall assume that the nuclei in the ligand bath couple to an applied external magnetic field in the standard Zeeman way; that is,

$$H_{ext} = \sum_k g_{n_k} \mu_n \vec{I}_k \cdot \vec{H}_{ext} \tag{2.38}$$

2.4.5 Coupling to Phonons

Both the super-exchange/exchange and nuclear spin couplings are local in the sense that their ranges do not extend outside of a given molecule; it is enough to treat their effects on a "per molecule" basis. In this section we shall, following the treatment given in [92], introduce couplings of a single molecule with phonon fields which at low energies have long wavelengths and as such owe their properties to the details of the crystal lattice.

The presence of phonons in the crystal can be dealt with by introducing strain and rotation fields which are written respectively as [92]

$$\epsilon_{\alpha\gamma} = \frac{1}{2}\left(\partial_\alpha u_\gamma + \partial_\gamma u_\alpha\right) \quad , \qquad \omega_{\alpha\gamma} = \frac{1}{2}\left(\partial_\alpha u_\gamma - \partial_\gamma u_\alpha\right)$$

where

$$u_\alpha(\vec{r}) = \sum_{k\lambda} \left[\frac{\hbar}{2NM\omega_{k\lambda}}\right]^{1/2} e_\alpha^{(\lambda)} \left[a_{k\lambda}^\dagger + a_{k\lambda}\right]$$

are the displacements at $\vec{r}$ caused by a phonon field whose creation/annihilation operators are given by $\{a_{k\lambda}^\dagger, a_{k\lambda}\}$ and $e_\alpha^{(\lambda)}$ is the magnitude of the polarization vector. λ labels the branch and includes in general both optical and acoustic phonons. M is the mass of the unit cell and N is the total number of unit cells.

These local strains and rotations cause there to be introduced into the Hamiltonian terms mediated by the phonons. For example, imagine the effect of a local rotation of a particular spin on the $D_{ij}S_iS_j$ term in (2.20), and in particular on the $D_{zz}S_zS_z$ component;

$$S_z \rightarrow S_z + \omega_{zx}S_x + \omega_{zy}S_y \tag{2.39}$$

and

$$D_{zz}S_z^2 \rightarrow D_{zz}\left(S_z^2 + \omega_{zx}^2 + \omega_{zy}^2\omega_{zx}\{S_z, S_x\} + \omega_{zy}\{S_z, S_y\}\right) \tag{2.40}$$

In general one can show [92] that the spin orbit interaction leads to an effective coupling between the ionic spins and the phonon fields of the form

$$H_{sp} = i\sum_{\vec{q}\lambda}\sum_{l=1}^{8}\left[\frac{\hbar}{2NM\omega_{q\lambda}}\right]^{1/2} q\left[a_{\vec{q}\lambda}^\dagger V_{\vec{q}\lambda}(\vec{S}_l) - a_{\vec{q}\lambda}V_{\vec{q}\lambda}^\dagger(\vec{S}_l)\right] \tag{2.41}$$

where

$$V_{\vec{q}\lambda}(\vec{S}_l) = B_{\alpha\beta}^{(l)}S_l^\alpha S_l^\beta + \left(\vec{\xi}_{\vec{q}\lambda} \times \hat{q}\right) \cdot \vec{S}_l \tag{2.42}$$

Here $\vec{\xi}_{\vec{q}\lambda}$ is the polarization vector of the phonon involved. The terms $B_{\alpha\beta}^{(l)}$ can in principle be calculated from knowledge of the crystal symmetry and have been estimated to be $\sim 0.01\ mK$ for the Mn_{12} material [93]. One must keep in mind that in order to do

this one must use the symmetries appropriate for the individual ions and not the full symmetry of the crystal. The term linear in $\vec{S}$ arises from treating the spin as being locked to the lattice due to spin-orbit effects. This term is likely to be much smaller than the $B_{\alpha\beta}$ terms (see [92] for a discussion of this point).

2.4.6 Coupling to Photons

The coupling to the photon field is taken to be of magnetic dipolar origin [94]. The magnetic field due to the photon field can be written

$$\vec{B}_\gamma = \vec{\nabla} \times \vec{A} = \sum_{\lambda \vec{k}} \left[\frac{2\pi\hbar c^2}{V\tilde{\omega}_{k\lambda}} \right]^{1/2} e^{i\vec{k}\cdot\vec{r}} \left(c_{k\lambda} + c^\dagger_{-k\lambda} \right) \left(\vec{\nabla} \times \vec{\xi}_{\vec{k}\lambda} \right) \tag{2.43}$$

where V is the volume of the sample, $\{c^\dagger_{k\lambda}, c_{k\lambda}\}$ are the creation/annihilation operators for the photon field and $\vec{\xi}_{\vec{k}\lambda}$ is the polarization vector for the $\{\vec{k}, \lambda\}$ mode. The coupling to the electronic spins is then straightforward and is given by

$$H_{s\gamma} = \sum_{l=1}^{8} g\mu_B \vec{B}_\gamma \cdot \vec{S}_l \tag{2.44}$$

2.4.7 Bringing all the Terms Together–The Bare Fe_8 Hamiltonian

The description of the systems under scrutiny given in the previous section contains seven terms, namely (2.23), (2.24), (2.36), (2.37), (2.38), (2.41) and (2.44). Explicitly we have, for our effective Hamiltonian, an expression of the form

$$\begin{aligned} H &= \sum_{p=1}^{8} \left[G_p^{\alpha_1\alpha_2\alpha_3\alpha_4\alpha_5}(\vec{H}) \; S^p_{\alpha_1} S^p_{\alpha_2} S^p_{\alpha_3} S^p_{\alpha_4} S^p_{\alpha_5} + g\mu_B \vec{S}_p \cdot \vec{H} \right. \\ &+ \left. g_{n_p}\mu_n \left[A^{p\alpha\beta} S^p_\alpha I^p_\beta + R^{p\alpha\beta} H_\alpha I^p_\beta \right] \right] + \sum_{p<q=1}^{8} J^{\alpha\beta}_{pq} S^p_\alpha S^q_\beta \\ &+ \sum_{k=1}^{N+8} \left[\sum_{l=1}^{8} g_{n_k}\mu_n M^{\alpha\beta}_{lk} S^l_\alpha I^k_\beta + \frac{eQ_k}{6I_k(2I_k-1)} V^{k\alpha\beta} I^k_{\alpha\beta} \right] \end{aligned}$$

$$+ \quad \frac{\mu_0 \mu_n^2}{4\pi} \sum_{l<k=1}^{N} \frac{g_{n_l} g_{n_k}}{r_{lk}^3} \left[\vec{I}_l \cdot \vec{I}_k - 3(\vec{I}_l \cdot \hat{r}_{lk})(\vec{I}_k \cdot \hat{r}_{lk}) \right] + \sum_{k=1}^{N} g_{n_k} \mu_n \vec{I}_k \cdot \vec{H}_{ext}$$

$$+ \quad i \sum_{\vec{q}\lambda} \sum_{l=1}^{8} \left[\frac{\hbar}{2NM\omega_{q\lambda}} \right]^{1/2} q \left[a_{\vec{q}\lambda}^{\dagger} V_{\vec{q}\lambda}(\vec{S}_l) - a_{\vec{q}\lambda} V_{\vec{q}\lambda}^{\dagger}(\vec{S}_l) \right] + \sum_{l=1}^{8} g \mu_B \vec{B}_\gamma \cdot \vec{S}_l \quad (2.45)$$

Let us review what we know about each term in this expression. The first term is a sum over all the single ion Fe^{3+} spin Hamiltonians. In order to evaluate the coupling energies $G_p^{\alpha_1\alpha_2\alpha_3\alpha_4\alpha_5}$ we could do the following. First, we identify the symmetry of the crystalline field surrounding each iron ion. This reduces the number of non-zero couplings (as we saw in the exactly cubic case in (2.22)). We then pick a set of axes, aligned so as to simplify the spin Hamiltonian of one of the ions. Next we determine the angles necessary to rotate each iron ion from the axes chosen by its local crystal field to our chosen basis and apply these rotations. This procedure allows us to approximately evaluate the $G_p^{\alpha_1\alpha_2\alpha_3\alpha_4\alpha_5}$ for Fe_8. We do not know for certain what the magnitudes of these couplings are, although as mentioned earlier for Fe^{3+} in a cubic field they are typically in the mK range [77]. We shall not explicitly perform this task for a reason that will soon be made clear. This term also contains couplings between the electronic spin and external field, which we have approximated as being isotropic ($g^{\alpha\beta} \sim g = 2$), the "contact" interaction between the nuclear and electronic spin and the interaction between the external field and the nuclear spin. These two last will not in general be isotropic.

The second term is the exchange/superexchange term coupling the electronic wavefunctions of the iron ions. Extracting quantitative predictions about how large the $J_{pq}^{\alpha\beta}$ are is a difficult task and has yet to be performed satisfactorily [18]. It is not known whether the anisotropicity here is important. As we mentioned earlier, preliminary investigations indicate that these couplings are in the tens to hundreds of Kelvin [18].

The third, fourth and fifth terms are the non-local coupling between nuclear spins and Fe^{3+} electronic spins, nuclear-nuclear dipole interactions and nuclear spin-external

field coupling respectively. All of the quantities in these term are either known or can be calculated (we do this explicitly for all the nuclei in the molecule in chapter 3). The coupling energies here are found to be bounded above by $\sim 5\ mK$.

The sixth term is the phonon-electronic spin coupling. Here the only term that we do not know is the value of the $B_{\alpha\beta}$ terms in (1.21), although these have been estimated to be on the order of 0.01 mK in Mn_{12} [93]. The seventh and final term is the dipolar magneto-optical coupling. Here the photon field in the material will be changed to a renormalized (by optical phonons) "polariton" field and therefore the frequencies $\tilde{\omega}_{k\lambda}$ are not known exactly, although methods to approximate these are available [95].

2.5 Exchange/Superexchange and the Giant Spin Picture

As was discussed in the introductory chapter, the low-energy phenomenology of the Fe_8 system indicates that somehow the electronic spins "lock together" into some fixed-spin object. Because the exchange/superexchange coupling energies are much larger than all the other energy scales in our Hamiltonian (2.45), we are presented with a mechanism whereby we can understand how this can happen. In a numerical diagonalization study performed in [18], it was suggested that the groundstate of the Hamiltonian (2.24) is given by a state where six of the Fe^{3+} align parallel to each other while the other two align themselves anti-parallel, giving a "quantum rotator" with excess spin of $S = 6 \cdot 5/2 - 2 \cdot 5/2 = 10$. Because the $J_{kl}^{\alpha\beta}$ are large, there exists a sizeable gap to excitations out of this ground state, whose magnitude these authors suggest is on the order of $\Delta E \sim 30K$.

This locking together of the electronic spins profoundly affects the ultimate form of the low-energy effective description. To begin with, as excitations from the ground state are energetically inaccessible as long as $k_B T \ll \Delta E$ (we will ultimately be interested in

the mK range so this is reasonable), we may consider the term in our effective description (2.24) to be simply a constant which we henceforth remove from consideration. Note that this does not mean that the dynamics of the electronic spins are frozen–it is simply that the effective degree of freedom that they represent is, for $k_BT \ll \Delta E$, a single collective "quantum rotator" or "giant spin" which is still very much a dynamical quantity.

Now it is quite a difficult matter to actually *derive* an effective description in terms of this new collective degree of freedom from the Hamiltonian (2.45). In order to do this one would have to first determine the ground state of the electronic spins and then perform perturbations out of this ground state in a similar way done for the single ion case. Instead what we shall do is, following [74], make the following hypothesis.

We simply assume that the exchange/superexchange couplings lock the electronic spins together into a quantum rotator or "giant spin" $\vec{S}$ with $S = 10$, where six (two) of the electronic spins point parallel (antiparallel) to the direction of $\vec{S}$, as indicated by [18]. This we refer to as the *giant spin hypothesis.* We then, as a corollary to this hypothesis, rewrite (2.45) in the form

$$\begin{aligned} H &= \tilde{G}^{\alpha_{i_1}\ldots\alpha_{i_{20}}}\ S_{\alpha_{i_1}}S_{\alpha_{i_2}}\ldots S_{\alpha_{i_{20}}} + g\mu_B\vec{H}\cdot\sum_{p=1}^{8}\vec{S}_p + \sum_{p=1}^{8} g_{n_p}\mu_n\left[A^{p\alpha\beta}S^p_\alpha I^p_\beta + R^{p\alpha\beta}H_\alpha I^p_\beta\right] \\ &+ \sum_{k=1}^{N+8}\left[\sum_{l=1}^{8} g_{n_k}\mu_n M^{\alpha\beta}_{lk}S^l_\alpha I^k_\beta + \frac{eQ_k}{6I_k(2I_k-1)}V^{k\alpha\beta}I^k_{\alpha\beta}\right] \\ &+ \frac{\mu_0\mu_n^2}{4\pi}\sum_{l<k=1}^{N}\frac{g_{n_l}g_{n_k}}{r^3_{lk}}\left[\vec{I}_l\cdot\vec{I}_k - 3(\vec{I}_l\cdot\hat{r}_{lk})(\vec{I}_k\cdot\hat{r}_{lk})\right] + \sum_{k=1}^{N} g_{n_k}\mu_n\vec{I}_k\cdot\vec{H}_{ext} \\ &+ i\sum_{\vec{q}\lambda}\sum_{l=1}^{8}\left[\frac{\hbar}{2NM\omega_{q\lambda}}\right]^{1/2} q\left[a^\dagger_{\vec{q}\lambda}V_{\vec{q}\lambda}(\vec{S}_l) - a_{\vec{q}\lambda}V^\dagger_{\vec{q}\lambda}(\vec{S}_l)\right] + \sum_{l=1}^{8} g\mu_B\vec{B}_\gamma\cdot\vec{S}_l \end{aligned} \tag{2.46}$$

where $S_{\alpha_{i_j}} = S_x$, S_y, S_z or the identity. What we have done here is replace the sum over single-ion spin Hamiltonians and the exchange/superexchange terms with a giant spin Hamiltonian $H_{GS} = \tilde{G}^{\alpha i_1\ldots\alpha_{i_{20}}}S_{\alpha_{i_1}}S_{\alpha_{i_2}}\ldots S_{\alpha_{i_{20}}}$. As we discussed in the single ion case, the spin Hamiltonian can contain in general terms up to $2S^{th}$ order in spin operators, which

in this case is 20^{th} order. We can however reduce the total number of terms significantly in the case of Fe_8, because the giant spin Hamiltonian must contain the symmetry of the full crystalline lattice, which in the case of Fe_8 is triclinic [23]. Note however that we are not going to derive any of these terms. As we saw in the introductory chapter much effort has been expended in trying to *measure* what the relevant couplings $\tilde{G}^{\alpha_{i_1}\cdots\alpha_{i_{20}}}$ are. Unfortunately because there are so many of these, even after the crystal symmetry has been taken into account, most have been ignored as their magnitudes decrease quickly with increasing order in S_i. This is however quite dangerous as these small ignored terms can contribute greatly to the physics, in particular to the magnitude of tunneling amplitudes between different $|m_S>$ states of the giant spin (twenty one of which, ranging for $S = 10$ from $|-10>$ to $|+10>$) [25].

The remaining terms are identical to their forms in (2.45). The only difference is that now we must remember that each individual electronic spin is locked to the giant spin.

2.6 Investigation of the Giant Spin Hamiltonian in the Absence of Environmental Couplings

If we completely neglect all environments in (2.46) and fix $\vec{S} = \sum_{l=1}^{8} \vec{S}_l$ we obtain

$$H = \tilde{G}^{\alpha_{i_1}\cdots\alpha_{i_{20}}} \; S_{\alpha_{i_1}} S_{\alpha_{i_2}} ... S_{\alpha_{i_{20}}} + g\mu_B \vec{H} \cdot \vec{S} \tag{2.47}$$

We are going to digress somewhat at this point from our focus on Fe_8. We will in what follows consider all possible crystal symmetries and not just the Fe_8 triclinic symmetry. This we do because there are other similar molecular magnets (Mn_{12}, for example) that may have giant spin descriptions of this sort that possess different crystal symmetries (for Mn_{12} this is tetragonal [28]) and for this reason it is worthwhile to say some general things about the description (2.47).

Now as we discussed earlier, the spin Hamiltonian can contain terms up to $2S^{th}$ order in the spin variables. It is however difficult to keep all of these terms in our description for large S, and furthermore it is not clear that all of these terms can be directly measured anyway. What is usually done is that only the lowest order terms in S consistent with the crystal symmetry are kept, and all higher order terms are thrown away. In what follows we shall follow this tack. We emphasize however that even if the higher order terms are "small" they can still significantly affect the physics, in particular the amplitudes of the tunneling matrix elements between states of the giant spin.

2.6.1 Exact Solution for Tunneling Matrix Elements via Diagonalization

We shall begin our study of (2.47) by exactly diagonalizing some particular subsets of it and thereby extracting tunneling matrix elements as functions of $\{\tilde{G}\}$, $|\vec{S}|$ and $\vec{H}$. Our plan of attack is as follows. We begin in each case by choosing one of the seven crystal symmetries so as to determine the allowed form of $\{\tilde{G}\}$. In the specific cases of the tetragonal, orthorhombic and hexagonal systems we then diagonalize a truncated version of the resultant Hamiltonian for a range of externally applied DC fields, for central spin values $|\vec{S}| = 1$, 10 and 15. In each of these cases we assume the existence of an easy axis which we identify with the z axis. We calculate the tunnelling splittings between the two lowest lying states ($|+S>$ and $|-S>$), corresponding to the giant spin pointing in the $\pm\hat{z}$ directions, which we then plot as functions of the parameters in the bare Hamiltonian.

The Cubic System

A crystal with underlying cubic symmetry possesses a spin Hamiltonian obeying the symmetries

$$[S_x \to S_y \quad S_y \to -S_x] \quad , \quad [S_x \to S_z \quad S_z \to -S_x] \quad , \quad [S_y \to S_z \quad S_z \to -S_y]$$

This restricts the allowed terms in the spin Hamiltonian. If we only include the two lowest order terms obeying these symmetries the giant spin Hamiltonian can be written [96]

$$H = -D\left(S_x^4 + S_y^4 + S_z^4\right) + E\left(S_x^6 + S_y^6 + S_z^6 + 30S_x^2S_y^2S_z^2\right) + g\mu_B\vec{S}\cdot\vec{H} \qquad (2.48)$$

The case of cubic crystal symmetry is somewhat anomalous in that it is the only case we shall encounter where an axis (easy or hard) is not singled out by the crystal field–as we see from the symmetry requirements, all three axes in the crystal are equivalent. We shall not say more about this crystal symmetry. However, it is worth noting that the physics of cubic molecular magnets should be particularly entertaining because of the lack of an easy/hard axis.

The Tetragonal System

In systems with tetragonal symmetry, the symmetries

$$[S_x \to S_y \quad S_y \to -S_x] \quad ,[S_z \to -S_z] \qquad (2.49)$$

must be preserved (see figure 2.2). Keeping only the lowest order terms gives a spin Hamiltonian of the form

$$H = -DS_z^2 + \alpha_4\left(S_+^4 + S_-^4\right) + g\mu_B\vec{S}\cdot\vec{H} \qquad (2.50)$$

Shown in figures 2.3 and 2.4 are results of exact diagonalization of (2.50) for a variety of parameter regimes. Note that in zero external field, if $|\vec{S}|$ is odd the tunneling splitting between the two lowest levels here is zero. This is known as Kramer's degeneracy [47, 97], and it arises here because there exists no path by which our Hamiltonian can connect the states $|S>$ and $|-S>$ if S is odd.

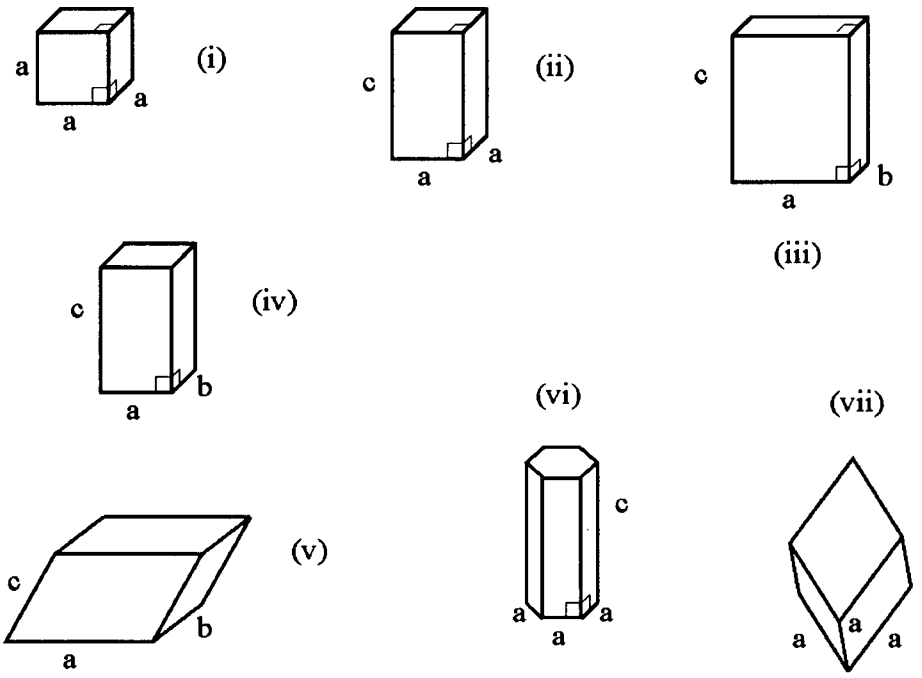

Figure 2.2: All of the unit cells (after Ashcroft and Mermin [138]). (i) Cubic, (ii) Tetragonal, (iii) Orthorhombic, (iv) Monoclinic, (v) Triclinic, (vi) Hexagonal and (vii) Trigonal.

The Orthorhombic System

In systems with orthorhombic symmetry, the symmetries

$$[S_x \to -S_x \quad S_y \to -S_y \quad S_z \to -S_z] \tag{2.51}$$

must be preserved (figure 2.2). Keeping only the lowest order terms leads to the Hamiltonian

$$H = -DS_z^2 + \alpha_2 \left(S_+^2 + S_-^2\right) + g\mu_B \vec{S} \cdot \vec{H} \tag{2.52}$$

Shown in figures 2.5 and 2.6 are results of exact diagonalization of (2.52) for a variety of parameter regimes.

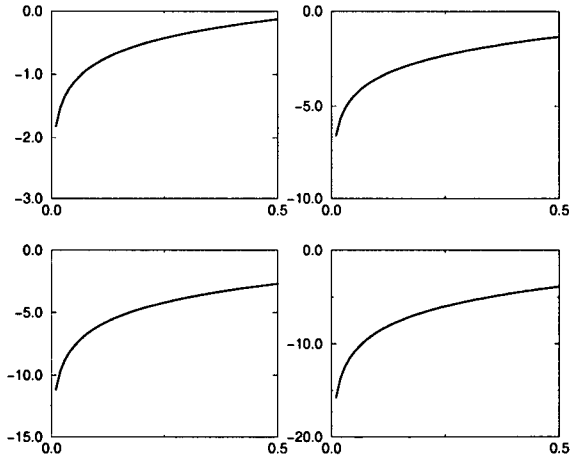

Figure 2.3: Variation of $\Delta_{S,-S}$ with α_4/D for four different $|\vec{S}|$ values (clockwise from top left, $|\vec{S}|$ =2, 6, 10, and 14); tetragonal symmetry. On the x axis is plotted $\alpha_4 S^2/D$ and on the y axis $\log_{10} \Delta_{S,-S}$. Here we have taken the external field to be zero.

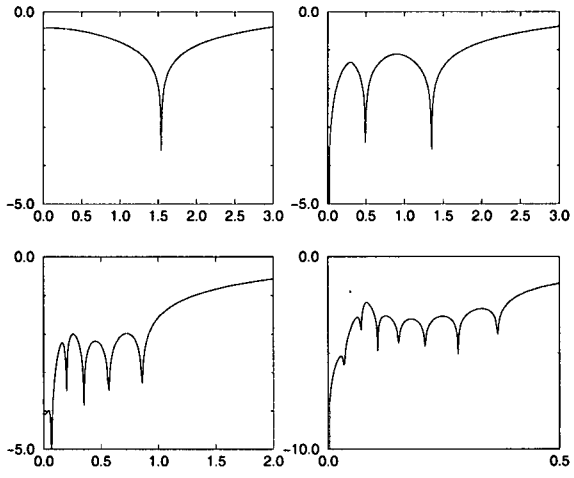

Figure 2.4: Variation of $\Delta_{S,-S}$ with H_x/D for $\alpha_4 S^2/D = 0.25$ for four different $|\vec{S}|$ values (clockwise from top left, $|\vec{S}|$ =2, 5, 10, and 15); tetragonal symmetry. On the x axis is plotted H_x/DS^2 and on the y axis $\log_{10} \Delta_{S,-S}$.

The Monoclinic System

Systems with monoclinic symmetry contain as a special case the orthorhombic symmetry. Because of this the spin Hamiltonian for these systems must contain the orthorhombic symmetries. In addition we shall have quartic terms, giving

$$H = -DS_z^2 + \alpha_2\left(S_+^2 + S_-^2\right) + \alpha_4^{(+)}S_+^4 + \alpha_4^{(-)}S_-^4 + g\mu_B\vec{S}\cdot\vec{H} \tag{2.53}$$

The Triclinic System

Triclinic symmetry is obtained via a distortion of monoclinic symmetry. As such the description of the triclinic case must contain the symmetry of the monoclinic case. In addition, we pick up a diagonal quartic spin term;

$$H = -DS_z^2 - D_0S_z^4 + \alpha_2\left(S_+^2 + S_-^2\right) + \alpha_4^{(+)}S_+^4 + \alpha_4^{(-)}S_-^4 + g\mu_B\vec{S}\cdot\vec{H} \tag{2.54}$$

The Trigonal System

In systems with trigonal symmetry, rotations around the body diagonal are three-fold symmetric.

$$H = -DS_z^2 + \alpha_3\left\{S_z, S_+^3 + S_-^3\right\} + g\mu_B\vec{S}\cdot\vec{H} \tag{2.55}$$

The Hexagonal System

In systems with hexagonal symmetry, the symmetries

$$\left[S_x \to e^{i\pi/3}S_x\right] \quad , \quad \left[S_y \to e^{i\pi/3}S_y\right] \quad , \quad \left[S_z \to -S_z\right] \tag{2.56}$$

must be preserved. This implies, keeping only the lowest order spin terms, a Hamiltonian

$$H = -DS_z^2 + \alpha_6\left(S_x^6 + S_y^6\right) + g\mu_B\vec{S}\cdot\vec{H} \tag{2.57}$$

Shown in figures 2.7 and 2.8 are results of exact diagonalization of (2.57) for a variety of parameter regimes.

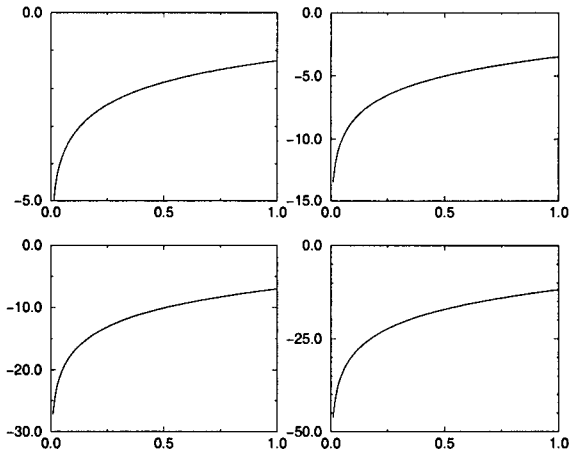

Figure 2.5: Variation of $\Delta_{S,-S}$ with α_2/D for four different $|\vec{S}|$ values (clockwise from top left, $|\vec{S}|$ =2, 5, 10, and 15); orthorhombic symmetry. On the x axis is plotted α_2/D and on the y axis $\log_{10} \Delta_{S,-S}$. Here we have taken the external field to be zero.

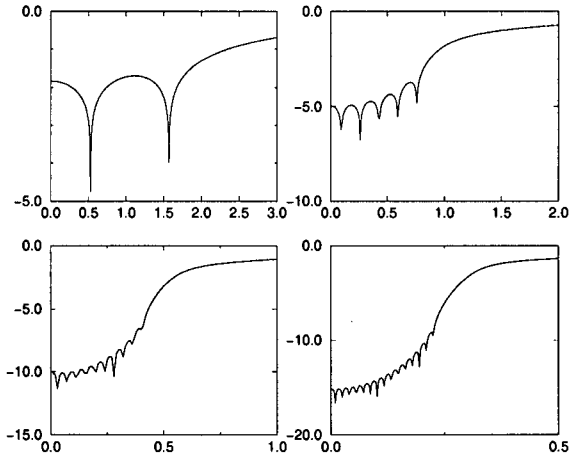

Figure 2.6: Variation of $\Delta_{S,-S}$ with H_x/D for $\alpha_2/D = 0.25$ for four different $|\vec{S}|$ values (clockwise from top left, $|\vec{S}|$ =2, 5, 10, and 15); orthorhombic symmetry. On the x axis is plotted H_x/DS^2 and on the y axis $\log_{10} \Delta_{S,-S}$.

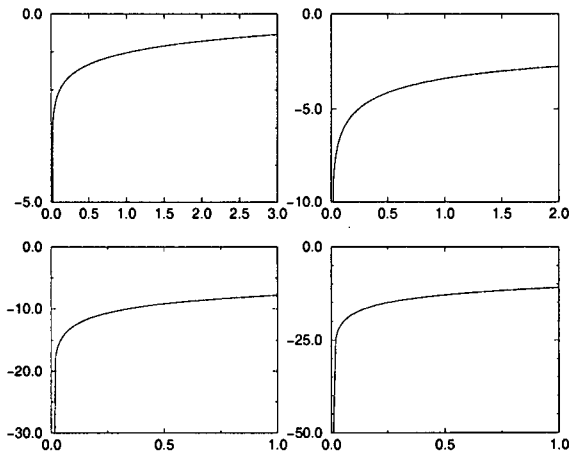

Figure 2.7: Variation of $\Delta_{S,-S}$ with α_6/D for four different $|\vec{S}|$ values (clockwise from top left, $|\vec{S}|$ =2, 6, 10, and 14); hexagonal symmetry. On the x axis is plotted $\alpha_6 S^4/D$ and on the y axis $\log_{10} \Delta_{S,-S}$. Here we have taken the external field to be zero.

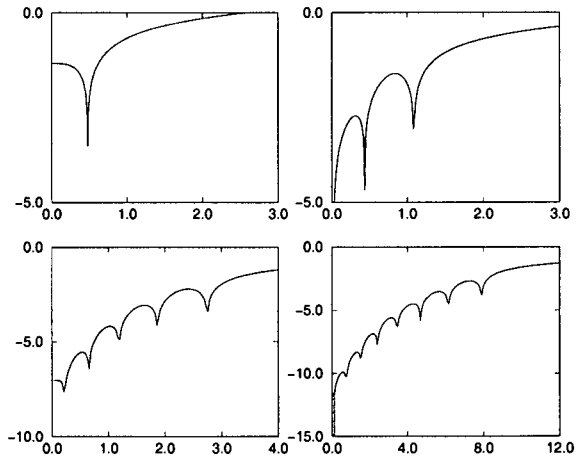

Figure 2.8: Variation of $\Delta_{S,-S}$ with H_x/D for $\alpha_6 S^4/D = 0.25$ for four different $|\vec{S}|$ values (clockwise from top left, $|\vec{S}|$ =2, 5, 10, and 15); hexagonal symmetry. On the x axis is plotted H_x/DS^2 and on the y axis $\log_{10} \Delta_{S,-S}$.

2.6.2 Tunneling Matrix Elements via Perturbation Theory

The calculation of tunneling matrix elements via perturbation theory in the terms that break the easy axis symmetry ($\hat{z} \leftrightarrow -\hat{z}$) is quite straightforward as long as there is only one such term in the Hamiltonian. For these cases we shall just state the results, all of which have been previously calculated elsewhere [70].

Hamiltonian	$\Delta_{S,-S}$
$-DS_z^2 + \alpha_2\left(S_+^2 + S_-^2\right)$	$\frac{\alpha_2^S (2S)!}{4^{S-1} D^{S-1} [(S-1)!]^2}$
$-DS_z^2 + \alpha_4\left(S_+^4 + S_-^4\right)$	$\frac{\alpha_4^{S/2} (2S)!}{4^{S-2} D^{S/2-1} [(S/2-1)!]^2}$
$-DS_z^2 + \alpha_6\left(S_+^6 + S_-^6\right)$	$\frac{\alpha_6^{S/3} (2S)!}{4^{S-3} D^{S/3-1} [(S/3-1)!]^2}$
$-DS_z^2 + H_x\left(S_+ + S_-\right)$	$\frac{H_x^{2S} (2S)}{D^{2S-1} [(2S-1)!]}$
$-DS_z^2 + \alpha_3\left\{S_z, \left(S_+^3 + S_-^3\right)\right\}$	$\frac{\alpha_3^{2S/3} (2S)!}{D^{2S/3-1} 6^{2S/3-2} [(S/3-1)!]^2}$

Table 2.1: Perturbation theory results for some simple Hamiltonians, from [70].

When the number of symmetry breaking terms in the Hamiltonian is increased, the solution for Δ using perturbation theory becomes a little more complicated. This is because of the competition between these terms in deciding which are the preferred paths between the low lying states.

2.6.3 Tunneling Matrix Elements via WKB Methods

It has been shown [25, 26] that the Hamiltonian

$$H = -DS_z^2 + \alpha_k \left(S_+^k + S_-^k \right) \tag{2.58}$$

leads to

$$\Delta_{S,-S} = \frac{DS}{\pi} \left(\frac{2\alpha_k S^{k-2}}{D} \right)^{2S/k} \tag{2.59}$$

as long as $\alpha_k S^k \ll DS^2$ and the ambient energy E is such that $E \ll DS^2$.

2.6.4 Tunneling Matrix Elements via Instanton Techniques

The final approximate method of solution for tunneling matrix elements in spin Hamiltonians that we shall consider involves using instanton techniques. We will explicitly perform one such calculation in section (2.8), obtaining the following form for an orthorhombic (ie. easy-axis easy-plane) Hamiltonian (see (2.52))

$$\Delta_{S,-S} = \frac{2\sqrt{6}}{\sqrt{\pi}} S^{3/2} (D - 2\alpha_2)^{3/4} \alpha_2^{1/4} \exp \left[-S \sqrt{\frac{D - 2\alpha_2}{\alpha_2}} \right] \tag{2.60}$$

The same type of procedure may be followed in principle with any spin Hamiltonian that possesses well-defined semi-classical trajectories between its minima. However in practice one runs up against problems with all but the easiest quadratic spin terms. We believe that it is possible to derive forms similar to (2.60) but have left this task to future investigations [98].

2.6.5 Comparison of Approximate Methods to Exact Solutions

In order to give some idea about how effective these different approximation schemes actually are, we now compare the results of the preceding sections to the exact results for the tetragonal and orthorhombic crystal symmetries. Shown in figure 2.9 is the

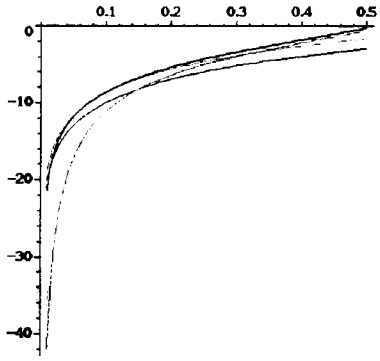

Figure 2.9: Comparison of perturbation theory, WKB results and instanton results to the exact solution for the tunneling splitting between the two lowest levels of the Hamiltonian of orthorhombic symmetry with S=10. Plotted on the horizontal axis is α_2/D, and on the vertical axis $\log_{10}\Delta_{S,-S}$. Legend: Black, exact solution; Green, instanton solution; Red, perturbation theory and Blue, WKB.

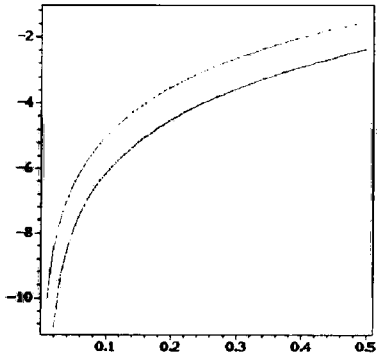

Figure 2.10: Comparison of perturbation theory and WKB results to the exact solution for the tunneling splitting between the two lowest levels of the Hamiltonian of tetragonal symmetry with S=10. Plotted on the horizontal axis is $\alpha_4 S^2/D$, and on the vertical axis $\log_{10}\Delta_{S,-S}$. Legend: Yellow, exact solution; Red, perturbation theory and Green, WKB.

comparison for the orthorhombic case. Here we see that, as we could have expected, the instanton solution fails quite spectacularly if α_2/D is small. This is simply because when we calculated our instanton action we assumed that the fluctuations around the semi-classical paths were small, which of course they aren't if α_2/D is small. When α_2/D is large, the instanton solution is quite good. The WKB solution we see is quite bad. It turns out that the functional form in α_2/D is correct but the prefactor is not. Perturbation theory works quite well for the entire range of $\alpha_2/D < 0.5$ studied.

We next turn our attention to the tetragonal case, shown in figure 2.10. Here we see a similar story. The WKB solution gets the functional form correct but again the prefactor is wrong. Perturbation theory works quite well in the small α_4/D regime.

2.7 Back to the Full Hamiltonian–Separation of Tunneling Energy Scale Using an Instanton Technique

As was discussed in the introduction and to a lesser degree in section (2.6), it is simply not feasible to measure all of the non-zero components of the tensor $\tilde{G}^{\alpha_{i_1}\cdots\alpha_{i_{20}}}$ experimentally. Because of this what is usually done is that the lower order terms in S_i allowed by crystal symmetry are kept and the rest of the terms thrown away. The coefficients of the kept terms are then used to fit experimental data.

In the case of the Fe_8 spin Hamiltonian, the form that we shall adopt is

$$H_{GS} = \tilde{G}^{\alpha_{i_1}\cdots\alpha_{i_{20}}} S_{i_1}...S_{i_{20}} = -DS_z^2 + E(S_+^2 + S_-^2) + C(S_-^4 + S_+^4) \tag{2.61}$$

This form, with $D = 0.292K$, $E = 0.046K$ and $C = -2.1 \cdot 10^{-5}K$, is good enough to accurately fit both the period of the "Aharonov-Bohm" oscillations and magnitude of the tunneling splitting [51] in recent experiments. Note however that it is clear that a large number of terms have simply been chopped off the "true" spin Hamiltonian (for example, even the quartic diagonal spin term has not been included).

The effects of thermal phonons and polaritons at low enough temperatures *can be completely neglected* [20]. This is because processes involving these bosonic modes scale like their respective densities in the crystal, which are vanishingly small at low temperatures. If we are in the "quantum regime" demonstrated by Sangregorio et.al. [14] we are at temperatures less than $\sim 360\ mK$, and therefore $k_B T \ll DS$ [20]. We therefore write the quantum regime Hamiltonian in the form

$$\begin{aligned} H &= -DS_z^2 + E(S_+^2 + S_-^2) + C(S_-^4 + S_+^4) + g\mu_B \vec{H}\cdot\vec{S} \\ &+ \sum_{p=1}^{8} g_{n_p}\mu_n \left[A^{p\alpha\beta} S_\alpha^p I_\beta^p + R^{p\alpha\beta} H_\alpha I_\beta^p\right] + \sum_{k=1}^{N} g_{n_k}\mu_n \vec{H}\cdot\vec{I}_k \\ &+ \sum_{k=1}^{N+8}\left[\sum_{l=1}^{8} g_{n_k}\mu_n M_{lk}^{\alpha\beta} S_\alpha^l I_\beta^k + \frac{eQ_k}{6I_k(2I_k-1)} V^{k\alpha\beta} I_{\alpha\beta}^k\right] \\ &+ \frac{\mu_0\mu_n^2}{4\pi}\sum_{l<k=1}^{N} \frac{g_{n_l} g_{n_k}}{r_{lk}^3}\left[\vec{I}_l\cdot\vec{I}_k - 3(\vec{I}_l\cdot\hat{r}_{lk})(\vec{I}_k\cdot\hat{r}_{lk})\right] \end{aligned} \tag{2.62}$$

There still remains one feature of (2.62) that we can take advantage of in order to simplify it. An examination of the relative strengths of the terms in (2.63) reveals that the largest term is the single-molecule anisotropy term DS_z^2 in the spin Hamiltonian which is of the order of 29 K. All the other terms are small compared to this. We therefore see that if all ambient energies (primarily the lattice temperature and external field) are much less than the gap to the first excited level $D(S^2 - (S-1)^2)$ the giant spin will only be able to access the two lowest energy levels $S_z = \pm S$. At this low energy scale we shall define our final low energy effective description, within which the giant spin is mapped to a two-level system parametrized by a Pauli matrix $\vec{\tau}$, where $\hat{\tau}_z = \pm 1$ corresponds to $S_z = \pm S$ respectively. This description will be valid in the quantum regime $T < 360\ mK$ [14].

There is another case of interest where this mapping may be performed. If an external longitudinal field H_z is applied to the system, the effect is to *bias* the wells drawn in

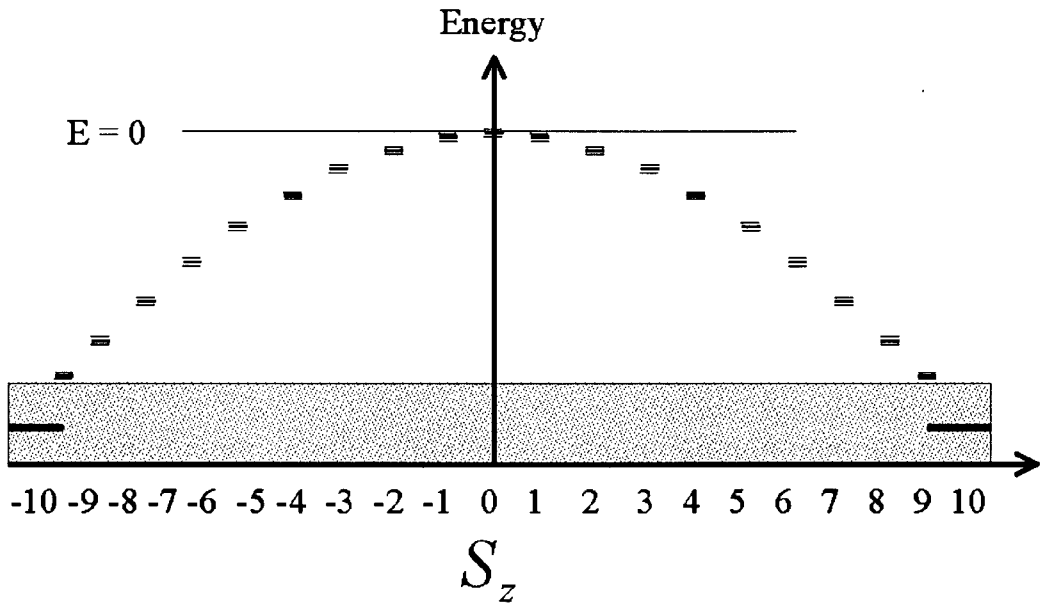

Figure 2.11: Z-projection of spin versus energy from H_{GS} for the Fe_8 system. The region of validity of the mapping to a two-state system is the region where excited states are forbidden (this region in shaded grey in the above).

figure 2.11. If the applied field is strong enough, it can bring to resonance one of our original states and a higher-energy state on the other side of the barrier (for example, the application of a positive H_z could lead to a resonance condition between $|+10>$ and $|-9>$). In this case, the dominant tunneling dynamics in the system still involve only two levels. However, one must exercise caution here, as the lower-lying states (in this example, $|-10>$) are connected to the two primary states by several mechanisms, most importantly phonon emission taking $|-9>$ to $|-10>$. Because of this complication,

in what follows we shall explicitly consider only the case where the externally applied longitudinal field is such that $H_z \ll DS$ and only the two levels $|\pm S>$ are involved, keeping in mind that in certain circumstances we may be able to generalize our results to larger values of H_z.

The dynamics of $\vec{\tau}$ in this regime are solely the product of tunneling from $|S> \leftrightarrow |-S>$. This observation leads to a natural separation of contributions coming from terms in (2.63) that are diagonal in S_z (and therefore are not involved in tunneling events) and terms that are not diagonal in S_z (and therefore coming into play only when the giant spin tunnels). This separation is helpful because it will turn out (we will show this) that the time scale for tunneling physics $\equiv \Delta^{-1}$ is much smaller than the time between tunneling events $\equiv \Omega_0^{-1}$ [20]. To see why this separation is helpful, consider the following argument.

Let us imagine a likely trajectory for the excess spin $\vec{S}(t)$, assuming an initial condition corresponding to $\vec{S}(0) = +S\,\hat{z}$. We assume that the time between tunneling events is much longer than the time over which tunneling occurs. We therefore expect the central spin to evolve dynamically in a similar way to that shown in figure 2.12. This "separation of scales" allows one to consider the effective description separately in two different regimes; one in the regions between tunneling events and one during the tunneling. The regime between tunneling events we shall refer to as the "diagonal" region (as only terms diagonal in $\hat{S}$ enter into play) and the contribution of these terms to the final effective description we can simply read off our equation (2.63). We find under these circumstances that the diagonal contribution can be written

$$\begin{aligned} H^D &= \frac{5}{2}\hat{\tau}_z \sum_{p=1}^{8}\left[(\pm)_p g_{n_p}\mu_n\left[A^{pz\beta}I_\beta^p + \sum_{k=1}^{N+8} M_{pk}^{z\beta} I_\beta^k\right]\right] + g\mu_B S H_z \hat{\tau}_z \\ &+ \sum_{p=1}^{8} g_{n_p}\mu_n R^{p\alpha\beta} H_\alpha I_\beta^p + \sum_{k=1}^{N} g_{n_k}\mu_n \vec{H}\cdot\vec{I}_k + \sum_{k=1}^{N}\left[\frac{eQ_k}{6I_k(2I_k-1)} V^{k\alpha\beta} I_{\alpha\beta}^k\right] \end{aligned}$$

$$+ \quad \frac{\mu_0 \mu_n^2}{4\pi} \sum_{l<k} \frac{g_{n_l} g_{n_k}}{r_{lk}^3} \left[\vec{I}_l \cdot \vec{I}_k - 3(\vec{I}_l \cdot \hat{r}_{lk})(\vec{I}_k \cdot \hat{r}_{lk}) \right] \tag{2.63}$$

where $(\pm)_p$ is shorthand for the direction in which the p^{th} ionic spin is pointing (see figure 2.1). Our labelling system has $(\pm)_p = 1$ for ionic spins $\{p_\uparrow\} = 1, 2, 4, 5, 6$ and 8 and $(\pm)_p = -1$ for spins $\{p_\downarrow\} = 3$ and 7 when the central spin is "up" (that is, $\hat{\tau}_z = +1$) with signs reversed if the central spin is "down".

We may rewrite this in the form

$$\begin{aligned} H^D &= \left(\frac{1+\hat{\tau}_z}{2} \right) \left[\sum_{p=1}^{8} \vec{\gamma}_p^{(1c)} \cdot \vec{I}_p + \sum_{k=1}^{N} \vec{\gamma}_k^{(1)} \cdot \vec{I}_k \right] + \left(\frac{1-\hat{\tau}_z}{2} \right) \left[\sum_{p=1}^{8} \vec{\gamma}_p^{(2c)} \cdot \vec{I}_p + \sum_{k=1}^{N} \vec{\gamma}_k^{(2)} \cdot \vec{I}_k \right] \\ &+ g\mu_B S H_z \hat{\tau}_z + \sum_{k=1}^{N} \left[+ \frac{eQ_k}{6I_k(2I_k-1)} V^{k\alpha\beta} I^k_{\alpha\beta} \right] \\ &+ \frac{\mu_0 \mu_n^2}{4\pi} \sum_{l<k} \frac{g_{n_l} g_{n_k}}{r_{lk}^3} \left[\vec{I}_l \cdot \vec{I}_k - 3(\vec{I}_l \cdot \hat{r}_{lk})(\vec{I}_k \cdot \hat{r}_{lk}) \right] \end{aligned} \tag{2.64}$$

where

$$\vec{\gamma}_p^{(1c)} = \frac{5}{2} g_{n_p} \mu_n (\pm)_p \left[A^{pz\beta} + R^{p\alpha\beta} H_\alpha \right] \tag{2.65}$$

$$\vec{\gamma}_p^{(2c)} = \frac{5}{2} g_{n_p} \mu_n (\pm)_p \left[-A^{pz\beta} + R^{p\alpha\beta} H_\alpha \right] \tag{2.66}$$

$$\vec{\gamma}_k^{(1)} = \vec{\gamma}_{kS}^{(1)} + \frac{5}{2} g_{n_k} \mu_n H^\beta = \frac{5}{2} g_{n_k} \mu_n \left[\sum_{p \in \{p_\uparrow\}} M_{pk}^{z\beta} - \sum_{p \in \{p_\downarrow\}} M_{pk}^{z\beta} + H^\beta \right] \tag{2.67}$$

$$\vec{\gamma}_k^{(2)} = \vec{\gamma}_{kS}^{(2)} + \frac{5}{2} g_{n_k} \mu_n H^\beta = \frac{5}{2} g_{n_k} \mu_n \left[- \sum_{p \in \{p_\uparrow\}} M_{pk}^{z\beta} + \sum_{p \in \{p_\downarrow\}} M_{pk}^{z\beta} + H^\beta \right] \tag{2.68}$$

The notation here is such that the β^{th} component of the expressions on the right corresponds to the β^{th} component of the vector on the left.

One can think of the expression (2.64) in the following way. There are two electronic spin configurations (1,2) that correspond to before (1) and after (2) the central spin

complex flips. In each of these configurations, each nuclear spin in the system feels a magnetic field coming from the ionic spins and the externally applied field. In the above expression, these fields are represented by $\vec{\gamma}_k^{(1)}$, $\vec{\gamma}_k^{(1c)}$, $\vec{\gamma}_k^{(2)}$ and $\vec{\gamma}_k^{(2c)}$. The sign changes in going from $\vec{\gamma}_k^{(1)} \rightarrow \vec{\gamma}_k^{(2)}$ and $\vec{\gamma}_k^{(1c)} \rightarrow \vec{\gamma}_k^{(2c)}$ come from the fact that the central spin object has reversed its direction along the easy axis.

One may write (2.64) in a more transparent fashion by defining unit vectors

$$\hat{m}_k = \frac{\vec{\gamma}_k^{(1)} + \vec{\gamma}_k^{(2)}}{|\vec{\gamma}_k^{(1)} + \vec{\gamma}_k^{(2)}|} \quad , \qquad \vec{l}_k = \frac{\vec{\gamma}_k^{(1)} - \vec{\gamma}_k^{(2)}}{|\vec{\gamma}_k^{(1)} - \vec{\gamma}_k^{(2)}|} \tag{2.69}$$

for k labelling the ligand spins $k = 1..N$ and

$$\hat{m}_k = \frac{\vec{\gamma}_k^{(1c)} + \vec{\gamma}_k^{(2c)}}{|\vec{\gamma}_k^{(1c)} + \vec{\gamma}_k^{(2c)}|} \quad , \qquad \vec{l}_k = \frac{\vec{\gamma}_k^{(1c)} - \vec{\gamma}_k^{(2c)}}{|\vec{\gamma}_k^{(1c)} - \vec{\gamma}_k^{(2c)}|} \tag{2.70}$$

for k labelling the possible ^{57}Fe nuclear spins $k = N+1..N+8$. We also define energies

$$\omega_k^{||} = |\vec{I}_k| g_{n_k} \mu_n |\vec{\gamma}_k^{(1)} - \vec{\gamma}_k^{(2)}| \quad , \quad \omega_k^{\perp} = |\vec{I}_k| g_{n_k} \mu_n |\vec{\gamma}_k^{(1)} + \vec{\gamma}_k^{(2)}| \tag{2.71}$$

for ligand spins $k = 1..N$ and

$$\omega_k^{||} = |\vec{I}_k| g_{n_k} \mu_n |\vec{\gamma}_k^{(1c)} - \vec{\gamma}_k^{(2c)}| \quad , \quad \omega_k^{\perp} = |\vec{I}_k| g_{n_k} \mu_n |\vec{\gamma}_k^{(1c)} + \vec{\gamma}_k^{(2c)}| \tag{2.72}$$

for ^{57}Fe spins $k = N+1..N+8$. With these we can write

$$\begin{aligned} H^D &= \sum_{k=1}^{N+8} \left[\frac{\omega_k^{\perp}}{2} \hat{I}_k \cdot \hat{m}_k + \frac{\hat{\tau}_z}{2} \omega_k^{||} \hat{I}_k \cdot \hat{l}_k \right] + g \mu_B S H_z \hat{\tau}_z \\ &+ \sum_{k=1}^{N} \left[\frac{eQ_k}{6I_k(2I_k-1)} V^{k\alpha\beta} I^k_{\alpha\beta} \right] + \frac{\mu_0 \mu_N^2}{4\pi} \sum_{l<k} \frac{g_{n_l} g_{n_k}}{r_{lk}^3} \left[\vec{I}_l \cdot \vec{I}_k - 3(\vec{I}_l \cdot \hat{r}_{lk})(\vec{I}_k \cdot \hat{r}_{lk}) \right] \end{aligned} \tag{2.73}$$

This form is similar to that derived by Prokofiev and Stamp [20]. It differs in two respects. Firstly, it shows explicitly what the energies $\omega_k^{||}, \omega_k^{\perp}$ and unit vectors $\hat{m}_k, \hat{l}_k$ are in terms of parameters in the higher energy descriptions (and allows us to calculate these–we shall

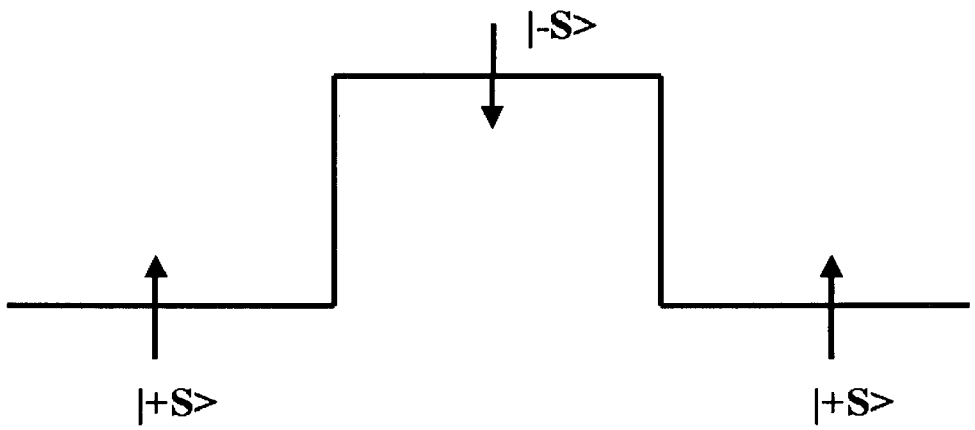

Figure 2.12: Typical evolution of the projection of the excess spin $\vec{S}(t)$ along the easy-axis. We see two regimes; one where S evolves without tunneling (diagonal in $\hat{\tau}$), and one where S tunnels from $|+S> \leftrightarrow |-S>$ (off-diagonal in $\hat{\tau}$). Note the separation of scales; the time between tunneling events is much greater than the tunneling time.

do this in the next chapter). Secondly, it includes the effect of quadrupolar couplings between higher spin nuclei in the ligand bath and electric field gradients in the molecule.

The "off-diagonal" contribution to the effective Hamiltonian is somewhat harder to extract, and a different approach will be required.

2.8 Off-Diagonal Terms and the Instanton Method

A method has been developed by Tupitsyn et.al. [74] that allows the extraction of the "off-diagonal" terms in the effective Hamiltonian, ie. those that act when the central spin object tunnels. Two objections have recently been raised which question the validity of this method [101]). In this section we shall review the method and point out the objections.

2.8.1 Review of the Method of Tupitsyn et.al.

In the effective description (2.63) we have reduced the Hilbert space of the central degree of freedom down to dimension $D = 2$. These states are collective objects of the form $\vec{S} = \sum_l \vec{S}_l$; that is, they are formed of electronic spins that have locked together. In the approach to the Fe_8 molecule that we have adopted, we have chosen a model where all the electronic spins lock together such that each lies parallel or antiparallel to the easy axis. We shall in what follows treat this collective state as a spin 10 quantum rotator, pointing out when this description must be modified because of the "true" eight spin nature of the object.

The states $|\alpha>$ and $|\beta>$ are collective states with $\alpha = |+\vec{S}>$ and $\beta = |-\vec{S}>$, ie. referring to the central spin "pointing in the up/down directions". The transition amplitude between these states can be defined to be

$$\Gamma_{\alpha\beta}(t) = \int_{|\alpha>}^{|\beta>} D(\theta,\phi) \exp\left(-\int_0^t d\tau \left(L_0(\tau) + L_N(\tau)\right)\right) \tag{2.74}$$

where $L_0(\tau)$ and $L_N(\tau)$ are the Lagrangians corresponding to the bare spin Hamiltonian plus the external field term

$$H_0 = -DS_z^2 + E(S_+^2 + S_-^2) + C(S_+^4 + S_-^4) + g\mu_B \vec{S}\cdot\vec{H} \tag{2.75}$$

and the contributions from the nuclear spins respectively. The spherical angles θ and ϕ are introduced so as to characterize $\vec{S}$ in the standard way; that is,

$$S_x = |\vec{S}|\cos\phi\sin\theta \quad , \quad S_y = |\vec{S}|\sin\phi\sin\theta \quad , \quad S_z = |\vec{S}|\cos\theta \tag{2.76}$$

If we assume that the "bounce time" between minima Ω_0^{-1} is much smaller than the time between transitions Δ_0^{-1}, the evolution operator connecting the two minima will be given by

$$\left(H^{ND}\right)_{\alpha\beta} = \frac{i}{t}\Gamma_{\alpha\beta}(t) \quad , \qquad (\alpha \neq \beta, \Omega_0^{-1} \ll t \ll \Delta_0^{-1}) \tag{2.77}$$

where H^{ND} is the non-diagonal part of the effective Hamiltonian that we are looking for. This means that in order to calculate H^{ND} it suffices to calculate $\Gamma_{\alpha\beta}(t)$, and this we can attempt to do by solving for the instanton (semiclassical) solutions of (2.74).

2.8.2 The Tunneling Lagrangian

In the calculation that follows we shall explicitly use the easy-axis easy-plane spin Hamiltonian, vis.

$$H_0 = -(D - 2E)S_z^2 + 4ES_x^2 \tag{2.78}$$

However, the tactics we employ here can be used for any spin Hamiltonian admitting clearly defined semiclassical paths between the minima $|\alpha>$ and $|\beta>$. Note that this spin Hamiltonian is equivalent to the one experimentally obtained for Fe_8 if the quartic spin terms in this latter are neglected. Using the relationship $S^2 = S_x^2 + S_y^2 + S_z^2$ we can show that (2.78) is equivalent to

$$H_0 = -DS_z^2 + E(S_+^2 + S_-^2) \tag{2.79}$$

This truncation is performed simply for convenience, as inclusion of the quartic terms makes the analytic calculations that follow very difficult. As we discussed earlier in this chapter, the "true" spin Hamiltonian contains many terms that are inaccessible experimentally, and therefore dropping the quartic term simply emphasizes the point that in using a form like (2.78) we really are using a phenomenological description–the effect of dropping higher order terms on the amplitude of tunneling matrix elements can be drastic [164]. This being said, what is important in this case is the instanton trajectory, and this is not expected to be strongly affected by higher order terms [74].

For the easy-axis easy-plane model (2.78) one can show that the equations of motion

are

$$i\,\dot{\theta}\sin\theta + 4ES\sin^2\theta\sin 2\phi = 0 \tag{2.80}$$

and

$$\dot{\phi}\sin\theta - i4ES(\frac{D-2E}{4E} + \cos^2\phi)\sin 2\theta = 0 \tag{2.81}$$

Solutions of the classical equations of motion are simply

$$\phi = \eta\frac{\pi}{2} - i\sinh^{-1}\sqrt{\frac{D-2E}{4E}} \tag{2.82}$$

and

$$\dot{\theta}(t) = \sin\theta(t) = \frac{1}{\cosh\Omega_0 t} \quad , \quad \Omega_0 = 4ES\sinh\left[2\sinh^{-1}\sqrt{\frac{D-2E}{4E}}\right] \tag{2.83}$$

where $\eta = \pm$ labels rotations clockwise and counter-clockwise in the easy plane. Now in the standard treatment, one assumes that the classical equations of motion are attractors in the sense that a small perturbation away from these costs action. If this is true then one can perform a gaussian integration over small fluctuations away from the classical equations of motion in the manner suggested by Tupitsyn et.al. [74].

However it was recently pointed out by Unruh [101] that if we perturb the variable ϕ in the equation of motion (2.81) we obtain

$$\delta\dot{\phi} = -8ES\sin(2\sinh^{-1}\sqrt{\frac{D-2E}{4E}})\cos\theta\,\delta\phi \tag{2.84}$$

Now we see that as long as $\cos\theta > 0$ any perturbation of ϕ is attracted to the classical solution. However we see from our solutions that $\cos\theta$ changes sign at $\theta = \pi/2$. Thus it would appear that at this point the variable ϕ is pushed away from its stable point. If this is true it brings into question the validity of the gaussian integration technique.

2.8.3 An Assumption is Made

In what follows we shall make the assumption that we may perform gaussian integrations over small fluctuations in ϕ around the solutions of the classical equations of motion. As Unruh has pointed out [101] it is not clear that this assumption holds even in the limit where $\frac{D-2E}{4E} \ll 1$–the case treated by Tupitsyn et.al. [74]. Furthermore in our case we have that $\frac{D-2E}{4E} = 2.67$. That this number is large means the potential that holds ϕ close to the classical solutions is not very steep, so that the assumption that gaussian integrations can be performed is questionable (however our results of comparing the exact solution to the instanton solution for the tunneling amplitude show good agreement in this case–see figures 2.9, 6.1 and 6.2).

The Formal Calculation

Explicitly the Lagrangians appearing in (2.74) are

$$\begin{aligned} L_0 &= -iS\phi\dot{\theta}\sin\theta + (D-2E)S^2\sin^2\theta + 4ES^2\sin^2\theta\cos^2\phi \\ &- S\left(H_x\sin\theta\cos\phi + H_y\sin\theta\sin\phi + H_z\cos\theta\right) \end{aligned}$$

and

$$\begin{aligned} L_N &= \sum_{p=1}^{8} g_{n_p}\mu_n\left[A^{p\alpha\beta}S^p_\alpha I^p_\beta + R^{p\alpha\beta}H_\alpha I^p_\beta\right] + \sum_{k=1}^{N} g_{n_k}\mu_n\vec{H}\cdot\vec{I}_k \\ &+ \sum_{k=1}^{N}\left[\sum_{p=1}^{8} g_{n_k}\mu_n M^{\alpha\beta}_{pk}S^p_\alpha I^k_\beta + \frac{eQ_k}{6I_k(2I_k-1)}V^{k\alpha\beta}I^k_{\alpha\beta}\right] \\ &+ \frac{\mu_0\mu_n^2}{4\pi}\sum_{l<k=1}^{N}\frac{g_{n_l}g_{n_k}}{r^3_{lk}}\left[\vec{I}_l\cdot\vec{I}_k - 3(\vec{I}_l\cdot\hat{r}_{lk})(\vec{I}_k\cdot\hat{r}_{lk})\right] \end{aligned} \tag{2.85}$$

We shall assume that the instanton bounce time Ω_0^{-1} is such that $\Omega_0^{-1} \ll T_2^{-1}$, where T_2^{-1} is the time scale over which the nuclear-nuclear flip-flop processes mediated by the last term in the above expression occur. In this limit, the nuclear-nuclear term provides

a static bias field acting on each nucleus and therefore we can rewrite our Langrangian in the form

$$\begin{aligned} L_N &= \sum_{p=1}^{8} g_{n_p}\mu_n \left[A^{p\alpha\beta}S_\alpha^p I_\beta^p + R^{p\alpha\beta}H_\alpha^p I_\beta^p\right] + \sum_{k=1}^{N} g_{n_k}\mu_n \vec{H}_k \cdot \vec{I}_k \\ &+ \sum_{k=1}^{N}\left[\sum_{p=1}^{8} g_{n_k}\mu_n M_{pk}^{\alpha\beta} S_\alpha^p I_\beta^k + \frac{eQ_k}{6I_k(2I_k-1)} V^{k\alpha\beta} I_{\alpha\beta}^k\right] \end{aligned} \tag{2.86}$$

where now the static field at each nucleus is given by the sum of the external field plus some contribution from the nuclear-nuclear term.

In our model, each electronic spin is locked to the central spin. This means that

$$\vec{S}_p = (\pm)_p \vec{S}\frac{|\vec{S}_p|}{|\vec{S}|} \tag{2.87}$$

and therefore

$$\begin{aligned} &\sum_{p=1}^{8} g_{n_p}\mu_n A^{p\alpha\beta}S_\alpha^p I_\beta^p + \sum_{k=1}^{N}\sum_{p=1}^{8} g_{n_k}\mu_n M_{pk}^{\alpha\beta} S_\alpha^p I_\beta^k \rightarrow \\ &\frac{S_\alpha}{4}\left[g_{n_p}\mu_n\left[\sum_{p\in\{p_\uparrow\}} A^{p\alpha\beta}I_\beta^p - \sum_{p\in\{p_\downarrow\}} A^{p\alpha\beta}I_\beta^p\right] + \sum_{k=1}^{N} g_{n_k}\mu_n I_\beta^k\left[\sum_{p\in\{p_\uparrow\}} M_{pk}^{\alpha\beta} - \sum_{p\in\{p_\downarrow\}} M_{pk}^{\alpha\beta}\right]\right] \end{aligned} \tag{2.88}$$

2.8.4 Solution for the Free Instanton Trajectory

We assume that fluctuations in the variable ϕ are small in our model. This will only strictly be true for $4E/(D-2E)$ large (see figure 2.9). In our case we have seen that $4E/(D-2E) \sim 0.37$. Looking back to our comparison of the exact solution with the instanton solution for orthorhombic symmetry we see that in this regime the instanton solution is off by about a factor of two from the exact one in the determination of Δ_0. Nevertheless we shall adopt this method in this case. Doing this allows us to perform a Gaussian integration over ϕ. This will leave us with an effective description in terms

of only one path-valued parameter $\theta(\tau)$ which is the angle between $\vec{S}$ and the z axis during the instanton trajectory. In the case where the giant spin is not coupled to the environmental spins and there is no external magnetic field it is known that this effective description reduces to (here we include only terms that affect the equations of motion) [75]

$$L_{eff}(\theta) = \frac{S^2}{4\widetilde{E}}\dot{\theta}^2 + \widetilde{D}\sin^2\theta \tag{2.89}$$

where we have defined $\widetilde{E} = 4E\sum_p |\vec{S}_p|^2$ and $\widetilde{D} = (D-2E)\sum_p |\vec{S}_p|^2$, following [75]. The classical equation of motion is readily found from (2.89) and is

$$\dot{\theta} = \sin\theta(\tau) = 1/\cosh(\Omega_0\tau) \quad , \Omega_0 = \frac{S}{2}\sqrt{\widetilde{E}\widetilde{D}} \tag{2.90}$$

There are two things worth noting here. First is that the form of the instanton after the gaussian integrations have been performed is the same as the bare classical form with renormalized Ω_0. Second is that the parameters $\widetilde{D}$ and $\widetilde{E}$ depend on the fact that we are really dealing with an eight spin object. In the case of a spin 10 object, $\widetilde{E} = 2ES^2 = 200E$, while for us $\widetilde{E} = 2E\sum_p |\vec{S}_p|^2 = E \cdot 8 \cdot 25/4 = 100E$; likewise for $\widetilde{D}$. Substituting this extremal trajectory into the effective Lagrangian and integrating over τ gives for the instanton action

$$A_{eff} = A_0 + i\eta\pi S \quad , \quad A_0 = 2S\sqrt{\frac{D-2E}{4E}}$$

where $\eta = \pm$ corresponds to clockwise and counterclockwise paths respectively. Note that neither the Haldane phase $\eta\pi S$ nor A_0 depends on the eight spin nature of the collective central spin [75].

2.8.5 Inclusion of the External Magnetic Field and the Nuclear Spins

We now make the assumption that the applied magnetic field and the couplings to the environmental spins are weak. Specifically we require that

$$\frac{\omega_k^{||}}{\Omega_0} << 1 \quad , \frac{\omega_k^{\perp}}{\Omega_0} << 1 \quad , \frac{|\vec{H}|}{\Omega_0} << 1 \tag{2.91}$$

It is known [74] that the modifications to the instanton trajectory calculated above (2.90) coming from the external field and the spin bath first appear to second order in an expansion in powers of $\mathcal{E}/\Omega_0$ where $\mathcal{E}$ is one of $\omega_k^{||}$, $\omega_k^{\perp}$ or the external field magnitude $|\vec{H}|$. This means that if we are only interested in first-order corrections due to these effects (which we are) we can neglect these and use the trajectory (2.90) in the presence of the external field and the spin bath (as long, of course, as the conditions (2.91) hold).

It must be noted here that the validity of this approach has been questioned [101]- in particular the assumption that the trajectory of the central spin responds to second order in the external fields.

Substitution of the extremal trajectory into the general effective lagrangian and integrating over τ yields the following effective action,

$$A_{eff} = A_0 + i\eta\pi S - i\eta\vec{A}_H \cdot \vec{H} + \eta \sum_{k=1}^{N+8} \vec{A}_{N,D}^k \cdot \vec{I}_k \tag{2.92}$$

where $\vec{A}_H$ is the contribution due to the external magnetic field $\vec{H}$ and the $\vec{A}_{N,D}^k$ terms are the contribution due to the presence of the environmental spins. Explicitly these are

$$\vec{A}_H = \frac{\pi S g \mu_B}{\Omega_0}\hat{y} - i\frac{S^2 \pi g \mu_B}{2\tilde{E}}\hat{x} \tag{2.93}$$

$$\vec{A}_{N,D}^k = \frac{S\pi}{4\Omega_0} g_{n_k}\mu_n \left[\left[\sum_{p\in\{p_\uparrow\}} M_{pk}^{y\beta} - \sum_{p\in\{p_\downarrow\}} M_{pk}^{y\beta}\right] - i\sqrt{\frac{D-2E}{4E}}\left[\sum_{p\in\{p_\uparrow\}} M_{pk}^{x\beta} - \sum_{p\in\{p_\downarrow\}} M_{pk}^{x\beta}\right]\right] \tag{2.94}$$

for $k = 1..N$ representing the ligand nuclear spins and

$$\vec{A}^k_{N,D} = (\pm)_k \frac{S\pi}{4\Omega_0} g_{n_k}\mu_n \left[A^{py\beta} - i\sqrt{\frac{D-2E}{4E}} A^{px\beta} \right] \tag{2.95}$$

for $k = N+1..N+8$ representing the ^{57}Fe ions. In both cases the β^{th} component of the tensors on the left hand sides are identified with the β^{th} component of the vectors on the right hand side. These expressions should be compared to equations (2.27) and (2.28) in [20], noting of course that here the hard direction is the x direction whilst in [20] it is the y direction. Aside from this the only differences here are that the terms due to the presence of the nuclear spins have been explicitly written in terms of parameters in a higher energy Hamiltonian and the nuclear spins can have arbitrary spin numbers.

The tunneling splitting in zero field Δ_0 is given in this instanton picture by

$$\Delta_0 = \Omega_0 \sqrt{\frac{3A_0}{2\pi}} \exp(-A_0) \tag{2.96}$$

As we have seen earlier, this expression for Δ_0 is off by approximately a factor of two from the exact solution for $(D-2E)/4E \sim 0.37$ (figure 2.9).

As discussed previously, for times $\Omega_0^{-1} << t << \Delta_0^{-1}$, the relationship between the transition amplitude and the off-diagonal part of the effective Hamiltonian is

$$H^{ND} = \frac{i}{t} \left(\hat{\tau}_- \Gamma_{\downarrow\uparrow}(t) + h.c. \right) \tag{2.97}$$

where

$$\Gamma_{\downarrow\uparrow}(t) = it\Delta_0 \sum_{\eta=\pm} \exp(-A_{eff}) \tag{2.98}$$

and $\hat{\tau}_-$ is a Pauli lowering operator in the subspace of the two-level Neel vector. Using our expression (2.92) for A_{eff} and the criteria (2.91) allows us to write the off-diagonal part of the effective Hamiltonian as

$$H^{ND} = 2\Delta_0 \hat{\tau}_- \cos(\Phi - i \sum_{k=1}^{N+8} \vec{A}^k_{N,D} \cdot \vec{I}_k) + h.c. \tag{2.99}$$

where

$$\Phi = \pi S - \vec{A}_H \cdot \vec{H} \tag{2.100}$$

2.9 The Final Single Molecule Effective Hamiltonian

As a result of all the above considerations we find that the form of the single molecule effective Hamiltonian is

$$\begin{aligned} H &= \sum_{k=1}^{N+8} \left[\frac{\omega_k^{\perp}}{2} \hat{I}_k \cdot \hat{m}_k + \frac{\hat{\tau}_z}{2} \omega_k^{\parallel} \hat{I}_k \cdot \hat{l}_k \right] + g\mu_B S H_z \hat{\tau}_z + 2\Delta_0 \hat{\tau}_- \cos(\Phi - i \sum_{k=1}^{N+8} \vec{A}_{N,D}^{k} \cdot \vec{I}_k) + h.c. \\ &+ \sum_{k=1}^{N} \left[\frac{eQ_k}{6I_k(2I_k-1)} V^{k\alpha\beta} I_{\alpha\beta}^{k} \right] + \frac{\mu_0 \mu_n^2}{4\pi} \sum_{l<k} \frac{g_{n_l} g_{n_k}}{r_{lk}^3} \left[\vec{I}_l \cdot \vec{I}_k - 3(\vec{I}_l \cdot \hat{r}_{lk})(\vec{I}_k \cdot \hat{r}_{lk}) \right] \end{aligned} \tag{2.101}$$

At this point we reiterate that objections as to the validity of the instanton calculation have been raised [101]. The term that is affected is the off-diagonal constribution. We shall find later on that the predictions that we obtain from the use of this term match both exact diagonalization and experimental results extremely well in the low field regime that we are considering. We treat this as evidence (but certainly not proof) that the approximations made in the instanton calculation are valid.

Chapter 3

Nuclear Spin Couplings in Fe_8 and the Isotope Effect

Here we present our results for the quantities $\vec{\gamma}_{kS}^{(1)}$ and $\vec{\gamma}_{kS}^{(2)}$ (for definitions see (2.67) and (2.68)) in Fe_8, which represent the dipolar fields due to the Fe^{3+} ions at the k^{th} nuclear spin before and after the central spin complex tunnels respectively. We are going to do this using two different methods. The first will treat each Fe^{3+} ion in the molecule as a point magnetic dipole (and as such we call this the "point dipole approximation"). The second method we shall use is to model the actual spatial spin distribution near the iron ions by using previously calculated Hartree-Fock wavefunctions for free Fe^{3+} ions. This "spreading out" of the magnetic dipole changes the values for the fields at the nuclei.

These fields (and therefore $\vec{\gamma}_k^{(1)}$ and $\vec{\gamma}_k^{(2)}$) are then used to calculate the dipolar coupling energies $\omega_k^{||}$ and $\omega_k^{\perp}$. The conversion of field units to energy units is calculated using the dipole-dipole interaction using known nuclear g-factors and assuming that the Fe^{3+} g factor is isotropic and equal to 2.

We then use $\{\omega_k^{||}\}$ and $\{\omega_k^{\perp}\}$, together with known contact hyperfine couplings due to the presence of $^{57}Fe^{3+}$ ions, to calculate the orthogonality blocking parameter κ, the topological decoherence parameter λ and the full linewidth of the nuclear spins $\mathcal{W}$ for arbitrary isotopic concentration. We find that all these quantities show a significant isotope effect.

3.1 Units and Constants

We choose to work in the SI system of units. We therefore have that

$$\frac{\mu_0}{4\pi} = 10^{-7} \ \frac{N}{A^2} \tag{3.1}$$

The Bohr Magneton is

$$\mu_B = 0.9271203 \cdot 10^{-23} \ \frac{J}{T} \tag{3.2}$$

and the nuclear magneton is

$$\mu_n = 0.505038 \cdot 10^{-26} \ \frac{J}{T} = 7.622462 \ \frac{MHz}{T} \tag{3.3}$$

The proton and electronic iron g-factors are

$$g_{pr} = 5.58510 \quad , \quad g_{Fe} = 2 \tag{3.4}$$

Here we have assumed an isotropic spin-only g-factor for the electronic spin of the Fe^{3+} ions [?].

The unit conversion factors we shall use are

$$20.837 \ GHz = 1 \ K = 1.3807 \cdot 10^{-23} \ J = 0.695045 \ cm^{-1} = 8.617 \cdot 10^{-5} \ eV \tag{3.5}$$

3.2 The Point Dipole Approximation

Here we begin the problem of calculating the magnetic fields created by the iron ions. The tack we use here is to treat the iron ions as point dipoles. This is a "first order" approach which will only be useful if the spatial extent of the iron wavefunctions is much less than the distance between the iron ions and the protons. We will attempt a more careful treatment in the following section and compare its results to those obtained using the point dipole approximation.

3.2.1 Magnetic Field at $\vec{r}$ due to a "Point Dipole" at $\vec{0}$

The field at $\vec{r}$ due to a point dipole at the origin is

$$\vec{\gamma}(\vec{r}) = -\frac{\mu_0}{4\pi}\frac{1}{|\vec{r}|^3}\left[\vec{m} - 3(\vec{m}\cdot\hat{r})\hat{r}\right] \tag{3.6}$$

where $\vec{m}$ is the magnetic dipole moment of the dipole at the origin, which in our case is

$$\vec{m} = g_{Fe}\mu_B\vec{s} = g_{Fe}\mu_B s\hat{s} \tag{3.7}$$

Therefore we find that

$$\vec{\gamma}(\vec{r}) = -\frac{\mu_0}{4\pi}\frac{1}{|\vec{r}|^3}g_{Fe}\mu_B s\left[\hat{s} - 3(\hat{s}\cdot\hat{r})\hat{r}\right] \tag{3.8}$$

which is equivalent to

$$\vec{\gamma}(\vec{r}) = 4.636\frac{1}{|\vec{r}|^3}\left[3(\hat{s}\cdot\hat{r})\hat{r} - \vec{s}\,\right]\ \ T \tag{3.9}$$

where $\vec{r}$ is measured in Angstroms.

3.2.2 Magnetic Field at $\vec{r}_p$ due to Eight "Point Dipoles" at $\vec{r}_{Fe_{1..8}}$

Define the vector joining the p^{th} nucleus and j^{th} iron ion to be $\vec{r}_{pj} = \vec{r}_p - \vec{r}_j$. Then the total field at the p^{th} nucleus due to the eight iron ions in the point dipole approximation is

$$\vec{\gamma}(\vec{r}_p) = 4.636\sum_{j=1}^{8}\frac{1}{|\vec{r}_{pj}|^3}\left[3(\hat{s}_j\cdot\hat{r}_{pj})\hat{r}_{pj} - \vec{s}_j\right]\ \ T \tag{3.10}$$

where again distances are measured in Angstroms.

3.2.3 Isotopic Concentrations, Nuclear g-factors and Quadrupolar Moments in Fe_8

In table 3.1 we present information on the properties of the various nuclei that can be found in the Fe_8 molecule. The nuclear magnetic moments are equal to $g\mu_n|I|$ and are listed in units of nuclear magnetons.

Species	Concentration	$\|\vec{I}\|$	Nuclear Moment $[\mu_n]$	Quadrupole Moment Q $[10^{-24}cm^2]$
^1H	99.98	1/2	2.79255	0
^2H	0.02	1	0.857354	0.00273
^{12}C	98.88	0	0	0
^{13}C	1.12	1/2	0.70225	0
^{14}N	99.62	1	0.40365	0.02
^{15}N	0.38	1/2	-0.2830	0
^{16}O	99.757	0	0	0
^{17}O	0.039	5/2	-1.8935	-0.005
^{18}O	0.204	0	0	0
^{56}Fe	91.068	0	0	0
^{57}Fe	2.20	1/2	0.05	0
^{79}Br	50.56	3/2	2.10576	0.335
^{81}Br	49.47	3/2	2.2696	0.280

Table 3.1: Nuclear spin information for nuclei occuring in Fe_8. From [48].

The isotopic concentrations shown in table 3.1 are the "naturally occuring" concentrations. It is quite possible to alter these concentrations and as such in what follows we shall treat the general case where the particular isotopic concentrations in the material may be varied.

3.2.4 Definition and Evaluation of $\vec{\gamma}_k^{(1)}$, $\vec{\gamma}_k^{(2)}$, $\omega_k^{||}$ and $\omega_k^{\perp}$

$\vec{\gamma}_k^{(1)}$ and $\vec{\gamma}_k^{(2)}$ are the dipolar fields (in Tesla) at the point $\vec{r}_k$ before/after the central spin flips respectively, for all nuclei $k = 1..N+8$ (see (2.67) and (2.68)). Note that in the absence of an externally applied magnetic field we have $\vec{\gamma}_k^{(2)} = -\vec{\gamma}_k^{(1)}$ (the field due to the central spin cluster just flips its direction when the central object tunnels).

The energy of interaction of the nuclear dipole at $\vec{r}_k$ with the external field is

$$\begin{aligned} U_k &= g_n\mu_n\vec{I}_k\cdot\vec{\gamma}_k \\ &= \frac{1+\hat{\tau}_z}{2}\left[g_n\mu_n\vec{I}_k\cdot\vec{\gamma}_k^{(1)}\right]+\frac{1-\hat{\tau}_z}{2}\left[g_n\mu_n\vec{I}_k\cdot\vec{\gamma}_k^{(2)}\right] \\ &= \frac{g_n\mu_n}{2}\left[\vec{I}_k\cdot(\vec{\gamma}_k^{(1)}+\vec{\gamma}_k^{(2)})+\hat{\tau}_z\vec{I}_k\cdot(\vec{\gamma}_k^{(1)}-\vec{\gamma}_k^{(2)})\right] \end{aligned} \tag{3.11}$$

As before we take

$$\hat{m}_k=\frac{\vec{\gamma}_k^{(1)}+\vec{\gamma}_k^{(2)}}{|\vec{\gamma}_k^{(1)}+\vec{\gamma}_k^{(2)}|}\quad,\quad \hat{l}_k=\frac{\vec{\gamma}_k^{(1)}-\vec{\gamma}_k^{(2)}}{|\vec{\gamma}_k^{(1)}-\vec{\gamma}_k^{(2)}|}\quad, \tag{3.12}$$

$$\omega_k^{\|}=|\vec{I}_k|g_n\mu_n|\vec{\gamma}_k^{(1)}-\vec{\gamma}_k^{(2)}|\quad,\quad \omega_k^{\perp}=|\vec{I}_k|g_n\mu_n|\vec{\gamma}_k^{(1)}+\vec{\gamma}_k^{(2)}| \tag{3.13}$$

which gives an interaction term of the form (compare to (2.73))

$$U_k=\frac{\omega_k^{\perp}}{2}\hat{I}_k\cdot\hat{m}_k+\frac{\hat{\tau}_z}{2}\omega_k^{\|}\hat{I}_k\cdot\hat{l}_k \tag{3.14}$$

3.2.5 Contact Hyperfine Coupling Energies for $^{57}Fe^{3+}$

There is another contribution due to contact hyperfine interactions due to the presence of any ^{57}Fe nuclei in the material. As was discussed in chapter 2, this coupling is of the form (see (2.61))

$$U_p^c=g_{n_k}\mu_n A^{p\alpha\beta}S_\alpha^p I_\beta^p \tag{3.15}$$

We are going to make the approximation in what follows that the off-diagonal elements of the tensor $A^{p\alpha\beta}$ are zero. This gives the form

$$U_p^c=\omega_p^c\,\vec{I}_p\cdot\vec{S}_p \tag{3.16}$$

where $\vec{S}_p$ and $\vec{I}_p$ are the electronic and nuclear spin of the p^{th} ^{57}Fe ion respectively. Similarly to what we did with the dipolar term we write, with $\vec{S}_p^{(1)}$ and $\vec{S}_p^{(2)}$ the p^{th}

electronic spin before and after the central spin flips respectively,

$$\begin{aligned} U_p^c &= \omega_p^c \, \vec{I}_p \cdot \vec{S}_p \\ &= \frac{1+\hat{\tau}_z}{2}\left[\omega_p^c \vec{I}_p \cdot \vec{S}_p^{(1)}\right] + \frac{1-\hat{\tau}_z}{2}\left[\omega_p^c \vec{I}_p \cdot \vec{S}_p^{(2)}\right] \\ &= \frac{\omega_p^c}{2}\left[\vec{I}_p \cdot (\vec{S}_p^{(1)} + \vec{S}_p^{(2)}) + \hat{\tau}_z \vec{I}_p \cdot (\vec{S}_p^{(1)} - \vec{S}_p^{(2)})\right] \end{aligned} \tag{3.17}$$

Define

$$\hat{m}_p^c = \frac{\vec{S}_p^{(1)} + \vec{S}_p^{(2)}}{|\vec{S}_p^{(1)} + \vec{S}_p^{(2)}|} \quad , \quad \hat{l}_p^c = \frac{\vec{S}_p^{(1)} - \vec{S}_p^{(2)}}{|\vec{S}_p^{(1)} - \vec{S}_p^{(2)}|} \quad , \tag{3.18}$$

$$\omega_p^{\|c} = |\vec{I}_p| \omega_p^c |\vec{S}_p^{(1)} - \vec{S}_p^{(2)}| \quad , \quad \omega_p^{\perp c} = |\vec{I}_p| \omega_p^c |\vec{S}_p^{(1)} + \vec{S}_p^{(2)}| \tag{3.19}$$

Then we may write the interaction term in the form

$$U_p^c = \frac{\omega_p^{\perp c}}{2} \hat{I}_p \cdot \hat{m}_p^c + \frac{\hat{\tau}_z}{2} \omega_p^{\|c} \hat{I}_p \cdot \hat{l}_p^c \tag{3.20}$$

The value of the field at the nucleus of a free $^{57}Fe^{3+}$ ion due to polarization of the s electrons by the outer shell $3d$ electrons has been previously calculated and was found to be $H_c \sim 63\ T$ [99]. If we take the nuclear g-factor of the ^{57}Fe ion to be $g = 0.05$ [166], this gives a zero field longitudinal contact hyperfine coupling of

$$\omega_p^{\|c} \sim 48 \ \ MHz \quad \forall\, p \tag{3.21}$$

These completely overwhelm the dipolar coupling energies $\omega^{\|}_{k=N+1..N+8}$ and $\omega^{\perp}_{k=N+1..N+8}$, as the dipolar fields at the iron nuclei are on the order of $300 - 800$ gauss (see table 3.10).

Because of this, it is easiest to think about the "diagonal" effects of the nuclear spins in the following way. All nuclear spins in the molecule $k = 1..N+8$ are involved in dipole-dipole interactions via (3.14). However, the ^{57}Fe nuclei $k = N+1..N+8$ also are involved in contact hyperfine interactions which absolutely swamp the dipole-dipole

interactions of the ^{57}Fe nuclei. Therefore the interaction term in our Hamiltonian is

$$U = \sum_{k=1}^{N+8} \left[\frac{\omega_k^{\perp}}{2} \hat{I}_k \cdot \hat{m}_k + \frac{\hat{\tau}_z}{2} \omega_k^{||} \hat{I}_k \cdot \hat{l}_k \right] \tag{3.22}$$

where it is understood that the terms for $k = 1..N$ are the dipole-dipole terms (3.14) but the terms for $k = N+1..N+8$ are contact terms from (3.20).

3.2.6 Calculation of $\omega_k^{||}$ and $\omega_k^{\perp}$ from Knowledge of Atomic Positions

In the Fe_8 molecule, we know where all the atoms are in the molecule. This allows us to calculate what the parameters $\omega_k^{||}$ and $\omega_k^{\perp}$ are, for $k = 1..N$, via the use of (3.10) and (3.13) together with the knowledge of the directions in which the central spin object points in the two lowest lying energy levels $|+10>$ and $|-10>$. This last is calculated as follows.

The central spin Hamiltonian for Fe_8, when truncated to terms of quartic order or less in S, can be written in the presence of an external field $\vec{H}$ in the form

$$H_0 = -DS_z^2 + E\left(S_x^2 - S_y^2\right) + C(S_+^4 + S_-^4) + g\mu_B \vec{H} \cdot \vec{S} \tag{3.23}$$

as discussed in chapter 2. Here we take $D = 0.292K$, $E = 0.046K$ and $C = -2.9 \cdot 10^{-5}K$ in keeping with the findings of Wernsdorfer et.al. [51]. If we write $\vec{S}$ in spherical coordinates $S_x \to S\sin\theta\sin\phi$, $S_y \to S\cos\phi\sin\theta$ and $S_z \to S\cos\theta$ and substitute these into (3.23) it is then a simple exercise to find the angles (θ, ϕ) and therefore the quantities $\vec{s}_j$ for all the electronic spins in the molecule as functions of $\vec{H}$. We assume that the individual electronic spins are locked to the direction in which the effective central spin is pointing, with relative signs given by taking $|+10>$ and $|-10>$ to correspond to the Fe^{3+} spins being $\{\uparrow,\uparrow,\downarrow,\uparrow,\uparrow,\uparrow,\downarrow,\uparrow\}$ and $\{\downarrow,\downarrow,\uparrow,\downarrow,\downarrow,\downarrow,\uparrow,\downarrow\}$ respectively, where the labelling $1 \to 8$ corresponds to that in table 3.2. All coordinate positions are in Angstroms.

We present information on the zero field values of the $\omega_k^{||}$ in the following manner. We label all the nuclei in the molecule such that the hydrogen atoms are tagged 1..120, the bromines 121..128, the nitrogens 129..146, the irons 147..154, the carbons 155..190 and the oxygens 191..213 (the positions of each of these are given in section 2.5). For each nucleus there are a variety of possible isotopes. Shown in figure (3.1) are the values for the zero field $\omega_k^{||}$ shown as functions of nucleus label for ^1H, ^{79}Br, ^{14}N, ^{57}Fe, ^{13}C and ^{17}O.

This information is presented in a different manner in figures (3.2) through (3.13). In these figures we bin the hyperfine values, in each case assuming that the isotope in question represents 100% of the element in question (for example, in figure (3.2) we assume a 100% concentration of ^1H).

3.2.7 Calculation of the Orthogonality Blocking Parameter κ

The Prokof'ev and Stamp theory [20] contains a parameter κ which is defined to be

$$\kappa = -\ln\left[\prod_{k=1}^{N+8}\cos\beta_k\right] \tag{3.24}$$

where

$$\cos 2\beta_k = -\hat{\gamma}_k^{(1)}\cdot\hat{\gamma}_k^{(2)} \tag{3.25}$$

Since we know what the fields $\vec{\gamma}_k^{(1)}$ and $\vec{\gamma}_k^{(2)}$ are, we may calculate the β_k and then κ. If the nuclear spin in question is a ^{57}Fe then because the contact hyperfine field is so much larger than the dipolar field ($63\,T$ and $\sim 0.3-0.8\,T$ respectively) we can take

$$\cos 2\beta_k = -\hat{S}_k^{(1)}\cdot\hat{S}_k^{(2)} \tag{3.26}$$

Note that for all nuclei β_k is a strong function of the externally applied DC magnetic field. Shown in figures 3.14 and 3.15 is κ as a function of a DC field applied in the x

Nuclear Label	x	y	z
Fe1	5.737857	.064911	1.58115
Fe2	6.912112	-2.210346	3.04665
Fe3	6.656427	3.323106	.33915
Fe4	5.327499	2.408451	3.17265
Fe5	5.198078	-2.412666	-3.16665
Fe6	3.616621	2.196296	-2.98815
Fe7	3.888089	-3.321701	-.29265
Fe8	4.848748	-.043695	-1.54365

Table 3.2: Positions of the iron ions, units in Angstoms.

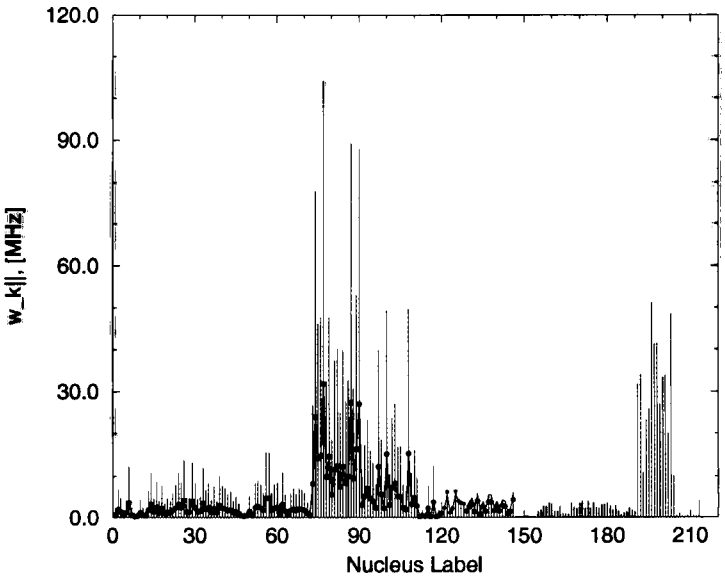

Figure 3.1: $\omega_k^{||}$ for all nuclei in Fe_8. Labeling is as indicated in the text. The dots represent values for ^2H (labels 1..120), ^{81}Br (labels 121..128), and ^{15}N (labels 129..146).

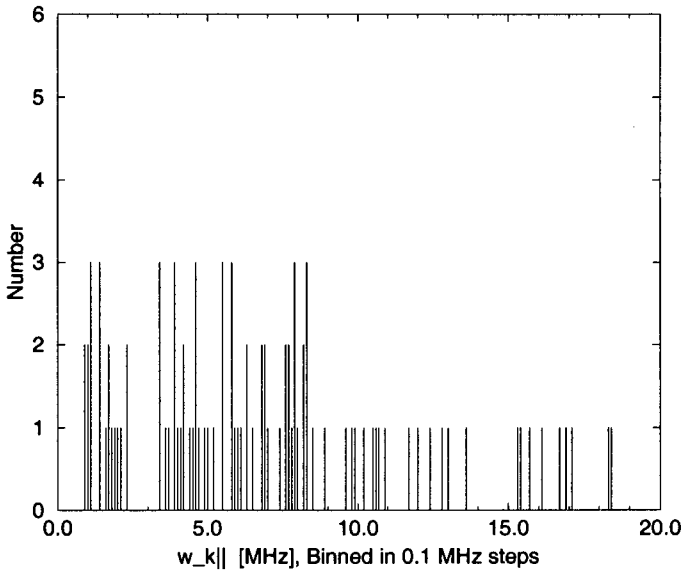

Figure 3.2: ^1H, emphasizing low end of the spectrum.

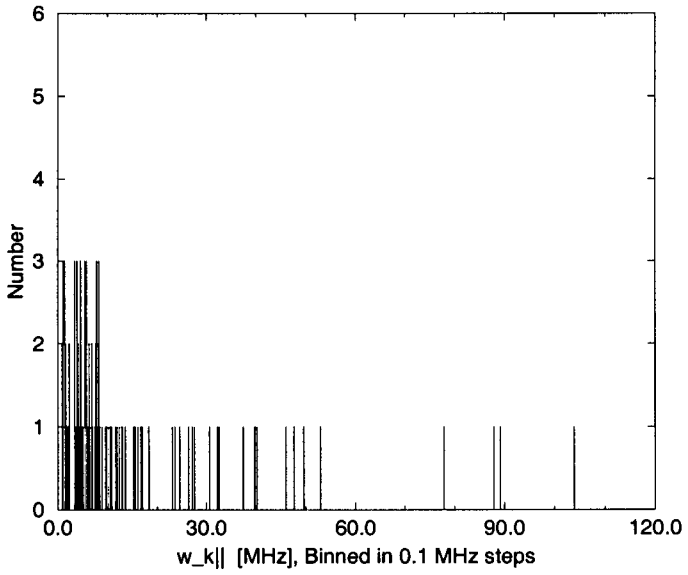

Figure 3.3: ^1H, high end of the spectrum.

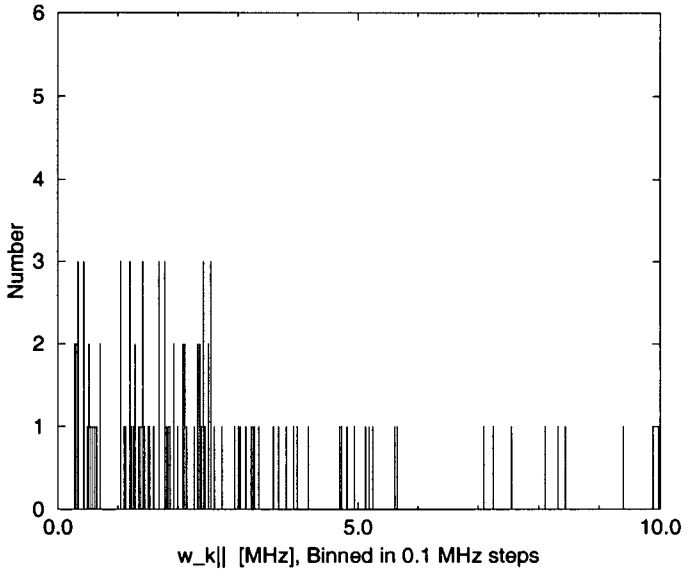

Figure 3.4: ^2H, low end of spectrum.

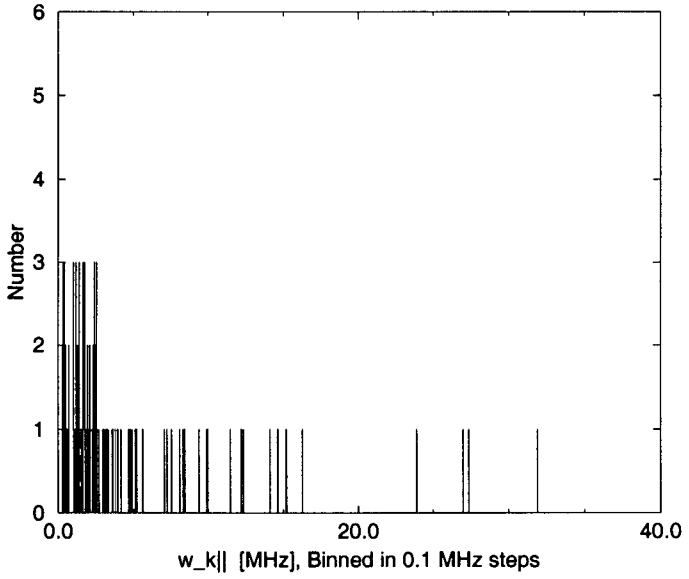

Figure 3.5: ^2H, entire spectrum.

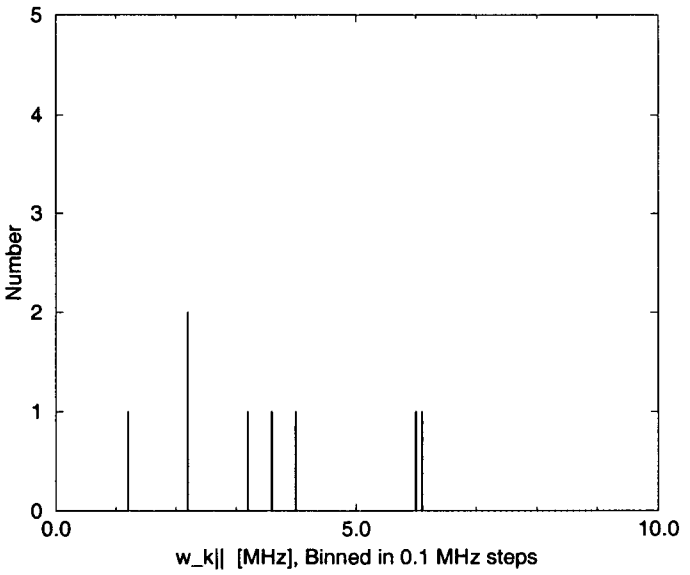

Figure 3.6: ^{79}Br, entire spectrum.

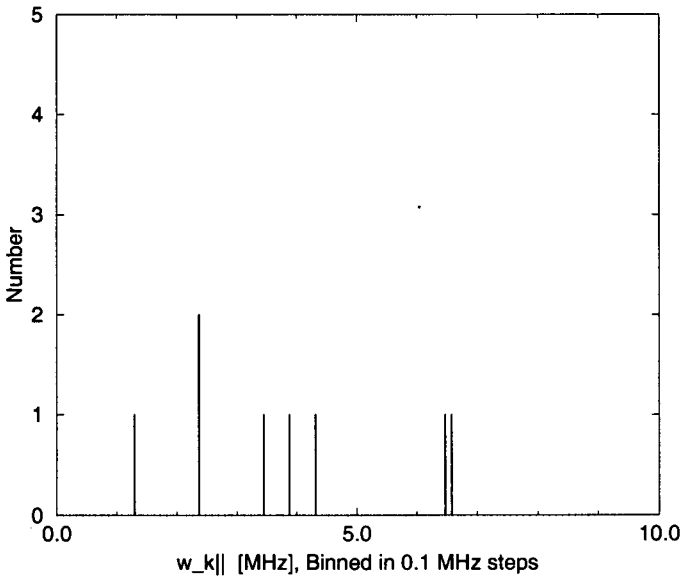

Figure 3.7: ^{81}Br, entire spectrum.

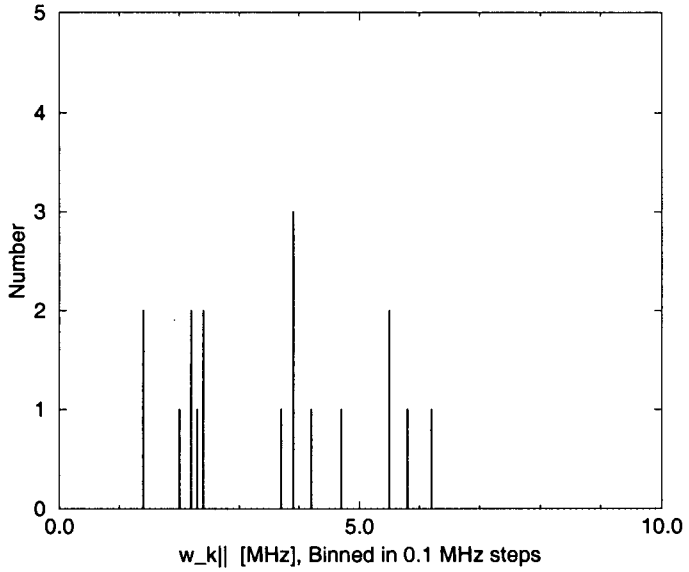

Figure 3.8: ^{14}N, entire spectrum.

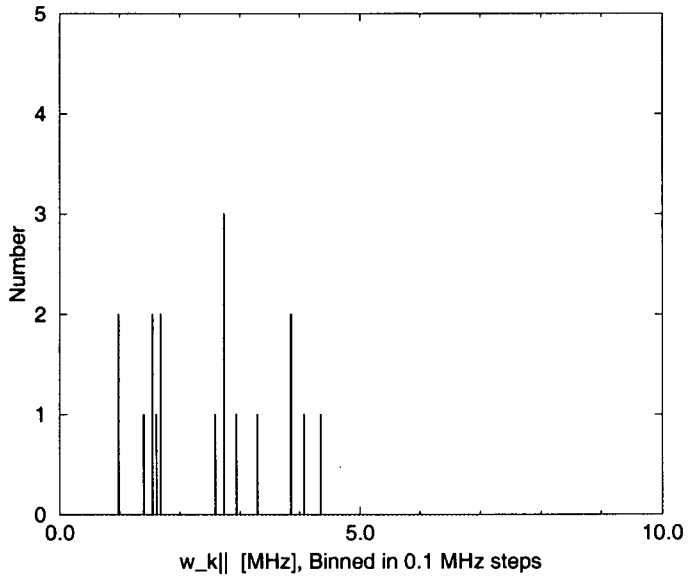

Figure 3.9: ^{15}N, entire spectrum.

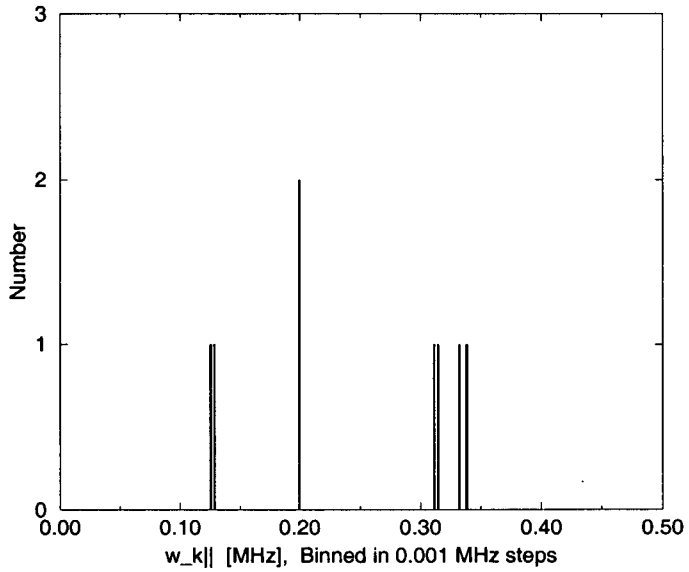

Figure 3.10: ^{57}Fe, entire spectrum.

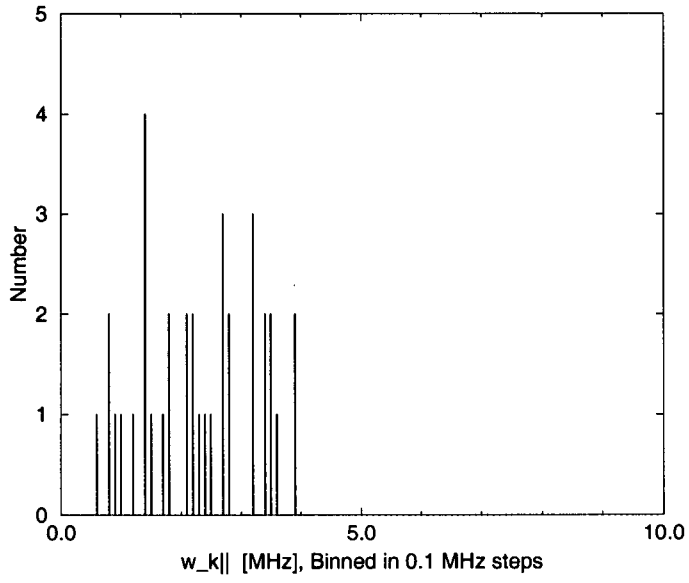

Figure 3.11: ^{13}C, entire spectrum.

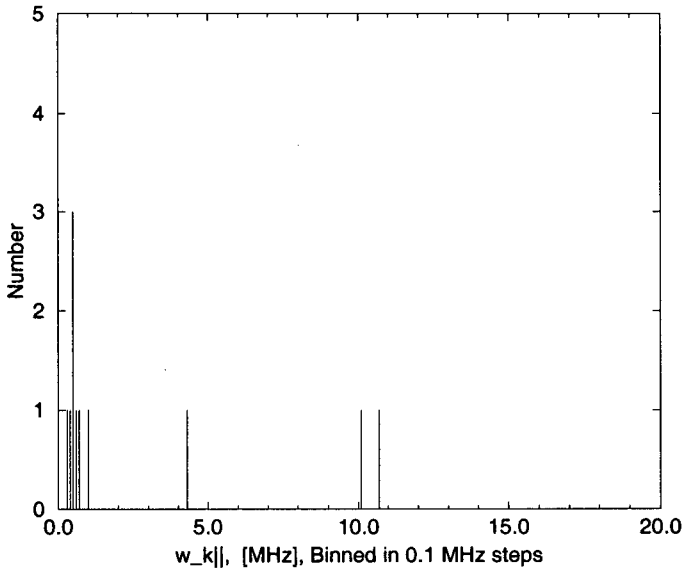

Figure 3.12: ^{17}O, low end of spectrum.

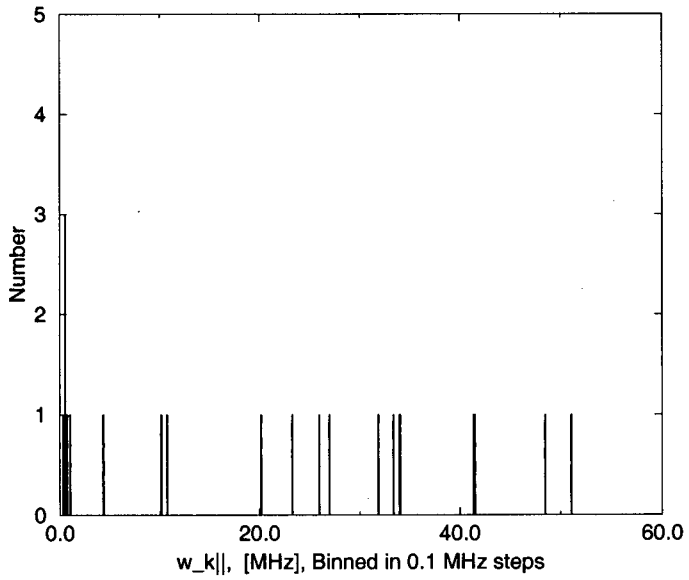

Figure 3.13: ^{17}O, entire spectrum.

direction for an Fe_8 molecule with 100% concentrations of ^1H, ^{81}Br, ^{14}N, ^{57}Fe, ^{13}C and ^{17}O. We shall call this material Fe_8^{max}. Note that the contribution to κ from the presence of ^{57}Fe is minimal because the minima of $\vec{S}$ don't change much as functions of field.

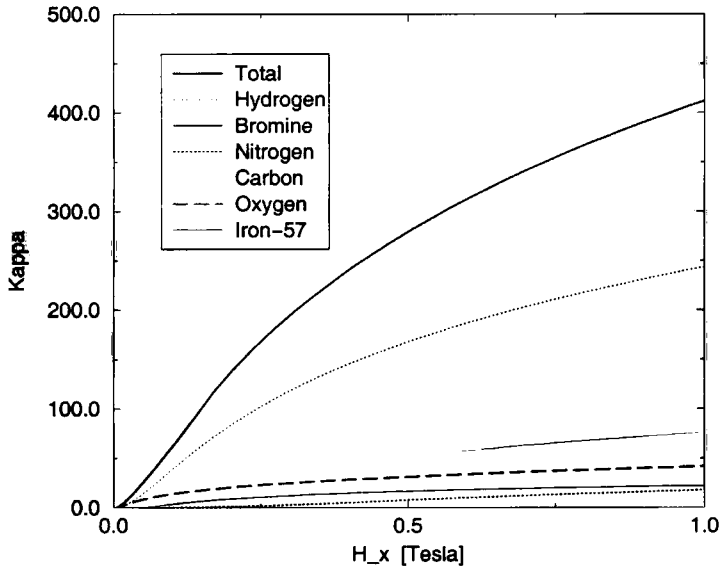

Figure 3.14: The orthogonality blocking parameter κ over a large range of external fields applied in the x direction for the Fe_8^{max} material.

3.2.8 Calculation of E_0

The quantity E_0 is related to the spread in energy space due to the presence of many nuclear spins. From (3.14) we see that in the absence of quadrupolar or contact interactions and in zero external magnetic field the k^{th} nuclear spin has $2I+1$ equally spaced energy levels between $\pm\omega_k^{||}/2$. In the presence of an applied field the situation is similar. The variance in the distribution of the energy levels for this nucleus is defined to be $\sigma^2 =< E^2 > - < E >^2$ where E is the energy of the nucleus. If we make the approximation that the probability of each level being occupied is identical (effectively

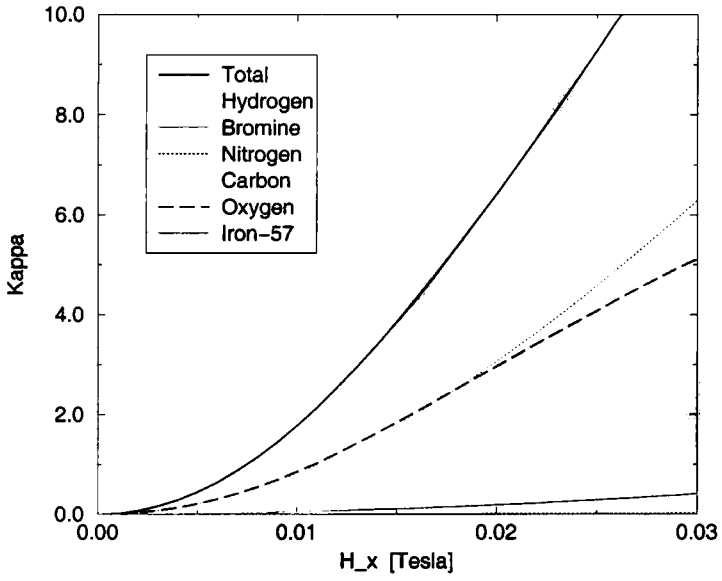

Figure 3.15: The parameter κ for small values of external field applied in the x direction for the Fe_8^{max} material.

an infinite spin temperature approximation) then $< E >= 0$ and

$$\begin{aligned} \sigma^2 &= < E^2 >= \sum_{i=1}^{2I+1} p_i E_i^2 = \frac{1}{2I+1} \frac{\omega_k^{\|^2}}{4} \left[\sum_{i=1}^{2I+1} \left(\frac{2I - 2(i-1)}{2I} \right)^2 \right] \\ &= \frac{I+1}{12I} \omega_k^{\|^2} \end{aligned} \tag{3.27}$$

Here $p_i = \frac{1}{2I+1}$ is the probability of the i^{th} energy level of the nucleus being occupied. The total variance of the distribution of all nuclear levels is then given by the central limit theorem as

$$\bar{\sigma}^2 = \sum_{k=1}^{N} \sigma_j^2 \tag{3.28}$$

where N is the total number of nuclear spins. In the case of Fe_8 this gives

$$4\bar{\sigma}^2 = \sum_{k_{1_H}} \left(\omega_{k_{1_H}}^{\|^2} \right) + \frac{2}{3} \sum_{k_{2_H}} \left(\omega_{k_{2_H}}^{\|^2} \right) + \frac{5}{9} \sum_{k_{79_{Br}}} \left(\omega_{k_{79_{Br}}}^{\|^2} \right)$$

$$+ \frac{5}{9}\sum_{k_{81_{Br}}}\left(\omega^{||}_{k_{81_{Br}}}{}^2\right) + \frac{2}{3}\sum_{k_{14_N}}\left(\omega^{||}_{k_{14_N}}{}^2\right) + \sum_{k_{15_N}}\left(\omega^{||}_{k_{15_N}}{}^2\right)$$
$$+ \sum_{k_{13_C}}\left(\omega^{||}_{k_{13_C}}{}^2\right) + \frac{7}{15}\sum_{k_{17_O}}\left(\omega^{||}_{k_{17_O}}{}^2\right) + \sum_{k_{57_{Fe}}}\left(\omega^{||}_{k_{57_{Fe}}}{}^2\right)$$
$$+ \sum_{k_{57_{Fe}}}\left(\omega^{||c}_{k_{57_{Fe}}}{}^2\right) \tag{3.29}$$

The relation between the halfwidth of the distribution W, E_0 and $\bar{\sigma}$ is found via

$$e^{-\epsilon^2/2\bar{\sigma}^2} = e^{-2\epsilon^2/E_0^2} = e^{-\epsilon^2/W^2} \tag{3.30}$$

or

$$E_0^2 = 4\bar{\sigma}^2 = 2W^2 \tag{3.31}$$

The full width of the distribution is

$$\mathcal{W} = 2W = \sqrt{2}E_0 \tag{3.32}$$

The width $\mathcal{W}$ is of course a function of the isotopic concentration in a particular Fe_8 sample. For example, if we pick the easiest case where we have 100% concentrations of ^1H, ^{79}Br, ^{14}N, ^{16}O, ^{56}Fe and ^{12}C (we shall call this material Fe_{8*}) then we find, in zero external field in the point dipole approximation, that

$$\sum_{k_{1_H}=1}^{120}\omega^{||}_{k_{1_H}}{}^2 = 71887.545\ [MHz]^2$$
$$\frac{5}{9}\sum_{k_{79_{Br}}=1}^{8}\omega^{||}_{k_{79_{Br}}}{}^2 = 70.27\ [MHz]^2$$
$$\frac{2}{3}\sum_{k_{14_N}=1}^{18}\omega^{||}_{k_{14_N}}{}^2 = 181.8184\ [MHz]^2 \tag{3.33}$$

which gives

$$E_0 = 268.6\ MHz \quad , \quad \mathcal{W} = 379.8\ MHz = 18.23\ mK \tag{3.34}$$

What we have calculated here is an intrinsic linewidth due to spreading caused by the presence of the nuclear spins in the molecule. Note that these numbers are sensitive to which isotopic concentrations we choose for our molecule. This should lead to a clear isotope effect in this intrinsic linewidth which is easy to calculate using our formalism (it just amounts to changing the spin and nuclear moments for the new isotopes). For example, if we replace all the hydrogen nuclei by deuterium (we shall call this material Fe_{8D}), which has $I = 1$ and $g = 0.857354\ \mu_n$, we find that

$$\sum_{k_{1_H}=1}^{120} {\omega^{||}_{k_{1_H}}}^2 \to \frac{2}{3} \sum_{k_{2_H}=1}^{120} {\omega^{||}_{k_{1_H}}}^2 \left(\frac{0.857354}{2.79255}\right)^2 \tag{3.35}$$

which gives

$$E_0 = 69.06\ MHz \quad , \quad \mathcal{W} = 97.67\ MHz = 4.687\ mK \tag{3.36}$$

Note as well that because $\omega^{||}_k$ is a function of external magnetic field (because the minima of $\vec{S}$ are), the linewidth E_0 is also a function of external magnetic field. Shown in figure 3.16 is the intrinsic linewidth as a function of a field applied in the x direction due to specific isotopes for 100% concentrations of these isotopes (in other words, if the isotope is ^1H we are assuming that all the hydrogens are ^1H; if the isotope is ^{81}Br then we assume all the bromines are ^{81}Br, etc.).

The addition of ^{57}Fe to the mix significantly changes the value of the linewidth. This is because the contact hyperfine coupling energies ω^c_k are large. Let us define the material $^{57}Fe_8$ to be identical to Fe_{8*} in every way except that every iron ion is a ^{57}Fe ion; ie. 100% concentrations of ^1H, ^{79}Br, ^{15}N, ^{57}Fe, ^{12}C and ^{16}O. Then the contribution to the zero-field linewidth coming from the contact terms is, via (3.29),

$$\sum_{k=1}^{8} {\omega^{||c}_k}^2 \sim \sum_{k=1}^{8} 2304\ MHz^2 = 18432\ MHz^2 \tag{3.37}$$

which is a significant fraction of the contribution from the protons (see (3.33)). Addition

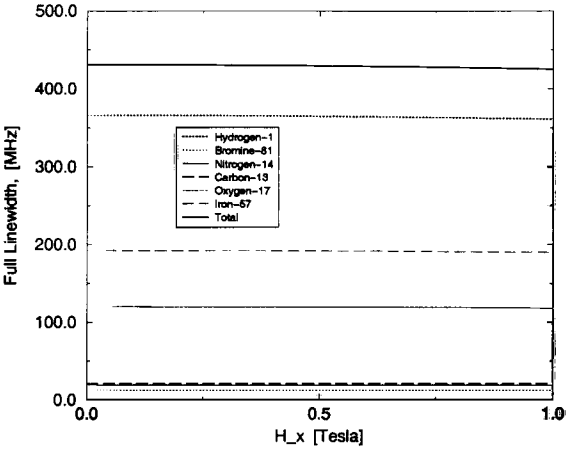

Figure 3.16: Intrinsic linewidth $\mathcal{W}$ due to particular isotopes as a function of H_x for 100% concentrations of these isotopes. Note that $\omega_k^{||}$ and therefore $\mathcal{W}$ drops slowly with field. This effect comes about because as the external field is raised, the two minima of the central spin complex are forced closer together (no longer are they antiparallel). The curve shown as "total" is the total result for a material containing 100% of the isotopes shown.

of this term gives the linewidth

$$E_0 = 301.0\ MHz \quad , \quad \mathcal{W} = 425.6\ MHz = 20.43\ mK \tag{3.38}$$

which is 1.12 times the linewidth for Fe_{8*}.

3.2.9 Calculation of Topological Decoherence Parameters $\vec{A}^k_{N,D}$ and λ

If we assume for the moment that there are no ^{57}Fe nuclei in our molecule, then we can see from (2.89) that all parameters can be calculated in the expression for $\vec{A}^k_{N,D}$. In addition, if we assume that the contact interaction is of the form (3.16) then we can calculate the general form for $\vec{A}^k_{N,D}$. Furthermore, we see that these are not functions of the external magnetic field, unlike the orthogonality blocking parameters. Because the coupling energies ω_k are much less than the energy scale Ω_0, all of the $\vec{A}^k_{N,D}$ turn out to

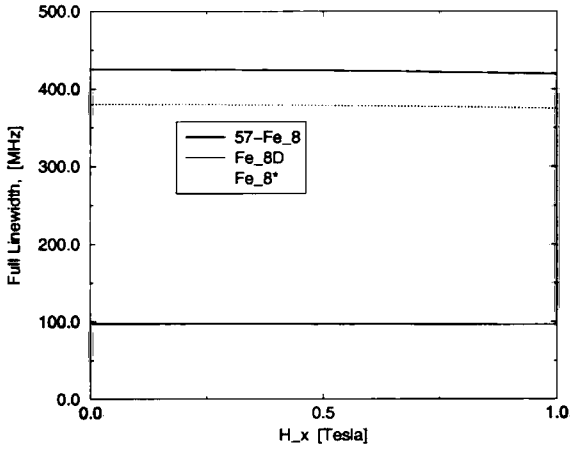

Figure 3.17: Intrinsic linewidth $\mathcal{W}$ as a function of H_x for Fe_{8*}, Fe_{8D} and $^{57}Fe_8$.

be small (see figure 3.18).

The topological decoherence parameter λ [20] is given in this limit by

$$\lambda = \frac{1}{2}\sum_{k=1}^{N+8} |\vec{A}^k_{N,D}|^2 \tag{3.39}$$

This is found to be $\lambda = 4.45 \cdot 10^{-5}$, $\lambda = 8.87 \cdot 10^{-5}$ and $\lambda = 1.38 \cdot 10^{-5}$ for the Fe_{8*}, $^{57}Fe_8$ and Fe_{8D} materials respectively. Note that these are extremely small! λ is roughly the number of nuclear spins flipped per central spin tunneling event.

3.3 Using Free Fe^{3+} Hartree-Fock Wavefunctions to Model Actual Spin Distributions

In this section we attempt to do a little better than the point dipole approximation. Here what we shall do is instead of treating the magnetic dipole nature of the Fe^{3+} ion as a point we shall assume that it is "spread out" in a way dictated by the spatial spread of the Fe^{3+} wavefunction.

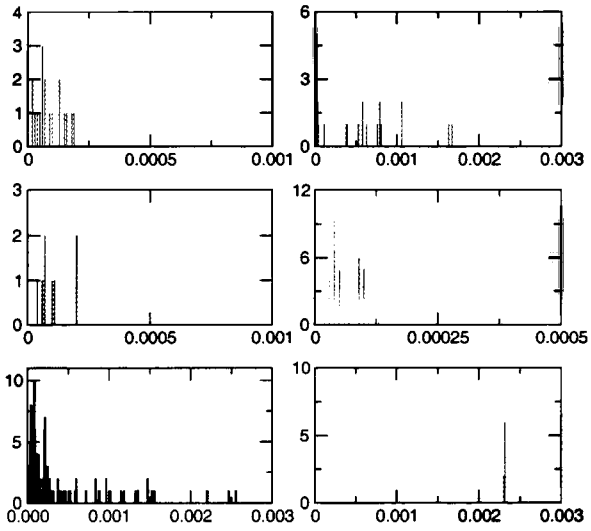

Figure 3.18: Binned topological decoherence parameters $|\vec{A}^k_{N,D}|$ for all nuclei, assuming 100% concentrations of (clockwise from bottom left) ^1H, ^{79}Br, ^{14}N, ^{17}O, ^{13}C and ^{57}Fe, using the point dipole approximation. The bin width here is 0.0001; plotted on the x axis is $|\vec{A}^k_{N,D}|$ and on the y axis "number of nuclei". Note that the contribution to $|\vec{A}^k_{N,D}|$ from ^{57}Fe is almost entirely from the contact interaction.

Specifically, we are interested in the five $3d$ electrons in the Fe^{3+} ion (its electronic configuration is of course $[Ar]3d^5$). In a free Fe^{3+} ion, these five d electrons are spin-aligned due to the Hund's rule which asks for maximized spin angular momentum giving a total spin of 5/2. We can write down what the field at a point $\vec{r}$ is due to a Fe^{3+} ion at the origin; it is

$$\vec{\gamma}(\vec{r}) = -\frac{\mu_0}{4\pi}\sum_{j=1}^{5}\int d^3\vec{r}'\psi_j^\dagger(\vec{r}')\psi_j(\vec{r}')\frac{1}{|\vec{r}-\vec{r}'|^3}\left[\vec{m}_j - \frac{3}{|\vec{r}-\vec{r}'|^2}(\vec{m}_j\cdot[\vec{r}-\vec{r}'])(\vec{r}-\vec{r}')\right] \quad (3.40)$$

where

$$\vec{m} = g_{Fe}\mu_B\vec{s} = g_{Fe}\mu_B\frac{1}{2}\hat{s} \quad (3.41)$$

because the spin of each d electron is one half. Here the sum over j is over the five d electrons, and the integration $\vec{r}'$ is over all space. We assume that the wavefunctions $\psi_j(\vec{r}')$ are properly normalized.

Since the total angular momentum of the Fe^{3+} in its ground state is zero, the spin of the d electrons is distributed spherically and therefore we can approximate (3.40) by the expression

$$\vec{\gamma}(\vec{r}) = -\frac{\mu_0}{4\pi}\int d^3\vec{r'}\psi^\dagger(\vec{r'})\psi(\vec{r'})\frac{1}{|\vec{r}-\vec{r'}|^3}\left[\vec{m} - \frac{3}{|\vec{r}-\vec{r'}|^2}(\vec{m}\cdot[\vec{r}-\vec{r'}])(\vec{r}-\vec{r'})\right] \quad (3.42)$$

where $\psi(\vec{r'})$ represents the spin distribution around the iron ion.

The wavefunction $\psi(\vec{r'})$ for a free Fe^{3+} ion has been previously calculated using a Hartree-Fock approach [100]. We can fit the numerical results of this calculation using the form

$$\psi(r) = (A + Br + Cr^2)r^2\exp(-r/d) \quad (3.43)$$

where

$$A = -60.786097 \quad , B = 68.94202\frac{1}{\dot{A}} \quad , C = -22.48757\frac{1}{\dot{A}^2} \quad , d = 0.282745\dot{A} \quad (3.44)$$

This is the form we shall use in the following. Note that it is not exactly correct as immersion in the crystal will change the electronic distributions and therefore the spin distribution. However it is clear that using the free Hartree-Fock wavefunction here will give more realistic results than the point dipole approximation (it remains to see how different these are).

The integrations in (3.42) are handled as follows. Instead of trying to do these analytically, we shall do them numerically using the following technique. We pick P points out of the $|\psi(r)|^2$ distribution to represent one iron ion wavefunction. This will be exact as $P \to \infty$. Then

$$\vec{\gamma}(\vec{r}) \approx -\frac{\mu_0}{4\pi}\frac{1}{P}\sum_{p=1}^{P}\frac{1}{|\vec{r}-\vec{r}_p|^3}\left[\vec{m} - \frac{3}{|\vec{r}-\vec{r}_p|^2}(\vec{m}\cdot[\vec{r}-\vec{r}_p])(\vec{r}-\vec{r}_p)\right] \quad (3.45)$$

Convergence is reached for $P \sim 80$ for all nuclei (the closer to an iron nucleus a proton is, the larger number of points are required for convergence). If the point dipole approximation were exact, then $P = 1$ would suffice (one point). Shown in figure (3.20)

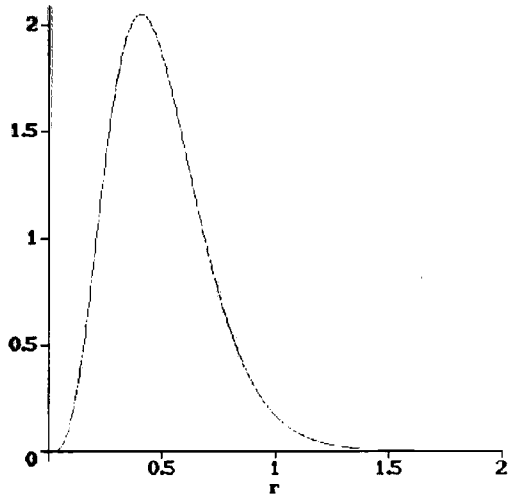

Figure 3.19: Hartree-Fock results for the free Fe^{3+} wavefunction.

is a comparison of the $\omega_k^{\|}$ values obtained using the point dipole approximation and the Hartree-Fock method, using the Fe_8^{max} material (100% ^1H, ^{81}Br, ^{14}N, ^{17}O, ^{13}C and ^{57}Fe). We find that the lower energy nuclei are not affected by the change to the Hartree-Fock wavefunction. Only the higher energy nuclei are affected significantly. This however could be meaningful for several quantities of interest, primarily the intrinsic linewidth $\mathcal{W}$ which is sensitive to the higher energy couplings. Shown in figures (3.21) through (3.32) are the binned hyperfine values obtained using the Hartree-Fock wavefunction–these are the HF analogues of figures (3.2) through (3.13).

We may recalculate κ for the new fields generated in this approach. Shown in figures (3.33) and (3.34) are the analogues of figures (3.14) and (3.15), using the Hartree-Fock wavefunctions instead of the point dipole approximation. We may repeat our calculations for the intrinsic linewidth as well. With our new field values the numbers for Fe_{8*}

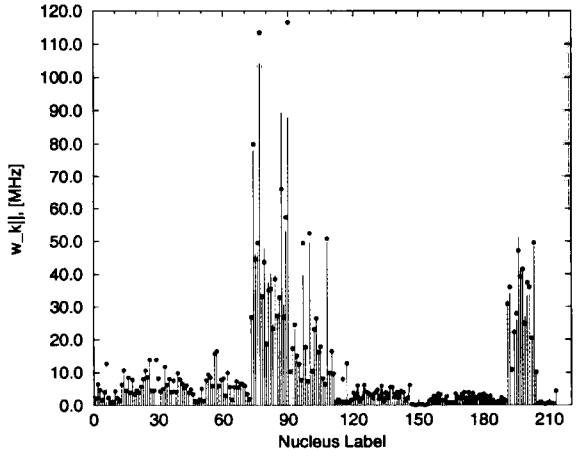

Figure 3.20: Comparison of point dipole and Hartree-Fock methods; zero field $\omega_k^{||}$ values in Fe_8^{max}. The Hartree-Fock results are shown as dots.

are, in zero external field using the Hartree-Fock wavefunction approximation,

$$\sum_{k_H=1}^{120} {\omega_{k_H}^{||}}^2 = 71512.22[MHz]^2$$

$$\frac{5}{9}\sum_{k_{Br}=1}^{8} {\omega_{k_{Br}}^{||}}^2 = 71.21[MHz]^2$$

$$\frac{2}{3}\sum_{k_N=1}^{18} {\omega_{k_N}^{||}}^2 = 180.93[MHz]^2 \tag{3.46}$$

which gives

$$E_0 = 258.9\ MHz \quad , \quad \mathcal{W} = 366.2\ MHz = 17.57\ mK \tag{3.47}$$

Note that the values obtained are quite close to those obtained using the point dipole approximation. Note however that this did not have to be the case, as some of the larger $\omega_k^{||}$ increased and some decreased in going from the point dipole to Hartree-Fock approximations.

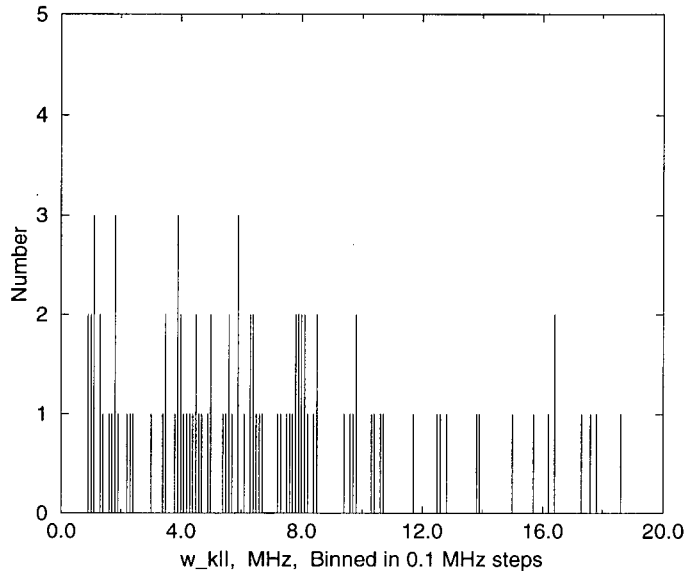

Figure 3.21: ^1H, Hartree-Fock, emphasizing low end of the spectrum.

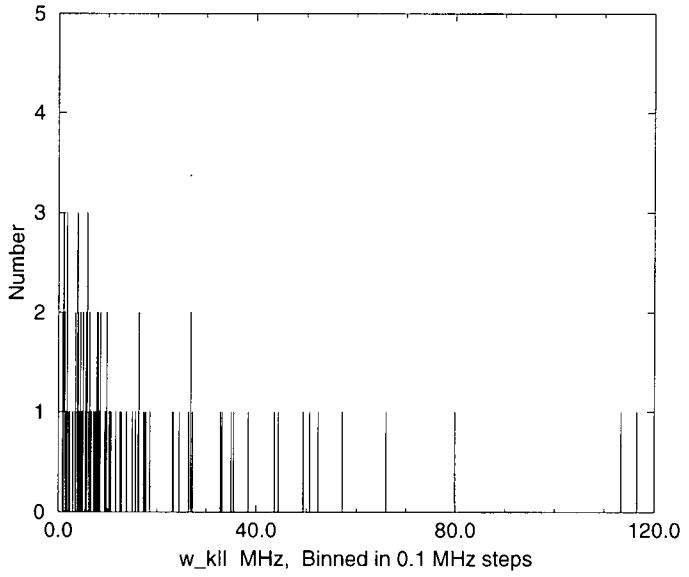

Figure 3.22: ^1H, Hartree-Fock, high end of the spectrum.

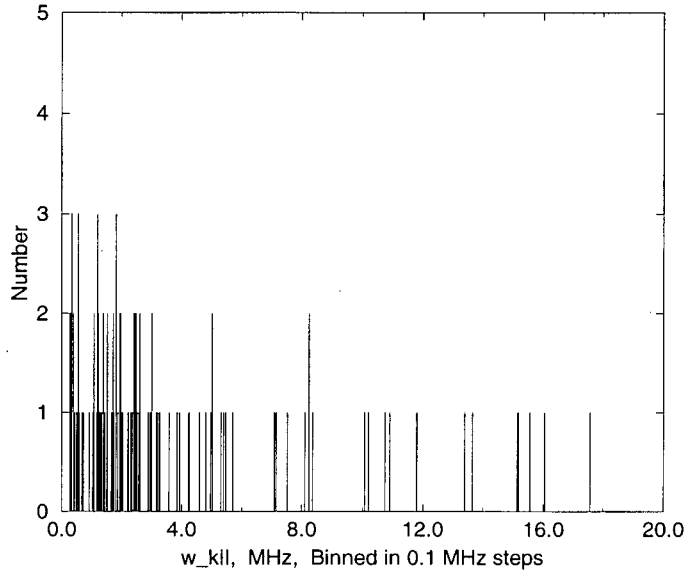

Figure 3.23: ^2H, Hartree-Fock, low end of spectrum.

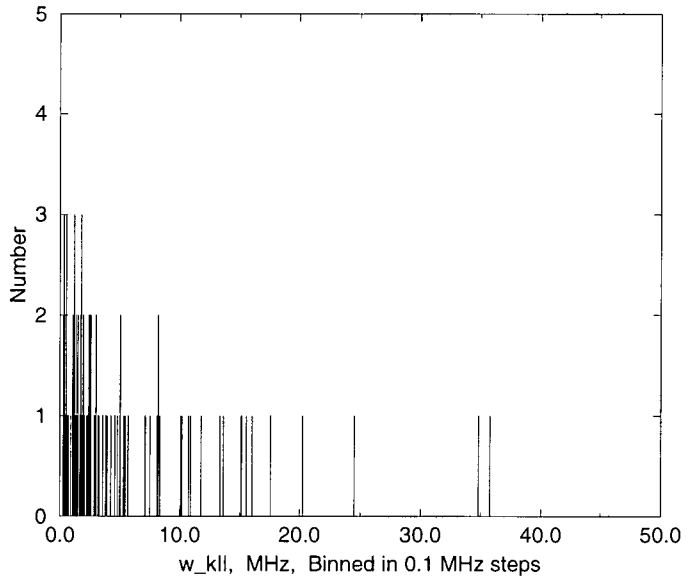

Figure 3.24: ^2H, Hartree-Fock, entire spectrum.

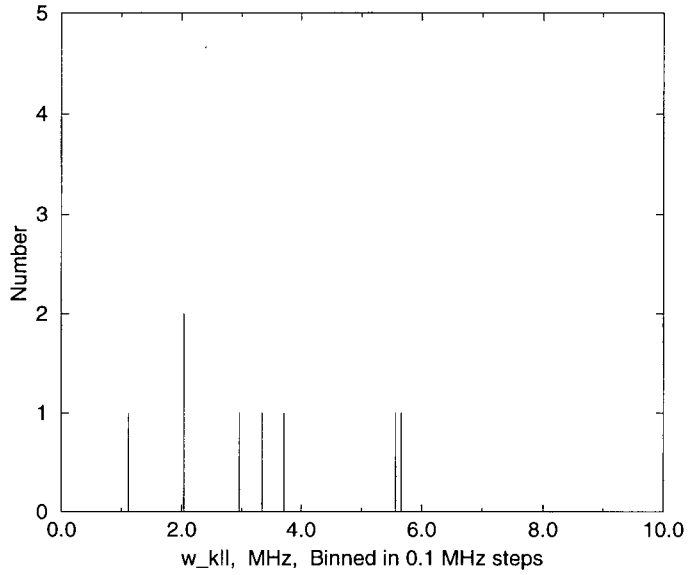

Figure 3.25: ^{79}Br, Hartree-Fock, entire spectrum.

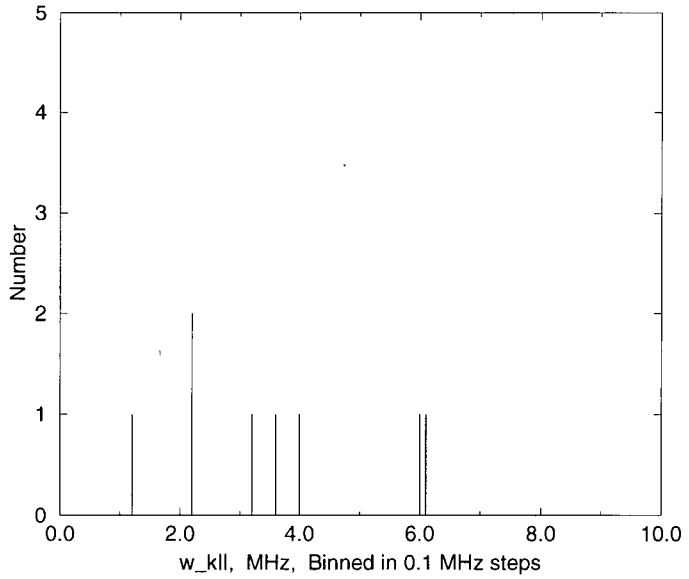

Figure 3.26: ^{81}Br, Hartree-Fock, entire spectrum.

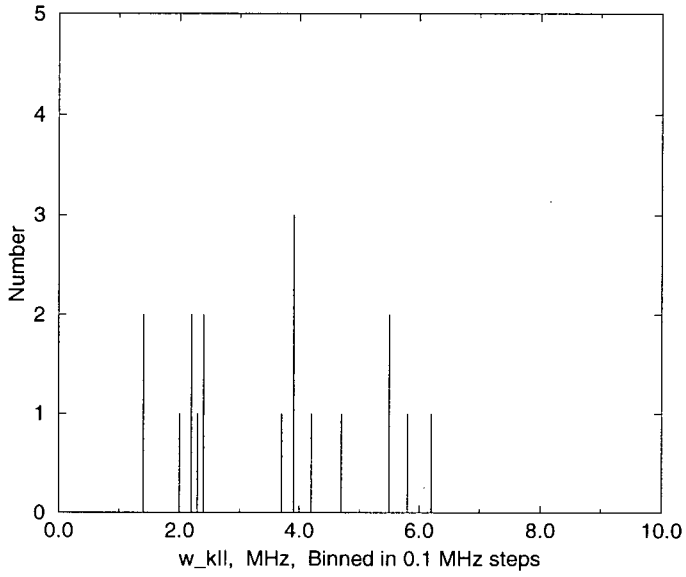

Figure 3.27: ^{14}N, Hartree-Fock, entire spectrum.

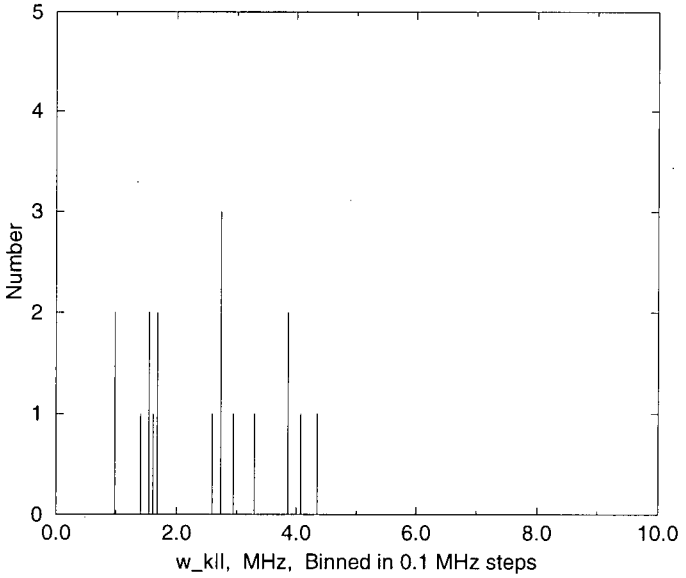

Figure 3.28: ^{15}N, Hartree-Fock, entire spectrum.

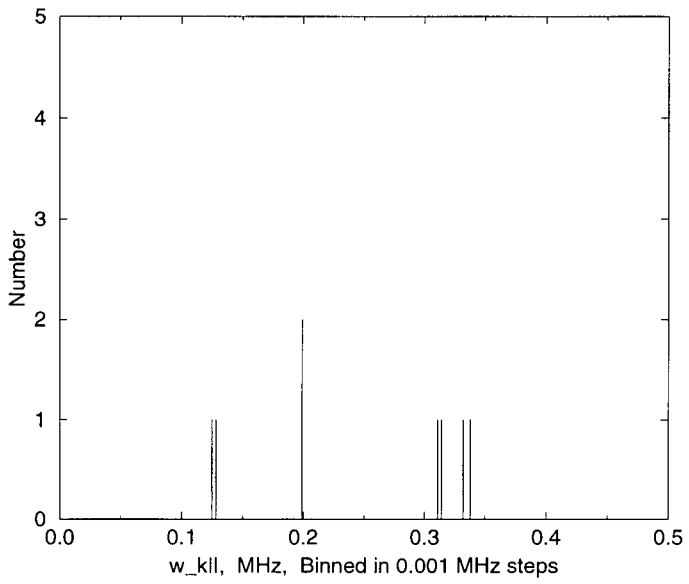

Figure 3.29: ^{57}Fe, Hartree-Fock, entire spectrum.

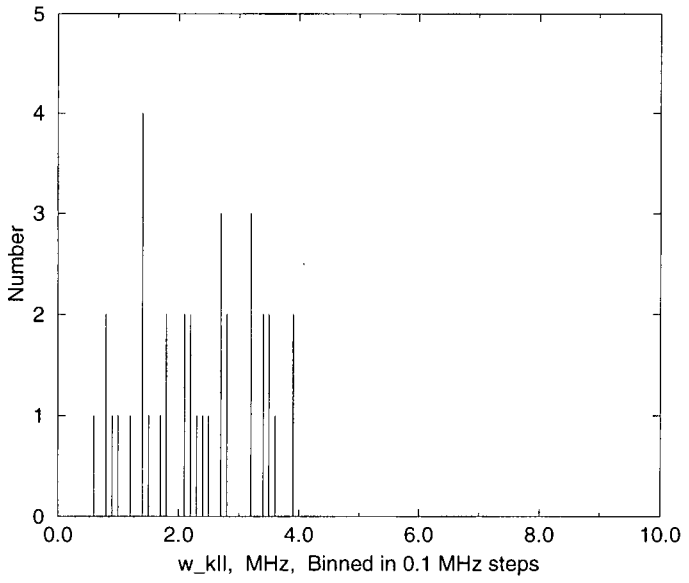

Figure 3.30: ^{13}C, Hartree-Fock, entire spectrum.

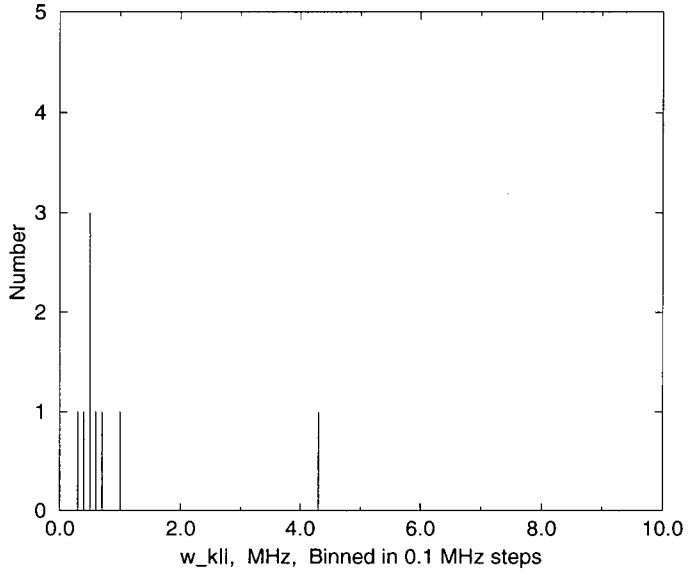

Figure 3.31: ^{17}O, Hartree-Fock, low end of spectrum.

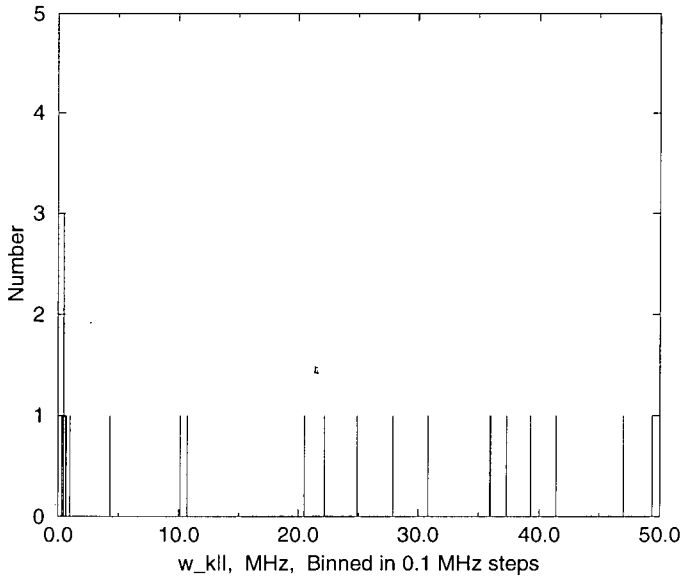

Figure 3.32: ^{17}O, Hartree-Fock, entire spectrum.

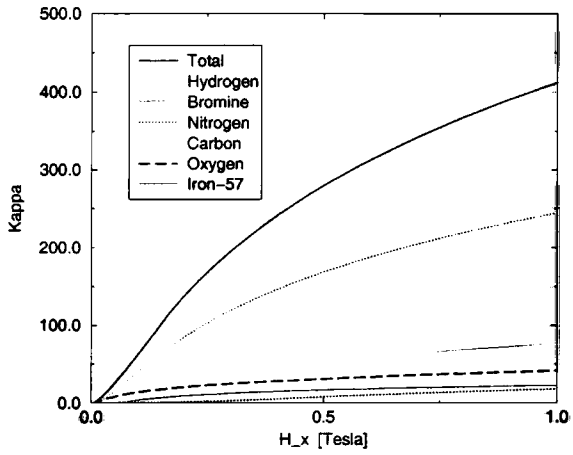

Figure 3.33: The orthogonality blocking parameter κ as a function of H_x in the Hartree-Fock wavefunction picture.

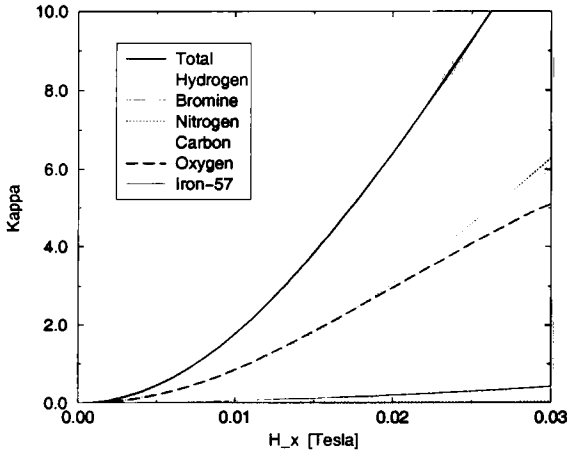

Figure 3.34: The orthogonality blocking parameter κ as a function of H_x in the Hartree-Fock wavefunction picture, focusing on small fields.

As before, we can redo this calculation with any isotopic concentration. Here we treat the case where all protons are replaced by deuterium. This gives

$$\sum_{k_H=1}^{120} {\omega_{k_H}^{||}}^2 \rightarrow \frac{2}{3} \sum_{k_D=1}^{120} {\omega_{k_H}^{||}}^2 \left(\frac{0.857354}{2.79255}\right)^2 \tag{3.48}$$

which gives

$$E_0 = 68.32\ MHz \quad , \quad \mathcal{W} = 96.62\ MHz = 4.676\ mK \tag{3.49}$$

which is very close to the point dipole result.

Similarly to what we did in the point dipole case we compute the intrinsic linewidth $\mathcal{W}$ as a function of H_x for the three materials Fe_{8*}, Fe_{8D} and $^{57}Fe_8$ and show the results in figure (3.35).

We conclude by recalculating the topological decoherence parameters. Using our new field values we find that $\lambda = 4.23 \cdot 10^{-5}$, $8.73 \cdot 10^{-5}$, and $1.35 \cdot 10^{-5}$ for the Fe_{8*}, $^{57}Fe_8$ and Fe_{8D} materials respectively. Values for $|\vec{A}^k_{N,D}|$ are shown in figure 3.36.

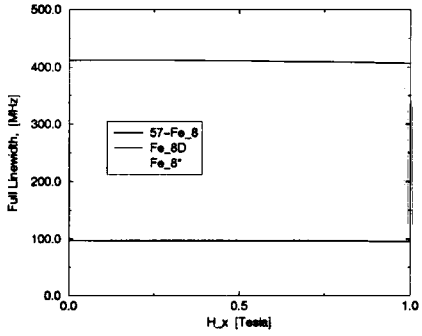

Figure 3.35: Intrinsic linewidth $\mathcal{W}$ as a function of H_x for Fe_{8*}, Fe_{8D} and $^{57}Fe_8$ in the Hartree-Fock picture.

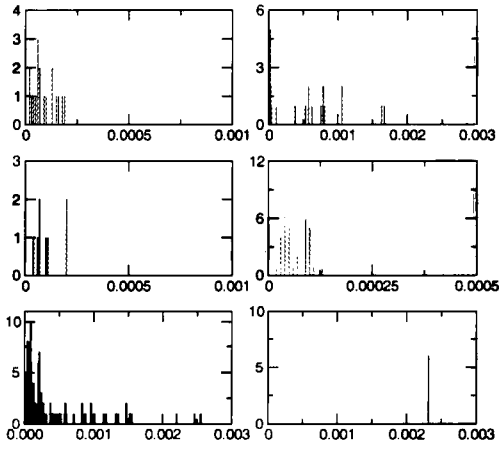

Figure 3.36: Binned topological decoherence parameters $|\vec{A}^{k}_{N,D}|$ for all nuclei, assuming 100% concentrations of (clockwise from bottom left) ^{1}H, ^{79}Br, ^{14}N, ^{17}O, ^{13}C and ^{57}Fe, using the Hartree Fock approximation. The bin width here is 0.0001; plotted on the x axis is $|\vec{A}^{k}_{N,D}|$ and on the y axis "number of nuclei". Note that the contribution to $|\vec{A}^{k}_{N,D}|$ from ^{57}Fe is almost entirely from the contact interaction.

3.4 Tables of Nuclear Positions, Fields at Nuclei and Hyperfine Coupling Energies

In what follows we shall be considering only the case where the external magnetic field is zero for clarity of presentation. In these tables we indicate the locations of each ion in the molecule, presented in Cartesian coordinates (x,y,z) in Angstroms. As well we present the magnitude of the field at each nucleus due to the eight iron spins (note that in zero external field this magnitude is the same for both configurations of the central spin complex) both for the point dipole approximation and the Hartree-Fock approximation. We also present the hyperfine coupling energies $\omega_k^{||}$ for both point dipole and Hartree-Fock cases ($\omega_k^{\perp}$ is zero when the external field is zero).

Here we have chosen the following isotopes in order to convert from field to energy units: ^1H, ^{79}Br, ^{14}N, ^{57}Fe, ^{13}C, and ^{17}O.

Nuclear Label	x	y	z	$\|\vec{\gamma}^{(1)}\|$ $[T]$ (P.D.)	$\omega^{\|\|}$ $[MHz]$ (P.D.)	$\|\vec{\gamma}^{(1)}\|$ $[T]$ (H.F.)	$\omega^{\|\|}$ $[MHz]$ (H.F.)
H1	10.8	3.58	1.92	.0509	2.167	.0521	2.22
H2	9.38	2.12	1.38	.161	6.854	.152	6.476
H3	9.6	2.61	-.66	.112	4.757	.112	4.76
H4	10.3	4.3	-.173	.0422	1.797	.0415	1.772
H5	9.07	5.17	-1.88	.0978	4.168	.0943	4.016
H6	7.29	4.78	-2.37	.284	12.055	.298	12.676
H7	8.03	6.8	-1.13	.0556	2.365	.0577	2.46
H8	9.54	6.61	-.0732	.0242	1.026	.0246	1.052
H9	9.52	7.18	2.03	.0277	1.175	.0274	1.172
H10	8.24	6.26	2.61	.0988	4.209	.101	4.292
H11	9.94	5.34	3.62	.054	2.301	.054	2.304
H12	10.6	5.61	2.36	.0347	1.477	.0345	1.472
H13	3.4	5.03	3.38	.15	6.383	.149	6.344
H14	3.68	4.34	4.85	.256	10.939	.251	10.708
H15	5.91	5.96	5.19	.106	4.532	.104	4.444
H16	5.79	5.65	3.57	.2	8.519	.2	8.532
H17	7.62	4.27	7.01	.0927	3.945	.0924	3.944
H18	5.88	4.07	6.59	.179	7.632	.183	7.824
H19	10.8	-.193	5.82	.0807	3.436	.0821	3.504
H20	10.2	-1.76	6.24	.109	4.626	.109	4.628
H21	11	-2.19	4.4	.0924	3.938	.0924	3.944
H22	10.3	-1.09	3.45	.137	5.832	.136	5.776
H23	6.01	1.8	7.08	.186	7.915	.189	8.056
H24	7.02	1.88	6.14	.249	10.634	.249	10.628
H25	2.87	.67	5.39	.195	8.311	.201	8.58
H26	3.72	2.35	5.84	.321	13.67	.326	13.88
H27	1.63	2.12	3.77	.11	4.68	.108	4.592
H28	2.01	.981	2.96	.109	4.656	.107	4.572
H29	6.79	-2.16	-5.9	.307	13.088	.326	13.94
H30	7.63	-.505	-5.25	.195	8.328	.192	8.196

Table 3.3: Data for Hydrogen.

Nuclear Label	x	y	z	$\|\vec{\gamma}^{(1)}\|$ [T] (P.D.)	$\omega^{\|}$ [MHz] (P.D.)	$\|\vec{\gamma}^{(1)}\|$ [T] (H.F.)	$\omega^{\|}$ [MHz] (H.F.)
H31	8.61	-1.06	-2.96	.104	4.423	.101	4.316
H32	8.83	-2.19	-3.93	.118	5.023	.118	5.032
H33	6.52	-4.3	-5.18	.277	11.756	.277	11.784
H34	6.88	-5.19	-3.84	.153	6.517	.148	6.312
H35	4.57	-5.64	-3.71	.194	8.255	.19	8.1
H36	4.24	-5.96	-5.37	.0985	4.201	.0971	4.136
H37	4.52	-3.93	-6.69	.174	7.418	.178	7.568
H38	2.79	-4.09	-7.02	.0938	4.004	.0962	4.1
H39	3.43	-1.79	-6.2	.234	9.961	.232	9.884
H40	4.47	-1.73	-7.13	.179	7.632	.186	7.924
H41	4.21	5.46	-3	.163	6.943	.156	6.664
H42	3.44	5.64	-4.65	.131	5.581	.127	5.404
H43	.303	.862	-3.45	.145	6.198	.144	6.136
H44	-.515	1.95	-4.2	.0924	3.938	.0919	3.916
H45	.385	1.99	-6	.116	4.964	.115	4.916
H46	-.312	.338	-5.82	.0798	3.4	.0807	3.44
H47	1.19	-7.11	-2.18	.0331	1.409	.0326	1.392
H48	.406	-6.44	-1.32	.0274	1.169	.0272	1.16
H49	.0679	-5.37	-3.3	.042	1.785	.0425	1.812
H50	1.72	-5.16	-3.29	.124	5.287	.118	5.048
H51	1.75	-6.92	.851	.0333	1.423	.0321	1.372
H52	3.39	-5.77	1.73	.193	8.218	.18	7.676
H53	6.48	-3.54	6.51	.21	8.967	.221	9.436
H54	8.07	-3.5	6.48	.186	7.915	.199	8.492
H55	8.47	-1.16	7.11	.14	5.949	.138	5.904
H56	6.89	-1.24	5.94	.364	15.498	.368	15.716
H57	3.61	1.38	-5.96	.361	15.383	.387	16.488
H58	2.01	1.26	-7.1	.137	5.862	.14	5.96
H59	2.3	3.54	-6.3	.188	8.014	.184	7.856
H60	3.84	3.65	-6.53	.195	8.302	.192	8.188

Table 3.4: Data for Hydrogen.

Nuclear Label	x	y	z	$\|\vec{\gamma}^{(1)}\|$ $[T]$ (P.D.)	$\omega^{\|\|}$ $[MHz]$ (P.D.)	$\|\vec{\gamma}^{(1)}\|$ $[T]$ (H.F.)	$\omega^{\|\|}$ $[MHz]$ (H.F.)
H61	.623	-2.88	.611	.08	3.407	.0718	3.056
H62	1.95	-1.71	.255	.251	10.708	.232	9.884
H63	1.75	-4.88	2.25	.129	5.505	.132	5.612
H64	.617	-5.23	.629	.0481	2.05	.0439	1.868
H65	8.72	-5.09	3.6	.137	5.85	.131	5.604
H66	9.24	-4.12	5.09	.165	7.021	.171	7.284
H67	6.92	-5.64	4.83	.131	5.57	.129	5.52
H68	6.26	-5.47	3.17	.163	6.965	.157	6.708
H69	1.1	4.07	-4.8	.16	6.83	.154	6.572
H70	1.72	4.94	-3.24	.142	6.053	.139	5.916
H71	.272	-2.64	-1.92	.0859	3.662	.0828	3.532
H72	-.208	-4.22	-1.48	.0453	1.927	.0446	1.904
H73	8.05	-.671	4.23	.622	26.468	.629	26.844
H74	7.98	-2.98	2.43	1.82	77.829	1.87	79.864
H75	5.76	-3.43	3.78	1.08	46.004	1.04	44.464
H76	7.86	3.23	1.98	1.12	47.703	1.16	49.468
H77	7.11	2.81	-1.02	2.44	103.95	2.65	113.492
H78	6.67	5.16	.275	.758	32.286	.779	33.22
H79	3.8	2.86	2.4	1.12	47.649	1.02	43.636
H80	7.07	3.95	4.32	.432	18.397	.439	18.688
H81	4.83	.935	4.13	.877	37.415	.823	35.084
H82	5.68	-.979	-4.05	.943	40.203	.833	35.512
H83	3.59	-3.76	-4.2	.579	24.676	.547	23.344
H84	6.76	-3.06	-2.37	.934	39.825	.903	38.492
H85	2.49	.701	-4.22	.647	27.551	.64	27.288
H86	4.9	3.6	-3.77	.765	32.557	.772	32.876
H87	2.54	2.85	-2.31	2.09	89.109	1.55	66.084
H88	3.73	-5.2	-.498	.72	30.655	.631	26.856
H89	2.7	-2.96	-1.82	1.24	53.006	1.34	57.224
H90	3.58	-2.99	1.29	2.06	87.885	2.74	116.536

Table 3.5: Data for Hydrogen.

Nuclear Label	x	y	z	$\|\vec{\gamma}^{(1)}\|$ $[T]$ (P.D.)	$\omega^{\|\|}$ $[MHz]$ (P.D.)	$\|\vec{\gamma}^{(1)}\|$ $[T]$ (H.F.)	$\omega^{\|\|}$ $[MHz]$ (H.F.)
H91	8.78	.0423	5.01	.231	9.837	.242	10.316
H92	7.92	2.02	3.9	.403	17.188	.406	17.348
H93	5.34	-1.03	3.83	.542	23.124	.575	24.52
H94	6.2	-4.09	1.14	.371	15.776	.354	15.064
H95	8.76	3.34	2.78	.303	12.891	.293	12.54
H96	3.29	.719	1.14	.187	7.979	.182	7.756
H97	7.21	3.45	-1.76	.934	39.767	1.16	49.388
H98	7.9	-.733	1.32	.432	18.425	.415	17.656
H99	7.15	6.11	.465	.181	7.7	.172	7.32
H100	5.05	3.95	1.35	1.16	49.5	1.23	52.368
H101	2.81	3.16	2.39	.242	10.279	.246	10.492
H102	2.66	.832	-1.47	.556	23.686	.544	23.176
H103	5.85	1.45	-3.24	.638	27.153	.622	26.464
H104	2.57	-2.02	-3.9	.392	16.747	.38	16.208
H105	5.99	-.381	-4.76	.396	16.94	.42	17.892
H106	7.21	-.719	-1.14	.185	7.888	.193	8.208
H107	2.99	-4.75	-5.18	.15	6.398	.152	6.488
H108	5.45	-3.95	-1.35	1.17	49.671	1.19	50.76
H109	7.68	-3.16	-2.34	.249	10.567	.23	9.792
H110	4.29	4.05	-1.14	.378	16.101	.387	16.488
H111	1.72	-.0423	-5.01	.227	9.663	.226	9.652
H112	7.97	7.92	7.83	.0219	.934	.0222	.948
H113	2.53	6.18	7.14	.0427	1.817	.0427	1.824
H114	6.65	6.66	9.57	.0265	1.133	.027	1.152
H115	3.35	-6.11	-.465	.182	7.755	.187	7.992
H116	7.55	5.74	10.6	.0242	1.033	.0246	1.048
H117	1.73	-3.34	-2.78	.291	12.401	.3	12.828
H118	2.95	8.36	4.44	.0227	.969	.0229	.976
H119	3.85	7.44	5.43	.0389	1.662	.0396	1.688
H120	9.69	-.874	.24	.0877	3.742	.0891	3.804

Table 3.6: Data for Hydrogen.

Nuclear Label	x	y	z	$\|\vec{\gamma}^{(1)}\|$ $[T]$ (P.D.)	$\omega^{\|\|}$ $[MHz]$ (P.D.)	$\|\vec{\gamma}^{(1)}\|$ $[T]$ (H.F.)	$\omega^{\|\|}$ $[MHz]$ (H.F.)
Br1	10.2	2.65	5.67	.0521	2.215	.0537	2.293
Br2	3.37	-2.3	4.91	.137	5.856	.142	6.063
Br3	5.2	7.11	7.43	.0289	1.23	.0298	1.273
Br4	.265	-2.64	-5.66	.0516	2.201	.0535	2.279
Br5	7.09	2.28	-4.91	.14	5.957	.145	6.167
Br6	7.64	-4.75	.0737	.091	3.878	.0943	4.015
Br7	1.06	1.08	-.26	.0816	3.481	.0844	3.604
Br8	3.7	5.53	.2	.0734	3.132	.076	3.243

Table 3.7: Data for Bromine.

Nuclear Label	x	y	z	$\lvert\vec{\gamma}^{(1)}\rvert\ [T]$ (P.D.)	$\omega^{\lvert\rvert}\ [MHz]$ (P.D.)	$\lvert\vec{\gamma}^{(1)}\rvert\ [T]$ (H.F.)	$\omega^{\lvert\rvert}\ [MHz]$ (H.F.)
N1	8.52	-1.05	5.1	.0547	2.332	.053	2.26
N2	8.73	-3.03	3.35	.0891	3.796	.0849	3.62
N3	6.48	-3.78	4.49	.112	4.765	.108	4.61
N4	8.87	3.76	1.97	.0486	2.073	.0479	2.04
N5	8.09	3.55	-.923	.138	5.892	.14	5.95
N6	7.75	5.71	.515	.0333	1.419	.0392	1.67
N7	3.45	3.02	3.18	.0917	3.908	.0807	3.44
N8	6.55	4.24	4.89	.0525	2.242	.0577	2.46
N9	4.83	1.44	4.98	.13	5.526	.132	5.63
N10	5.7	-1.4	-4.92	.13	5.533	.136	5.78
N11	3.96	-4.13	-4.86	.0582	2.476	.0525	2.24
N12	7	-3.14	-3.23	.0929	3.964	.0884	3.77
N13	2.01	1.12	-5.06	.0568	2.423	.0638	2.72
N14	4.07	3.86	-4.4	.1	4.283	.0896	3.82
N15	1.77	2.92	-3.2	.0927	3.947	.083	3.54
N16	2.73	-5.67	-.426	.0342	1.459	.045	1.92
N17	1.7	-3.67	-1.94	.0532	2.268	.0605	2.58
N18	2.48	-3.44	.983	.146	6.228	.145	6.18

Table 3.8: Data for Nitrogen.

Nuclear Label	x	y	z	$\|\vec{\gamma}^{(1)}\|$ $[T]$ (P.D.)	$\omega^{\|\|}$ $[MHz]$ (P.D.)	$\|\vec{\gamma}^{(1)}\|$ $[T]$ (H.F.)	$\omega^{\|\|}$ $[MHz]$ (H.F.)
C1	10	-1.15	5.49	.0352	1.499	.0357	1.52
C2	10.2	-1.83	4.1	.0422	1.797	.0441	1.88
C3	8.52	-4.37	4.1	.0659	2.807	.069	2.94
C4	6.95	-4.98	4.11	.0638	2.72	.0615	2.62
C5	7.21	-3.19	6.03	.0833	3.553	.0805	3.43
C6	7.76	-1.57	6.15	.0762	3.254	.0758	3.23
C7	9.72	3.16	1.34	.035	1.487	.035	1.49
C8	9.51	3.41	-.168	.035	1.491	.0342	1.46
C9	8.22	4.94	-1.55	.0633	2.703	.0615	2.62
C10	8.46	6.13	-.569	.0217	.925	.0221	.941
C11	8.82	6.22	2	.0206	.878	.0213	.908
C12	9.69	5.27	2.58	.0194	.829	.0198	.844
C13	3.94	4.46	3.98	.0837	3.572	.0819	3.49
C14	5.59	5.22	4.4	.0598	2.553	.0615	2.62
C15	6.6	3.79	6.3	.0507	2.162	.0518	2.21
C16	6.18	2.13	6.23	.0812	3.456	.0821	3.5
C17	3.43	1.57	5.12	.0936	3.993	.0919	3.92
C18	2.45	1.85	3.65	.0521	2.224	.0495	2.11
C19	7.07	-1.45	-5.07	.0919	3.915	.088	3.75
C20	8.09	-1.88	-3.72	.0521	2.216	.0528	2.25
C21	6.36	-4.53	-4.28	.0851	3.631	.0821	3.5
C22	4.7	-5.22	-4.55	.0568	2.416	.0577	2.46
C23	3.83	-3.64	-6.35	.0507	2.162	.0488	2.08
C24	4.26	-2.07	-6.27	.0758	3.233	.0795	3.39
C25	2.73	1.66	-6.12	.0753	3.205	.0748	3.19
C26	3.2	3.26	-5.96	.0805	3.432	.0823	3.51
C27	3.5	4.96	-3.95	.0643	2.739	.0643	2.74
C28	.382	1.66	-4.01	.0432	1.835	.0418	1.78
C29	1.88	4.27	-3.84	.0666	2.837	.0687	2.93
C30	.49	1.26	-5.37	.0361	1.536	.038	1.62
C31	1.25	-6.23	-1.68	.0153	.652	.0147	.627
C32	1.13	-5.13	-2.69	.0253	1.081	.0249	1.06
C33	.645	-3.34	-1.37	.0298	1.273	.0307	1.31
C34	1.4	-2.74	.183	.0551	2.348	.0558	2.38
C35	1.68	-4.91	1.25	.0425	1.814	.0434	1.85
C36	2.44	-5.92	.938	.0333	1.424	.0331	1.41

Table 3.9: Data for Carbon.

Nuclear Label	x	y	z	$\|\vec{\gamma}^{(1)}\|$ $[T]$ (P.D.)	$\omega^{\|\|}$ $[MHz]$ (P.D.)	$\|\vec{\gamma}^{(1)}\|$ $[T]$ (H.F.)	$\omega^{\|\|}$ $[MHz]$ (H.F.)
FE1	5.72	.0651	1.58	.00729	.311	.00729	.311
FE2	6.9	-2.21	3.05	.00467	.199	.00467	.199
FE3	6.65	3.34	.339	.003	.128	.003	.128
FE4	5.31	2.41	3.18	.00793	.338	.00793	.338
FE5	5.19	-2.43	-3.17	.00779	.332	.00779	.332
FE6	3.61	2.2	-2.99	.00467	.199	.00467	.199
FE7	3.89	-3.33	-.293	.00293	.125	.00293	.125
FE8	4.84	-.0439	-1.55	.00737	.314	.00737	.314

Table 3.10: Data for Iron.

Nuclear Label	x	y	z	$\|\vec{\gamma}^{(1)}\|$ $[T]$ (P.D.)	$\omega^{\|\|}$ $[MHz]$ (P.D.)	$\|\vec{\gamma}^{(1)}\|$ $[T]$ (H.F.)	$\omega^{\|\|}$ $[MHz]$ (H.F.)
O1	6.9	1.68	3.29	.746	31.831	.699	29.8
O2	5.4	-1.44	2.99	.798	34.036	.877	37.4
O3	5.57	-3.6	1.31	.253	10.783	.249	10.6
O4	4.14	.682	1.88	.544	23.202	.518	22.1
O5	7.59	-.53	2.12	.608	25.926	.671	28.6
O6	5.8	3.68	1.76	1.2	51.071	1.06	45
O7	6.14	1.37	.185	.969	41.303	.931	39.7
O8	4.5	-1.34	-.115	.973	41.493	.978	41.7
O9	3	.503	-2.03	.633	26.96	.612	26.1
O10	5.13	1.44	-2.94	.783	33.367	.887	37.8
O11	3.65	-1.68	-3.24	.798	33.975	.877	37.4
O12	6.5	-.649	-1.85	.471	20.113	.483	20.6
O13	4.74	-3.71	-1.76	1.14	48.459	1.15	49.2
O14	4.94	3.55	-1.29	.239	10.154	.251	10.7
O100	8.98	8.16	7.79	.0121	.516	.012	.512
O20	1.58	6.01	7.14	.0246	1.046	.0258	1.1
O30	-1.02	6.85	5.61	.012	.51	.0116	.493
O40	11.4	7.23	9.35	.00868	.37	.00901	.384
O50	6.85	6.23	10.6	.0155	.662	.0153	.651
O60	3.56	8.15	4.43	.0182	.775	.0174	.741
O70	9.32	5.56	10.5	.0139	.593	.0134	.571
O80	1.11	8.53	4.67	.0115	.492	.0116	.496
O90	8.96	-1.17	.278	.101	4.302	.0973	4.15

Table 3.11: Data for Oxygen.

Chapter 4

An Introduction to the Generalized Landau-Zener Problem

An introduction to the standard Landau-Zener problem is presented. Three methods of solution are considered; one involves solving directly for the wavefunctions of the two-level system, the second is a perturbation expansion in the tunneling term and the third uses a complex analysis technique usually referred to as Dychne's formula. We demonstrate that it is possible to solve a more general version of the simple Landau-Zener Hamiltonian and present the solutions (see [102] for a complementary analysis).

4.1 Introduction to and Exact Solution of the Landau-Zener Problem

Consider a two-level system (TLS) with time-dependent Hamiltonian

$$H(t) = v\,t\,\hat{\sigma}_z + \Delta\,\hat{\sigma}_x \tag{4.1}$$

where $\{\hat{\sigma}\}$ are the Pauli matrices. This rather generic effective description was first considered by Landau [103], Zener [104] and Stuckelberg [105]. Landau and Stuckelberg used this Hamiltonian to model the evolution of two atoms scattering off each other, while Zener used it to model the evolution of the electronic states of a bi-atomic molecule. It has since been used in a large number of different contexts; chemical reaction kinetics [106], biophysics [107], examination of the solar neutrino puzzle [108], aspects of nuclear magnetic resonance [109], behaviour of atoms in photon fields [110], surface scattering [111], electric breakdown in solids [112] and many more. The reason for its wide usage is evident. There are many real physical systems that for one reason or another can be

modeled as two level systems–either they really are two level systems (for example, the spin Hilbert space of a spin 1/2 particle) or they can be mapped to one (for example, the $\mathcal{O}(DS)$ low energy effective Hamiltonian derived in chapter 2). It is often useful to know how these systems respond to an externally applied time-dependent perturbation. It is clear that the simplest effective description of a two level system coupled to a time dependent perturbation is that given in (4.1). We have sketched the energy levels of this Hamiltonian as functions of time in figure 4.1.

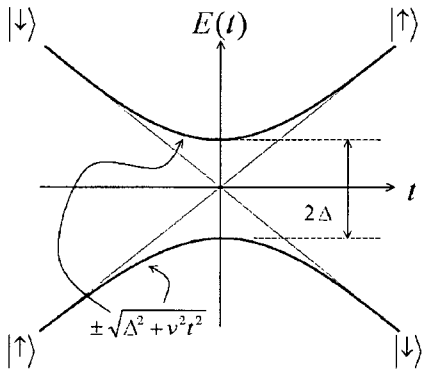

Figure 4.1: Energy levels of the Landau-Zener Hamiltonian. Shown are both the eigenstates of $\hat{\sigma}_z$, which are linear in time, and the eigenstates of $H(t)$, $E_{\pm}(t) = \pm(\Delta^2+v^2t^2)^{1/2}$.

One of the most useful features of the description (4.1) is that one can solve it exactly, in the sense that one can solve for the wavefunctions explicitly as functions of time. In order get a feel for the model, we shall outline in the following how these wavefunctions are extracted.

Insertion of (4.1) into the Schrodinger equation (we choose a system of units such

that $\hbar = 1$)

$$i\frac{d}{dt}\begin{pmatrix}\psi_a\\ \psi_b\end{pmatrix} = H(t)\begin{pmatrix}\psi_a\\ \psi_b\end{pmatrix} \tag{4.2}$$

yields

$$\begin{aligned} i\frac{d\psi_a}{dt} &= vt\psi_a + \Delta\psi_b \\ i\frac{d\psi_b}{dt} &= \Delta\psi_a - vt\psi_b \end{aligned} \tag{4.3}$$

eliminating ψ_a allows us to write

$$\ddot{\psi}_b + \left(v^2t^2 + \Delta^2 - iv\right)\psi_b = 0 \tag{4.4}$$

where overdots denote derivatives with respect to t. This is the equation for a parabolic cylinder function. It has two solutions which may be written

$$\begin{aligned} \psi_b^{(1)} &= \frac{1}{\sqrt{t}}W_{\frac{1}{4}-\frac{i\Delta^2}{4v},\frac{1}{4}}\left(ivt^2\right) \\ \psi_b^{(2)} &= \frac{1}{\sqrt{t}}W_{-\frac{1}{4}+\frac{i\Delta^2}{4v},\frac{1}{4}}\left(-ivt^2\right) \end{aligned} \tag{4.5}$$

where W is the Whittaker function [113]. If we consider the asymptotic forms of these solutions as $t \to -\infty$, we find that

$$\begin{aligned} |\psi_b^{(1)}|^2 &\overset{t\to-\infty}{\longrightarrow} 1 \\ |\psi_b^{(2)}|^2 &\overset{t\to-\infty}{\longrightarrow} 0 \end{aligned} \tag{4.6}$$

This indicates that the choice of one of the two solutions is equivalent to the choice of an initial condition on the wavefunction ψ_b. The analysis of the other wavefunction ψ_a proceeds in an identical manner; solving

$$\ddot{\psi}_a + \left(v^2t^2 + \Delta^2 + iv\right)\psi_a = 0 \tag{4.7}$$

gives two solutions

$$\psi_a^{(1)} = \frac{1}{\sqrt{t}} W_{\frac{1}{4}+\frac{i\Delta^2}{4v},\frac{1}{4}}\left(-ivt^2\right)$$

$$\psi_a^{(2)} = \frac{1}{\sqrt{t}} W_{-\frac{1}{4}-\frac{i\Delta^2}{4v},\frac{1}{4}}\left(ivt^2\right) \tag{4.8}$$

which have deep past asymptotics

$$|\psi_a^{(1)}|^2 \quad \stackrel{t\to-\infty}{\longrightarrow} \quad 1$$

$$|\psi_a^{(2)}|^2 \quad \stackrel{t\to-\infty}{\longrightarrow} \quad 0 \tag{4.9}$$

This is consistent with our interpretation of the choice of one of these being equivalent to the choice of initial conditions. That is, preparation of the system in state ψ_a at time $t = -\infty$ requires that we use solutions $\psi_a^{(1)}$ and $\psi_b^{(2)}$. Similarly, preparation in the state ψ_b requires the use of $\psi_a^{(2)}$ and $\psi_b^{(1)}$.

Finding the transition probabilities is now a straightforward exercise. The probability of finding the system in state ψ_a at time t given that it started in state $\psi_a = |\uparrow>$ at time $t = -\infty$ is simply

$$P_\uparrow(t) = |\psi_a^{(1)}(t)|^2 = \left|\frac{1}{\sqrt{t}} W_{\frac{1}{4}+\frac{i\Delta^2}{4v},\frac{1}{4}}(-ivt^2)\right|^2 \tag{4.10}$$

This solution is plotted in figure 4.2. As $t \to +\infty$ (4.10) asymptotically approaches

$$P_\uparrow(t \to \infty) = 1 - e^{-\frac{\pi\Delta^2}{v}} \tag{4.11}$$

and therefore the probability to make a transition is

$$P_{\uparrow\downarrow}(t \to \infty) = e^{-\frac{\pi\Delta^2}{v}} \tag{4.12}$$

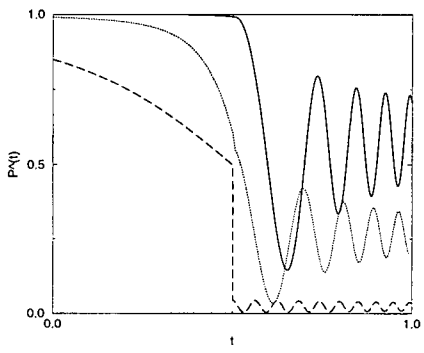

Figure 4.2: Transition probability (4.10) as a function of t (in units of Δ) . Here we have taken $\Delta^2/v = 0.63$, 1 and 5 for the solid, dotted and dashed lines respectively.

4.1.1 Alternate Method of Solution for the Transition Probability

I. All Orders Perturbation Expansion

It is also possible to solve for the transition probabilities without first finding the wave-functions [104]. Consider the amplitude

$$A_{a\to b} =< b|U(t_f,t_i)|a > \tag{4.13}$$

where

$$U(t_f,t_i) = Te^{i\int_{t_i}^{t_f} H(\tau)d\tau} \tag{4.14}$$

is the time evolution operator (T meaning "time ordered") and a, b can be either "up" or "down" ($\hat{\sigma}_z = \pm 1$, respectively). Splitting the Hamiltonian into diagonal and off-diagonal (in $\hat{\sigma}$) parts $H(t) = H_d(t) + H_\Delta$ allows us to rewrite the evolution operator in the more convenient form [71]

$$U(t_2,t_1) = e^{-i\int_{t_i}^{t_f} H_d(\tau)d\tau} Te^{-i\int_{t_i}^{t_f} \widetilde{H}_\Delta d\tau} \tag{4.15}$$

where

$$\widetilde{H}_\Delta(t) = e^{i\int_{t_i}^{t} H_d(\tau)d\tau} H_\Delta e^{-i\int_{t_i}^{t} H_d(\tau)d\tau} \tag{4.16}$$

Expansion of the time-ordered exponential yields

$$A_{a\to b} = \sum_{n=0}^{\infty}(-i)^n \int_{t_i}^{t_f} dt_n \int_{t_i}^{t_n} dt_{n-1} \ldots \int_{t_i}^{t_2} dt_1 < b|e^{i\int_{t_n}^{\infty} d\tau v\tau\hat{\sigma}_z}\Delta\hat{\sigma}_x$$
$$e^{i\int_{t_{n-1}}^{t_n} d\tau v\tau\hat{\sigma}_z}\Delta\hat{\sigma}_x \ldots e^{i\int_{t_1}^{t_2} d\tau v\tau\hat{\sigma}_z}\Delta\hat{\sigma}_x e^{i\int_{-\infty}^{t_1} d\tau v\tau\hat{\sigma}_z}|a> \qquad (4.17)$$

Let us assume that $a = b$, and furthermore that $|a>=|\uparrow>$ (the solution for $|a>=|\downarrow>$ is similar, differing only in an overall phase factor). Inspection of (4.17) shows that in this case only paths with n even contribute, and furthermore that the inner product in $\hat{\sigma}$-space is easy to perform. Explicitly we find

$$A_{\uparrow\uparrow} = e^{i\varphi}\sum_{n=0}^{\infty}\Delta^{2n}\int_{-t_i}^{t_f} dt_{2n}\int_{t_i}^{t_{2n}} dt_{2n-1}\ldots\int_{t_i}^{t_2} dt_1 e^{-iv\sum_{j=1}^{2n}(-1)^j t_j^2} \qquad (4.18)$$

where φ is an uninteresting phase. One sees that all of the time integrals may now be performed *if* we take $t_i = -\infty$ and $t_f = +\infty$; otherwise we are stuck. That is, it seems as though this approach gives us less information than the solution for the wavefunctions performed in the preceding section; this is somewhat strange, as usually if a problem is solvable in terms of known special functions in one representation it is usually solvable in all of them. In any case, we shall now take $t_i = -\infty$ and $t_f = +\infty$. In this case the integrations over the time set $\{t_j\}$ can be performed explicitly, giving

$$A_{\uparrow\uparrow} = e^{i\varphi}\sum_{n=0}^{\infty}\frac{1}{n!}\left(\frac{\Delta^2\pi}{2|v|}\right)^n \qquad (4.19)$$

with subsequent probability

$$P_{\uparrow\downarrow} = 1 - |A_{\uparrow\uparrow}|^2 = e^{-\frac{\pi\Delta^2}{|v|}} \qquad (4.20)$$

as before.

4.1.2 Alternate Method of Solution for the Transition Probability II. Dychne's Formula

The final method that we shall review for extracting results from (4.1) was first suggested by Landau [114] but later became known as Dychne's formula [?]. This method uses arguments from the theory of complex analysis in order to extract transition amplitudes from two level time dependent Hamiltonians such as the Landau Zener model (4.1). We shall not give a detailed analysis of this method, but just present its basic result.

We begin by defining the standard rotation matrix

$$R = \begin{bmatrix} \cos\theta/2 & -\sin\theta/2 \\ \sin\theta/2 & \cos\theta/2 \end{bmatrix} \tag{4.21}$$

which, if θ is a function of time, can diagonalize the general Hamiltonian

$$H = V_{||}(t)\hat{\sigma}_z + \Delta(t)\hat{\sigma}_x = \begin{bmatrix} V_{||}(t) & \Delta(t) \\ \Delta(t) & -V_{||}(t) \end{bmatrix} \tag{4.22}$$

giving

$$RHR^{\dagger} = \begin{bmatrix} E_-(t) & 0 \\ 0 & E_+(t) \end{bmatrix} \tag{4.23}$$

where

$$E_{\pm}(t) = \pm\sqrt{\Delta^2(t) + V_{||}^2(t)} \tag{4.24}$$

are the adiabatic energy levels. In the case of the simple Landau Zener Hamiltonian, we find that

$$E_{\pm}(t) = \pm\sqrt{\Delta^2 + v^2t^2} \tag{4.25}$$

The result of Landau and Dychne states that the probability for making a transition from one eigenstate of $\hat{\sigma}_z$ to the other if the Hamiltonian is evolved over the range

$-\infty < t < \infty$ is approximately

$$P_{a\to b} = e^{-2Im\xi(t_c)} \tag{4.26}$$

where

$$\xi(t) = 2\int^t E(\tau)d\tau \tag{4.27}$$

and t_c is the zero of $E(t)$ in the upper half plane that is closest to the real axis. Note that this requires that we analytically continue the time variable throughout the complex plane. The error in this expression comes from the neglect of the contribution of all the other zeroes of $E(t)$ in the upper half complex plane which are omitted here. Generally speaking, one can tell whether or not this method will give useful results by looking at the structure of the zeroes of $E(t)$. If there are many closely spaced zeroes in $E(t)$ off the real axis, then the contributions from subdominant terms will grow and this method will fail. For example, in the case of the simple Landau Zener model, there are only two points in the complex time plane where $E(t)$ vanishes, namely $t_c = \pm i\Delta/\sqrt{v}$, and only on of these is in the upper half plane. Because of this we expect that in this case the results obtained using Dychne's formula should be exact. This result is interesting as it provides insight into the reasons why this model is exactly solvable and many other similar models are not–for example, changing the time dependence from linear to say cubic in $V_{||}(t)$ causes the methods used in the preceding chapters to fail to produce exact results. This is most probably related to the existence of now *two* zeroes of $E(t)$ in the upper half plane which introduce errors into the formula (4.26). It is quite likely that there is a deep connection here between the theory of special functions and issues in complex analysis. However, we do not choose to pursue this avenue at the present time–we shall only mention it in passing.

Let us now apply Dychne's formula to the Landau Zener Hamiltonian. We find that

$$\xi(t) = 2\int^{t} \sqrt{\Delta^2 + v^2\tau^2}d\tau = t\sqrt{\Delta^2 + v^2t^2} + \frac{\Delta^2}{v}\ln\left(vt + \sqrt{\Delta^2 + v^2t^2}\right) \tag{4.28}$$

and therefore

$$Im\ \xi(t_c) = \frac{\Delta^2\pi}{2|v|} \tag{4.29}$$

and

$$P_{a\to b} = e^{-\frac{\Delta^2\pi}{|v|}} \tag{4.30}$$

which agrees with our previous exact results.

4.1.3 Analysis of the Transition Formula

We now wish to step back from the preceding technical exercise and draw some conclusions from this analysis. From the outset it should have been clear that the presence of the tunneling term $\Delta\hat{\sigma}_x$ in the Hamiltonian would mix the two states that we are calling $\psi_{a,b}$. Furthermore one expects that the dimensionless parameter Δ^2/v should be important in the final transition expression. Both these suspicions, as we have seen (4.12), turn out to be justified. What else can we say about this solution?

Perhaps the key point here is that as we are dealing with a two-level system the equations for the wavefunctions have to be second order homogeneous differential equations. For the specific Hamiltonian that we were working with (4.1) this differential equation turned out to be one that is a well-studied specific case of the hypergeometric equation. This allowed us to write down general solutions. Supplanting these solutions with information about the asymptotic behaviour of the system then gave us the specific transition probabilities that we were after. This realization suggests that there exists a class of two level time dependent Hamiltonians whose wavefunctions are obtainable in terms

of known special functions, and that this class is that whose Schrodinger equation can be mapped to the hypergeometric equation. The full determination of what is required of the Hamiltonian in order for it to belong to this class is a difficult task. We shall in the following demonstrate the method for some specific cases.

4.1.4 Generalization of the Two-Level Landau-Zener Problem

I. Exact Solution for $\Delta(t) \sim V_{||}(t)$

Let us now consider a more general case of (4.1), namely [102]

$$H(t) = V_{||}(t)\hat{\sigma}_z + \Delta(t)\hat{\sigma}_x \tag{4.31}$$

We may perform the same type of analysis as we did in section 5.1. The Schrodinger equation

$$i\frac{d}{dt}\begin{pmatrix} \psi_a \\ \psi_b \end{pmatrix} = H(t)\begin{pmatrix} \psi_a \\ \psi_b \end{pmatrix} \tag{4.32}$$

yields

$$i\frac{d\psi_a}{dt} = V_{||}(t)\psi_a + \Delta(t)\psi_b$$

$$i\frac{d\psi_b}{dt} = \Delta(t)\psi_a - V_{||}(t)\psi_b \tag{4.33}$$

eliminating ψ_a allows us to write

$$\ddot{\psi}_b - \frac{\dot{\Delta}}{\Delta}\dot{\psi}_b + \left(V_{||}^2 + \Delta^2 - i\left[\dot{V}_{||} - V_{||}\frac{\dot{\Delta}}{\Delta}\right]\right)\psi_b = 0 \tag{4.34}$$

where again the overdot represents a time derivative. As before, we have to supplant this equation with a specification of the initial conditions; here we shall assume that

$$|\psi_b(t = -\infty)|^2 = 1 \tag{4.35}$$

ie. that the system has been prepared in state ψ_b in the deep past.

The equation (4.34) cannot be solved with known special functions for general $V_{||}(t)$ and $\Delta(t)$. However, it is possible to recast it in a form that allows solution for quite a few interesting specific cases. We map

$$t \to z(t) \tag{4.36}$$

where the only requirement we have at this stage being that the map is *onto*, ie. $1 \to 1$. With differentiation with respect to z denoted by primes, (4.34) becomes

$$\psi_b'' + \left[\frac{\dot{z}'}{\dot{z}} - \frac{\Delta'}{\Delta}\right]\psi_b' + \left[\frac{V_{||}^2 + \Delta^2}{\dot{z}^2} - \frac{i}{\dot{z}}\left[V_{||}' - V_{||}\frac{\Delta'}{\Delta}\right]\right]\psi_b = 0 \tag{4.37}$$

We now choose the mapping such that

$$\dot{z} \equiv \Delta(t) \tag{4.38}$$

We then find that

$$\psi_b'' + \left[1 + \frac{V_{||}^2}{\Delta^2} - \frac{i}{\Delta}\left[V_{||}' - V_{||}\frac{\Delta'}{\Delta}\right]\right]\psi_b = 0 \tag{4.39}$$

Writing our equation in this form highlights the fact that if $V_{||}$ and Δ are constant multiples of each other, ie.

$$V_{||} = \kappa\Delta \tag{4.40}$$

with κ constant, then (4.39) reduces to

$$\psi_b'' + \left(1 + \kappa^2\right)\psi_b = 0 \tag{4.41}$$

Define $\gamma^2 = 1 + \kappa^2$; then

$$\psi_b(z) = c_0 e^{-i\gamma z} + c_1 e^{i\gamma z} \tag{4.42}$$

is the general solution of (4.41). In order to determine the normalization constants we require the following. Firstly, we want the solution for the probability to be bounded everywhere by 1; explicitly,

$$|\psi_b|^2 = |c_0|^2 + |c_1|^2 + c_0^* c_1 e^{2iz\gamma} + c_1^* c_0 e^{-2iz\gamma} \leq 1 \tag{4.43}$$

As well, we know the solution for $V_{||} = 0$ with our initial condition is simply

$$|\psi_b|^2 = |c_0|^2 + |c_1|^2 + c_0^* c_1 e^{2iz} + c_1^* c_0 e^{-2iz} = \cos^2(z) \tag{4.44}$$

These fix the constants to be $c_0 = c_1 = 1/2$, and

$$|\psi_b(z)|^2 = \cos^2(\gamma z) \tag{4.45}$$

In terms of our original parameters this transition probability is written

$$|\psi_b(t)|^2 = \cos^2\left[(1+\kappa^2)^{1/2} \int^t \Delta(\tau) d\tau\right] \tag{4.46}$$

This result has been derived previously by different methods [115]. We may pause now and ask how this exact solution compares to that obtained using Dychne's formula. In this particular case, we find that

$$E_{\pm}(t) = \pm\sqrt{\Delta^2(t) + V_{||}^2(t)} = \pm\sqrt{1+\kappa^2}|\Delta(t)| \tag{4.47}$$

and that the zeroes of $E_{\pm}(t)$ are simply the zeroes of $\Delta(t)$ (where, of course, we analytically continue the time t throughout the entire complex plane). The transition probability from Dychne's formula is then

$$P_{\uparrow\downarrow} \equiv <\downarrow |U(-\infty, +\infty)| \uparrow> \approx e^{-4\sqrt{1+\kappa^2} Im \int^{t_c} |\Delta(\tau)| d\tau} \tag{4.48}$$

where t_c is the zero of $\Delta(t)$ closest to the real axis in the upper half plane.

Let us solve for the transition probabilities for some specific potentials using our exact result. One that occurs quite regularly in this type of problem is a "pulse" potential that looks like

$$\Delta(t) = \frac{\Delta}{\cosh \omega t} \tag{4.49}$$

The indefinite integral of $\Delta(t)$ is

$$\int^t \Delta(\tau) d\tau = \frac{\Delta}{\omega} \tan^{-1}(\sinh \omega t) + c_2 \tag{4.50}$$

To be consistent with our initial condition (4.35) we take $c_2 = \Delta\pi/2\omega$. The transition probability from our exact result is then

$$|\psi_b(t)|^2 = \cos^2\left[(1+\kappa^2)^{1/2}\frac{\Delta}{\omega}\left[\tan^{-1}(\sinh \omega t) + \frac{\pi}{2}\right]\right] \tag{4.51}$$

The $t \to \infty$ asymptotic of (4.51) is

$$P_{\uparrow\downarrow} \equiv \cos^2\left[\frac{\Delta\pi}{\omega}\sqrt{1+\kappa^2}\right] \tag{4.52}$$

If we were to try to use Dychne's formula for this case, we would find that it fails. This is because since our energy levels are asymptotically approaching zero as $t \to \infty$, there is no zero of $E(t)$ that is closest to the real axis and therefore one cannot find a unique t_c. This breakdown of Dychne's formula in this regime has been noted previously [102].

Our exact solution is quite interesting. We see that the $t \to \infty$ transition probability may be varied between zero and one by altering an external parameter (Δ or ω). A train of such pulses with these varied could be used as "quantum logic gates". The reason that this particular application is interesting is that there is absolutely no source of decoherence present in this system–phase coherence is sustained throughout the evolution of the system simply because there is nothing coupled to the two level system that can remove it. We shall not say anything further about this potential application; some embellishment of this basic idea may be found in recent reviews [102].

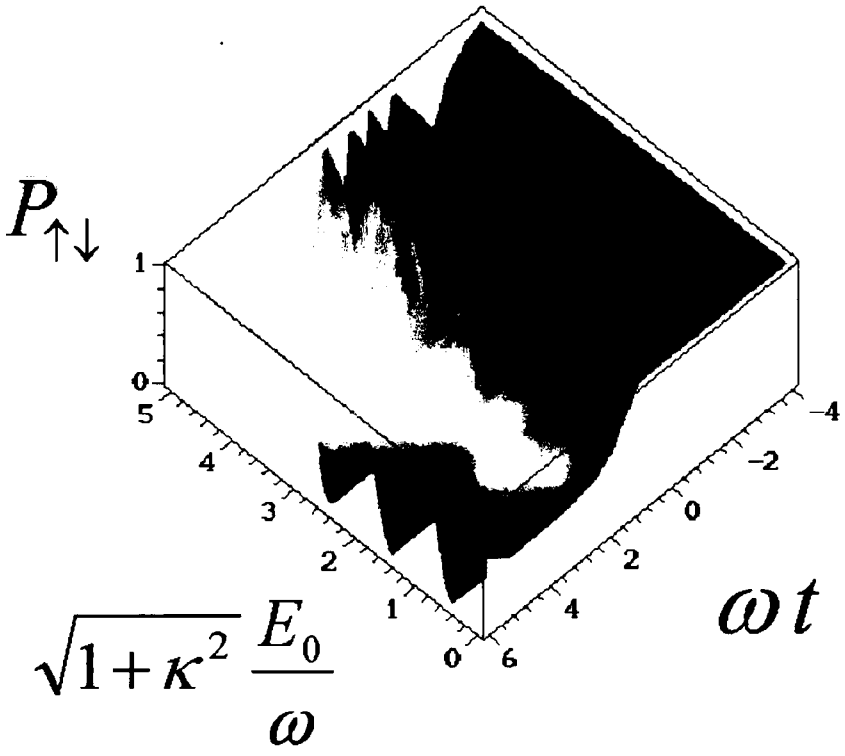

Figure 4.3: Transition probabilities for the pulse potential.

Another potential of interest is the following one;

$$\Delta(t) = 0 \quad , \qquad |t| > t_0$$
$$\Delta(t) = \Delta \sin \omega(t + t_0) \quad , \qquad |t| < t_0 \tag{4.53}$$

where we fix $t_0 = n\pi/2\omega$. Here we find that for $|t| < t_0$

$$|\psi_b(t)|^2 = \cos^2\left[(1+\kappa^2)^{1/2}\frac{\Delta}{\omega}\left[\cos\omega(t+t_0) - 1\right]\right] \tag{4.54}$$

with dynamics frozen for $|t| > t_0$. This solution is shown in figure (4.4). Note that here

we also have a tunable switching effect, this time also depending on the value of n that we pick.

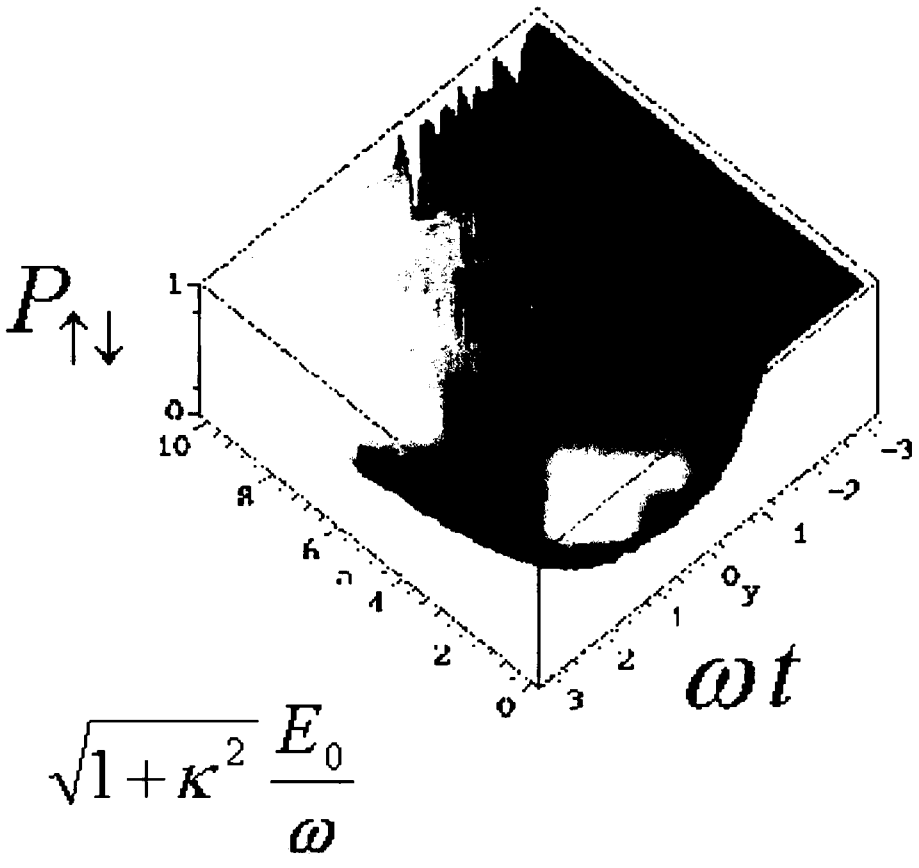

Figure 4.4: Transition probabilities for the sinusoidal potential.

4.1.5 Generalization of the Two-Level Landau-Zener Problem

II. Exact Solution by Mapping to Riemann's Differential Equation

There is a similar approach to the solution of (4.31) that generates solutions for a different class of functions $V_{||}(t)$ and $\Delta(t)$. Let us take the mapping

$$z(t) = \frac{1}{2}\left[\tanh \omega t + 1\right] \tag{4.55}$$

Then (4.31) becomes

$$\psi_b'' + \left[\frac{1}{z} + \frac{1}{z-1} - \frac{\Delta'}{\Delta}\right]\psi_b' + \frac{1}{z(z-1)}\left[\frac{V_{||}^2 + \Delta^2}{4\omega^2 z(z-1)} + \frac{i}{2\omega}\left[\frac{\Delta V_{||}' - V_{||}\Delta'}{\Delta}\right]\right]\psi_b = 0 \tag{4.56}$$

which is suspiciously close to Riemann's differential equation (RDE) [113]. We have been able to map this equation into the RDE in two specific cases, which we shall review.

Let us take

$$V_{||}(t) = A\tanh \omega t \quad , \qquad \Delta(t) = (\Delta^2 + A^2)^{1/2}\frac{1}{\cosh \omega t} \tag{4.57}$$

As functions of z, these are

$$V_{||}(z) = A(2z-1) \quad , \qquad \Delta(z) = (A^2 + \Delta^2)^{1/2} 2\sqrt{z(1-z)} \tag{4.58}$$

This models some scenario where the tunneling between the two states is externally enhanced near $t = 0$ and killed for $|t| >> 1$ while the two levels are crossed. Insertion of these into (4.56) yields

$$\psi_b'' + \frac{1}{2}\left[\frac{1}{z} + \frac{1}{z-1}\right]\psi_b' + \frac{1}{z(z-1)}\left[-\frac{k}{z} + \frac{k}{z-1} - A_1^2\right]\psi_b = 0 \tag{4.59}$$

where

$$A_0 = \frac{A}{2\omega} \quad , \qquad A_1 = \frac{\Delta}{\omega}, \qquad k = A_0^2 - i\frac{A_0}{2} \tag{4.60}$$

This is a specific case of the RDE. Its solutions are

$$\psi_b = z^{\alpha}(z-1)^{\gamma}\left[CF[a,b;c;z] + Dz^{1-c}F[1+a-c,1+b-c;2-c;z]\right] \tag{4.61}$$

where C and D are constants chosen such that $|\psi_b(z=0)|^2 = 0$. In order to determine what the constants α, γ, a, b and c are, we refer to Abramowitz and Stegun [113]. Using their nomenclature,

$$\begin{aligned} 1-\alpha-\alpha^{'} = 1/2 \quad , \qquad & 1-\gamma-\gamma^{'} = 1/2 \\ \alpha\alpha^{'} = k \quad , \qquad & \beta\beta^{'} = -A_1^2 \\ \gamma\gamma^{'} = k \quad , \qquad & a+b = 1+\alpha-\alpha^{'}+\gamma-\gamma^{'} \\ & c = 1+\alpha-\alpha^{'} \end{aligned} \tag{4.62}$$

In terms of our original parameters we find that

$$\begin{aligned} \alpha = \frac{1}{2}(1+2A_0 i) \quad , \qquad & \gamma = -A_0 i \\ a = \frac{1}{2} - A_1 \quad , \qquad & b = \frac{1}{2} + A_1 \\ & c = 1 + \frac{1+4A_0 i}{2} \end{aligned} \tag{4.63}$$

and our general solution becomes

$$\begin{aligned} \psi_b \;=\; & z^{(1+2A_0 i)/2}(z-1)^{-A_0 i}\left[CF[\frac{1}{2}-A_1, \frac{1}{2}+A_1; \frac{3}{2}+2A_0 i; z]\right. \\ +\; & \left. Dz^{-(1+4A_0 i)/2}F[-2A_0 i - A_1, -2A_0 i + A_1; \frac{1}{2} - 2A_0 i; z]\right] \end{aligned} \tag{4.64}$$

The condition

$$|\psi_b(z=0)|^2 = 0 \tag{4.65}$$

gives $D = 0$. The solution that we require is the $t \to \infty$ asymptotic; this corresponds to the $z \to 1$ limit. Near $z = 1$ we find that

$$\psi_b(z=1) = e^{\pi A_0} C \frac{\Gamma(\frac{3}{2}+2A_0 i)\Gamma(\frac{1}{2}+2A_0 i)}{\Gamma(1+2A_0 i + A_1)\Gamma(1+2A_0 i - A_1)} \tag{4.66}$$

Using the reflection formulae

$$\Gamma(\frac{1}{2}+iy)\Gamma(\frac{1}{2}-iy) = \frac{\pi}{\cosh \pi y}$$
$$\Gamma(1+iy)\Gamma(1-iy) = \frac{\pi y}{\sinh \pi y} \tag{4.67}$$

we find that

$$|\psi_b|^2 = \frac{C^2 e^{2\pi A_0}(1+16A_0^2)}{4(4A_0^2+A_1^2)}\left[1-\frac{\cos^2 \pi A_1}{\cosh^2 2A_0\pi}\right] \tag{4.68}$$

As we require that the probability be bounded above by one we take

$$C^2 \equiv \frac{4(4A_0^2+A_1^2)}{e^{2\pi A_0}(1+16A_0^2)} \tag{4.69}$$

which gives, in terms of our original parameters, the final transition probability

$$|\psi_b(t\to\infty)|^2 = 1-\frac{\cos^2 \frac{\Delta\pi}{\omega}}{\cosh^2 \frac{A\pi}{\omega}} \tag{4.70}$$

We emphasize that this result is *exact.* To the best of our knowledge, this result has not been published previously. This solution is sketched in figure (4.5).

If we try to compare this exact result to that obtained from Dychne's formula, we encounter another interesting conundrum. In order to obtain closed form solutions for Dychne's formula, one has to be able to obtain the indefinite integral of $E(t) = \sqrt{V_{||}^2(t)+\Delta^2(t)}$. Now it is evident that the presence of the square root will make the set of $V_{||}(t)$ and $\Delta(t)$ that can be dealt with quite small. The present case is an example of a Hamiltonian that produces time-dependent energy eigenstates that do not produce closed form solutions to this integration. This line of thought is quite interesting, as it seems to relate the integrability of square root functions to the solution of second order differential equations. It is plausible that progress could be made in the study of these kinds of indefinite integrals via the connection that has been established here to the hypergeometric equation.

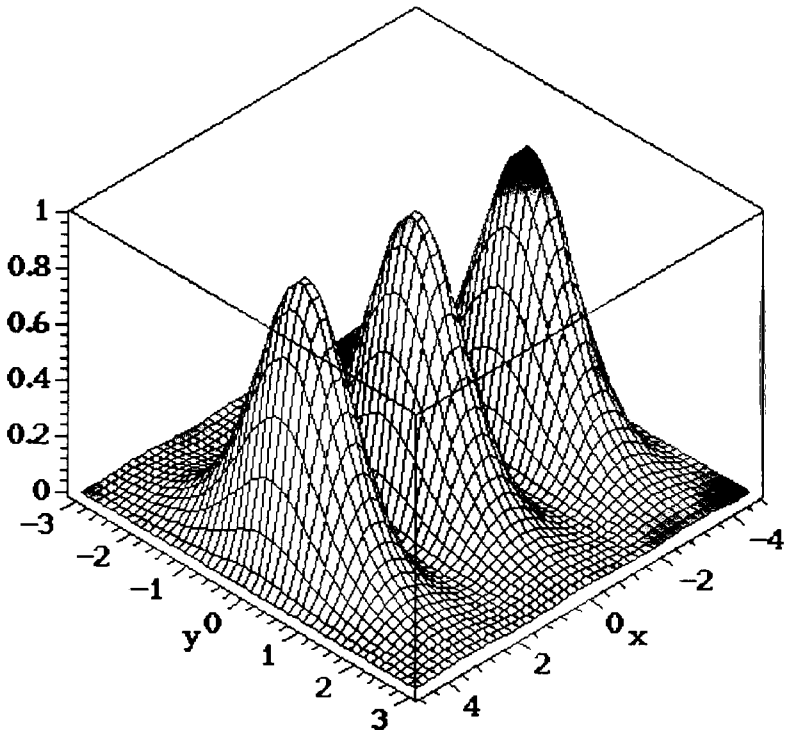

Figure 4.5: Transition probability $P_{\uparrow\downarrow}$ for the pulse/ramp scenario. Plotted is $\Delta\pi/\omega$ on the x axis and $A\pi/\omega$ on the y axis.

There is another case where we can map exactly to the RDE, and that is for the parameter set

$$V_{||}(t) = A \tanh \omega t \quad , \qquad \Delta(t) = \Delta \tag{4.71}$$

This is similar to the previous example, except that the tunneling term is constant for all time. The procedure is identical to that done explicitly in the preceeding; we shall

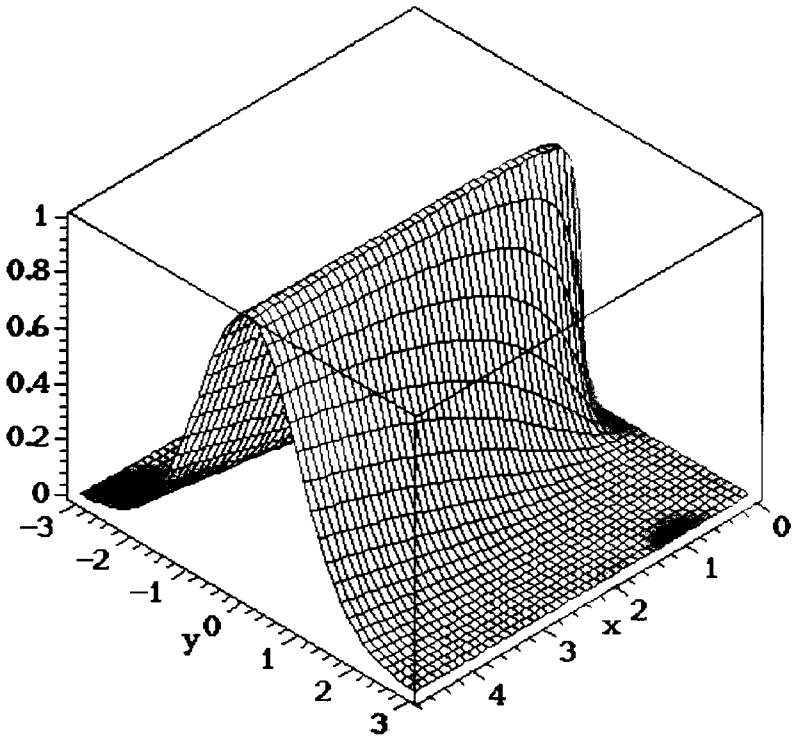

Figure 4.6: Transition probability $P_{\uparrow\downarrow}$ for the ramp scenario. Plotted on the x axis is A/ω and on the y axis $\frac{\Delta}{\omega}$.

just state the result. We find that

$$|\psi_b(t \to \infty)|^2 = \frac{\sinh^2 \frac{A\pi}{\omega}}{\sinh^2 \frac{\pi}{\omega}(A^2 + \Delta^2)^{1/2}} \tag{4.72}$$

Note that for $\Delta/A << 1$, this reduces to the standard Landau-Zener result (4.12). This is another new exact result. This solution is shown in graphical form in figure (4.6).

Chapter 5

The Landau-Zener Problem in the Presence of a Spin Bath

At temperatures $T < 360\ mK$ thermal occupation of all but the two lowest lying levels in the Fe_8 molecular magnet is vanishingly small (see figure 1.11 for experimental evidence of this and chapter 2 for theoretical justification). This means, as discussed in chapter 2, that in this "quantum regime" the central spin complex of the Fe_8 molecular magnet can be described by a two level system. In the presence of an externally applied time-dependent magnetic field, the Hamiltonian of an isolated molecule is of the generalized Landau-Zener form (4.31) with the added complication that the central two level degree of freedom is coupled to an environmental spin bath. In this chapter we solve for the transition probability between $\hat{\tau}_z$ eigenstates of the central spin object in the presence of an external AC field. We use this general result to calculate the one-molecule relaxation rate for any system with a Hamiltonian of the form (5.6). We then calculate the one-molecule relaxation rates for the specific case of the Fe_8 system.

5.1 The Addition of an Environment to the Landau-Zener Problem: General Considerations

Whenever we study a condensed matter system, there is of necessity a distinction made between a (perhaps collective) degree of freedom and "everything else". When we write down an evolution operator (such as (4.31)) for this interesting degree of freedom without considering the "everything else" of the system we run the risk of misunderstanding what is actually happening inside the material. While the exact solution of toy models such

as (4.31) may perhaps be pleasing to the aesthetic sense, it does little to further physical understanding. It is not even clear that questions of principle in quantum mechanics may be settled via the use of toy models such as these.

As we discussed at length in chapter 2, there exist standard ways of obtaining realistic effective Hamiltonians for some condensed matter systems. These effective descriptions, no matter what the material under study, always require us to specify a subset of the total information contained in them to be the "degrees of freedom of interest", while relegating all the "uninteresting degrees of freedom" to an *environment* [20, 21, 22, 74, 75]. This split, while not necessary in principle, is usually necessary to make the study of the system tractable (for, as we have seen, realistic effective Hamiltonians are complicated objects!).

The consequences of this (artificial) distinction between system and environment are still not fully understood. Some of the ramifications, both physical and philosophical, were addressed in previous chapters and in earlier classic works [74, 20, 21, 22]. In this section, however, we shall consider some of the *technical* problems that arise due to the inclusion of an environment.

5.2 The Quantum Regime Effective Hamiltonian: Inclusion of a Spin Environment

The form of the low energy effective Hamiltonian for the Fe_8 molecular magnet was derived in chapter 2. We may ask how this Hamiltonian is changed by the application of an external time-dependent magnetic field. Looking back to (2.101) we see that there are four terms that will be affected; one due to direct interaction of the field with the nuclear spins ($\omega_k^{\perp}\hat{m}_k$) ; one due to the field acting on the nuclear spins coming from the central spin whose minima are functions of the external field ($\omega_k^{||}\hat{l}_k$); and two due

to the interaction of the field with the central spin (the diagonal term $\sim \hat{\tau}_z H_z$ and the off-diagonal terms in the phase Φ).

The first of these is

$$\omega_k^{\perp}\hat{m}_k = |\vec{I}_k| g_{n_k}\mu_n(\vec{\gamma}_k^{(1)} + \vec{\gamma}_k^{(2)}) = |\vec{I}_k| g_{n_k}\mu_n(\vec{\gamma}_{kS}^{(1)} + \vec{\gamma}_{kS}^{(2)} + \vec{H}(t) + \vec{H}(t+\Omega_0^{-1})) \quad (5.1)$$

where we have defined the fields

$$\vec{\gamma}_{kS}^{(1,2)} = g_{n_k}\mu_n \left[\sum_{p\in\{p_\uparrow\}} M_{pk}^{\alpha\beta} S_\alpha^{p(1,2)} - \sum_{p\in\{p_\downarrow\}} M_{pk}^{\alpha\beta} S_\alpha^{p(1,2)} \right] \quad (5.2)$$

to be those due to the central spin before/after the central spin flips respectively at the k^{th} nucleus, t is the time at which the flip occured and Ω_0^{-1} is the tunneling time for the central spin complex. If we assume that Ω_0^{-1} is much less than the timescale over which the externally applied field changes, then we find that

$$\omega_k^{\perp}\hat{m}_k(t) \approx |\vec{I}_k| g_{n_k}\mu_n(\vec{\gamma}_{kS}^{(1)} + \vec{\gamma}_{kS}^{(2)} + 2\vec{H}(t)) \quad (5.3)$$

This assumption also leads to $\omega_k^{||}\hat{l}_k$ being time independent, since

$$\omega_k^{||}\hat{l}_k = |\vec{I}_k| g_{n_k}\mu_n(\vec{\gamma}_k^{(1)} - \vec{\gamma}_k^{(2)}) = |\vec{I}_k| g_{n_k}\mu_n(\vec{\gamma}_{kS}^{(1)} - \vec{\gamma}_{kS}^{(2)} + \vec{H}(t) - \vec{H}(t+\Omega_0^{-1})) \approx \omega_k^{||}\hat{l}_k \quad (5.4)$$

Also we find that in general the phase Φ becomes time dependent if the external field contains transverse components that vary with time. In the particular case of the easy-axis easy-plane Hamiltonian in the limit studied in chapter 2 (that is, the DC bias field $|\vec{H}| \ll \Omega_0$ and $4E/(D-2E)$ not too small (so that the instanton calculation is valid, see chapter 2)) we find that

$$\Phi = \pi S - \left[-i\frac{\pi S^2 g\mu_B}{2\tilde{E}} H_x + \frac{\pi S g\mu_B}{\Omega_0} H_y \right] \rightarrow \Phi(t) = \pi S + i\frac{\pi S^2 g\mu_B}{2\tilde{E}} H_x(t) - \frac{\pi S g\mu_B}{\Omega_0} H_y(t) \quad (5.5)$$

Together with the obvious diagonal coupling to the external field we find that in the presence of a general external time-dependent field the one-molecule effective Hamiltonian is

$$\begin{aligned} H(t) &= \sum_{k=1}^{N+8}\left[\frac{\omega_k^{\perp}}{2}\hat{I}_k\cdot\hat{m}_k(t)+\frac{\hat{\tau}_z}{2}\omega_k^{\parallel}\hat{I}_k\cdot\hat{l}_k\right]+g\mu_B S H_z(t)\hat{\tau}_z \\ &+ 2\Delta_0\hat{\tau}_-\cos\left(\Phi(t)-i\sum_{k=1}^{N+8}\vec{A}^k_{N,D}\cdot\vec{I}_k\right)+h.c. \\ &+ \sum_{k=1}^{N}\left[\frac{eQ_k}{6I_k(2I_k-1)}V^{k\alpha\beta}I^k_{\alpha\beta}\right]+\frac{\mu_0\mu_n^2}{4\pi}\sum_{l<k}\frac{g_{n_l}g_{n_k}}{r^3_{lk}}\left[\vec{I}_l\cdot\vec{I}_k-3\left(\vec{I}_l\cdot\hat{r}_{lk}\right)\left(\vec{I}_k\cdot\hat{r}_{lk}\right)\right] \end{aligned} \tag{5.6}$$

where the notation is the same as that introduced in chapter 2. From this point onwards we shall drop all g-factors and magnetons for reasons of notational simplicity. Whenever confusion may arise we shall explicitly include them.

This expression is still quite complicated; however, one notes that it has the form of a generalized Landau-Zener Hamiltonian which has been coupled to a spin environment. Note that the phonon bath does not enter into the quantum regime effective description, for reasons detailed in chapter 2 (although of course the oscillator bath is present when relaxation becomes temperature dependent–a proper treatment of these baths is under construction. Note that there are several (often conflicting) treatments of oscillator baths in this context [116, 117]).

We shall now simplify the expression (5.6) by restricting our attention to the following two kinds of externally applied field. In all that follows we shall be considering this external field to be either a longitudinal sinusoidal field plus a static component in an arbitrary direction

$$\vec{H}^{\cos}(t)=(A\cos\omega t+\xi)\ \ \hat{z}+H_x\ \ \hat{x}+H_y\ \ \hat{y} \tag{5.7}$$

or a longitudinally applied sawtooth field plus a static component in an arbitrary direction

$$\begin{aligned}\vec{H}^{saw}(t) &= \left(\frac{2A\omega}{\pi}\sum_{n=-\infty}^{\infty}\left[\Theta\left(\frac{2n+1}{\omega}-t\right)\Theta\left(t-\frac{2n-1}{\omega}\right)\right]\left(t-\frac{2n}{\omega}\right)+\xi\right)\ \hat{z} \\ &+ H_x\ \hat{x}+H_y\ \hat{y} \end{aligned} \tag{5.8}$$

Note that we have chosen to use the notation that the longitudinal component of the externally applied field is denoted by $H_z \to \xi$. Now because neither of these two fields have time-dependent transverse components, we find that the phase Φ remains time independent. This simplifies our expression somewhat. To emphasize the relation of our effective Hamiltonian to the simpler Landau-Zener models studied previously, we rewrite it in the form

$$H(t) = \hat{g}(t) + \hat{V}_{||}(t)\hat{\tau}_z + \hat{\Delta}\hat{\tau}_- + h.c. \tag{5.9}$$

where

$$\hat{g}(t) = \hat{\zeta}(t) + \frac{\mu_0}{4\pi}\sum_{l<k}\frac{1}{r_{lk}^3}\left[\vec{I}_l\cdot\vec{I}_k - 3\left(\vec{I}_l\cdot\hat{r}_{lk}\right)\left(\vec{I}_k\cdot\hat{r}_{lk}\right)\right] \tag{5.10}$$

$$\hat{V}_{||}(t) = \hat{\Upsilon} + H_z(t) \tag{5.11}$$

$$\hat{\Delta} = 2\Delta_0\cos\left(\Phi - i\sum_{k=1}^{N+8}\vec{A}_{N,D}^{k}\cdot\vec{I}_k\right) \tag{5.12}$$

and we have defined

$$\hat{\zeta}(t) = \sum_{k=1}^{N+8}\hat{\zeta}_k(t) = \sum_{k=1}^{N+8}\frac{\omega_k^{\perp}}{2}\hat{I}_k\cdot\hat{m}_k(t) + \sum_{k=1}^{N}\left[\frac{eQ_k}{6I_k(2I_k-1)}V^{k\alpha\beta}I_{\alpha\beta}^{k}\right] \tag{5.13}$$

and

$$\hat{\Upsilon} = \sum_{k=1}^{N+8}\hat{\Upsilon}_k = \sum_{k=1}^{N+8}\frac{\omega_k^{||}}{2}\hat{I}_k\cdot\hat{l}_k \tag{5.14}$$

Note that $\hat{g}(t)$, $\hat{V}_{||}(t)$, $\hat{\Delta}$ and $\vec{A}_{N,D}^{k}$ are all operators in the $\{\vec{I}_k\}$ (environmental spin) subspaces.

5.3 General AC Field Solution in Fast Passage

We understand from looking at the effective description (5.9) that it will not be possible to compute the transition probabilities from the solution of a simple second-order differential equation. This is because all the environmental spins are dynamic and coupled to the central degree of freedom, vastly increasing the Hilbert space, and requiring the solution of (for a bath of N spin I nuclei) a $(2I+1)^{Nth}$ order differential equation which proves to be quite impossible in practice. We therefore must look for a different method of solution.

Consider the perturbation expansion presented in section 4.1.1. We saw in the simple case presented there that there exists a natural perturbation parameter Δ^2/v, which is small if the time it takes the external field to sweep through the resonance is much smaller than the "bounce time" Δ^{-1}. We see explicitly in this case that if the sweep velocity is large enough, it is sufficient to calculate only to first order in this quantity.

Let us set up this perturbation expansion for our effective description. As we indicated earlier, our externally applied field will be either sinusoidal or a sawtooth function. Often we shall find that analytic results are easier to obtain with the latter. Whenever possible we shall solve for interesting quantities for both shapes.

Before we proceed with our technical investigation, let us pause and consider what the dynamics of the central spin complex should look like. When calculating the time evolution of this collective degree of freedom we can either calculate the evolution *amplitude* from our initial time (say, $t = 0$) to our final time t or we can choose a "coarse graining" time $t_c < t$ and only evolve the system from $t = 0$ to t_c. After this shorter-time evolution, we calculate probabilities and piece together a series of these, assuming that each piece is *independent of the other pieces.* Now in the usual case of a model like (4.31) it is clearly not permissible to do this, as the dynamics of the central degree of freedom

at any particular time interfere (in the quantum mechanical sense) with dynamics at all other times. Another way of saying this is that it is necessary to calculate the evolution amplitude over the entire time range of interest–there is no *decoherence* (loss of phase information) in this system.

However, the coupling to the environmental spin bath in (5.9) changes this story. Because the spin bath is dynamically active, both because of its internal dynamics (coming from the nuclear dipole-dipole term in the Hamiltonian) and its response to the dynamics of the central spin moments, it absorbs phase information from the central spin complex [64, 167]. This has the effect of *decorrelating* successive sweeps of the AC field through resonance–while the evolution of the *entire system* is of course unitary, the evolution of the central spin degree of freedom is not. One can understand why this should be so from the following argument. During each sweep of the AC field through resonance, the central spin configuration can flip, and in so doing it can flip or rearrange the distribution of the environmental spins. This rearranges the density matrix of the spin environment, which can in general contain off-diagonal terms. Now as the sweeping field moves off-resonance, the nuclear spin-spin relaxation mechanism tries to equilibrate the environmental spin set. If the sweeping frequency is larger than $\sim \Gamma_0$, where Γ_0 is the energy range over which the nuclei sweep due to nuclear dipole-dipole interactions, by the time the sweeping field comes back to a resonance the off-diagonal spin bath elements will still be present (note that the energy scale Γ_0 is roughly $\Gamma_0 \sim \sqrt{N}T_2^{-1}$ for an ensemble of N nuclei, where T_2^{-1} is the standard spin-spin relaxation time). This means that for high enough sweeping frequencies one cannot neglect quantum correlations between successive passes of the field. In this case one could invoke methods from the so-called Floquet theory [118]. However, if Γ_0 is much larger than ω, then the spin bath does have time to equilibrate itself between passes of the field, and we can therefore neglect all quantum correlations between successive passes, treating each sweep as being "decorrelated from its history".

This consideration presents us with a natural "coarse graining time", the time it takes for one full sweep through a resonance by the AC field (which is $t_c = \pi/\omega$ for both the sinusoidal and sawtooth fields). If the timescale for the readjustment of the density matrix of the system (which is $t_b \approx 1/\Gamma_0$) is such that $t_b/t_c < 1$ then this coarse graining procedure is justified. Typically in magnetic insulators at mK temperatures $T_2^{-1} \sim 10^4 - 10^6 Hz$ [48, 64]. In the specific case of Fe_8 we can calculate Γ_0 (see table 5.2); we find that $\Gamma_0 \sim 3 - 13 MHz$, depending on the nuclear spin isotopes present. This gives us an approximate gauge of the highest frequencies that we can apply before the coarse graining approximation breaks down. For a sinusoidal sweep, $t_b/t_c \approx \pi\Gamma_0/\omega$, which gives

$$\omega < \pi\Gamma_0 <\sim 10\ MHz \tag{5.15}$$

In the experiments that have been performed to date on the Fe_8 and Mn_{12} materials, the sweeping frequencies are much less than this; in the Fe_8 experiments these frequencies were in the range $0.01 - 5\ Hz$ [51]. We shall therefore use the coarse graining approximation in what follows. It is worth noting here that this point gives ample warning that temporal quantum coherence of the central degree of freedom in this system on timescales of the order of t_c will be difficult to maintain, as the nuclear spin bath has ample time to both absorb phase information from the central spin and bias the system between sweeps of the AC field–and therefore processes mediated by the AC field will most likely be incoherent in the sense that each sweep through resonance is decorrelated from all other such sweeps.

5.3.1 A List of Approximations Invoked in the Calculations That Follow

For the sake of clarity we shall list in this subsection all the approximations that we shall be making in the sections that follow. Whenever one of these is invoked, we shall refer

the reader to the following list.

(i) The coarse graining approximation. This approximation is described in some detail in the preceding section. To recap, whenever the condition

$$\omega < \pi\Gamma_0$$

is met, one can neglect quantum mechanical correlations between successive sweeps of the AC field. This is because the internal dynamics of the spin bath mediated by nuclear-nuclear terms in the Hamiltonian carry phase information away from the central spin.

(ii) The fast passage limit. The justification for taking this limit was presented in the preceding section. Formally in this limit we consider only the regime where

$$\frac{\Delta^2}{A\omega} \ll 1$$

where A and ω are the amplitude and frequency of the sweeping field respectively.

(iii) Nuclear spins with a given polarization group M are in thermal equilibrium at a polarization group temperature $\beta_M = 0$. The "polarization group" of our set of $N+8$ nuclear spins is defined to be [20]

$$M = \sum_{k=1}^{N+8} I_{kz}$$

We note that this quantity explicitly depends on which axes of quantization we pick for the nuclear spins. What we choose to do in this work is to pick the axes of quantization of the nuclear spins to be such that $\hat{z}_k = \hat{\gamma}_k^{(1)}$; that is, the z direction for the k^{th} nuclear spin corresponds to the direction of the field at the spin when the central spin complex is in its $+\hat{\tau}_z$ eigenstate. Because the internal field due to the iron spins is quite inhomogeneous, these axes will only be mutually aligned in the case where the external field $\vec{H}$ is much larger than the internal fields (which we have seen in chapter 3 are in the $0.01 - 0.26$ Tesla range).

5.3.2 General Strategy for Calculating Relaxation Rates

The core of the calculation of the one-molecule relaxation rate is the calculation of the transition probability between the $\hat{\tau}_z$ eigenstates of the central spin complex during one sweep of the AC field. Before we begin to attack this problem, we shall explicitly describe the general strategy that shall be used to calculate these probabilities and hence the one-molecule relaxation rates.

Qualitatively the situation that we have to deal with is similar to that examined in the previous sections dealing with the simple Landau-Zener transition. The big difference here is that the Hilbert space of the system now contains not one two level system but a two level system plus the full Hilbert space of the environment. This means that when we calculate the transition amplitudes (and then the probabilities) between the $\hat{\tau}_z$ eigenstates, we also have to explicitly include the effects of the other $N + 8$ systems. Formally we can see how this is done by noting the following. For the Hamiltonian (5.6) the amplitude to go from some initial $\hat{\tau}_z$ eigenstate $|\alpha>$ to some final $\hat{\tau}_z$ eigenstate $|\beta>$ during a single sweep of the AC field can be written

$$A^{if}_{\alpha\beta} \equiv < \beta| < I^f|e^{i\int_0^{t_c} H(\tau)d\tau}|I^i > |\alpha > \tag{5.16}$$

where we have defined $|I^i>$ and $|I^f>$ to be the initial and final states of the spin bath respectively. Let us take a moment and explicitly detail the formalism that we shall use in order to describe the spin bath states.

In a general molecular magnet there can be many species of environmental spins included in the effective Hamiltonian. For example in Fe_8 we have 120 protons, 18 nitrogens, 8 bromines, 8 irons, 36 carbons and 23 oxygens. Our formalism must be able to handle these different species. To this end we shall define the following notation. The symbol

$$N^{\mu}_{s} \tag{5.17}$$

represents the number of environmental spins of spin s and species μ. The k^{th} spin of the subset N_s^μ is labeled $k_\mu = 1..N_s^\mu$. The total number of spins in the spin bath is $N = \sum_\mu N_s^\mu$. As an example, consider the Fe_{8*} material. Here we have that

$$N_{1/2}^H = 120 \quad , \quad N_1^N = 18 \quad , \quad N_{3/2}^{Br} = 8 \tag{5.18}$$

With this notation the spin bath states $|I^i>$ and $|I^f>$ can be written in the form

$$|I^i> \equiv \prod_\mu \left\{ \prod_{k_\mu=1}^{N_s^\mu} |I_{k_\mu}^i> \right\} \equiv \prod_\mu \left\{ |I_{1_\mu}^i> \otimes |I_{2_\mu}^i> ... \otimes |I_{N_s^\mu}^i> \right\}$$

$$|I^f> \equiv \prod_\mu \left\{ \prod_{k_\mu=1}^{N_s^\mu} |I_{k_\mu}^f> \right\} \equiv \prod_\mu \left\{ |I_{1_\mu}^f> \otimes |I_{2_\mu}^f> ... \otimes |I_{N_s^\mu}^f> \right\}$$

The transition probability is then simply

$$P_{\alpha\beta}^{if} = A_{\alpha\beta}^{if\dagger} A_{\alpha\beta}^{if} \tag{5.19}$$

This expression for the "per sweep" transition probability contains explicit reference to the initial and final states of the spin bath. Now in any actual experiment performed on these materials, what is actually measured is a relaxation rate. In the calculation of this rate we will have to specify the distribution and characteristics of the initial and final spin bath states during a sweep of the external AC field.

Now because of reasons elaborated in the preceding section, the strategy that we shall use in specifying the form of the initial states of the spin bath is the following. We shall define the set of states $|M_\mu>$ to be all the allowed spin bath states with polarization group M_μ in the μ^{th} subset of nuclear spins. That is, we explicitly treat each species of nuclear spin separately, defining a polarization group for each. We shall see later that in this calculation all the environmental spin subspaces separate; this means that it is permissible here to treat each species as being independent of all the other species. We define the number of states in the polarization group M_μ to be $\mathcal{C}_{M_\mu}$. We have then

$p = 1..\mathcal{C}_{M_\mu}$ states with

$$\sum_{k_\mu=1}^{N_s^\mu} I_{k_\mu z} = M_\mu$$

which we label

$$|M_\mu^p >= \left\{ \prod_{k_\mu=1}^{N_s^\mu} |I_{k_\mu}^i > \right\} \tag{5.20}$$

Because this notation may at first sight appear confusing, let us explain here again what each of the symbols represent. The state $|M_\mu^p >$ is a *particular* state which is a member of the set of states $|M_\mu >$. The states $|M_\mu >$ have particular polarization groups M_μ fixed for each species. For example, imagine a fictitious material with 2 protons and 2 nitrogen atoms. We begin by fixing (say) $M_H = 0$ and $M_N = 1$. Then the states $|M_\mu >$ are the set of particular states M_μ^p with polarization group M_μ. So in this example we could label our states

$$|M_H^1 >= |+1/2, -1/2> \quad , \quad |M_H^2 >= |-1/2, +1/2>$$

and

$$|M_N^1 >= |1, 0> \quad , \quad |M_N^2 >= |0, 1>$$

the former of which constitute the set $|M_H >$ and the latter the set $|M_N >$.

Because of our approximation *(iii)* in the previous section we may define a density matrix for the spin state set $|M_\mu >$ of the form

$$\rho_{M_\mu} \equiv \frac{1}{\mathcal{Z}_{M_\mu}(\beta_{M_\mu})} e^{-\beta_{M_\mu} E_\mu^p} |M_\mu^p >< M_\mu^p| \to \frac{1}{\mathcal{Z}_{M_\mu}(\beta_{M_\mu})} |M_\mu^p >< M_\mu^p| \tag{5.21}$$

with partition function

$$\mathcal{Z}_{M_\mu}(\beta_{M_\mu}) = \sum_{i=1}^{\mathcal{C}_{M_\mu}} e^{-\beta_{M_\mu} E_\mu^p} \to \mathcal{C}_{M_\mu} \tag{5.22}$$

These definitions allow us to write down the transition probability for the central spin complex in the form

$$P_{\alpha\beta} \equiv \sum_{APG} \prod_{\mu} \left[W_{M_\mu} P_{\alpha\beta}^{M_\mu} \right] \tag{5.23}$$

where the sum is over all possible configurations of All Polarization Groups (APG) and

$$P_{\alpha\beta}^{M_\mu} = Tr \left\{ \rho_{M_\mu} \sum_{|I^f>} P_{\alpha\beta}^{if} \right\} \tag{5.24}$$

where we have summed over all final spin bath states for our transition probability (any state of the spin bath is acceptable as a final state). Here the ensemble average over all possible configurations of all polarization group states APG is normalized such that

$$\sum_{APG} \prod_{\mu} W_{M_\mu} = 1$$

For a single species spin 1/2 bath,

$$W_M = \frac{1}{2^N} \begin{pmatrix} N \\ \frac{|N-M|}{2} \end{pmatrix} \tag{5.25}$$

The way this works is as follows. Each particular molecule begins its quantum mechanical evolution in one of the nuclear spin states $\prod_\mu |M_\mu>$. The probability of its making a transition from central spin state $|\alpha>$ to central spin state $|\beta>$ is then $\prod_\mu P_{\alpha\beta}^{M_\mu}$. The relaxation rate which we are after will involve contributions from all molecules in the crystal, which will of course be in different polarization groups. Therefore in order to extract the quantity of interest we need to perform an ensemble average over all these contributions. This ensemble average is given by (5.23).

We can write the expression (5.24) in a simpler form by explicitly summing over all final spin bath states, using the completeness relation $\sum_{|I^f>} |I^f><I^f| = 1$. Performing the sum gives

$$P_{\alpha\beta}^{M_\mu} = Tr \left\{ \rho_{M_\mu} < \alpha | e^{-i \int_0^{t_c} H(\tau) d\tau} | \beta >< \beta | e^{i \int_0^{t_c} H(\tau) d\tau} | \alpha > \right\} \tag{5.26}$$

In order to finish our job, we need to translate this transition probability into a relaxation rate. We can do this by noting that since this is a "per sweep" transition probability, the relaxation rate can be obtained by dividing this quantity by the time for one sweep (which is of course simply the coarse-graining time t_c). Furthermore, we may without loss of generality here choose $|\alpha>=|\uparrow>$ and $|\beta>=|\downarrow>$. Therefore the one-molecule relaxation rate, with the molecule's polarization group state initially $\prod_\mu |M_\mu>$, is

$$\tau_{M_\mu}^{-1} = \frac{1}{t_c} Tr \left\{ \rho_{M_\mu} <\uparrow |e^{-i\int_0^{t_c} H(\tau)d\tau}| \downarrow><\downarrow |e^{i\int_0^{t_c} H(\tau)d\tau}| \uparrow> \right\} \tag{5.27}$$

and the final ensemble averaged relaxation rate is, from (5.23),

$$\tau^{-1} = \sum_{APG} \prod_\mu \left[W_{M_\mu} \tau_{M_\mu}^{-1} \right] \tag{5.28}$$

We now turn to the explicit evaluation of this quantity.

5.3.3 Processing of the Transition Amplitude

In this subsection we shall recast the transition amplitude (5.16) in a new form that is easier to deal with. We begin with our original definition

$$A_{\alpha\beta}^{if} \equiv <\beta| < I^f|e^{i\int_0^{t_c} H(\tau)d\tau}|I^i> |\alpha> \tag{5.29}$$

This form is correct to all orders in Δ. As it is our wish to do perturbation theory in this flipping term we may rewrite this in the form

$$\begin{aligned} A_{\alpha\beta}^{if} \equiv & \sum_{n=0}^{\infty} i^n \int_0^{t_c} dt_n \int_0^{t_n} dt_{n-1} ... \int_0^{t_2} dt_1 <\beta| < I^f|e^{i\int_{t_n}^{t_c} d\tau H_d(\tau)} H_\Delta e^{i\int_{t_{n-1}}^{t_n} d\tau H_d(\tau)} \\ * & H_\Delta e^{i\int_{t_{n-2}}^{t_{n-1}} d\tau H_d(\tau)} ... H_\Delta e^{i\int_0^{t_1} d\tau H_d(\tau)} |I^i> |\alpha> \end{aligned} \tag{5.30}$$

where $H_d(t)$ contains all terms in the Hamiltonian diagonal in the $\hat{\tau}$ representation

$$H_d(t) = \hat{g}(t) + \hat{V}_{||}(t)\hat{\tau}_z \tag{5.31}$$

and H_Δ contains all off-diagonal terms

$$H_\Delta = \hat{\Delta}\hat{\tau}_- + h.c. \tag{5.32}$$

This amplitude can be thought of as a sum over diagrams containing n "blips" (see figure (5.1a)).

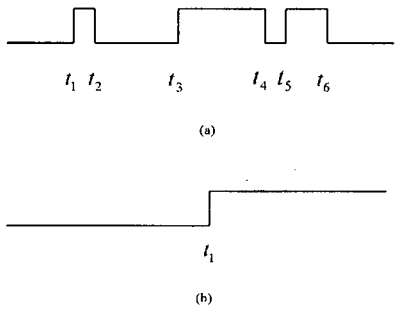

Figure 5.1: Transition amplitude as a train of blips.

Taking $|\alpha>=|\uparrow>$ and $|\beta>=|\downarrow>$ we find that the leading order diagram contains only one blip (see figure (5.1b). This leading order term is simply

$$A^{if}_{\uparrow\downarrow} = i\int_0^{t_c} dt_1 <\downarrow| < I^f|e^{i\int_{t_1}^{t_c} d\tau H_d(\tau)} H_\Delta e^{i\int_0^{t_1} d\tau H_d(\tau)}|I^i> |\uparrow> \tag{5.33}$$

Now it turns out that the presence of the nuclear dipole-dipole term in $H_d(t)$ introduces unnecessary complications into our calculation. This is because it couples the subspaces of all the environmental spins; that is, one cannot consider each environmental spin subspace separately if this term is explicitly present. However we may use the following physical argument to rewrite this term in a different way. The nuclear dipole-dipole term has the effect of causing a time-varying random field acting on the central spin, coming from the fast nuclear-nuclear dynamics in the bath. The transverse components of this field may be absorbed into the already existing transverse terms in the Hamiltonian. As

long as these latter are much larger than the amplitude of the nuclear-nuclear noise $\sim \Gamma_0$ we may neglect them–we shall assume this is the case for now and then explicitly show in section 5.6 that this holds. The longitudinal terms, however, may not be so absorbed. This is because the energy scale that we must compare these to is Δ_0, which is much smaller than Γ_0.

Therefore we shall replace our microscopic and deterministic description with an equivalent *stochastic* form, following [20]. In this stochastic version the internal dynamics of the spin bath are replaced by a randomly varying time-dependent field acting on the central spin complex which models the dynamics generated by the original nuclear dipole-dipole term and each environmental spin subspace is assumed to be decoupled from all others. In terms of our Hamiltonian this entails replacing the intra-nuclear term in (5.10) with a term $\delta\xi(t)\hat{\tau}_z$, where $\delta\xi(t)$ represents the longitudinal component of the fluctuating nuclear-nuclear bias field. Explicitly we have that

$$\begin{aligned} H(t) &= \hat{g}(t) + \hat{V}_{||}(t)\hat{\tau}_z + \hat{\Delta}\hat{\tau}_- + h.c. \rightarrow \\ \bar{H}(t) &= \hat{\zeta}(t) + \left(\hat{V}_{||}(t) + \delta\xi(t)\right)\hat{\tau}_z + \hat{\Delta}\hat{\tau}_- + h.c. \end{aligned} \tag{5.34}$$

We have denoted this new stochastic Hamiltonian via an overbar; that is, we write $H(t)$ for the original Hamiltonian and $\bar{H}(t)$ for the stochastic approximation.

Because our new Hamiltonian now contains this stochastic term, we shall use a slightly different notation for the amplitude, writing

$$\bar{A}^{if}_{\uparrow\downarrow} = i\int_0^{t_c} dt_1 <\downarrow| < I^f|e^{i\int_{t_1}^{t_c} d\tau \bar{H}_d(\tau)} H_\Delta e^{i\int_0^{t_1} d\tau \bar{H}_d(\tau)}|I^i> |\uparrow>$$

with the overbar reminding us that we are now using $\bar{H}(t)$ to evolve the system, and not $H(t)$.

With this choice, the inner product in the $\hat{\tau}$ subspace can be taken, yielding

$$\bar{A}^{if}_{\uparrow\downarrow} = i\int_0^{t_c} dt_1 < I^f|e^{i\int_{t_1}^{t_c} d\tau\{\hat{\zeta}(\tau)-\hat{F}(\tau)\}}\hat{\Delta}^* e^{i\int_0^{t_1} d\tau\{\hat{\zeta}(\tau)+\hat{F}(\tau)\}}|I^i> \tag{5.35}$$

where we have defined

$$\hat{F}(\tau) \;=\; \hat{V}_{||}(\tau) + \delta\xi(\tau) = \hat{\Upsilon} + A\cos\omega\tau + \xi + \delta\xi(\tau) \tag{5.36}$$

Here we have chosen for the sake of concreteness the sinusoidal form for the sweeping field. For the sake of notational simplicity we shall separate terms in $\hat{\zeta}$ that are time-dependent from those that aren't, writing

$$\hat{\zeta}(\tau) \equiv \sum_{k=1}^{N+8}\left[\hat{\zeta}_k + A\cos\omega\tau\hat{I}_{zk}\right] \tag{5.37}$$

where

$$\hat{\zeta}_k = \left[\frac{\vec{\gamma}_{kS}^{(1)} + \vec{\gamma}_{kS}^{(2)}}{2} + (\xi\hat{z} + H_x\hat{x} + H_y\hat{y})\right]\cdot\hat{I}_k + \sum_{k=1}^{N}\left[\frac{eQ_k}{6I_k(2I_k-1)}V^{k\alpha\beta}I^k_{\alpha\beta}\right] \tag{5.38}$$

$$\hat{\zeta} = \sum_{k=1}^{N+8}\hat{\zeta}_k \tag{5.39}$$

and the time-dependent piece is the Zeeman interaction between the external AC field and the nuclear spin. We find that, after performing the τ integrals in the exponents,

$$\bar{A}^{if}_{\uparrow\downarrow} = i\int_0^{t_c} dt_1 e^{i\sin\omega t_1\sum_\mu\frac{A}{\omega}\left[M_{i\mu}-M_{f\mu}\right]} < I^f|e^{i\left[\{\hat{\zeta}-\hat{\Upsilon}-\xi\}(t_c-t_1)+\frac{A}{\omega}\sin\omega t_1-\int_{t_1}^{t_c}d\tau\delta\xi(\tau)\right]}$$
$$\hat{\Delta}^* e^{i\left[\{\hat{\zeta}+\hat{\Upsilon}+\xi\}t_1+\frac{A}{\omega}\sin\omega t_1+\int_0^{t_1}d\tau\delta\xi(\tau)\right]}|I^i> \tag{5.40}$$

We have defined the initial and final polarization groups of the μ^{th} species to be

$$M_{i\mu} = \sum_{k_\mu=1}^{N_s^\mu} I^i_{zk_\mu} \quad , \quad M_{f\mu} = \sum_{k_\mu=1}^{N_s^\mu} I^f_{zk_\mu} \tag{5.41}$$

Because we are always in the limit that

$$\frac{Sg\mu_B}{Ng_n\mu_n} \gg 1 \tag{5.42}$$

we can drop the direct field-nucleus interaction $\sim A$ term from our expression.

Because all the environmental spin spaces are independent in $\bar{H}(t)$ we may separate each contribution. Rewriting the cosine coming from the flip term as a sum of exponentials

$$\hat{\Delta} = 2\Delta_0 \cos\left(\Phi - i\sum_{k=1}^{N+8} \vec{A}^k_{N,D}\cdot\vec{I}_k\right) = \Delta_0 \sum_{h=\pm 1} e^{ih\Phi} \prod_{k=1}^{N+8} e^{h\vec{A}^k_{N,D}\cdot\vec{I}_k}$$

we find that

$$\bar{A}^{if}_{\uparrow\downarrow} = \Delta_0 i \int_0^{t_c} dt_1 e^{i\left[\frac{2A}{\omega}\sin\omega t_1 - \int_{t_1}^{t_c} d\tau\delta\xi_{if}(\tau) + \int_0^{t_1} d\tau\delta\xi_{if}(\tau) + \xi(t_c - t_1)\right]}$$
$$\sum_{h=\pm 1} e^{ih\Phi} \prod_{k=1}^{N+8} < I^f_k | e^{i\{\hat{\zeta}_k - \hat{\Upsilon}_k\}(t_c - t_1)} e^{h\vec{A}^k_{N,D}\cdot\vec{I}_k} e^{i\{\hat{\zeta}_k + \hat{\Upsilon}_k\}t_1} | I^i_k > \tag{5.43}$$

where $|I^i_k>$ ($|I^f_k>$) is the initial (final) state of the k^{th} nuclear spin and $\delta\xi_{if}$ is the (time dependent) nuclear-nuclear longitudinal bias field acting during the transition from $|I^i>$ to $|I^f>$. This is the form of the transition amplitude that is best suited for using as input into the calculation of the transition probability.

5.3.4 Processing of the Transition Probability

(i) The Formal Expression

The next step on our journey towards the final one-molecule relaxation rate is the computation of the transition probability from the result (5.43). As we noted in our introduction of the problem, the transition probability from the state $|\uparrow> \otimes |I^i>$ to the state $|\downarrow> \otimes |I^f>$ with Hamiltonian $H(t)$ is simply

$$P^{if}_{\uparrow\downarrow} = A^{if\dagger}_{\uparrow\downarrow} A^{if}_{\uparrow\downarrow} \tag{5.44}$$

Now in our case we are working with the transformed Hamiltonian $\bar{H}(t)$. Does this change this expression? Looking at the form of our transition amplitude (5.43) we realize that it contains explicit mention of the time-varying random field $\delta\xi(t)$. This field has to be

averaged over in the final expression for the transition probability. This means that if we use $\bar{H}(t)$, the expression for the transition probability becomes

$$\bar{P}^{if}_{\uparrow\downarrow} = \int \mathcal{D}[\delta\xi_{if}(t)]\mathcal{P}[\delta\xi_{if}(t)]\bar{A}^{if\dagger}_{\uparrow\downarrow}\bar{A}^{if}_{\uparrow\downarrow} \tag{5.45}$$

where we have explicitly included a functional average over the fluctuating bias field. Using our result (5.43) we find that this transition probability is

$$\begin{aligned}\bar{P}^{if}_{\uparrow\downarrow} = \Delta_0^2 \int_0^{t_c} dt_1 \int_0^{t_c} dt_2 \int \mathcal{D}\left[\delta\xi_{if}(t)\right] \mathcal{P}[\delta\xi_{if}(t)] e^{i\left[\frac{2A}{\omega}(\sin\omega t_1 - \sin\omega t_2) - 2\int_{t_1}^{t_2} d\tau \delta\xi_{if}(\tau) + \xi(t_1-t_2)\right]} \\ \sum_{h,m=\pm 1} e^{i(h\Phi - m\Phi^*)} \prod_{k=1}^{N+8} < I^i_k | e^{-i\{\hat{\zeta}_k + \hat{\Upsilon}_k\}t_2} e^{m\vec{A}^{k*}_{N,D}\cdot\vec{I}_k} e^{-i\{\hat{\zeta}_k - \hat{\Upsilon}_k\}(t_c - t_2)} | I^f_k > \\ < I^f_k | e^{i\{\hat{\zeta}_k - \hat{\Upsilon}_k\}(t_c - t_1)} e^{h\vec{A}^k_{N,D}\cdot\vec{I}_k} e^{i\{\hat{\zeta}_k + \hat{\Upsilon}_k\}t_1} | I^i_k >\end{aligned} \tag{5.46}$$

To translate this into the form $\bar{P}^{M_\mu}_{\uparrow\downarrow}$ we sum over all final states of the spin bath (using the completeness relation) and restrict the set of initial spin bath states to be those with polarization group M_μ, giving

$$\begin{aligned}\bar{P}^{M_\mu}_{\uparrow\downarrow} = \Delta_0^2 \int_0^{t_c} dt_1 \int_0^{t_c} dt_2 e^{i\left[\frac{2A}{\omega}(\sin\omega t_1 - \sin\omega t_2) + \xi(t_1-t_2)\right]} \\ \sum_{h,m=\pm 1} e^{i(h\Phi - m\Phi^*)} \int \mathcal{D}\left[\delta\xi_{M_\mu}(t)\right] \mathcal{P}[\delta\xi_{M_\mu}(t)] e^{-2i\int_{t_1}^{t_2} d\tau \delta\xi_{M_\mu}(\tau)} \sum_{p\in M^p_\mu} \frac{1}{\mathcal{C}_{M_\mu}} \\ \prod_{k_\mu=1}^{N^\mu_s} < M^{pk}_\mu | e^{-i\{\hat{\zeta}_k + \hat{\Upsilon}_k\}t_2} e^{m\vec{A}^{k*}_{N,D}\cdot\vec{I}_k} e^{-i\{\hat{\zeta}_k - \hat{\Upsilon}_k\}(t_1 - t_2)} e^{h\vec{A}^k_{N,D}\cdot\vec{I}_k} e^{i\{\hat{\zeta}_k + \hat{\Upsilon}_k\}t_1} | M^{pk}_\mu >\end{aligned} \tag{5.47}$$

where $|M^{pk}_\mu>$ is the initial state of the k^{th}_μ nuclear spin in the p^{th} spin bath state having polarization group M_μ and $\delta\xi_{M_\mu}$ is the fluctuating longitudinal bias term coming from the nuclear spins in the M_μ polarization group.

5.3.5 Processing of the Transition Probability

(ii) Averaging over the Randomly Fluctuating T_2 Noise

We see from the preceding that the contributions from the effective nuclear-nuclear term in our Hamiltonian $\bar{H}(t)$ coming from the μ^{th} species are wholly described by the expression

$$\int \mathcal{D}\left[\delta\xi_{M_\mu}(t)\right] \mathcal{P}[\delta\xi_{M_\mu}(t)] e^{-2i\int_{t_1}^{t_2} d\tau \delta\xi_{M_\mu}(\tau)} \tag{5.48}$$

In order to explicitly evaluate this contribution we first need to specify the probability functional $P[\delta\xi_{M_\mu}(t)]$. We assume that this random process is gaussian and therefore take

$$\mathcal{P}\left[\delta\xi_{M_\mu}(t)\right] = e^{-\frac{1}{2}\int ds_1 \int ds_2 \delta\xi_{M_\mu}(s_1) K_{M_\mu}(s_1-s_2) \delta\xi_{M_\mu}(s_2)} \tag{5.49}$$

where the quantity K_{M_μ} can be understood in terms of the following. The probability functional is defined so that the average of any operator over it is simply

$$< \mathcal{A}(\delta\xi_{M_\mu}(t)) > \equiv \int \mathcal{D}[\delta\xi_{M_\mu}(t)] \mathcal{A}[\delta\xi_{M_\mu}(t)] \mathcal{P}[\delta\xi_{M_\mu}(t)] \tag{5.50}$$

It follows therefore that the autocorrelation function of the noise is

$$< \delta\xi_{M_\mu}(s_1)\delta\xi_{M_\mu}(s_2) > = \int \mathcal{D}[\delta\xi_{M_\mu}(t)] \delta\xi_{M_\mu}(s_1)\delta\xi_{M_\mu}(s_2) e^{-\frac{1}{2}\int ds_1 \int ds_2 \delta\xi_{M_\mu}(s_1) K_{M_\mu}(s_1-s_2) \delta\xi_{M_\mu}(s_2)} \tag{5.51}$$

The formal solution to this equation is [119]

$$< \delta\xi_{M_\mu}(s_1)\delta\xi_{M_\mu}(s_2) > = K^{-1}_{M_\mu}(s_1 - s_2) \tag{5.52}$$

where $K^{-1}_{M_\mu}$ is defined by

$$\int ds' K_{M_\mu}(s_1 - s') K^{-1}_{M_\mu}(s' - s_2) = \delta(s_1 - s_2) \tag{5.53}$$

In our case, we are interested in a noise functional $\delta\xi_{M_\mu}(t)$ which changes by roughly $\delta\omega_{M_\mu}$ in a time T_2/N_s^μ (this quantity is related to the spread in energy space of the M_μ^{th} polarization group Γ_{M_μ}–simply $\Gamma_{M_\mu} = \sqrt{N_s^\mu}\delta\omega_{M_\mu}$). It then diffuses in energy space with diffusion constant

$$D_{\delta\xi_{M_\mu}} = \frac{N_s^\mu(\delta\omega_{M_\mu})^2}{2T_2} = \frac{\Lambda_{M_\mu}^3}{2} \tag{5.54}$$

where we have defined $\Lambda_{M_\mu}^3 = \frac{\Gamma_{M_\mu}^2}{T_2}$. This now allows us to find out what $K_{M_\mu}^{-1}(s_1 - s_2)$ is for our problem. This is because

$$\begin{aligned} < \left(\delta\xi_{M_\mu}(s_1) - \delta\xi_{M_\mu}(s_2)\right)^2 > &= < (\delta\xi_{M_\mu}(s_1))^2 > + < (\delta\xi_{M_\mu}(s_2))^2 > -2 < \delta\xi_{M_\mu}(s_1)\delta\xi_{M_\mu}(s_2) > \\ &= 2D_{\delta\xi_{M_\mu}}|s_1 - s_2| = \Lambda_{M_\mu}^3|s_1 - s_2| \end{aligned} \tag{5.55}$$

and therefore

$$< \delta\xi_{M_\mu}(s_1)\delta\xi_{M_\mu}(s_2) >= K_{M_\mu}^{-1}(s_1 - s_2) = \frac{\Lambda_{M_\mu}^3}{2}\left(|s_1| + |s_2| - |s_1 - s_2|\right) + \delta\xi_{M_\mu}^2(0) \tag{5.56}$$

We now introduce the characteristic functional $\Phi[Q_{M_\mu}]$ dual to our probability functional

$$\begin{aligned} \Phi[Q_{M_\mu}(t)] &= \int \mathcal{D}\delta\xi_{M_\mu}(t) e^{i\int dt Q_{M_\mu}(t)\delta\xi_{M_\mu}(t)}\mathcal{P}[\delta\xi_{M_\mu}(t)] \\ \mathcal{P}[\delta\xi_{M_\mu}(t)] &= \int \mathcal{D}Q_{M_\mu}(t) e^{-i\int dt Q_{M_\mu}(t)\delta\xi_{M_\mu}(t)}\Phi[Q_{M_\mu}(t)] \end{aligned} \tag{5.57}$$

For a gaussian probability functional it follows that

$$\Phi[Q_{M_\mu}(t)] = e^{i\int ds Q_{M_\mu}(s)\delta\xi_{M_\mu}(s)} e^{-\frac{1}{2}\int ds_1 \int ds_2 Q_{M_\mu}(s_1)K_{M_\mu}^{-1}(s_1 - s_2)Q_{M_\mu}(s_2)} \tag{5.58}$$

The quantity that we are trying to evaluate (5.48) is simply $\Phi[-2]$. Because we know what $K_{M_\mu}^{-1}(s_1 - s_2)$ is from physical grounds, we may now write

$$\begin{aligned} &\int \mathcal{D}\left[\delta\xi_{M_\mu}(t)\right]\mathcal{P}[\delta\xi_{M_\mu}(t)] e^{-2i\int_{t_1}^{t_2} d\tau \delta\xi_{M_\mu}(\tau)} = \Phi[-2] \\ &= e^{-2i\int_{t_1}^{t_2} ds \delta\xi_{M_\mu}(s)} e^{-\frac{1}{2}\int_{t_1}^{t_2} ds_1 \int_{t_1}^{s_1} ds_2 \frac{\Lambda_{M_\mu}^3}{2}(|s_1| + |s_2| - |s_1 - s_2|) + \Gamma_{M_\mu}^2 \delta(s_1 - s_2)} \end{aligned} \tag{5.59}$$

Performing the s integrals gives

$$\int \mathcal{D}\left[\delta\xi_{M_\mu}(t)\right]\mathcal{P}[\delta\xi_{M_\mu}(t)]e^{-2i\int_{t_1}^{t_2}d\tau\delta\xi_{M_\mu}(\tau)} = e^{-\frac{\Lambda_{M_\mu}^3}{3}(t_2-t_1)^3-\Gamma_{M_\mu}^2(t_2-t_1)^2} \tag{5.60}$$

We find therefore that

$$\begin{aligned}\bar{P}_{\uparrow\downarrow}^{M_\mu} &= \Delta_0^2\int_0^{t_c}dt_1\int_0^{t_c}dt_2 e^{i\left[\frac{2A}{\omega}(\sin\omega t_1-\sin\omega t_2)+\xi(t_1-t_2)\right]}e^{-\frac{\Lambda_{M_\mu}^3}{3}(t_2-t_1)^3-\Gamma_{M_\mu}^2(t_2-t_1)^2}\\ &\sum_{h,m=\pm1}e^{i(h\Phi-m\Phi^*)}\sum_{p\in M_\mu^p}\frac{1}{\mathcal{C}_{M_\mu}}\\ &\prod_{k_\mu=1}^{N_s^\mu}<M_\mu^{pk}|e^{-i\{\hat{\zeta}_k+\hat{\Upsilon}\}t_2}e^{m\vec{A}_{N,D}^{k_*}\cdot\vec{I}_k}e^{-i\{\hat{\zeta}_k-\hat{\Upsilon}_k\}(t_1-t_2)}e^{h\vec{A}_{N,D}^{k}\cdot\vec{I}_k}e^{i\{\hat{\zeta}_k+\hat{\Upsilon}_k\}t_1}|M_\mu^{pk}>\end{aligned} \tag{5.61}$$

Note that since $\Lambda_{M_\mu} \ll \Gamma_{M_\mu}$ (that is, $\Gamma_{M_\mu} \gg T_2^{-1}$) for the systems under consideration, we can always drop the cubic term in $(t_1 - t_2)$ in the above expression. We therefore find that

$$\begin{aligned}\bar{P}_{\uparrow\downarrow}^{M_\mu} &= \Delta_0^2\int_0^{t_c}dt_1\int_0^{t_c}dt_2 e^{i\left[\frac{2A}{\omega}(\sin\omega t_1-\sin\omega t_2)+\xi(t_1-t_2)\right]}e^{-\Gamma_{M_\mu}^2(t_2-t_1)^2}\sum_{h,m=\pm1}e^{i(h\Phi-m\Phi^*)}\sum_{p\in M_\mu^p}\frac{1}{\mathcal{C}_{M_\mu}}\\ &\prod_{k_\mu=1}^{N_s^\mu}<M_\mu^{pk}|e^{-i\{\hat{\zeta}_k+\hat{\Upsilon}_k\}t_2}e^{m\vec{A}_{N,D}^{k_*}\cdot\vec{I}_k}e^{-i\{\hat{\zeta}_k-\hat{\Upsilon}_k\}(t_1-t_2)}e^{h\vec{A}_{N,D}^{k}\cdot\vec{I}_k}e^{i\{\hat{\zeta}_k+\hat{\Upsilon}_k\}t_1}|M_\mu^{pk}>\end{aligned} \tag{5.62}$$

5.4 Solution Without Spin Bath

The expression (5.62) is still quite opaque. In order to see how one extracts meaningful results, we shall see how to resolve it in the situation where the spin bath is absent. Here the Hamiltonians $H(t)$ and $\bar{H}(t)$ are identical and $\hat{\zeta}_k = \hat{\Upsilon}_k = \vec{A}_{N,D}^k = \Gamma_M = 0$. Since $\prod_{k=1}^{N+8} < M_k^i|M_k^i >= 1$ and $P_{\uparrow\downarrow}^M \to P_{\uparrow\downarrow}$, we may write (5.62) as

$$P_{\uparrow\downarrow} = \Delta_0^2\int_0^{t_c}dt_1\int_0^{t_c}dt_2 e^{i\left[\frac{2A}{\omega}(\sin\omega t_1-\sin\omega t_2)+\xi(t_1-t_2)\right]}\sum_{h,m=\pm1}e^{i(h\Phi-m\Phi^*)} \tag{5.63}$$

The sums over $\{h, m\}$ collapse, and we have

$$P_{\uparrow\downarrow} = 2\Delta_0^2 |\cos\Phi|^2 \int_0^{t_c} dt_1 \int_0^{t_c} dt_2 e^{i\left[\frac{2A}{\omega}(\sin\omega t_1 - \sin\omega t_2) + \xi(t_1 - t_2)\right]} \tag{5.64}$$

These integrals can now be performed, with result

$$P_{\uparrow\downarrow} = \frac{\Delta_0^2\pi^2}{\omega^2}|\cos\Phi|^2 \left[\mathcal{J}^2_{-\frac{2\xi}{\omega}}\left(\frac{2A}{\omega}\right) + \mathcal{E}^2_{-\frac{2\xi}{\omega}}\left(\frac{2A}{\omega}\right)\right] \tag{5.65}$$

where $\mathcal{J}$ and $\mathcal{E}$ are the Anger and Weber functions respectively [113]. This result, normalized to the transition probability for the standard Landau-Zener process

$$P^{(0)}_{\uparrow\downarrow} = \frac{\Delta^2\pi}{v} = \frac{\Delta_0^2|\cos\Phi|^2\pi}{A\omega} \tag{5.66}$$

is

$$\frac{P_{\uparrow\downarrow}}{P^{(0)}_{\uparrow\downarrow}} = \frac{\pi A}{\omega}\left[\mathcal{J}^2_{-\frac{2\xi}{\omega}}\left(\frac{2A}{\omega}\right) + \mathcal{E}^2_{-\frac{2\xi}{\omega}}\left(\frac{2A}{\omega}\right)\right] \tag{5.67}$$

This quantity is a function only of A/ω and ξ/ω. We have plotted it as a function of ξ/ω for three fixed values of A/ω in the figures that follow.

Note that similar transition amplitudes have been calculated previously for related problems [115, 120, 121]. Perhaps the most closely related problem for which a published solution exists is for the Hamiltonian [115]

$$H = \begin{bmatrix} \xi - A\cos\omega t & \Delta_0 \\ \Delta_0 & -\xi \end{bmatrix} \tag{5.68}$$

The published result is the transition probability over one entire cycle of the field, which is a time which is double that of the coarse-graining time we are using, and it is given by

$$P_{\uparrow\downarrow} = \frac{\Delta_0^2\pi^2}{\omega^2} J^2_{-\frac{2\xi}{\omega}}\left(\frac{2A}{\omega}\right) \tag{5.69}$$

where $J_\mu(x)$ is a μ^{th} order Bessel function.

We may also solve this problem for the case of a sawtooth field. In this case we have that

$$P_{\uparrow\downarrow} = 4\Delta_0^2|\cos\Phi|^2 \int_{-t_c/2}^{t_c/2} dt_1 \int_{-t_c/2}^{t_c/2} dt_2 e^{i\left[\frac{A\omega}{\pi}(t_1^2-t_2^2)+\xi(t_1-t_2)\right]} \tag{5.70}$$

These integrals may be performed, giving error functions [113] which can be easily plotted. This result, again normalized to $P_{\uparrow\downarrow}^{(0)}$, is compared to the results obtained from the sinusoidal perturbation in the figures that follow.

Note that what we have calculated here is the transition probability for one sweep. Because we do not have the spin bath to absorb phase information from the central spin we cannot really claim to have calculated a "relaxation rate", as each sweep of the field here is correlated (in the quantum mechanical sense) and this calculation implicitly assumes a decorrelation.

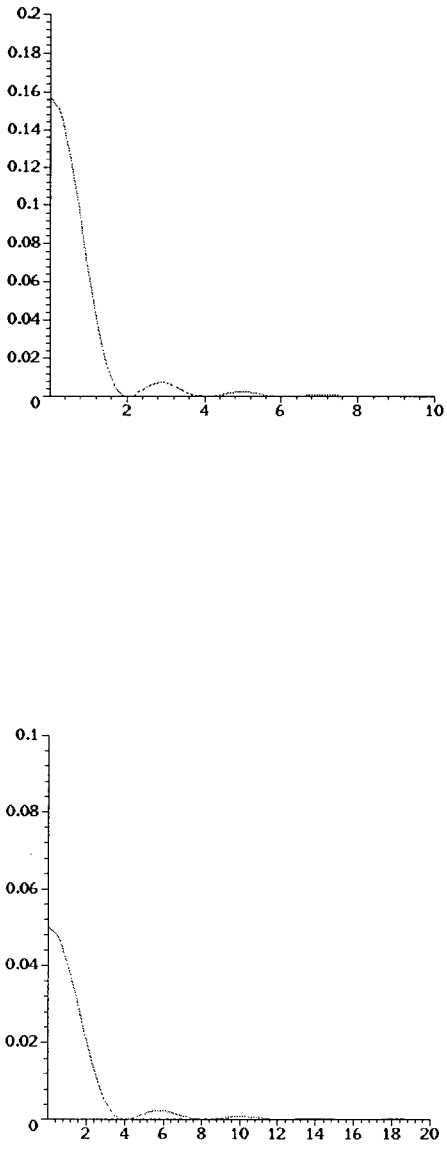

Figure 5.2: Transition probability normalized to the standard Landau-Zener transition probability $P_{\uparrow\downarrow}/P_{\uparrow\downarrow}^{(0)}$ plotted against $2\xi/\omega$ for $2A/\omega = 0.1$. The top (bottom) graph is for the sinusoidal (sawtooth) perturbation.

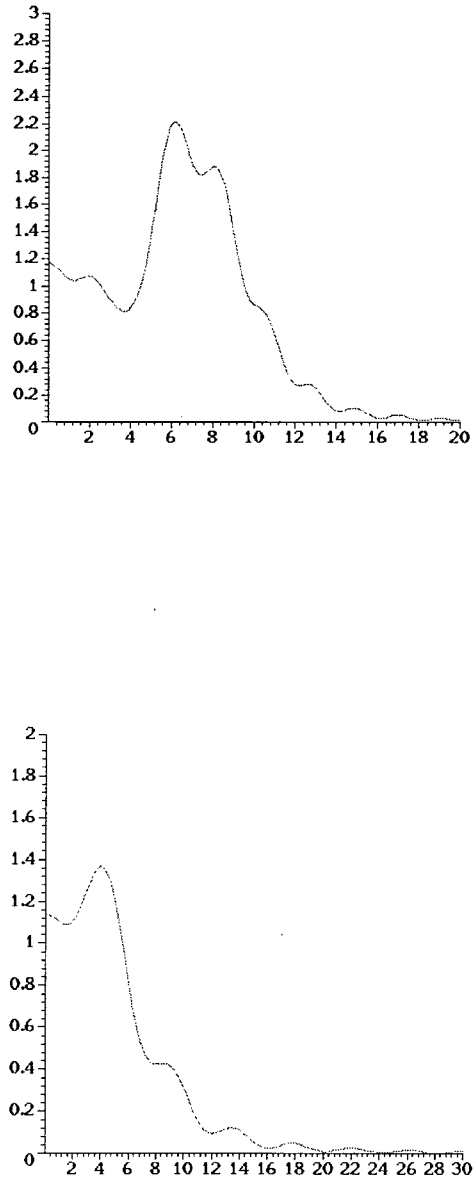

Figure 5.3: Transition probability normalized to the standard Landau-Zener transition probability $P_{\uparrow\downarrow}/P_{\uparrow\downarrow}^{(0)}$ plotted against $2\xi/\omega$ for $2A/\omega = 10$. The top (bottom) graph is for the sinusoidal (sawtooth) perturbation.

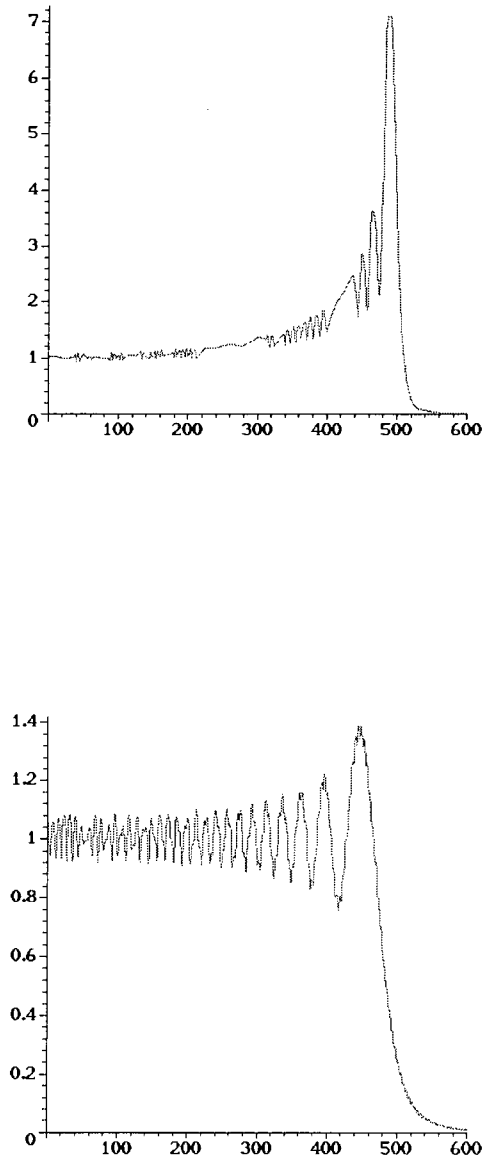

Figure 5.4: Transition probability normalized to the standard Landau-Zener transition probability $P_{\uparrow\downarrow}/P_{\uparrow\downarrow}^{(0)}$ plotted against $2\xi/\omega$ for $2A/\omega = 500$. The top (bottom) graph is for the sinusoidal (sawtooth) perturbation.

5.5 Solution For a Spin Bath with no Quadrupolar Contribution

If the spin bath contains only spin 1/2 nuclei, or if the contribution due to the electric quadrupolar term is omitted from the Hamiltonian, then the expression (5.62) simplifies considerably. In this section we shall calculate the full general relaxation rate produced by the effective Hamiltonian (5.6) in the limit where the terms representing the electric quadrupolar effects are taken to zero. Formally what we shall do is take

$$Q_k \to 0$$

It shall turn out in what follows that our choice of a sinusoidal sweeping field introduces technical difficulties in evaluating integrals when the spin bath is included. For this reason we shall in this section consider only the sawtooth perturbation (5.8). With this applied field (5.62) can be written

$$\bar{P}^{M_\mu}_{\uparrow\downarrow} = \Delta_0^2 \int_{-\pi/2\omega}^{\pi/2\omega} dt_1 \int_{-\pi/2\omega}^{\pi/2\omega} dt_2 e^{i\left[\frac{A\omega}{\pi}(t_1-t_2)^2+\xi(t_1-t_2)\right]} e^{-\Gamma^2_{M_\mu}(t_1-t_2)^2} \sum_{h,m=\pm 1} e^{i(h\Phi - m\Phi^*)}$$
$$\frac{1}{\mathcal{C}_{M_\mu}} \sum_{p\in M^p_\mu} \prod_{k_\mu=1}^{N^\mu_s} < M^{pk}_\mu | e^{-i\vec{\gamma}^{(1)}_{k_\mu}\cdot\hat{I}_{k_\mu}t_2} e^{m\vec{A}^{k_\mu *}_{N,D}\cdot\vec{I}_{k_\mu}} e^{-i\vec{\gamma}^{(2)}_{k_\mu}\cdot\hat{I}_{k_\mu}(t_1-t_2)} e^{h\vec{A}^{k_\mu}_{N,D}\cdot\vec{I}_{k_\mu}} e^{i\vec{\gamma}^{(1)}_{k_\mu}\cdot\hat{I}_{k_\mu}t_1} | M^{pk}_\mu > \tag{5.71}$$

5.5.1 Pure Orthogonality Blocking

In order to get a feel for how this calculation will go in the general case, let's start off with a particularly interesting limit–that of pure orthogonality blocking (for the definitions of orthogonality blocking, topological decoherence and degeneracy blocking we refer the reader to [20]). In this case we take the topological decoherence terms $\vec{A}^{k_\mu}_{N,D}$ to be zero. The reason that this limit is particularly simple is that without these terms, we may take the axes of quantization of each of the nuclear spins to be such that $\hat{\gamma}^{(1)}_{k_\mu} = \hat{z}$ without

having to worry about the effect that these rotations have on the form of the $\vec{A}^{\vec{k}_\mu}_{N,D}$. We find in this limit that

$$\bar{P}^{M_\mu}_{\uparrow\downarrow} = \Delta_0^2 |\cos\Phi|^2 \int_{-\pi/2\omega}^{\pi/2\omega} dt_1 \int_{-\pi/2\omega}^{\pi/2\omega} dt_2 e^{i\left[\frac{A\omega}{\pi}(t_1-t_2)^2+\xi(t_1-t_2)\right]} e^{-\Gamma^2_{M_\mu}(t_1-t_2)^2}$$
$$\frac{1}{\mathcal{C}_{M_\mu}} \sum_{p\in M^p_\mu} \prod_{k_\mu=1}^{N^\mu_s} e^{i|\vec{\gamma}^{(1)}_{k_\mu}| I_{k_\mu z}(t_1-t_2)} < M^{pk}_\mu | e^{-i\vec{\gamma}^{(2)}_{k_\mu}\cdot\hat{I}_{k_\mu}(t_1-t_2)} | M^{pk}_\mu > \tag{5.72}$$

where we have used notation such that $I_{k_\mu z}$ means the z state of the k^{th}_μ spin, normalized such that $-1 < I_{kz} < 1$. Note that we must be careful here, as the conversion from field to energy units contains a factor of $|\vec{I}_k|$. We now choose, without loss of generality,

$$\vec{\gamma}^{(2)}_{k_\mu} = c_0\hat{z} + c_1\hat{x} \tag{5.73}$$

where

$$c_0 = -|\vec{\gamma}^{(2)}_{k_\mu}|\cos 2\beta_{k_\mu} \quad , \qquad c_1 = |\vec{\gamma}^{(2)}_{k_\mu}|\sin 2\beta_{k_\mu} \tag{5.74}$$

with

$$\cos 2\beta_{k_\mu} \equiv -\hat{\gamma}^{(1)}_{k_\mu}\cdot\hat{\gamma}^{(2)}_{k_\mu} \tag{5.75}$$

Changing variables to

$$X = \omega(t_1 - t_2) \quad , \qquad Y = \omega\frac{t_1+t_2}{2} \tag{5.76}$$

allows us to write

$$\bar{P}^{M_\mu}_{\uparrow\downarrow} = \frac{\Delta_0^2|\cos\Phi|^2}{\omega^2} \int_{-\pi/2}^{\pi/2} dY \int_{-\infty}^{\infty} dX e^{i\left[\frac{2A}{\pi\omega}XY+\frac{\xi}{\omega}X\right]} e^{-\frac{\Gamma^2_{M_\mu}}{\omega^2}X^2}$$
$$\frac{1}{\mathcal{C}_{M_\mu}} \sum_{p\in M^p_\mu} \prod_{k_\mu=1}^{N^\mu_s} e^{i\frac{|\vec{\gamma}^{(1)}_{k_\mu}|}{\omega} I_{k_\mu z}X} < M^{pk}_\mu | e^{-i\frac{\vec{\gamma}^{(2)}_{k_\mu}}{\omega}\cdot\hat{I}_{k_\mu}X} | M^{pk}_\mu > \tag{5.77}$$

Here we have extended the limits on the X integral. This will be permissible as long as $\Gamma_{M_\mu} \gg \omega$ (which we assume here), as the gaussian term cuts off the large X contributions.

Similarly if $|\vec{\gamma}^{(1)}_{k_\mu}| < \sqrt{N_s^\mu}\Gamma_{M_\mu}$ (which we shall see is also the case–see table 5.2 and tables 2.3-2.11) we may expand the inner product to quadratic order in X, giving

$$\begin{aligned} &< M_\mu^{pk}|e^{-i\frac{\vec{\gamma}^{(2)}_{k_\mu}}{\omega}\cdot\hat{I}_{k_\mu}X}|M_\mu^{pk}> \approx \\ &1 - iX < M_\mu^{pk}|\frac{\vec{\gamma}^{(2)}_{k_\mu}}{\omega}\cdot\hat{I}_{k_\mu}|M_\mu^{pk}> - \frac{X^2}{2} < M_\mu^{pk}|\left(\frac{\vec{\gamma}^{(2)}_{k_\mu}}{\omega}\cdot\hat{I}_{k_\mu}\right)^2|M_\mu^{pk}> \end{aligned} \tag{5.78}$$

$$\begin{aligned} &= 1 + iXI_{k_\mu z}\frac{|\vec{\gamma}^{(2)}_{k_\mu}|}{\omega}\cos 2\beta_{k_\mu} - \frac{X^2|\vec{\gamma}^{(2)}_{k_\mu}|^2}{2\omega^2}\left[\frac{1}{2}\sin^2 2\beta_{k_\mu}\left(1 - \frac{I^2_{k_\mu z}}{2}\right) + \cos^2 2\beta_{k_\mu} I^2_{k_\mu z}\right] \\ &= e^{iXI_{k_\mu z}\frac{|\vec{\gamma}^{(2)}_{k_\mu}|}{\omega}\cos 2\beta_{k_\mu} - \frac{X^2|\vec{\gamma}^{(2)}_{k_\mu}|^2}{4\omega^2}\sin^2 2\beta_{k_\mu}\left(1-\frac{I^2_{k_\mu z}}{2}\right)} \end{aligned} \tag{5.79}$$

Insertion of this into (5.72) yields

$$\begin{aligned} \bar{P}^{M_\mu}_{\uparrow\downarrow} = &\frac{\Delta_0^2|\cos\Phi|^2}{\omega^2}\int_{-\pi/2}^{\pi/2}dY\int_{-\infty}^{\infty}dX e^{i\left[\frac{2A}{\pi\omega}XY + \frac{\xi}{\omega}X\right]}e^{-\frac{\Gamma^2_{M_\mu}}{\omega^2}X^2} \\ &\frac{1}{\mathcal{C}_{M_\mu}}\sum_{p\in M_\mu^p}\prod_{k_\mu=1}^{N_s^\mu} e^{2iXI_{k_\mu z}\frac{|\vec{\gamma}^{(2)}_{k_\mu}|}{\omega}\cos^2\beta_{k_\mu} - \frac{X^2|\vec{\gamma}^{(2)}_{k_\mu}|^2}{4\omega^2}\sin^2 2\beta_{k_\mu}\left(1-\frac{I^2_{k_\mu z}}{2}\right)} \end{aligned} \tag{5.80}$$

where we have used the fact that $|\vec{\gamma}^{(1)}_{k_\mu}| = |\vec{\gamma}^{(2)}_{k_\mu}|$ (ie. the magnitude of the field acting on the k_μ^{th} nuclear spin before/after the central spin complex flips is the same). Defining the quantities

$$\epsilon_1^\mu = 2\sum_{k_\mu=1}^{N_s^\mu} I_{k_\mu z}|\vec{\gamma}^{(1)}_k|\cos^2\beta_{k_\mu} \quad , \quad \rho^2_{1\mu} = \frac{1}{4}\sum_{k_\mu=1}^{N_s^\mu}|\vec{\gamma}^{(1)}_k|^2\sin^2 2\beta_{k_\mu}\left(1 - \frac{I^2_{k_\mu z}}{2}\right) \tag{5.81}$$

we can write this as

$$\bar{P}^{M_\mu}_{\uparrow\downarrow} = \frac{\Delta_0^2|\cos\Phi|^2}{\omega^2}\int_{-\pi/2}^{\pi/2}dY\int_{-\infty}^{\infty}dX e^{i\left[\frac{2A}{\pi\omega}XY + \frac{\xi}{\omega}X\right]}e^{-\frac{\Gamma^2_{M_\mu}}{\omega^2}X^2}\frac{1}{\mathcal{C}_{M_\mu}}\sum_{p\in M_\mu^p} e^{iX\frac{\epsilon_1^\mu}{\omega} - \frac{X^2\rho^2_{1\mu}}{\omega^2}} \tag{5.82}$$

The Sum Over Initial States $|M_\mu^p>$

We are now going to perform the sum over the initial states $|M_\mu^p>$. Before we begin, let us take a close look at the expression (5.82). We see that both ϵ_1^μ and $\rho_{1\mu}$ are functions of the particular state that the spin bath is in. Now what we are going to do now is to replace $\rho_{1\mu}^2$ with its average value; that is, we take

$$\rho_{1\mu}^2 \to \frac{1}{4}\sum_{k_\mu=1}^{N_s^\mu} |\vec{\gamma}_k^{(1)}|^2 \sin^2 2\beta_{k_\mu}\left(1 - \frac{\bar{I}_{k_\mu z}^2}{2}\right) \tag{5.83}$$

Since

$$\bar{I}_{k_\mu z}^2 = \frac{1}{I_\mu^2}\frac{2}{2I_\mu+1}\sum_{l=0}^{I_\mu}(I_\mu - l)^2 = \frac{1}{3}\frac{I_\mu+1}{I_\mu} \tag{5.84}$$

the average value of $\rho_{1\mu}^2$ is simply

$$\rho_{1\mu}^2 = \frac{5I_\mu - 1}{24I_\mu}\sum_{k_\mu=1}^{N_s^\mu} |\vec{\gamma}_k^{(1)}|^2 \sin^2 2\beta_{k_\mu} \tag{5.85}$$

The approximation of neglecting the width of the distribution of numbers $\{\rho_{1\mu}\}$ is justified whenever this width is much less than Γ_{M_μ} (which is certainly the case here). With this approximation the sum in question becomes

$$\frac{1}{\mathcal{C}_{M_\mu}} e^{-\frac{X^2\rho_{1\mu}^2}{\omega^2}} \sum_{p\in M_\mu^p} e^{i\frac{X}{\omega}\epsilon_1^\mu} \tag{5.86}$$

In order to clarify the procedure that we shall adopt in what follows, let us imagine how we would proceed in a specific case. As a typical example, let us consider how to deal with the protons in Fe_8.

In this situation, there are an enormous number of possible states because N_H (and therefore $\mathcal{C}_{M_H}$) is large. In Fe_8 there are 120 protons per molecule. This means that there are $2^{120} \sim 10^{36}$ states in $2N_H + 1 = 241$ polarization groups. The M_H^{th} polarization group contains N_H choose $|M_H - N_H|/2$ states, each of which contribute to the sum (5.86). In

addition, we note that the values that ϵ_1^μ can take are bounded. So the situation that we must deal with is one where we have an extraordinary number of states squashed into a bounded energy range. It is natural in this situation to convert the sum over initial states into an integral over ϵ_1^μ.

Now because of the exceedingly large number of states available to the spin bath, we may invoke the central limit theorem in order to supply an appropriate weighting function for the integration. That is, as we increase N_s^μ, the numbers that we get for ϵ_1^μ for each particular state of the spin bath will begin to approximate a gaussian distribution centered at some value $\epsilon_1^{M_\mu}$ with some width $\mathcal{W}(M_\mu)$. In this limit we find that

$$\epsilon_1^{M_\mu} \to \frac{2M_\mu}{N_s^\mu} \sum_{k_\mu=1}^{N_s^\mu} |\vec{\gamma}_k^{(1)}| \cos^2 \beta_k \tag{5.87}$$

Now the width $\mathcal{W}(M_\mu)$ is a little trickier to dealt with. In general it is apparent that this quantity has its maximum for $M_\mu = 0$ and monotonically decreases to zero for $|M_\mu| = N_s^\mu$. How it does this will in general be a function of how the fields $|\vec{\gamma}_{k_\mu}^{(1)}|$ are distributed. It turns out, however, that to a good approximation we can consider this width to be independent of M_μ. There are two factors that make this approximation reasonable. The first is that the number of states available in a given polarization group M_μ (which, for spin 1/2 nuclei, is simply N choose $|N - M|/2$), fall off sharply for $|M_\mu| >\sim \sqrt{N_s^\mu}$. This means that the behaviour of $\mathcal{W}(M_\mu)$ for $|M_\mu| > \sqrt{N_s^\mu}$ will be irrelevant, simply because there aren't enough states in these higher polarization groups to make any difference in the final relaxation rate. The second factor is that for $|M_\mu| < \sqrt{N_s^\mu}$, the width $\mathcal{W}(M_\mu)$ will be roughly of the form

$$\mathcal{W}(M_\mu) \sim \left(1 - \frac{|M_\mu|}{N_s^\mu}\right) \mathcal{W}(0_\mu) \quad , \quad |M_\mu| < \sqrt{N_s^\mu} \ll N_s^\mu \tag{5.88}$$

for N_s^μ large. The zero polarization group width we get from the central limit theorem;

it is simply

$$\mathcal{W}(0_\mu) \to \frac{2}{\sqrt{N_s^\mu}} \sum_{k_\mu=1}^{N_s^\mu} |\vec{\gamma}_k^{(1)}| \cos^2 \beta_k \tag{5.89}$$

Note that to be consistent here we must also take $\Gamma_{M_\mu} \to \Gamma_{0_\mu}$ for the same reason that we took $\mathcal{W}(M_\mu) \to \mathcal{W}(0_\mu)$. We shall hold off on using these approximations for the time being. We can make excellent progress in evaluating our expressions with unspecified Γ_{M_μ}, $\epsilon_1^{M_\mu}$ and $\mathcal{W}(M_\mu)$. Until we reach the point where we need to have explicit forms for these we shall just leave them as functions of the polarization group.

Using the gaussian weighting allows us to rewrite our sum in the form

$$\begin{aligned} e^{-\frac{X^2\rho_{1\mu}^2}{\omega^2}} \frac{1}{\mathcal{C}_{M_\mu}} \sum_{p\in M_\mu^p} e^{i\frac{\epsilon_1^\mu X}{\omega}} &= e^{-\frac{X^2\rho_{1\mu}^2}{\omega^2}} \frac{1}{\sqrt{2\pi}\mathcal{W}(M_\mu)} \int_{-\infty}^{\infty} d\epsilon_1^\mu e^{-\frac{(\epsilon_1^\mu - \epsilon_1^{M_\mu})^2}{2\mathcal{W}^2(M_\mu)}} e^{i\frac{\epsilon_1^\mu X}{\omega}} \\ &= e^{iX\frac{\epsilon_1^{M_\mu}}{\omega}} e^{-\frac{\mathcal{W}^2(M_\mu)/2+\rho_{1\mu}^2}{\omega^2}X^2} \end{aligned} \tag{5.90}$$

Substitution of (5.90) into the expression for the transition probability (5.82) yields

$$\bar{P}_{\uparrow\downarrow}^{M_\mu} = \frac{\Delta_0^2 |\cos\Phi|^2}{\omega^2} \int_{-\pi/2}^{\pi/2} dY \int_{-\infty}^{\infty} dX e^{i\left[\frac{2A}{\pi\omega}XY + \frac{\xi}{\omega}X\right]} e^{iX\frac{\epsilon_1^{M_\mu}}{\omega}} e^{-\frac{\mathcal{W}^2(M_\mu)/2+\rho_{1\mu}^2+\Gamma_{M_\mu}^2}{\omega^2}X^2} \tag{5.91}$$

Evaluation of the Ensemble Average Over Polarization Groups

Examination of $\bar{P}_{\uparrow\downarrow}^{M_\mu}$ reveals the following useful fact. Because the energy spreads in the different polarization groups overlap considerably, ie.

$$\frac{\mathcal{W}(M_\mu)}{\sqrt{N_s^\mu}} \ll \sqrt{\mathcal{W}^2(M_\mu)/2 + \rho_{1\mu}^2 + \Gamma_{M_\mu}^2} \tag{5.92}$$

we may approximate the ensemble average over all polarization groups by integrations. Formally this is done by taking

$$\sum_{APG} \prod_\mu W_{M_\mu} \to \prod_\mu \left[\frac{1}{\sqrt{2\pi N_s^\mu}} \int_{-\infty}^{\infty} dM_\mu e^{-M_\mu^2/2N_s^\mu} \right] \tag{5.93}$$

where we have extended the integration limits (the gaussian cuts off the large M contributions). From (5.28) we have

$$\begin{aligned} P_{\uparrow\downarrow} &= \sum_{APG} \prod_{\mu} \left[W_{M_\mu} P_{\uparrow\downarrow}^{M_\mu} \right] \\ &= \frac{\Delta_0^2 |\cos\Phi|^2}{\omega^2} \int_{-\pi/2}^{\pi/2} dY \int_{-\infty}^{\infty} dX e^{i\left[\frac{2A}{\pi\omega}XY + \frac{\xi}{\omega}X\right]} \\ &\quad \prod_{\mu} \left[\frac{1}{\sqrt{2\pi N_s^\mu}} \int_{-\infty}^{\infty} dM_\mu e^{-M_\mu^2/2N_s^\mu} e^{i\frac{M_\mu}{\sqrt{N_s^\mu}}\frac{\mathcal{W}(M_\mu)}{\omega}X} \right] e^{-\frac{\sum_\mu \left[\mathcal{W}^2(M_\mu)/2 + \rho_{1\mu}^2 + \Gamma_{M_\mu}^2\right]}{\omega^2} X^2} \end{aligned} \tag{5.94}$$

where we have written $\epsilon_1^{M_\mu}$ explicitly as a function of M_μ using (5.87). In order to perform the integrals over the set $\{M_\mu\}$ we now invoke our $\mathcal{W}(M_\mu) \to \mathcal{W}(0_\mu)$ approximation. The integrals over the set $\{M_\mu\}$ are then easily performed, giving

$$P_{\uparrow\downarrow} = \frac{\Delta_0^2 |\cos\Phi|^2}{\omega^2} \int_{-\pi/2}^{\pi/2} dY \int_{-\infty}^{\infty} dX e^{i\left[\frac{2A}{\pi\omega}XY + \frac{\xi}{\omega}X\right]} e^{-\frac{W^2}{\omega^2}X^2} \tag{5.95}$$

where we have defined the full energy width

$$W^2 = \sum_{\mu} \left[\mathcal{W}^2(0_\mu) + \Gamma_{0_\mu}^2 + \rho_{1\mu}^2 \right] \tag{5.96}$$

where all these quantities are evaluated for the zero polarization group spin set for each species.

Evaluation of the X and Y Integrals

The X integral can now be performed, yielding

$$P_{\uparrow\downarrow} = \frac{\Delta_0^2 |\cos\Phi|^2}{\sqrt{\pi}\omega W} \int_{-\pi/2}^{\pi/2} dY \exp\left[-\frac{\omega^2}{4W^2} \left(\frac{2AY}{\pi\omega} + \frac{\xi}{\omega} \right)^2 \right] \tag{5.97}$$

Changing variables to

$$Z = \frac{\omega}{2W} \left(\frac{2AY}{\pi\omega} + \frac{\xi}{\omega} \right) \tag{5.98}$$

allows us to write our relaxation rate in the final form

$$\tau^{-1} = \frac{\omega}{\pi} P_{\uparrow\downarrow} = \frac{\Delta_0^2 |\cos\Phi|^2}{\sqrt{\pi} A} \int_{Z_-}^{Z_+} dZ e^{-Z^2} \tag{5.99}$$

where

$$Z_\pm = \frac{\pm A + \xi}{2W} \tag{5.100}$$

Evaluation of the Relaxation Rate in Various Interesting Limits

In the limit where $|A| \gg \sqrt{\xi^2 + W^2}$ we recover our old large A result, which is of course independent of M_μ

$$\tau^{-1} = \frac{\Delta_0^2 |\cos\Phi|^2}{A} \tag{5.101}$$

If $|A| \ll \sqrt{\xi^2 + W^2}$ then the relaxation rate becomes

$$\tau^{-1} = \frac{\Delta_0^2 |\cos\Phi|^2}{\sqrt{\pi} W} \exp\left[-\frac{\xi^2}{4W^2}\right] \tag{5.102}$$

Discussion of Results:

I. Pure Orthogonality Blocking

The general result (5.99) produces two limiting cases (5.101, 5.102) that are both quite interesting. The first of these (5.101), valid for large A, tells us that in this limit orthogonality blocking effects *do not affect the relaxation rate at all.* How can we explain this physically?

In order to understand the result, we shall present a graphical depiction of how orthogonality blocking works in a molecular magnet. The central spin complex, a two-level system, begins its evolution in some $\hat{\tau}_z$ eigenstate which we choose without loss of generality to be $|\uparrow>$. Now for all the time that it remains in this state the nuclear spins

feel its dipolar field. The k^{th} nuclear spin initially is exposed to this field which we have called $\vec{\gamma}_k^{(1)}$.

We saw previously that because of the nature of pure orthogonality blocking we could choose the axis of quantization of the k^{th} nuclear spin freely and for convenience chose the z axis to be parallel to the direction of $\vec{\gamma}_k^{(1)}$. Physically what this means is that for this choice of basis the k^{th} nuclear spin feels only a longitudinal field as long as the central spin complex remains in its initial state $|\uparrow>$.

Now when the central spin complex tunnels to the other $\hat{\tau}_z$ eigenstate $|\downarrow>$, the k^{th} nuclear spin feels a different field $\vec{\gamma}_k^{(2)}$ *which contains transverse components.* This means, of course, that the k^{th} nuclear spin will *precess* in the new field $\vec{\gamma}_k^{(2)}$.

The diagram that we are evaluating in order to solve for the transition probability is the one shown in figure 5.5. We see that this process contains a length of time $t_1 - t_2$ where the central spin complex is in the state $|\downarrow>$. During this length of time the k^{th} nuclear spin precesses in the field $\vec{\gamma}_k^{(2)}$.

Now what does this have to do with our large A result (5.101)? Let us go back to an earlier expression (5.95) and look closely at the integrals involved. In particular, let us examine the Y integration. Notice that there is only one term under the integration that is a function of Y. This term may be isolated and is

$$\int_{-\pi/2}^{\pi/2} dY e^{i\frac{2A}{\pi\omega}XY} = \frac{\omega\pi}{AX}\sin\left(\frac{AX}{\omega}\right) \tag{5.103}$$

Now if A/ω is "large enough", we see that this expression will begin to approximate a delta function in X. How large is large enough? Looking back to the expression (5.95) we see that the X integral is now of the form

$$\int_{-\infty}^{\infty} dX \frac{\omega\pi}{AX}\sin\left(\frac{AX}{\omega}\right) e^{i\frac{\xi}{\omega}X} e^{-\frac{W^2}{\omega^2}X^2} \tag{5.104}$$

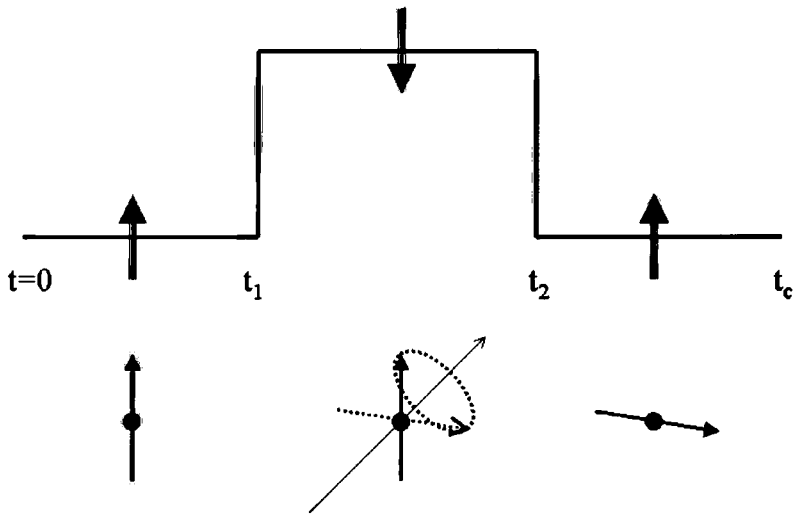

Figure 5.5: Depiction of the precession of the k^{th} nuclear spin during a "blip". The central spin is shown in black, with a schematic nuclear spin underneath. This nuclear spin feels a field $\vec{\gamma}_k^{(1)}$ for times $t < t_1$, which we choose to be the axis of quantization. After the central spin flips at t_1 the nuclear spin feels a different field $\vec{\gamma}_k^{(2)}$ which contains in general transverse components. This causes a precession of the nuclear spin. After the central spin flips back, the nuclear spin will be in a state that has less than full overlap with its original state.

Changing variables to $Z = AX/\omega$ allows us to write

$$\pi \int_{-\infty}^{\infty} dZ \frac{\sin Z}{Z} e^{i\frac{\xi}{A}Z} e^{-\frac{W^2}{A^2}Z^2} \tag{5.105}$$

Now here is the crux of the matter. If A is much bigger than ξ and W, then the terms in the exponentials grow slowly compared to the $\frac{\sin Z}{Z}$ term and we can neglect them, allowing for easy solution of (5.105). Moreover, we see that because these quantities drop out of the expression all references to the nuclear spins disappear! What has happened?

We see that this expression is dominated by small values of Z. But Z is nothing but $Z = AX/\omega = A(t_1 - t_2)$. Therefore contributions only come from $t_1 - t_2 <\sim \frac{1}{A}$. We see then that large A reduces the length of time that the central spin stays in the "blip"

and therefore the length of time that the nuclear spins can precess in the field $\vec{\gamma}_k^{(2)}$. This is the physical reason why orthogonality blocking does not affect our large A relaxation rate–the processes involved are completely dominated by short blips and therefore the nuclear spins don't have time to precess out of their initial states.

Let us now turn our attention to the other limiting case that we have worked out, that for small A (5.102). What we have found is that the relaxation rate falls off like a gaussian with applied bias ξ. This seemingly contradicts results obtained for $A = 0$ where the relaxation rate was found to be exponential with bias [20]

$$\tau^{-1} = \frac{\Delta^2}{\xi_0} e^{-|\xi|/\xi_0} \tag{5.106}$$

where ξ_0 is an energy scale in the Prokofi'ev and Stamp theory [20] such that $\Gamma_0 < \xi_0 < W$ (W is the full energy width of the nuclear spin distribution–in our case we shall find that it is $W \sim 100 - 400MHz$ depending on the choice of isotopes in the Fe_8). Why it is that our result seemingly disagrees with this earlier result can be traced to a subtle difference in the way that our expression (5.102) and the expression (5.106) were calculated.

When $A \equiv 0$ there is an additional constraint when we calculate the transition probability for the central spin, and that is that when the central spin complex tunnels $|\uparrow, M> \rightarrow |\downarrow, M'>$ it is necessary in order to conserve energy that $M' = -M$. That is, the total energy of the central spin plus the environmental spins has to be the same before and after a flip and therefore the environmental spins cannot go into any M' they want. Now in the calculation of (5.106) this constraint, which is explicitly used in the calculation of the transition probability, *is responsible for the exponential dependence on external bias.*

In our case we have not explicitly put in any such constraint. Instead we have allowed in our expression for the transition probability $|\uparrow, M> \rightarrow |\downarrow, M'>$ for any M'. The energy constraint here of course still exists (it is implicit in the expression for the

transition probability) but it is of a slightly different nature than when $A \equiv 0$. This is because when $A \neq 0$ the Hamiltonian is explicitly time-dependent and therefore the system of central spin plus nuclear spins does not in general conserve energy–energy may be exchanged with the external field. Moreover, our expression (5.102) is not valid for $A \equiv 0$ because we are in the fast passage limit $\Delta_0^2 \ll A\omega$.

So it appears that the exponential dependence on bias (5.106) arises solely because of the explicit addition of an energy constraint. Now in a molecular magnet, one can ask if this constraint is realistic. The answer here is that it is not. In these materials, there are dynamic external dipolar fields coming from all the other molecules in the crystal (in addition to any externally applied fields of the type that we are discussing). In terms of the structure of the transition probabilities we see that each individual molecular magnet *will have an explicitly time-dependent field acting on it from a external source.* This means that in calculating the one-molecule relaxation rates it is crucial to not put in any artificial energy constraints on the central spin plus nuclear spin system.

Let us now summarize our point of view on the discrepancy between our result and the $A \equiv 0$ result. The exponential dependence on bias found previously [74, 20] is a limiting case that is not relevant for a real molecular magnet, arising because of the addition of an explicit energy constraint. Our result, arising from an explicitly time-dependent Hamiltonian, is the description that is relevant for molecular magnets even in the absence of an externally applied time-varying field because of the presence of time-varying internal dipolar fields which can exchange energy with the one-molecule system.

5.5.2 The General Case; Inclusion of Topological Decoherence

We now turn our attention to the more general case, including the contributions due to the topological decoherence terms $\vec{A}^k_{N,D}$. The inclusion of these terms increases the technical difficulties involved in evaluating the trace over the spin bath for the following

reason. The basis in which the $\vec{A}^k_{N,D}$ are calculated is that of the spin Hamiltonian for the problem. That is, the axes of quantization of the nuclear spins cannot be chosen arbitrarily without properly rotating the $\vec{A}^k_{N,D}$ into this new basis. In order to get a concrete feel for why this presents a problem, let us consider the specific case of the easy-axis easy-plane spin Hamiltonian discussed at length in chapter 2. For molecules with this symmetry we showed that (2.73)

$$\vec{A}^k_{N,D} = \frac{\pi S}{4\Omega_0} g_{n_k}\mu_n \left[\sum_{p\in\{p_\uparrow\}} M^{y\beta}_{pk} - \sum_{p\in\{p_\downarrow\}} M^{y\beta}_{pk} - i\sqrt{\frac{D-E}{2E}} \left[\sum_{p\in\{p_\uparrow\}} M^{x\beta}_{pk} - \sum_{p\in\{p_\downarrow\}} M^{x\beta}_{pk} \right] \right] \tag{5.107}$$

for ligand nuclear spins $k = 1..N$ and

$$\vec{A}^k_{N,D} = \frac{S\pi\omega_k^{\|c}}{4\Omega_0} \left[\hat{y} - i\sqrt{\frac{D-E}{2E}}\hat{x} \right] \tag{5.108}$$

for any ^{57}Fe in the material. By splitting the real and imaginary parts of these we can write

$$\vec{A}^k_{N,D} = \tilde{\alpha}^{(1)}_k \tilde{\hat{n}}^k_1 + i\tilde{\alpha}^{(2)}_k \tilde{\hat{n}}^k_2 \tag{5.109}$$

where

$$\tilde{\alpha}^{(1)}_k = |Re\vec{A}^k_{N,D}| \quad , \quad \tilde{\alpha}^{(2)}_k = |Im\vec{A}^k_{N,D}| \tag{5.110}$$

and

$$\tilde{\hat{n}}^k_1 = \frac{Re\vec{A}^k_{N,D}}{\tilde{\alpha}^{(1)}_k} \quad , \quad \tilde{\hat{n}}^k_2 = \frac{Im\vec{A}^k_{N,D}}{\tilde{\alpha}^{(2)}_k} \tag{5.111}$$

for all nuclear spins $k = 1..N + 8$. Now as we did previously, we choose the axes of quantization to be such that $\hat{\gamma}^{(1)}_k = \hat{z}$ and $\hat{\gamma}^{(2)}_k = -\cos 2\beta_k \hat{z} + \sin 2\beta_k \hat{x}$ for all k. Then we see that since these new axes do not in general correspond to those of the spin

Hamiltonian, it is necessary to rotate the topological decoherence terms into these new bases. These rotations yield in general new topological decoherence terms

$$\vec{A}^k_{r,N,D} = \alpha^{(1)}_k \hat{n}^k_1 + i\alpha^{(2)}_k \hat{n}^k_2 \tag{5.112}$$

in terms of which we may write

$$\begin{aligned}
&\prod_\mu \bar{P}^{M_\mu}_{\uparrow\downarrow} = \Delta_0^2 \int_{-\pi/2\omega}^{\pi/2\omega} dt_1 \int_{-\pi/2\omega}^{\pi/2\omega} dt_2 e^{i\left[\frac{A\omega}{\pi}(t_1-t_2)^2+\xi(t_1-t_2)\right]} \sum_{h,m=\pm 1} e^{i(h\Phi - m\Phi^*)} \\
&\prod_\mu \Bigg[e^{-\Gamma^2_{M_\mu}(t_1-t_2)^2} \frac{1}{\mathcal{C}_{M_\mu}} \sum_{p\in M^p_\mu} \prod_{k_\mu=1}^{N^\mu_s} e^{iI_{k_\mu z}|\vec{\gamma}^{(1)}_k|(t_1-t_2)} \\
&< M^{pk}_\mu | e^{m\alpha^{(1)}_k \hat{n}^k_1 \cdot \vec{I}_{k_\mu} - im\alpha^{(2)}_k \hat{n}^k_2 \cdot \vec{I}_{k_\mu}} e^{-i(t_1-t_2)\vec{\gamma}^{(2)}_k \cdot \hat{I}_{k_\mu}} e^{h\alpha^{(1)}_k \hat{n}^k_1 \cdot \vec{I}_{k_\mu} + ih\alpha^{(2)}_k \hat{n}^k_2 \cdot \vec{I}_{k_\mu}} | M^{pk}_\mu > \Bigg]
\end{aligned} \tag{5.113}$$

Note that now that we have topological decoherence effects it is necessary to include all the nuclei (and therefore the product over species μ) here because the sum over m, h doesn't commute with the product over nuclei. Changing variables to

$$X = \omega(t_1 - t_2) \quad , \qquad Y = \frac{A\,(t_1+t_2)}{2\pi} \tag{5.114}$$

allows us to write

$$\begin{aligned}
&\prod_\mu \bar{P}^{M_\mu}_{\uparrow\downarrow} = \frac{\Delta_0^2 \pi}{\omega A} \int_{-A/2\omega}^{A/2\omega} dY \int_{-\infty}^{\infty} dX e^{i\left[XY + \frac{\xi}{\omega}X\right]} \sum_{h,m=\pm 1} e^{i(h\Phi - m\Phi^*)} \\
&\prod_\mu \Bigg[e^{-\frac{\Gamma^2_{M_\mu}}{\omega^2}X^2} \frac{1}{\mathcal{C}_{M_\mu}} \sum_{p\in M^p_\mu} \prod_{k_\mu=1}^{N^\mu_s} e^{i\frac{|\vec{\gamma}^{(1)}_k|}{\omega} I_{k_\mu z} X} \\
&< M^{pk}_\mu | e^{m\alpha^{(1)}_k \hat{n}^k_1 \cdot \vec{I}_{k_\mu} - im\alpha^{(2)}_k \hat{n}^k_2 \cdot \vec{I}_{k_\mu}} e^{-i\frac{\vec{\gamma}^{(2)}_k}{\omega} \cdot \hat{I}_{k_\mu} X} e^{h\alpha^{(1)}_k \hat{n}^k_1 \cdot \vec{I}_{k_\mu} + ih\alpha^{(2)}_k \hat{n}^k_2 \cdot \vec{I}_{k_\mu}} | M^{pk}_\mu > \Bigg]
\end{aligned} \tag{5.115}$$

where we have taken the limits on the X integral to infinity as before.

Evaluation of the Inner Product over Spin Bath States

As we saw previously in the case of pure orthogonality blocking, because the gaussian term (in X) coming from the average over the nuclear-nuclear bias field cuts off large X contributions to the expression (5.115), we may expand the orthogonality blocking term inside the spin inner product to quadratic order in X. As well, we shall restrict our attention to the case when all the $|\alpha_{k_\mu}^{(1,2)}| \ll 1$, which is again the physical limit for the materials in which we are interested. This allows us to expand the topological decoherence terms inside the inner product to quadratic order in $\alpha_{k_\mu}^{(1,2)}$ as well. Keeping only up to quadratic in X, $\alpha_{k_\mu}^{(1,2)}$ or products thereof allows us to write the environmental spin inner product in the form

$$
\begin{aligned}
&< M_\mu^{pk}|e^{m\alpha_k^{(1)}\hat{n}_1^k\cdot\vec{I}_{k_\mu}-im\alpha_k^{(2)}\hat{n}_2^k\cdot\vec{I}_{k_\mu}}e^{-i\frac{\vec{\gamma}_k^{(2)}}{\omega}\cdot\hat{I}_{k_\mu}X}e^{h\alpha_k^{(1)}\hat{n}_1^k\cdot\vec{I}_{k_\mu}+ih\alpha_k^{(2)}\hat{n}_2^k\cdot\vec{I}_{k_\mu}}|M_\mu^{pk}> \\
&\sim 1 - iX < M_\mu^{pk}|\frac{\vec{\gamma}_{k_\mu}^{(2)}}{\omega}\cdot\hat{I}_{k_\mu}|M_\mu^{pk}> -\frac{X^2}{2} < M_\mu^{pk}|\left(\frac{\vec{\gamma}_{k_\mu}^{(2)}}{\omega}\cdot\hat{I}_{k_\mu}\right)^2|M_\mu^{pk}> \\
&+ < M_\mu^{pk}|\left(m\vec{A}_{r,N,D}^{k_\mu *}\cdot\vec{I}_k + h\vec{A}_{r,N,D}^{k_\mu}\cdot\vec{I}_k\right)|M_\mu^{pk}> \\
&+\frac{1}{2} < M_\mu^{pk}|\left(\left[\vec{A}_{r,N,D}^{k_\mu *}\cdot\vec{I}_k\right]^2 + \left[\vec{A}_{r,N,D}^{k_\mu}\cdot\vec{I}_k\right]^2\right)|M_\mu^{pk}> \\
&+mh < M_\mu^{pk}|\left[\vec{A}_{r,N,D}^{k_\mu *}\cdot\vec{I}_k\right]\left[\vec{A}_{r,N,D}^{k_\mu}\cdot\vec{I}_k\right]|M_\mu^{pk}> \\
&-iX < M_\mu^{pk}|\left(m\left[\vec{A}_{r,N,D}^{k_\mu *}\cdot\vec{I}_k\right]\left[\frac{\vec{\gamma}_{k_\mu}^{(2)}}{\omega}\cdot\hat{I}_{k_\mu}\right] + h\left[\frac{\vec{\gamma}_{k_\mu}^{(2)}}{\omega}\cdot\hat{I}_{k_\mu}\right]\left[\vec{A}_{r,N,D}^{k_\mu}\cdot\vec{I}_k\right]\right)|M_\mu^{pk}>
\end{aligned}
\tag{5.116}
$$

We shall present results for these terms one by one and then combine the results after we are finished. We have that

$$
\begin{aligned}
&< M_\mu^{pk}|\left(m\vec{A}_{r,N,D}^{k_\mu *}\cdot\vec{I}_k + h\vec{A}_{r,N,D}^{k_\mu}\cdot\vec{I}_k\right)|M_\mu^{pk}> \\
&=< M_\mu^{pk}|\left(m+h\right)\alpha_{k_\mu}^{(1)}\hat{n}_{1k_\mu}\cdot\vec{I}_{k_\mu} - i(m-h)\alpha_k^{(2)}\hat{n}_{2k_\mu}\cdot\vec{I}_{k_\mu}|M_\mu^{pk}> \\
&= \left(m+h\right)\alpha_{k_\mu}^{(1)}\hat{n}_{1k_\mu z}I_{k_\mu z} - i(m-h)\alpha_k^{(2)}\hat{n}_{2k_\mu z}I_{k_\mu z}
\end{aligned}
\tag{5.117}
$$

The next term is

$$
\begin{aligned}
&< M_\mu^{pk}| \left(\left[\vec{A}_{r,N,D}^{k_\mu *} \cdot \vec{I}_k \right]^2 + \left[\vec{A}_{r,N,D}^{k_\mu} \cdot \vec{I}_k \right]^2 \right) |M_\mu^{pk}> \\
&= 2 < M_\mu^{pk}| \left[{\alpha_{k_\mu}^{(1)}}^2 (\hat{n}_{1k_\mu} \cdot \vec{I}_{k_\mu})^2 - {\alpha_{k_\mu}^{(2)}}^2 (\hat{n}_{2k_\mu} \cdot \vec{I}_{k_\mu})^2 \right] |M_\mu^{pk}> \\
&= 2 \left[\alpha_{k_\mu}^{(1)^2} \left[(1 - \hat{n}_{1k_\mu z}^2) \frac{\left(2I_\mu^2 - I_{k_\mu z}^2\right)}{4} + \hat{n}_{1k_\mu z}^2 I_{k_\mu z}^2 \right] \right. \\
&\left. -\alpha_{k_\mu}^{(2)^2} \left[(1 - \hat{n}_{2k_\mu z}^2) \frac{\left(2I_\mu^2 - I_{k_\mu z}^2\right)}{4} + \hat{n}_{2k_\mu z}^2 I_{k_\mu z}^2 \right] \right]
\end{aligned}
\tag{5.118}
$$

Next we have

$$
\begin{aligned}
&< M_\mu^{pk}| \left[\vec{A}_{r,N,D}^{k_\mu *} \cdot \vec{I}_k \right] \left[\vec{A}_{r,N,D}^{k_\mu} \cdot \vec{I}_k \right] |M_\mu^{pk}> \\
&=< M_\mu^{pk}| \left[{\alpha_{k_\mu}^{(1)}}^2 (\hat{n}_{1k_\mu} \cdot \vec{I}_{k_\mu})^2 + {\alpha_{k_\mu}^{(2)}}^2 (\hat{n}_{2k_\mu} \cdot \vec{I}_{k_\mu})^2 + i\alpha_{k_\mu}^{(1)} \alpha_{k_\mu}^{(2)} \left[\hat{n}_{1k_\mu} \cdot \vec{I}_{k_\mu}, \hat{n}_{2k_\mu} \cdot \vec{I}_{k_\mu} \right] \right] |M_\mu^{pk}> \\
&= \alpha_{k_\mu}^{(1)^2} \left[(1 - \hat{n}_{1k_\mu z}^2) \frac{\left(2I_\mu^2 - I_{k_\mu z}^2\right)}{4} + \hat{n}_{1k_\mu z}^2 I_{k_\mu z}^2 \right] \\
&+\alpha_{k_\mu}^{(2)^2} \left[(1 - \hat{n}_{2k_\mu z}^2) \frac{\left(2I_\mu^2 - I_{k_\mu z}^2\right)}{4} + \hat{n}_{2k_\mu z}^2 I_{k_\mu z}^2 \right] \\
&+I_{k_\mu z} \alpha_{k_\mu}^{(1)} \alpha_{k_\mu}^{(2)} \left(\hat{n}_{2k_\mu x} \hat{n}_{1k_\mu y} - \hat{n}_{2k_\mu y} \hat{n}_{1k_\mu x} \right)
\end{aligned}
\tag{5.119}
$$

And finally

$$
\begin{aligned}
&< M_\mu^{pk}| \left(m \left[\vec{A}_{r,N,D}^{k_\mu *} \cdot \vec{I}_k \right] \left[\frac{\vec{\gamma}_{k_\mu}^{(2)}}{\omega} \cdot \hat{I}_{k_\mu} \right] + h \left[\frac{\vec{\gamma}_{k_\mu}^{(2)}}{\omega} \cdot \hat{I}_{k_\mu} \right] \left[\vec{A}_{r,N,D}^{k_\mu} \cdot \vec{I}_k \right] \right) |M_\mu^{pk}> \\
&= -\frac{|\vec{\gamma}_{k_\mu}^{(1)}| \cos 2\beta_{k_\mu}}{\omega} I_{k_\mu z}^2 \left[\alpha_{k_\mu}^{(1)} \hat{n}_{1k_\mu z} (m + h) - i\alpha_{k_\mu}^{(2)} \hat{n}_{2k_\mu z} (m - h) \right] \\
&+\frac{|\vec{\gamma}_{k_\mu}^{(1)}| \sin 2\beta_{k_\mu}}{\omega} \left[\frac{\left(2I_\mu^2 - I_{k_\mu z}^2\right)}{4} \left\{ \alpha_{k_\mu}^{(1)} (m + h) \hat{n}_{1k_\mu x} - i\alpha_{k_\mu}^{(2)} (m - h) \hat{n}_{2k_\mu x} \right\} \right. \\
&\left. -i \frac{I_{k_\mu z}}{2} \left\{ \alpha_{k_\mu}^{(1)} (m - h) \hat{n}_{1k_\mu y} - i\alpha_{k_\mu}^{(2)} (m + h) \hat{n}_{2k_\mu y} \right\} \right]
\end{aligned}
\tag{5.120}
$$

We now substitute these results into the expression for the transition probability, giving

$$\prod_{\mu} \bar{P}_{\uparrow\downarrow}^{M_\mu} = \frac{2\Delta_0^2\pi}{\omega A}\int_{-A/2\omega}^{A/2\omega} dY \int_{-\infty}^{\infty} dX e^{i\left[XY+\frac{\xi}{\omega}X\right]} \sum_{m,h=\pm 1} e^{i(h\Phi - m\Phi^*)}$$
$$\prod_{\mu}\left[e^{-\frac{\Gamma_{M_\mu}^2}{\omega^2}X^2}\frac{1}{\mathcal{C}_{M_\mu}}\sum_{p\in M_\mu^p} e^{iX\frac{\epsilon_1^\mu}{\omega}-\frac{X^2\rho_{1\mu}^2}{\omega^2}} e^{(m+h)[\rho_{31\mu}-iX\rho_{41\mu}]-i(m-h)[\rho_{32\mu}-iX\rho_{42\mu}]+(1+mh)\rho_{21\mu}-(1-mh)\rho_{22\mu}}\right] \tag{5.121}$$

where we have defined

$$\begin{aligned}
\rho_{21\mu} &= \sum_{k_\mu=1}^{N_s^\mu} {\alpha_{k_\mu}^{(1)}}^2(1-n_{1k_\mu z}^2)\frac{(2I_\mu^2 - I_{k_\mu z}^2)}{4} + \frac{1}{2}\sum_{k_\mu=1}^{N_s^\mu} I_{k_\mu z}\alpha_{k_\mu}^{(1)}\alpha_{k_\mu}^{(2)}(\hat{n}_{2k_\mu x}\hat{n}_{1k_\mu y} - \hat{n}_{2k_\mu y}\hat{n}_{1k_\mu x}) \\
\rho_{22\mu} &= \sum_{k_\mu=1}^{N_s^\mu} {\alpha_{k_\mu}^{(2)}}^2(1-n_{2k_\mu z}^2)\frac{(2I_\mu^2 - I_{k_\mu z}^2)}{4} + \frac{1}{2}\sum_{k_\mu=1}^{N_s^\mu} I_{k_\mu z}\alpha_{k_\mu}^{(1)}\alpha_{k_\mu}^{(2)}(\hat{n}_{2k_\mu x}\hat{n}_{1k_\mu y} - \hat{n}_{2k_\mu y}\hat{n}_{1k_\mu x}) \\
\rho_{31\mu} &= \sum_{k_\mu=1}^{N_s^\mu} I_{k_\mu z}\alpha_{k_\mu}^{(1)}\hat{n}_{1k_\mu z} \\
\rho_{32\mu} &= \sum_{k_\mu=1}^{N_s^\mu} I_{k_\mu z}\alpha_{k_\mu}^{(2)}\hat{n}_{2k_\mu z} \\
\rho_{41\mu} &= \sum_{k_\mu=1}^{N_s^\mu} \frac{|\vec{\gamma}_{k_\mu}|}{\omega}\sin 2\beta_{k_\mu}\left[\frac{(2I_\mu^2 - I_{k_\mu z}^2)}{4}\alpha_{k_\mu}^{(1)}\hat{n}_{1k_\mu x} - \frac{I_{k_\mu z}}{2}\alpha_{k_\mu}^{(2)}\hat{n}_{2k_\mu y}\right] \\
\rho_{42\mu} &= \sum_{k_\mu=1}^{N_s^\mu} \frac{|\vec{\gamma}_{k_\mu}|}{\omega}\sin 2\beta_{k_\mu}\left[\frac{(2I_\mu^2 - I_{k_\mu z}^2)}{4}\alpha_{k_\mu}^{(2)}\hat{n}_{2k_\mu x} + \frac{I_{k_\mu z}}{2}\alpha_{k_\mu}^{(1)}\hat{n}_{1k_\mu y}\right]
\end{aligned} \tag{5.122}$$

and

$$\rho_{\alpha\beta} = \sum_{\mu}\rho_{\alpha\beta\mu} \tag{5.123}$$

In other words, if there is a μ subscript on one of these quantities then it refers to the species μ. For example, $\rho_{21\mu}$ is the quantity defined above for the specific subset of nuclear spins in species μ. If this subscript is not there then it refers to the sum over all species–for example, ρ_{21} is the sum over the contributions from all the species $\rho_{21} = \sum_\mu \rho_{21\mu}$.

The Large A Limit

Now there is a limit here where this simplifies considerably, and that is when A is much larger than all the other energy scales in this expression. In this case, the integral over Y gives a delta function in X, for reasons identical to those discussed in the pure orthogonality blocking case. This allows us to write

$$\prod_{\mu} \bar{P}_{\uparrow\downarrow}^{M_\mu} = \frac{2\Delta_0^2\pi}{\omega A} \sum_{m,h=\pm 1} e^{i(h\Phi - m\Phi^*)} \prod_{\mu} \left[\frac{1}{\mathcal{C}_{M_\mu}} \sum_{p \in M_\mu^p} \left[e^{(m+h)\rho_{31\mu} - i(m-h)\rho_{32\mu} + (1+mh)\rho_{21\mu} - (1-mh)\rho_{22\mu}} \right] \right] \tag{5.124}$$

The Sum Over States in the M_μ^{th} Polarization Group

All four quantities $\rho_{21\mu}$, $\rho_{22\mu}$, $\rho_{31\mu}$ and $\rho_{32\mu}$ depend explicitly on the state of the spin bath via their dependence on the set $\{I_{k_\mu z}\}$. At this stage of the calculation we wish to perform the sum over the states in the M_μ^{th} polarization group. In order to do this we define the quantities

$$\begin{aligned}
\bar{\rho}_{21\mu} &= \sum_{k_\mu=1}^{N_s^\mu} {\alpha_{k_\mu}^{(1)}}^2 (1 - n_{1k_\mu z}^2) \frac{(2I_\mu^2 - \bar{I}_{k_\mu z}^2)}{4} + \frac{1}{2}\frac{M_\mu}{N_s^\mu} \sum_{k_\mu=1}^{N_s^\mu} |\alpha_{k_\mu}^{(1)} \alpha_{k_\mu}^{(2)} (\hat{n}_{2k_\mu x}\hat{n}_{1k_\mu y} - \hat{n}_{2k_\mu y}\hat{n}_{1k_\mu x})| \\
&= \frac{I_\mu(5I_\mu - 1)}{12} \sum_{k_\mu=1}^{N_s^\mu} {\alpha_{k_\mu}^{(1)}}^2 (1 - n_{1k_\mu z}^2) + \frac{1}{2}\frac{M_\mu}{N_s^\mu} \sum_{k_\mu=1}^{N_s^\mu} |\alpha_{k_\mu}^{(1)} \alpha_{k_\mu}^{(2)} (\hat{n}_{2k_\mu x}\hat{n}_{1k_\mu y} - \hat{n}_{2k_\mu y}\hat{n}_{1k_\mu x})| \\
\bar{\rho}_{22\mu} &= \sum_{k_\mu=1}^{N_s^\mu} {\alpha_{k_\mu}^{(2)}}^2 (1 - n_{2k_\mu z}^2) \frac{(2I_\mu^2 - \bar{I}_{k_\mu z}^2)}{4} + \frac{1}{2}\frac{M_\mu}{N_s^\mu} \sum_{k_\mu=1}^{N_s^\mu} |\alpha_{k_\mu}^{(1)} \alpha_{k_\mu}^{(2)} (\hat{n}_{2k_\mu x}\hat{n}_{1k_\mu y} - \hat{n}_{2k_\mu y}\hat{n}_{1k_\mu x})| \\
&= \frac{I_\mu(5I_\mu - 1)}{12} \sum_{k_\mu=1}^{N_s^\mu} {\alpha_{k_\mu}^{(2)}}^2 (1 - n_{2k_\mu z}^2) + \frac{1}{2}\frac{M_\mu}{N_s^\mu} \sum_{k_\mu=1}^{N_s^\mu} |\alpha_{k_\mu}^{(1)} \alpha_{k_\mu}^{(2)} (\hat{n}_{2k_\mu x}\hat{n}_{1k_\mu y} - \hat{n}_{2k_\mu y}\hat{n}_{1k_\mu x})| \\
W_{2\mu} &= \frac{1}{2\sqrt{N_s^\mu}} \sum_{k_\mu=1}^{N_s^\mu} |\alpha_{k_\mu}^{(1)} \alpha_{k_\mu}^{(2)} (\hat{n}_{2k_\mu x}\hat{n}_{1k_\mu y} - \hat{n}_{2k_\mu y}\hat{n}_{1k_\mu x})| \\
\bar{\rho}_{31\mu} &= \frac{M_\mu}{N_s^\mu} \sum_{k_\mu=1}^{N_s^\mu} |\alpha_{k_\mu}^{(1)} \hat{n}_{1k_\mu z}| \quad , \quad \bar{\rho}_{32\mu} = \frac{M_\mu}{N_s^\mu} \sum_{k_\mu=1}^{N_s^\mu} |\alpha_{k_\mu}^{(2)} \hat{n}_{2k_\mu z}|
\end{aligned}$$

$$W_{31\mu} = \frac{1}{\sqrt{N_s^\mu}} \sum_{k_\mu=1}^{N_s^\mu} |\alpha_{k_\mu}^{(1)} \hat{n}_{1k_\mu z}| \quad , \quad W_{32\mu} = \frac{1}{\sqrt{N_s^\mu}} \sum_{k_\mu=1}^{N_s^\mu} |\alpha_{k_\mu}^{(2)} \hat{n}_{2k_\mu z}| \tag{5.125}$$

For reasons identical to those given in the section on pure orthogonality blocking we may now change the sum over states to an integration; explicitly we take

$$\begin{aligned}
&\frac{1}{\mathcal{C}_{M_\mu}} \sum_{p \in M_\mu^p} e^{(m+h)\rho_{31\mu} - i(m-h)\rho_{32\mu} + (1+mh)\rho_{21\mu} - (1-mh)\rho_{22\mu}} \rightarrow \\
&\frac{1}{\sqrt{2\pi} W_{31\mu}} \int_{-\infty}^{\infty} d\rho_{31\mu} e^{\frac{-(\rho_{31\mu} - \bar{\rho}_{31\mu})^2}{2W_{31\mu}^2}} \frac{1}{\sqrt{2\pi} W_{32\mu}} \int_{-\infty}^{\infty} d\rho_{32\mu} e^{\frac{-(\rho_{32\mu} - \bar{\rho}_{32\mu})^2}{2W_{32\mu}^2}} \\
&\frac{1}{\sqrt{2\pi} W_{2\mu}} \int_{-\infty}^{\infty} d\rho_{21\mu} e^{\frac{-(\rho_{21\mu}^2 - \bar{\rho}_{21\mu})}{2W_{2\mu}^2}} \frac{1}{\sqrt{2\pi} W_{2\mu}} \int_{-\infty}^{\infty} d\rho_{22\mu} e^{\frac{-(\rho_{22\mu}^2 - \bar{\rho}_{22\mu})}{2W_{2\mu}^2}} \\
&\exp\left[(m+h)\rho_{31\mu} - i(m-h)\rho_{32\mu} + (1+mh)\rho_{21\mu} - (1-mh)\rho_{22\mu}\right]
\end{aligned} \tag{5.126}$$

Note that the reason that these integrations can be taken to be independent is because we are only keeping to quadratic order in $|\alpha_k|$. These gaussian integrations are easily performed, giving

$$\begin{aligned}
&\frac{1}{\mathcal{C}_{M_\mu}} \sum_{p \in M_\mu^p} e^{(m+h)\rho_{31\mu} - i(m-h)\rho_{32\mu} + (1+mh)\rho_{21\mu} - (1-mh)\rho_{22\mu}} \rightarrow \\
&\exp\left[(1+mh)\left[W_{31\mu}^2 + \bar{\rho}_{21\mu}\right] - (1-mh)\left[W_{32\mu}^2 + \bar{\rho}_{22\mu}\right] + (m+h)\bar{\rho}_{31\mu} - i(m-h)\bar{\rho}_{32\mu}\right]
\end{aligned} \tag{5.127}$$

Inserting these results into (5.124) gives us

$$\begin{aligned}
&\prod_\mu \bar{P}_{\uparrow\downarrow}^{M_\mu} = \frac{2\Delta_0^2 \pi}{\omega A} \sum_{m,h=\pm 1} e^{i(h\Phi - m\Phi^*)} \\
&\exp\left[(1+mh)\left[W_{31}^2 + \bar{\rho}_{21}\right] - (1-mh)\left[W_{32}^2 + \bar{\rho}_{22}\right] + (m+h)\bar{\rho}_{31} - i(m-h)\bar{\rho}_{32}\right]
\end{aligned} \tag{5.128}$$

Evaluation of the Ensemble Average Over Polarization Groups

Our expression for $\prod_\mu P_{\uparrow\downarrow}^{M_\mu}$ depends explicitly on the set $\{M_\mu\}$ via the quantities $\bar{\rho}_{21}$, $\bar{\rho}_{22}$, $\bar{\rho}_{31}$ and $\bar{\rho}_{32}$. In order to perform the ensemble average over the set $\{M_\mu\}$ we perform the same calculation as was introduced in the section on pure orthogonality blocking; namely we take

$$\sum_{APG} \prod_\mu W_{M_\mu} \to \prod_\mu \left[\frac{1}{\sqrt{2\pi N_s^\mu}} \int_{-\infty}^{\infty} dM_\mu e^{-M_\mu^2/2N_s^\mu} \right] \tag{5.129}$$

Substitution of this into the expression for the relaxation rate

$$\tau^{-1} = \frac{\omega}{\pi} \sum_{APG} \prod_\mu \left[W_{M_\mu} P_{\uparrow\downarrow}^{M_\mu} \right] \tag{5.130}$$

gives

$$\tau^{-1} = \frac{2\Delta_0^2}{A} \sum_{m,h=\pm 1} e^{i(h\Phi - m\Phi^*)} \prod_\mu \left[\frac{1}{\sqrt{2\pi N_s^\mu}} \int_{-\infty}^{\infty} dM_\mu e^{-M_\mu^2/2N_s^\mu} \right]$$
$$\exp\left[(1+mh)\left[W_{31}^2 + \bar{\rho}_{21} \right] - (1-mh)\left[W_{32}^2 + \bar{\rho}_{22} \right] + (m+h)\bar{\rho}_{31} - i(m-h)\bar{\rho}_{32} \right] \tag{5.131}$$

Performing the $\{M_\mu\}$ integrals gives

$$\tau^{-1} = \frac{2\Delta_0^2}{A} \sum_{m,h=\pm 1} e^{i(h\Phi - m\Phi^*)} \exp\left[(1+mh)\left[W_{31}^2 + \frac{I_\mu(5I_\mu - 1)}{12} \right] \sum_{k_\mu=1}^{N_s^\mu} {\alpha_{k_\mu}^{(1)}}^2 (1 - n_{1k_\mu z}^2) \right.$$
$$\left. -(1-mh)\left[W_{32}^2 + \frac{I_\mu(5I_\mu - 1)}{12} \right] \sum_{k_\mu=1}^{N_s^\mu} {\alpha_{k_\mu}^{(2)}}^2 (1 - n_{2k_\mu z}^2) \right] \exp\left[\frac{1}{2} \left[(m+h)W_{31} - i(m-h)W_{32} \right]^2 \right] \tag{5.132}$$

We can now perform the $\{m, h\}$ sums. The result can be written

$$\tau^{-1} = \frac{4\Delta_0^2}{A} \left[e^{\lambda_1} \cosh 2\varphi_1 + e^{-\lambda_2} \cos 2\varphi_0 \right] \tag{5.133}$$

where we have defined

$$\lambda_1 = 4W_{31}^2 + \frac{I_\mu(5I_\mu - 1)}{6} \sum_\mu \sum_{k_\mu=1}^{N_s^\mu} {\alpha_{k_\mu}^{(1)}}^2 (1 - n_{1k_\mu z}^2) \tag{5.134}$$

$$\lambda_2 = 4W_{32}^2 + \frac{I_\mu(5I_\mu - 1)}{6} \sum_\mu \sum_{k_\mu=1}^{N_s^\mu} {\alpha_{k_\mu}^{(2)}}^2 (1 - n_{2k_\mu z}^2) \tag{5.135}$$

Defining new phases

$$\widetilde{\phi_0} \equiv \frac{1}{2} \cos^{-1} \left(e^{-\lambda_2} \cos 2\varphi_0 \right)$$

and

$$\widetilde{\phi_1} \equiv \frac{1}{2} \cosh^{-1} \left(e^{\lambda_1} \cosh 2\varphi_1 \right)$$

we write

$$\widetilde{\Phi} = \widetilde{\phi_0} + i\widetilde{\phi_1} \tag{5.136}$$

in terms of which the expression (5.133) can be written

$$\tau^{-1} = \frac{\Delta_0^2 |\cos \widetilde{\Phi}|^2}{A} \tag{5.137}$$

which is identical to the result without topological decoherence *except that the phase* Φ *has been renormalized by the interaction with the nuclei.* This is exactly what we would expect to have happen here. Note that the inclusion of topological decoherence does not change the result that in the large A limit orthogonality blocking effects disappear.

General Solution for Arbitrary A

Now let us attack the arbitrary A case, starting with (5.121). The strategy that we will use in this most general case is as follows.

1. First, we perform the sum over states in M_μ^p, by converting this sum to a set of integrals over quantities that are functions of the set $\{p \in M_\mu^p\}$; explicitly we take

$$\frac{1}{\mathcal{C}_{M_\mu}} \sum_{p \in M_\mu^p} \rightarrow$$
$$\frac{1}{\sqrt{2\pi} W_{31\mu}} \int_{-\infty}^{\infty} d\rho_{31\mu} e^{\frac{-(\rho_{31\mu}-\bar{\rho}_{31\mu})^2}{2W_{31\mu}^2}} \frac{1}{\sqrt{2\pi} W_{32\mu}} \int_{-\infty}^{\infty} d\rho_{32\mu} e^{\frac{-(\rho_{32\mu}-\bar{\rho}_{32\mu})^2}{2W_{32\mu}^2}}$$
$$\frac{1}{\sqrt{2\pi} W_{2\mu}} \int_{-\infty}^{\infty} d\rho_{21\mu} e^{\frac{-(\rho_{21\mu}^2-\bar{\rho}_{21\mu})}{2W_{2\mu}^2}} \frac{1}{\sqrt{2\pi} W_{2\mu}} \int_{-\infty}^{\infty} d\rho_{22\mu} e^{\frac{-(\rho_{22\mu}^2-\bar{\rho}_{22\mu})}{2W_{2\mu}^2}}$$
$$\frac{1}{\sqrt{2\pi}} \int_{-\infty}^{\infty} d\rho_{41\mu} \delta(\rho_{41\mu} - \bar{\rho}_{41\mu}) \frac{1}{\sqrt{2\pi}} \int_{-\infty}^{\infty} d\rho_{42\mu} \delta(\rho_{42\mu} - \bar{\rho}_{42\mu}) \frac{1}{\sqrt{2\pi}} \int_{-\infty}^{\infty} d\rho_{1\mu} \delta(\rho_{1\mu} - \bar{\rho}_{1\mu})$$
$$\frac{1}{\sqrt{2\pi}\mathcal{W}(M_\mu)} \int_{-\infty}^{\infty} d\epsilon_1^\mu e^{-\frac{(\epsilon_1^\mu - \epsilon_1^{M_\mu})^2}{2\mathcal{W}^2(M_\mu)}} \tag{5.138}$$

As we have seen previously, taking all these integrations to be independent is justified as long as we only keep to quadratic order in our small parameters. Note that the widths of the three distributions $\{\rho_{1\mu}\}$, $\{\rho_{41\mu}\}$ and $\{\rho_{42\mu}\}$ are all quadratic in small parameters and therefore have been dropped (because these appear in quartic order in small parameters after the integrations), effectively replacing integrations over gaussians with integrations over delta functions.

2. Next we perform the ensemble average over polarization groups M_μ. Explicitly we take

$$\sum_{APG} \prod_{\mu} W_{M_\mu} \rightarrow \prod_{\mu} \left[\frac{1}{\sqrt{2\pi N_s^\mu}} \int_{-\infty}^{\infty} dM_\mu e^{-M_\mu^2/2N_s^\mu} \right] \tag{5.139}$$

3. Next we integrate over the variable X, which represents the "blip length".

4. We then perform the sums over $\{m, h\}$.

5. Finally, we change variables from $Y \rightarrow Z$. This gives us our final answer.

Let us perform all five of these steps explicitly, starting with (5.121);

$$\prod_{\mu} \bar{P}_{\uparrow\downarrow}^{M_\mu} = \frac{2\Delta_0^2 \pi}{\omega A} \int_{-A/2\omega}^{A/2\omega} dY \int_{-\infty}^{\infty} dX e^{i\left[XY + \frac{\xi}{\omega} X\right]} \sum_{m,h=\pm 1} e^{i(h\Phi - m\Phi^*)}$$

$$\prod_{\mu}\left[e^{-\frac{\Gamma_{M_\mu}^2}{\omega^2}X^2}\frac{1}{\mathcal{C}_{M_\mu}}\sum_{p\in M_\mu^p}e^{iX\frac{\epsilon_1^\mu}{\omega}-\frac{X^2\rho_{1\mu}^2}{\omega^2}}e^{(m+h)[\rho_{31\mu}-iX\rho_{41\mu}]-i(m-h)[\rho_{32\mu}-iX\rho_{42\mu}]+(1+mh)\rho_{21\mu}-(1-mh)\rho_{22\mu}}\right] \tag{5.140}$$

In order to complete step *1.* we must calculate the following;

$$\frac{1}{\mathcal{C}_{M_\mu}}\sum_{p\in M_\mu^p}e^{iX\frac{\epsilon_1^\mu}{\omega}-\frac{X^2\rho_{1\mu}^2}{\omega^2}}e^{(m+h)[\rho_{31\mu}-iX\rho_{41\mu}]-i(m-h)[\rho_{32\mu}-iX\rho_{42\mu}]+(1+mh)\rho_{21\mu}-(1-mh)\rho_{22\mu}}\rightarrow$$

$$\frac{1}{\sqrt{2\pi}W_{31\mu}}\int_{-\infty}^{\infty}d\rho_{31\mu}e^{\frac{-(\rho_{31\mu}-\bar{\rho}_{31\mu})^2}{2W_{31\mu}^2}}\frac{1}{\sqrt{2\pi}W_{32\mu}}\int_{-\infty}^{\infty}d\rho_{32\mu}e^{\frac{-(\rho_{32\mu}-\bar{\rho}_{32\mu})^2}{2W_{32\mu}^2}}$$

$$\frac{1}{\sqrt{2\pi}W_{2\mu}}\int_{-\infty}^{\infty}d\rho_{21\mu}e^{\frac{-(\rho_{21\mu}^2-\bar{\rho}_{21\mu})}{2W_{2\mu}^2}}\frac{1}{\sqrt{2\pi}W_{2\mu}}\int_{-\infty}^{\infty}d\rho_{22\mu}e^{\frac{-(\rho_{22\mu}^2-\bar{\rho}_{22\mu})}{2W_{2\mu}^2}}$$

$$\frac{1}{\sqrt{2\pi}}\int_{-\infty}^{\infty}d\rho_{41\mu}\delta(\rho_{41\mu}-\bar{\rho}_{41\mu})\frac{1}{\sqrt{2\pi}}\int_{-\infty}^{\infty}d\rho_{42\mu}\delta(\rho_{42\mu}-\bar{\rho}_{42\mu})\frac{1}{\sqrt{2\pi}}\int_{-\infty}^{\infty}d\rho_{1\mu}\delta(\rho_{1\mu}-\bar{\rho}_{1\mu})$$

$$\frac{1}{\sqrt{2\pi}\mathcal{W}(M_\mu)}\int_{-\infty}^{\infty}d\epsilon_1^\mu e^{-\frac{(\epsilon_1^\mu-\epsilon_1^{M_\mu})^2}{2\mathcal{W}^2(M_\mu)}}e^{iX\frac{\epsilon_1^\mu}{\omega}-\frac{X^2\rho_{1\mu}^2}{\omega^2}}$$

$$\exp\left[(m+h)\left[\rho_{31\mu}-iX\rho_{41\mu}\right]-i(m-h)\left[\rho_{32\mu}-iX\rho_{42\mu}\right]+(1+mh)\rho_{21\mu}-(1-mh)\rho_{22\mu}\right] \tag{5.141}$$

Evaluating these integrals and inserting the results into (5.140) gives

$$\prod_{\mu}\bar{P}_{\uparrow\downarrow}^{M_\mu}=\frac{2\Delta_0^2\pi}{\omega A}\int_{-A/2\omega}^{A/2\omega}dY\int_{-\infty}^{\infty}dXe^{i\left[XY+\frac{\xi}{\omega}X\right]}\sum_{m,h=\pm1}e^{i(h\Phi-m\Phi^*)}$$

$$\prod_{\mu}\left[\exp\left[-\frac{X^2}{\omega^2}\left(\Gamma_{M_\mu}^2+\bar{\rho}_{1\mu}^2+\frac{\mathcal{W}_{M_\mu}^2}{2}\right)+i\frac{X}{\omega}\epsilon_1^{M_\mu}-iX\bar{\rho}_{41\mu}(m+h)-(m-h)X\bar{\rho}_{42\mu}\right]\right.$$

$$\left.\exp\left[(1+mh)(W_{31}^2+\bar{\rho}_{21})-(1-mh)(W_{32}^2+\bar{\rho}_{22})+(m+h)\bar{\rho}_{31}-i(m-h)\bar{\rho}_{32}\right]\right] \tag{5.142}$$

We now move on to step *2.* The relaxation rate is written (5.28)

$$\tau^{-1}=\sum_{APG}\prod_{\mu}\left[W_{M_\mu}\tau_{M_\mu}^{-1}\right]\rightarrow$$

$$\frac{2\Delta_0^2}{A}\int_{-A/2\omega}^{A/2\omega}dY\int_{-\infty}^{\infty}dXe^{i\left[XY+\frac{\xi}{\omega}X\right]}\sum_{m,h=\pm1}e^{i(h\Phi-m\Phi^*)}$$
$$\prod_{\mu}\left[\frac{1}{\sqrt{2\pi N_s^{\mu}}}\int_{-\infty}^{\infty}dM_{\mu}e^{-M_{\mu}^2/2N_s^{\mu}}\right.$$
$$\exp\left[-\frac{X^2}{\omega^2}\left(\Gamma_{M_{\mu}}^2+\bar{\rho}_{1\mu}^2+\frac{\mathcal{W}_{M_{\mu}}^2}{2}\right)+i\frac{X}{\omega}\epsilon_1^{M_{\mu}}-iX\bar{\rho}_{41\mu}(m+h)-(m-h)X\bar{\rho}_{42\mu}\right]$$
$$\left.\exp\left[(1+mh)(W_{31}^2+\bar{\rho}_{21})-(1-mh)(W_{32}^2+\bar{\rho}_{22})+(m+h)\bar{\rho}_{31}-i(m-h)\bar{\rho}_{32}\right]\right] \tag{5.143}$$

Performing the integrations over $\{M_{\mu}\}$ gives

$$\tau^{-1}=\frac{2\Delta_0^2}{A}\int_{-A/2\omega}^{A/2\omega}dY\int_{-\infty}^{\infty}dXe^{i\left[XY+\frac{\xi}{\omega}X\right]}\sum_{m,h=\pm1}e^{i(h\Phi-m\Phi^*)}\exp\left[(1+mh)\frac{\lambda_1}{2}-(1-mh)\frac{\lambda_2}{2}\right]$$
$$\exp\left[-\frac{W^2X^2}{\omega^2}+iX\left[(m+h)\frac{\lambda_3 W}{\omega}+i(m-h)\frac{\lambda_4 W}{\omega}\right]\right] \tag{5.144}$$

where W, λ_1 and λ_2 are as previously and

$$\lambda_3=\frac{\mathcal{W}_{0_{\mu}}}{W}W_{31} \tag{5.145}$$

$$\lambda_4=\frac{\mathcal{W}_{0_{\mu}}}{W}W_{32} \tag{5.146}$$

We now perform step *3.*, the integration over the blip length X. This gives

$$\tau^{-1}=\frac{2\Delta_0^2\pi^{1/2}\omega}{WA}\int_{-A/2\omega}^{A/2\omega}dY\sum_{m,h=\pm1}e^{i(h\Phi-m\Phi^*)}\exp\left[(1+mh)\frac{\lambda_1}{2}-(1-mh)\frac{\lambda_2}{2}\right]$$
$$\exp\left[-\frac{\omega^2}{4W^2}\left[Y+\frac{\xi}{\omega}+(m+h)\frac{\lambda_3 W}{\omega}-i(m-h)\frac{\lambda_4 W}{\omega}\right]^2\right] \tag{5.147}$$

We next perform step *4.*, the sums over $\{m,h\}$. This gives

$$\tau^{-1}=\frac{2\Delta_0^2\pi^{1/2}\omega}{WA}\int_{-A/2\omega}^{A/2\omega}dY\left[\exp\left[\lambda_1-\lambda_3^2-\frac{\omega^2}{4W^2}(Y+\frac{\xi}{\omega})^2\right]\cosh\left[2\varphi_1+\lambda_3\frac{\omega}{W}(Y+\frac{\xi}{\omega})\right]\right.$$
$$\left.+\exp\left[-\lambda_2+\lambda_4^2-\frac{\omega^2}{4W^2}(Y+\frac{\xi}{\omega})^2\right]\cos\left[2\varphi_0+\frac{\lambda_4\omega}{W}(Y+\frac{\xi}{\omega})\right]\right] \tag{5.148}$$

Finally, step *5.* is a change of variables

$$Z = \frac{\omega}{2W}(Y + \frac{\xi}{\omega}) \tag{5.149}$$

which allows us to write this in the form

$$\tau^{-1} = \frac{\Delta_0^2}{2\sqrt{\pi}A}\int_{Z_-}^{Z_+} dZ e^{-Z^2}\left[e^{\lambda_1-\lambda_3^2}\cosh\left[2\varphi_1 + 2\lambda_3 Z\right] + e^{-\lambda_2+\lambda_4^2}\cos\left[2\varphi_0 + 2\lambda_4 Z\right]\right] \tag{5.150}$$

where

$$Z_\pm = \left(\frac{\pm A + \xi}{2W}\right) \tag{5.151}$$

Defining new phases

$$\widetilde{\phi_0}(Z) \equiv \frac{1}{2}\cos^{-1}\left[e^{-\lambda_2+\lambda_4^2}\cos\left[2\varphi_0 + 2\lambda_4 Z\right]\right] \tag{5.152}$$

and

$$\widetilde{\phi_1}(Z) \equiv \frac{1}{2}\cosh^{-1}\left[e^{\lambda_1-\lambda_3^2}\cosh\left[2\varphi_1 + 2\lambda_3 Z\right]\right] \tag{5.153}$$

we write

$$\tilde{\Phi}(Z) = \widetilde{\phi_0}(Z) + i\widetilde{\phi_1}(Z) \tag{5.154}$$

in terms of which our final relaxation rate may be written

$$\tau^{-1} = \frac{\Delta_0^2}{\sqrt{\pi}A}\int_{Z_-}^{Z_+} dZ e^{-Z^2}\left|\cos\tilde{\Phi}(Z)\right|^2 \tag{5.155}$$

Evaluation of the General Relaxation Rate in the Small A Limit

When A is large the general relaxation rate reduces to that for pure topological decoherence (5.137). When A becomes small, however, we expect to see some interplay between

orthogonality blocking and topological decoherence effects. In this limit we may rewrite the relaxation rate in the form

$$\tau^{-1} \approx \frac{\Delta_0^2}{\sqrt{\pi}A}|Z_+ - Z_-|e^{-\left(\frac{Z_- + Z_+}{2}\right)^2}|\cos\tilde{\Phi}\left(\frac{Z_- + Z_+}{2}\right)|^2$$
$$= \frac{\Delta_0^2}{\sqrt{\pi}W}\exp\left[-\frac{\xi^2}{4W^2}\right]\left|\cos\tilde{\Phi}\left(\frac{\xi}{2W}\right)\right|^2 \tag{5.156}$$

We see from (5.156) that there is a seemingly unusual dependence upon the external DC bias field when both orthogonality blocking and topological decoherence effects are present. However the reason for this form is evident. As in the case of pure orthogonality blocking, we see that there exists a gaussian profile with external bias. As well, the topological phase term has acquired a longitudinal bias dependence. This last occurs because the axes of quantization of each of the k nuclear spins that we have chosen, that is $\hat{z}_k = \hat{\gamma}_k^{(1)}$ and $\hat{x}_k = \frac{\hat{\gamma}_k^{(2)} + \cos 2\beta_k \hat{\gamma}_k^{(1)}}{\sin 2\beta_k}$, do not in general correspond with the axes of the central spin Hamiltonian, which are also the axes with which the topological decoherence terms are described. When we calculate the values for the topological decoherence terms $\vec{A}_{N,D}^k$, these are by definition off-diagonal in the axes of the spin Hamiltonian. But when these are rotated into the axes defined by the orthogonality blocking parameters they acquire, in general, longitudinal components. It is these longitudinal components, coming from this mismatch of preferred axes, that gives rise to the presence of a longitudinal bias term in the topological phase in (5.155) and (5.156). When orthogonality blocking effects disappear, such as we found happens in the large A limit, this rotation of axes is not necessary and this effect is not present (5.137).

5.6 The General Single Molecule Relaxation Rate in Fe_8

We now wish to evaluate the quantities entering into (5.155) for the specific case of the Fe_8 molecular magnet. We will begin by evaluating the contributions that arise from

Quantity	Definition
ω_0	$\frac{1}{\sum_{k=1}^{N+8} 2I_k} \sum_{k=1}^{N+8} \omega_k^{\|\|}$
Γ_0^2	$\frac{1}{\sum_{k=1}^{N+8} 2I_k} \sum_{k=1}^{N+8} \left(\omega_k^{\|\|} - \omega_0\right)^2$
ρ_1^2	$\sum_\mu \frac{5I_\mu - 1}{24 I_\mu} \sum_{k_\mu=1}^{N_s^\mu} \lvert\vec{\gamma}_{k_\mu}^{(1)}\rvert^2 \sin^2 2\beta_{k_\mu}$
$\mathcal{W}^2(0)$	$\sum_\mu \frac{4}{N_s^\mu} \left[\sum_{k_\mu=1}^{N_s^\mu} \lvert\vec{\gamma}_{k_\mu}^{(1)}\rvert \cos^2 \beta_{k_\mu}\right]^2$
W^2	$\Gamma_0^2 + \rho_1^2 + \mathcal{W}^2(0)$

Table 5.1: Quantities coming from orthogonality and degeneracy blocking.

orthogonality and degeneracy blocking effects, namely ρ_1^2, Γ_0^2 and $\mathcal{W}(0)$. How these quantities are defined, in terms of the more fundamental quantities in the theory, is repeated for convenience in table 5.1. In table 5.2 we present zero field values for Γ_0 and ω_0 for the three species Fe_{8*}, Fe_{8D} and $^{57}Fe_8$. The quantities ρ_1 and $\mathcal{W}(0)$ will be functions of any external bias field present, both because of the field magnitudes $|\vec{\gamma}_{k_\mu}|$ and their changing directions, imbodied in the orthogonality blocking parameters β_{k_μ}. Shown in figures 5.6 through 5.11 are ρ_1, $\mathcal{W}(0)$ and Γ_0 as functions of an external static transverse magnetic field oriented along the x direction (as defined by the central spin Hamiltonian) in the Fe_8 molecular magnet, for various species. In figure 5.12 is shown the full width W for the three varieties Fe_{8*}, Fe_{8D} and $^{57}Fe_8$.

	Fe_8	Fe_{8D}	$^{57}Fe_8$
Γ_0	10.64	3.22	12.96
ω_0	8.32	2.93	10.04

Table 5.2: Zero external field values for Γ_0 and ω_0 for the three species shown. Units are in MHz.

We now consider the terms owing their existence only to topological decoherence effects. These terms, unlike the ones dealt with in the preceding, are not strong functions of an externally applied transverse field (although there is a small dependence, since the application of an external field shifts the minima of the central spin object, thereby changing the phase that it accumulates in tunneling from $|\uparrow>$ to $|\downarrow>$ or viceversa). Therefore it is enough to calculate their values in zero transverse field. The definitions of λ_1 and λ_2 are repeated in table 5.3. Contributions to these from different nuclear species are shown in table 5.4. Values for λ_1 and λ_2 for the three varieties Fe_{8*}, Fe_{8D} and $^{57}Fe_8$ are shown in table 5.5.

Quantity	Definition
λ_1	$\sum_\mu \left[\frac{4}{N_s^\mu}\left[\sum_{k_\mu=1}^{N_s^\mu} \lvert\alpha_{k_\mu}^{(1)}\hat{n}_{1k_\mu z}\rvert\right]^2 + \frac{I_\mu(5I_\mu-1)}{6}\sum_{k_\mu=1}^{N_s^\mu}\alpha_{k_\mu}^{(1)^2}(1-\hat{n}_{1k_\mu z}^2)\right]$
λ_2	$\sum_\mu \left[\frac{4}{N_s^\mu}\left[\sum_{k_\mu=1}^{N_s^\mu} \lvert\alpha_{k_\mu}^{(2)}\hat{n}_{2k_\mu z}\rvert\right]^2 + \frac{I_\mu(5I_\mu-1)}{6}\sum_{k_\mu=1}^{N_s^\mu}\alpha_{k_\mu}^{(2)^2}(1-\hat{n}_{2k_\mu z}^2)\right]$

Table 5.3: Quantities coming solely from topological decoherence effects.

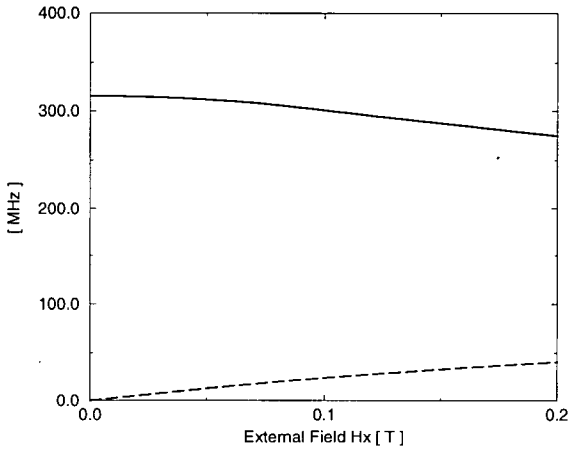

Figure 5.6: $\rho_{1\mu}$ (dashed) and $\mathcal{W}(0_\mu)$ (solid) for $\mu =^1 H$.

$\mu =$	^1H	^{79}Br	^{14}N	^{13}C	^{17}O	^{57}Fe
$\lambda_{1\mu}$	$1.45 \cdot 10^{-6}$	$0.06 \cdot 10^{-6}$	$0.03 \cdot 10^{-6}$	$0.66 \cdot 10^{-6}$	$0.11 \cdot 10^{-6}$	$0.18 \cdot 10^{-6}$
$\lambda_{2\mu}$	$12.8 \cdot 10^{-6}$	$0.13 \cdot 10^{-6}$	$0.13 \cdot 10^{-6}$	$0.61 \cdot 10^{-6}$	$0.31 \cdot 10^{-6}$	$0.60 \cdot 10^{-6}$

Table 5.4: Zero field values of the topological decoherence terms for species in Fe_8.

Finally, we consider terms that arise from the interplay of orthogonality blocking, degeneracy blocking and topological decoherence. These quantities are listed in table 5.6. These of course will be functions of any external transverse field because of the presence of the orthogonality blocking terms. Shown in figure 5.13 are λ_3 and λ_4 as functions of H_x for Fe_{8*}, Fe_{8D} and $^{57}Fe_8$.

The "bare" phase $\Phi = \varphi_0 + i\varphi_1$ is uniquely defined by the choice of a central spin

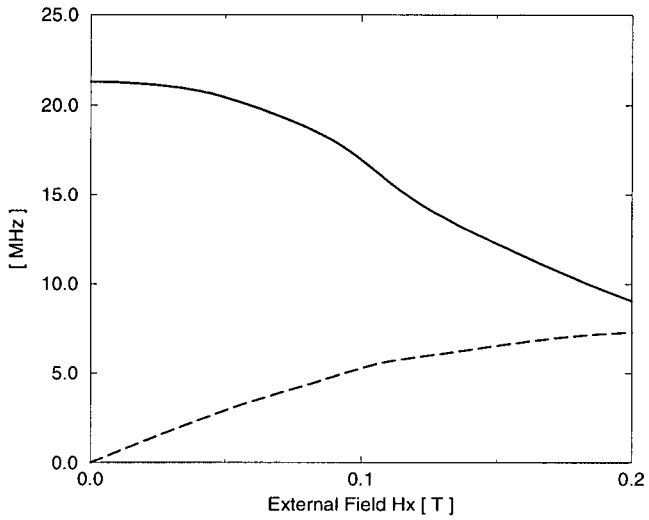

Figure 5.7: $\rho_{1\mu}$ (dashed) and $\mathcal{W}(0_\mu)$ (solid) for $\mu =^{79} Br$.

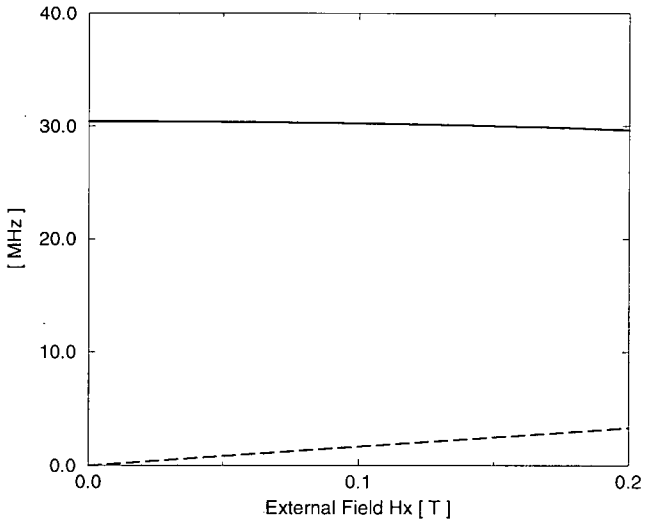

Figure 5.8: $\rho_{1\mu}$ (dashed) and $\mathcal{W}(0_\mu)$ (solid) for $\mu =^{14} N$.

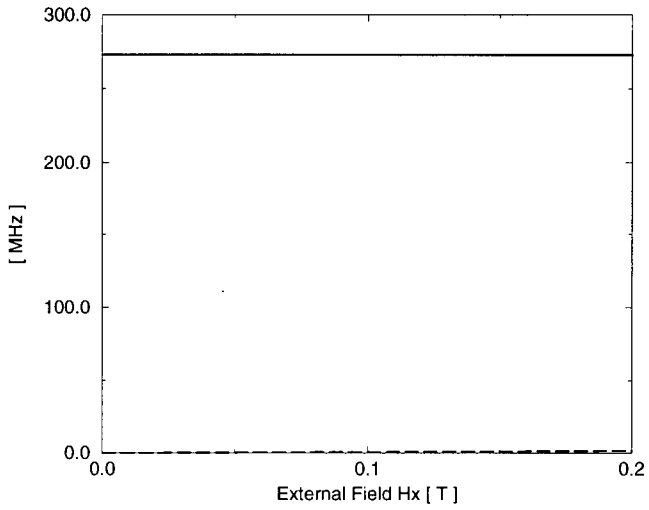

Figure 5.9: $\rho_{1\mu}$ (dashed) and $\mathcal{W}(0_\mu)$ (solid) for $\mu = ^{57} Fe$.

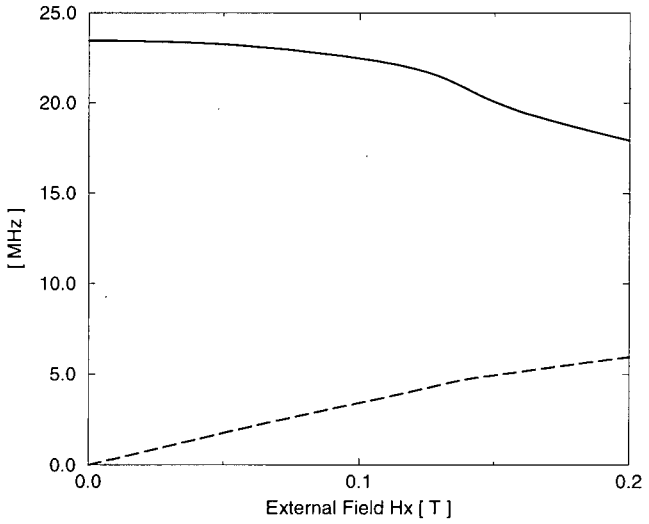

Figure 5.10: $\rho_{1\mu}$ (dashed) and $\mathcal{W}(0_\mu)$ (solid) for $\mu = ^{17} O$.

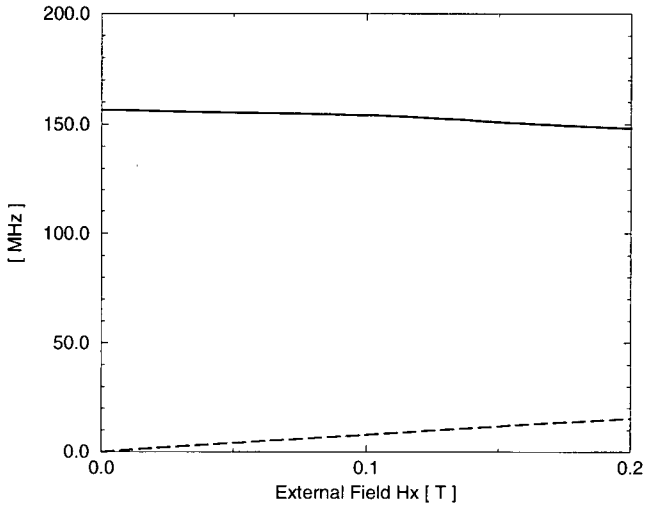

Figure 5.11: $\rho_{1\mu}$ (dashed) and $\mathcal{W}(0_\mu)$ (solid) for $\mu =^{13} C$.

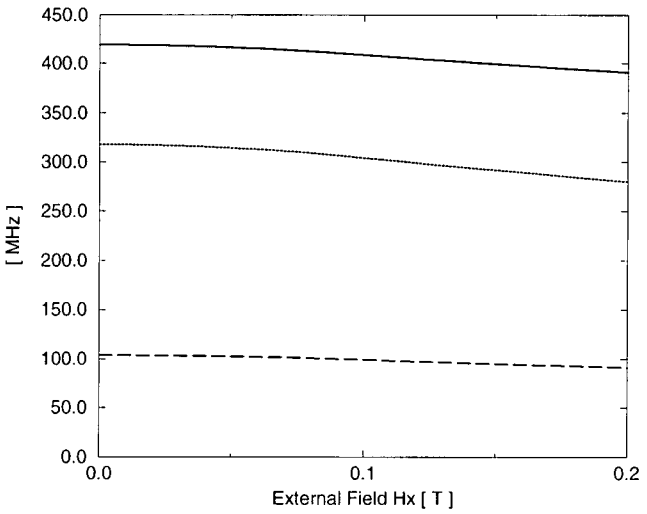

Figure 5.12: Full width W for Fe_{8*} (dotted), Fe_{8D} (dashed) and $^{57}Fe_8$ (solid).

	Fe_{8*}	Fe_{8D}	$^{57}Fe_8$
λ_1	$1.54 \cdot 10^{-6}$	$0.53 \cdot 10^{-6}$	$1.72 \cdot 10^{-6}$
λ_2	$13.06 \cdot 10^{-6}$	$4.16 \cdot 10^{-6}$	$13.66 \cdot 10^{-6}$

Table 5.5: Topological decoherence terms for three varieties of Fe_8.

Quantity	Definition
λ_3	$\sum_\mu \sum_{k_\mu=1}^{N_s^\mu} \frac{\mathcal{W}_{0\mu}}{\sqrt{N_s^\mu W}} \lvert \alpha_{k_\mu}^{(1)} \hat{n}_{1k_\mu z} \rvert$
λ_4	$\sum_\mu \sum_{k_\mu=1}^{N_s^\mu} \frac{\mathcal{W}_{0\mu}}{\sqrt{N_s^\mu W}} \lvert \alpha_{k_\mu}^{(2)} \hat{n}_{2k_\mu z} \rvert$

Table 5.6: Quantities that come about due to interplay between orthogonality blocking, degeneracy blocking and topological decoherence effects.

Hamiltonian. In our case we have chosen to use the spin Hamiltonian

$$H = -DS_z^2 + E(S_+^2 + S_-^2) + C(S_+^4 + S_-^4) \tag{5.157}$$

where $D = 0.292K$, $E = 0.046K$ and $C = -2.9 \cdot 10^{-5}K$. The bare tunneling splitting between nearly degenerate ground states $|\pm 10>$ can be found via exact diagonalization (see chapter 2) and is

$$\Delta_0 \approx 3.9 \cdot 10^{-8}K \tag{5.158}$$

Truncating the quartic spin term gives us an "easy-axis easy-plane" spin Hamiltonian

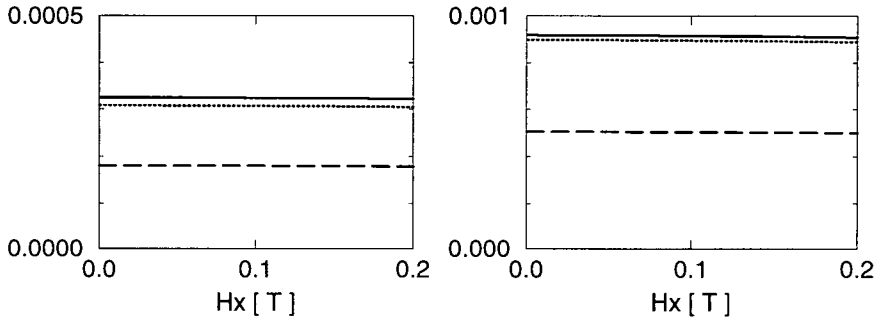

Figure 5.13: λ_3 (left) and λ_4 (right) for the three varieties Fe_{8*} (dotted), Fe_{8D} (dashed) and $^{57}Fe_8$ (solid).

which gives bare phases

$$\varphi_0 = \pi S - \frac{\pi S g \mu_B H_y}{\Omega_0} \quad , \quad \varphi_1 = \frac{S^2 \pi g \mu_B H_x}{2\tilde{E}} \tag{5.159}$$

Looking back at our general expression for the single molecule relaxation rate (5.155), we see that we have now calculated all of the parameters in this expression. Fixing the spin Hamiltonian gives a single molecule AC relaxation rate with no free parameters.

5.6.1 Effect of the Nuclear Spin Environment on the Large A Single Molecule Relaxation Rate in Fe_8

Shown in figure (5.14) are plots of two quantities. The first is the quantity $\Delta = \sqrt{A\tau^{-1}}$ calculated without the addition of any nuclear spins; that is,

$$\Delta = \Delta_0 |\cos \Phi| \tag{5.160}$$

The second is the quantity Δ, with the addition of nuclei to the effective Hamiltonian; that is,

$$\Delta = \Delta_0 |\cos \tilde{\Phi}| \tag{5.161}$$

We see that the phase renormalization $\Phi \rightarrow \tilde{\Phi}$ coming from the nuclei causes a tiny smoothing of the "nodes" seen in Δ calculated using the bare spin Hamiltonian. Furthermore, because we know how this renormalization depends on the nuclear spins we can predict the shape of this smoothing effect. This being said, it is obvious in this particular material that this effect is extremely weak, because of the small values of the topological decoherence parameters.

One should note that what we are calculating here is the *single molecule* relaxation rate. If we were to include many molecules, as is the case in a real crystal, we would have to include the effects of the transverse dipolar fields in Φ (ie. H_x and H_y don't only come from the external field; there are also internal dipolar fields of this kind). This is the basic reason why the data shown in figures 1.20 and 1.21 is so "smoothed"–this effect comes about because of non-zero H_y in the phase $\tilde{\Phi}$ coming from internal dipolar fields (we shall treat the multi-molecule case in the next chapter).

5.7 Summary and Discussion of Results

In this chapter we began with the full effective Hamiltonian (5.6) for a general molecular magnet in an external time dependent field. We derived a formal expression for the one-molecule relaxation rate in such a system, and solved it for the special case of a sawtooth external field in the absence of quadrupolar couplings to the nuclei. The general one-molecule relaxation rate in this case was found to be

$$\tau^{-1} = \frac{\Delta_0^2}{\sqrt{\pi}A} \int_{Z_-}^{Z_+} e^{-Z^2} \left|\cos \tilde{\Phi}(Z)\right|^2 \tag{5.162}$$

where needed definitions may be found in (5.151) and the equations that directly follow, (5.134), (5.135), (5.145) and (5.146).

This form for the relaxation rate simplifies in the limit that the sweeping amplitude is greater than both the energy width W and any external bias ξ. In this limit the

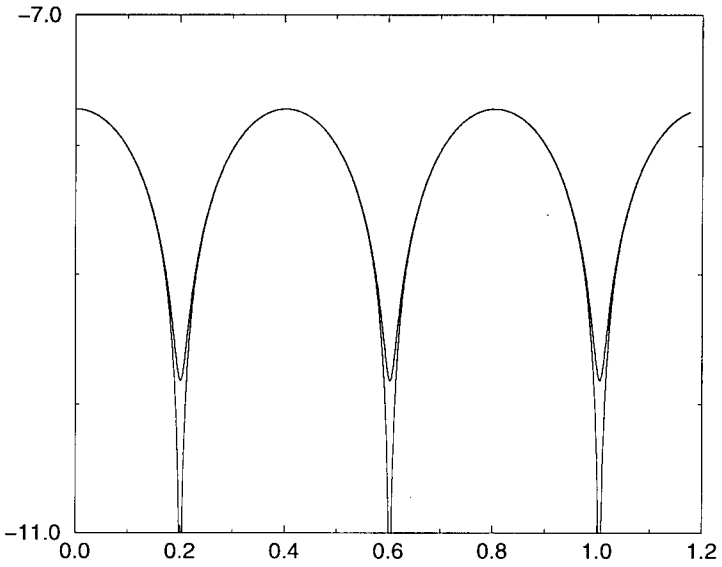

Figure 5.14: Presented here are (1) the bare result $\Delta_0|\cos\Phi|$ (the lower curve) and (2) the large A result with nuclear spins $\Delta_0|\cos\tilde{\Phi}|$ (the middle curve) plotted in units of Kelvin. Note the logarithmic vertical scale. The horizontal axis is H_x in Tesla–here we have $\varphi = 0$ ($H_y = 0$).

relaxation rate can be written

$$\tau^{-1} = \frac{\Delta_0^2|\cos\tilde{\Phi}|^2}{A} \tag{5.163}$$

where the nuclear spins have caused a renormalization of the Berry phase $\Phi \to \tilde{\Phi}$ in a way that we can calculate with no free parameters (once the positions of the nuclei are fixed). Note that in this case orthogonality blocking does not affect the relaxation rate at all. We saw in the case of the Fe_8 system that this phase renormalization coming from the nuclear spins was slight. However this need not be the case in general. We may draw some far reaching conclusions from this result– basically that the presence of spin environments that couple to magnetic degrees of freedom "randomize" the central Berry phase term, destroying Aharonov-Bohm type oscillations. This is hardly surprising. This

being said, we have shown quantitatively herein just how it happens and how to calculate the effects of a spin environment on this kind of topological decoherence.

When the amplitude of the sweeping field is much smaller than the total energy spread $|W + \xi|$ we find that

$$\tau^{-1} = \frac{\Delta_0^2}{\sqrt{\pi}W} \exp\left[-\frac{\xi^2}{4W^2}\right] \left|\cos\tilde{\Phi}\left(\frac{\xi}{2W}\right)\right|^2 \tag{5.164}$$

There are two things to note here. One is that the form for the one-molecule relaxation rate is *gaussian*, not exponential as is reported in the literature. We have explained the reasons behind this discrepancy and the reasons why we believe the gaussian form is more appropriate to the physics of molecular magnets. The second thing here is that there is an explicit interplay between topological decoherence and orthogonality blocking effects here which manifests itself in a ξ dependent Berry phase. However, we have shown that for the specific case of Fe_8, the oscillations in ξ coming from this term are far too small to be seen. Again, we do not expect this to hold in the general case–it is quite possible that in systems that have large amounts of topological decoherence coming from a spin bath the oscillations in $\tau^{-1}(\xi)$ will be apparent (these could be measured in a similar manner to recent experiments performed on Fe_8 which extract just this quantity).

We compared our general large A relaxation rate with that of the simple no-environment spin Hamiltonian (5.157). We found that the nuclear spins smooth out the cusps near the nodes in the relaxation rate. The effect of the nuclei considered is rather small in Fe_8; however, this need not be the case in general.

Chapter 6

AC Relaxation in a Crystal of Molecular Magnets

In this chapter we use the results obtained in the previous chapter to investigate what form the relaxation of the magnetization in a crystal of molecular magnets takes. In essence what we shall do is insert the one-molecule relaxation rate calculated in chapter 5 (5.155) into a master equation [15, 167] and solve it in various limits. In particular we shall be concerned with short-time relaxation in the presence of an external sawtooth field of arbitrary amplitude.

6.1 Preamble

The results derived in the previous section are single-molecule relaxation rates. In other words, in their derivation we have omitted completely from consideration all effects coming from intra-molecular terms in the full crystal Hamiltonian. The full Hamiltonian of a crystal of molecular magnets may be written in the form

$$H = \sum_i \mathcal{H}_i + \sum_{i<j} \mathcal{V}_{ij} \tag{6.1}$$

where $\mathcal{H}_i$ is the single-molecule Hamiltonian for the i^{th} molecule (including external fields) and $\mathcal{V}_{ij}$ gives the total interaction between the i^{th} and j^{th} molecules. This interaction will be dominated by magnetic dipolar interactions between off-site magnetic atoms. Now when we attempt to calculate the relaxation characteristics of the entire crystal, we see that it is not enough to know the single-molecule relaxation rates–there are other important terms in the crystal Hamiltonian.

In order to get a feel for the physics going on inside one of these crystals during a relaxation experiment, let's attempt to qualitatively describe this relaxation first before dealing directly with (6.1). This qualitative treatment will follow the course of the standard experiments of this type that are currently being performed on these systems (see chapter 1).

There are two standard ways of initially preparing these materials before their relaxation characteristics are measured. The first of these involves placing the sample in a large (5-8 T) DC magnetic field aligned along the $\hat{z}$ axis of the crystal at some high temperature, and then cooling the sample down slowly to the mK regime. This technique has the effect of preparing the material in an initially polarized state–all the magnetic ions will be such that each molecule will be in the "up" state at the beginning of the experiment. The second way to prepare the sample is to place the crystal in a smaller (0-5 T) $\hat{z}$ axis magnetic field at a high temperature, and then *quench* the system's temperature very quickly down to the mK regime. This has the effect of giving the crystal some less than full initial magnetization (which is a function of the strength of the original DC field) while making sure that there are no significant off-site correlations at the beginning of the experiment (why this consideration is important will soon become apparent!).

Let's begin our qualitative ponderings with some generally applicable remarks. In either of the above cases, each molecule in the sample will feel some bias field coming from the sum over the contributions of all the other molecules. These bias fields will have some distribution over the crystal, whose details depend on the sample shape. Now if the longitudinal (ie., along the $\hat{z}$-axis) bias on any particular molecule is much bigger than the "resonance window" given by our single-molecule relaxation rate (5.155), this molecule will be *frozen* in its original state. It is completely unable to relax! We note in passing that if we remove the effects of nuclear spins from our single-molecule relaxation rate, the resonance window shrinks down to encompass only external biases $\xi < \Delta_0$.

Because the values of the bare tunneling matrix elements in these materials are small (typically $< 10^{-6}K$), any significant longitudinal bias distribution will freeze the entire crystal. Typically the initial bias distribution in these materials varies over a range of $\sim 0.1 - 1\ K$, orders of magnitude larger than Δ_0! Because significant short-time relaxation is seen experimentally in both Fe_8 and Mn_{12}, we infer that the nuclear spins are actually *crucial* to the physics here [20, 51, 49].

Now let's imagine what will happen as the crystal starts to relax. We now have to specify the type of field applied during the relaxation process. There are two main possibilities for which experimental results have been obtained; either we apply a DC field in any direction, or we apply a longitudinal AC field. Now regardless of the form of the applied field, the following considerations apply. We have imagined that there exists a distribution of longitudinal biases in the crystal. Now there will be some fraction of the crystal for whom the bias is smaller than their resonance window (which is a function of the applied field through (5.155)). This fraction is able to relax. When one of these molecules does relax (by tunneling to the "down" state) it *rearranges the distribution of bias fields over the crystal.* This is because instead of contributing an "up" to the total internal field it now contributes a "down". We see therefore that the internal field distribution will *evolve* in time in a peculiar way–all molecules that are inside the bias window will begin to flip, and will "dig a hole" in the bias distribution near zero bias, sending their weight out into the distribution's wings. This will slow down the relaxation, as there are less and less molecules available in the resonance window as time progresses. As we have seen in chapter 1, this effect has recently been observed in Fe_8 [51]. Now in terms of a quantitative theory, what does this mean?

6.2 The Generalized Master Equation

There is one characteristic here that is apparent, and that is that as the crystal starts to relax, *correlations* between different sites begin to develop. That is, the relaxation of the crystal is strongly dependent on its history. It has been suggested [15] that these correlations may be dealt with similarly to the way that correlations in spin glasses are treated, namely by the definition of a series of many-molecule distribution functions which are related via an expression of the BBGKY type. We shall in what follows use this technique and see what results we can obtain and which remain elusive.

We begin by writing the magnetization of a crystal of molecular magnets in the form

$$M(t) = \sum_{\vec{r}} \int d\vec{H} M(\vec{r}, \vec{\mathcal{H}}, t) = \sum_{\vec{r}} \int d\vec{\mathcal{H}} (2P_{\uparrow}(\vec{r}, \vec{\mathcal{H}}, t) - 1) \tag{6.2}$$

where $P_{\uparrow}(\vec{r}, \vec{\mathcal{H}}, t)$ is the normalized probability of the central spin complex at site $\vec{r}$ to be "up" (ie. in state $|S_z = +S\rangle$) and in a DC bias field $\vec{\mathcal{H}}$ at time t.

To obtain a solution for $P_{\uparrow}(\vec{r}, \vec{\mathcal{H}}, t)$ we shall proceed in the following manner. We noted in the previous chapter that for frequencies lower than the nuclear T_2 energy scale $>\sim \Gamma_0$ each pass of the AC field through resonance is decorrelated from all other such passes. This means that we may calculate the transition probability for a single pass and by simply dividing this by the period of the ac field obtain a single-molecule relaxation rate $\tau^{-1}(A, \omega; \vec{\mathcal{H}})$. Knowledge of this rate allows us to write a kinetic or "master" equation of the form [15, 20]

$$\begin{aligned} \dot{P}_{\alpha}(\vec{r}, \vec{\mathcal{H}}, t) &= -\tau^{-1}(A, \omega; \vec{\mathcal{H}})\{P_{\alpha}(\vec{r}, \vec{\mathcal{H}}, t) - P_{-\alpha}(\vec{r}, \vec{\mathcal{H}}, t)\} \\ &- \sum_{\vec{r}', \alpha'} \int d\vec{\mathcal{H}}' \tau^{-1}(A, \omega, \vec{\mathcal{H}}')[P^{(2)}_{\alpha\alpha'}(\vec{r}, \vec{r}'; \vec{\mathcal{H}}, \vec{\mathcal{H}}'; t) - P^{(2)}_{\alpha\alpha'}(\vec{r}, \vec{r}'; \vec{\mathcal{H}} - \alpha\alpha' V_D(\vec{r} - \vec{r}'), \vec{\mathcal{H}}'; t)] + \ldots \end{aligned} \tag{6.3}$$

where $P^{(2)}$ is a 2-molecule distribution function, ie. the joint probability of two molecules

having the characteristics implied by their arguments. $V_D(\vec{r}-\vec{r}')$ represents the DC bias at $\vec{r}$ coming from the molecule at site $\vec{r}'$, which as we have mentioned is due to magnetic dipolar interactions. We have not explicitly written out the higher order multimolecular terms $P^{(3)}, P^{(4)}$, etc., representing these by an ellipsis (...). As the crystal relaxes, the influence of these higher order terms will begin to be significant. However, in the initial stages of relaxation, we shall assume that these can be neglected. This approximation will only hold for some limited time from the preparation of the initial state and it remains to be shown that this time is long enough to be significant.

6.3 Short Time Dynamics

In the early stages of the relaxation of a crystal of molecular magnets, there will be two dominant contributions to the physics. The first of these is given by the first term on the right-hand side of (6.3), and corresponds to "local" relaxation. If we were to neglect all terms but this first one we would find that the relaxation would be linear in time. Another way of saying this is that if all of the molecules relaxed independently of each other, then the total relaxation of the crystal has to be exponential (and therefore linear at short times). Defining the quantities

$$M(\vec{r},\vec{\mathcal{H}},t) \equiv P_{\uparrow}(\vec{r},\vec{\mathcal{H}},t) - P_{\downarrow}(\vec{r},\vec{\mathcal{H}},t) \quad , \quad M(\vec{\mathcal{H}},t) = \sum_{\vec{r}} M(\vec{r},\vec{\mathcal{H}},t) \quad , \quad M(t) = \int d\vec{H} M(\vec{\mathcal{H}},t)$$

allows us to write

$$\dot{P}_{\alpha}(\vec{r},\vec{\mathcal{H}},t) = -\tau^{-1}(A,\omega;\vec{\mathcal{H}})\{P_{\alpha}(\vec{r},\vec{\mathcal{H}},t) - P_{-\alpha}(\vec{r},\vec{\mathcal{H}},t)\} \tag{6.4}$$

in the form

$$\dot{M}(\vec{\mathcal{H}},t) = -\tau^{-1}(A,\omega;\vec{\mathcal{H}})M(\vec{\mathcal{H}},t) \tag{6.5}$$

Now if this is the whole story (ie. we neglect all corrections to this) this is easily solved, giving

$$M(\vec{\mathcal{H}},t) = M(\vec{\mathcal{H}},0)e^{-t/\tau(A,\omega;\vec{\mathcal{H}})} \tag{6.6}$$

and therefore

$$M(t) = \int d\vec{\mathcal{H}} M(\vec{\mathcal{H}},0)e^{-2/\tau(A,\omega;\vec{\mathcal{H}})} \tag{6.7}$$

which has short time behaviour

$$M(t) \sim 1 - t\int d\vec{\mathcal{H}}\; M(\vec{\mathcal{H}},0)\; \tau^{-1}(A,\omega;\vec{\mathcal{H}}) \tag{6.8}$$

which, as we have claimed, is linear in time.

Now we turn to the leading sub-dominant term in (6.3). How do we incorporate the leading corrections to the local term, and what effect will this have on the relaxation characteristics?

As the crystal begins to relax, the internal bias distribution (and therefore $M(\vec{\mathcal{H}},t)$) will change in time in a way that one can calculate analytically in an ellipsoidal crystal (see Appendix A). This redistribution of biases is exactly the effect that the leading correction term in (6.3) has on the relaxation. We can therefore take into account the leading corrections by simply inserting the form derived in Appendix A for $M(\vec{\mathcal{H}},t)$ into the local term (6.5). This gives us the following equation for the relaxation rate, incorporating both the local relaxation and the first corrections to it;

$$\dot{M}(t) = -\int d\vec{\mathcal{H}}\; \tau^{-1}(A,\omega;\vec{\mathcal{H}})\; M(\vec{\mathcal{H}},t) \tag{6.9}$$

where $M(\vec{\mathcal{H}},t)$ is the (evolving) distribution of biases derived in Appendix A and $\tau^{-1}(A,\omega;\vec{\mathcal{H}})$ is the general single-molecule relaxation rate derived in the previous chapter (5.155).

6.3.1 Strongly Annealed Samples and the Large A Limit

As we have seen earlier when the external sweeping amplitude is large enough to sweep all molecules through resonance, ie. when $A > H_z + W_D$, the relaxation rate simplifies considerably. We have also seen that in the Fe_8 material topological decoherence effects are minimal. If we ignore these we find that the relaxation rate can be written in the form

$$\tau^{-1}(A, H_x, H_y) = \frac{\Delta_0^2 \left|\cos \Phi(H_x, H_y)\right|^2}{A} \tag{6.10}$$

Let us now consider the experimentally relevant case of strong annealing, where the initial magnetization $M(t_0) \ll M_0$, the saturated magnetization. In this situation the initial magnetization distribution over the applied field is gaussian (see [200] and refs. therein)

$$M(\vec{H}, t_0) = \left(\frac{2}{\pi W_D^2(M)}\right)^{3/2} M(t_0) \exp\left[-\frac{2}{W_D^2(M)} \sum_{l=x,y,z} (H_l - H_l^0)\right] \tag{6.11}$$

The half-width $W_D(M)$ is directly measured in experiments [] and is much larger than E_0 for Fe_8. Note that the observation that W_D is a function of M and is directly extractable from experiment is due to work by Stamp and Tupitsyn [198].

Plugging (6.10) and (6.11) into (6.9) allows us to solve for $M(t)$. We find that

$$M(t) = M(t_0) \exp\left[-\Gamma_{AC}(\vec{H}, M)t\right] \tag{6.12}$$

where the relaxation rate is

$$\Gamma_{AC}(\vec{H}, M) = \frac{2\Delta_0^2}{\pi W_D^2(M) A} \int dH_x \int dH_y \left|\cos \Phi(H_x, H_y)\right|^2 \exp\left[\frac{-2}{W_D^2(M)} \left[(H_x - H_x^0)^2 + (H_y - H_y^0)^2\right]\right] \tag{6.13}$$

Now as we have stressed throughout this document, our analysis depends on the choice of a particular spin Hamiltonian (for Fe_8 this was the easy-axis easy-plane Hamiltonian).

The choice of the parameters in the spin Hamiltonian strongly affects the dependence of the tunneling matrix element on external transverse fields. This is relevant here as the dependence on H_x and H_y in the relaxation rate changes if we use a different spin Hamiltonian as we saw in chapter 2. In addition, in deriving our relaxation rate (6.9), we have assumed the instanton calculation which of course is not exact. In order to extract the correct tunneling amplitude as a function of external field, we have to exactly diagonalize the spin Hamiltonian plus the external field. That is, the correct expression takes our $\Delta_0|\cos\Phi(H_x,H_y)|$ to $|\Delta(H_x,H_y)|$ extracted by exact diagonalization.

There is a specific case where we can get around the first difficulty, and that is near the nodes of the tunneling amplitude–this case has been treated independently by Stamp and Tupitsyn [198, 200] and we will review their results in the following section. In this case the tunneling amplitude will be extracted by exact diagonalization and therefore comparing our results to theirs allows us to gauge the accuracy of our instanton approximation.

In the case where the spin Hamiltonian is the easy-axis easy-plane model we have seen that, in the limit being considered,

$$|\cos\Phi(H_x,H_y)|^2=\frac{1}{2}\left[\cos\left[2\pi S-\frac{2\pi Sg\mu_B(H_y+H_y^0)}{\Omega_0}\right]+\cosh\left[\frac{S^2\pi g\mu_B(H_x+H_x^0)}{\tilde{E}}\right]\right] \tag{6.14}$$

where we have split the transverse fields into two contributions, one from externally applied fields $H_{x,y}^0$ and one from internal transverse fields $H_{x,y}$. Integrating over the internal fields $H_{x,y}$ gives us our internal dipolar field-averaged relaxation rate

$$\Gamma_{AC}(\vec{H},M)=\frac{\Delta_0^2}{A}\left|\cos\bar{\Phi}(H_x^0,H_y^0)\right|^2 \tag{6.15}$$

where

$$\left|\cos\bar{\Phi}(H_x^0,H_y^0)\right|^2=\frac{1}{2}\left[e^{-\frac{2\pi^2S^2g^2\mu_B^2W_D^2(M)}{\Omega_0^2}}\cos\left[2\pi S-\frac{2\pi Sg\mu_BH_y^0}{\Omega_0}\right]+\right.$$

$$e^{\frac{S^4\pi^2 g^2 \mu_B^2 W_D^2(M)}{2\tilde{E}^2}} \cosh\left[\frac{S^2 \pi g \mu_B H_x^0}{\tilde{E}}\right]\Bigg] \tag{6.16}$$

The relaxation rates (6.15) are shown in figure 6.1 for several values of $W_D(M)$.

6.3.2 General Solution Near the Nodes

Stamp and Tupitsyn [200, 199] have demonstrated that near the nodes of $|\Delta(H_x, H_y)|^2$ one can expand $|\Delta(H_x, H_y)|$ around its zeroes, as $|\Delta(H_x, H_y)| = \Delta_0 \cosh \mathcal{Z}$, where for the Fe_8 biaxial symmetry

$$\mathcal{Z} = \psi_x + i\psi_y = \left[(H_y/F_y) + i(H_x - H_c^{(n)})/F_x\right] \tag{6.17}$$

(see [200] for complete details of this calculation). The "periods" F_x and F_y vary slowly with H_x and H_y, and so we expand as $F_l(H_l) = F_l(0) + F_l(0)'' H_l^2/2 + ...$ We can thus solve for the AC relaxation rate around the n^{th} "nodal field" $\vec{H}_\perp^{(n)}$;

$$\Gamma_{AC}^{(n)}(\vec{H}_\perp^0, M) = \frac{\Delta_0^2}{A}\left[C_n(M) + (\psi_x^2 + \psi_y^2)\right] \tag{6.18}$$

$$C_n(M) = \frac{\pi^2}{4} W_D^2(M)\left[F_x^{-2}(H_x^{(n)}) + F_y^{-2}(0)\right] \tag{6.19}$$

This is a parabolic increase around minima with values exactly proportional to the independently measurable $W_D^2(M)$.

Choosing a specific form for the Fe_8 spin Hamiltonian (such as the easy-axis easy-plane model we have been considering) allows us to use (6.13) to plot $\Gamma_{AC}(\vec{H}_\perp^{(0)}, M)$ over the whole range of $\vec{H}_\perp^0$ for different values of M (see figure 6.2). By varying M, the field angle $\theta = \sin^{-1}(H_y^0/H_x^0)$ and $\left|\vec{H}_0\right|$, AC relaxation measurements ought to obtain information about the giant spin Hamiltonian inaccessible to ESR experiments [200].

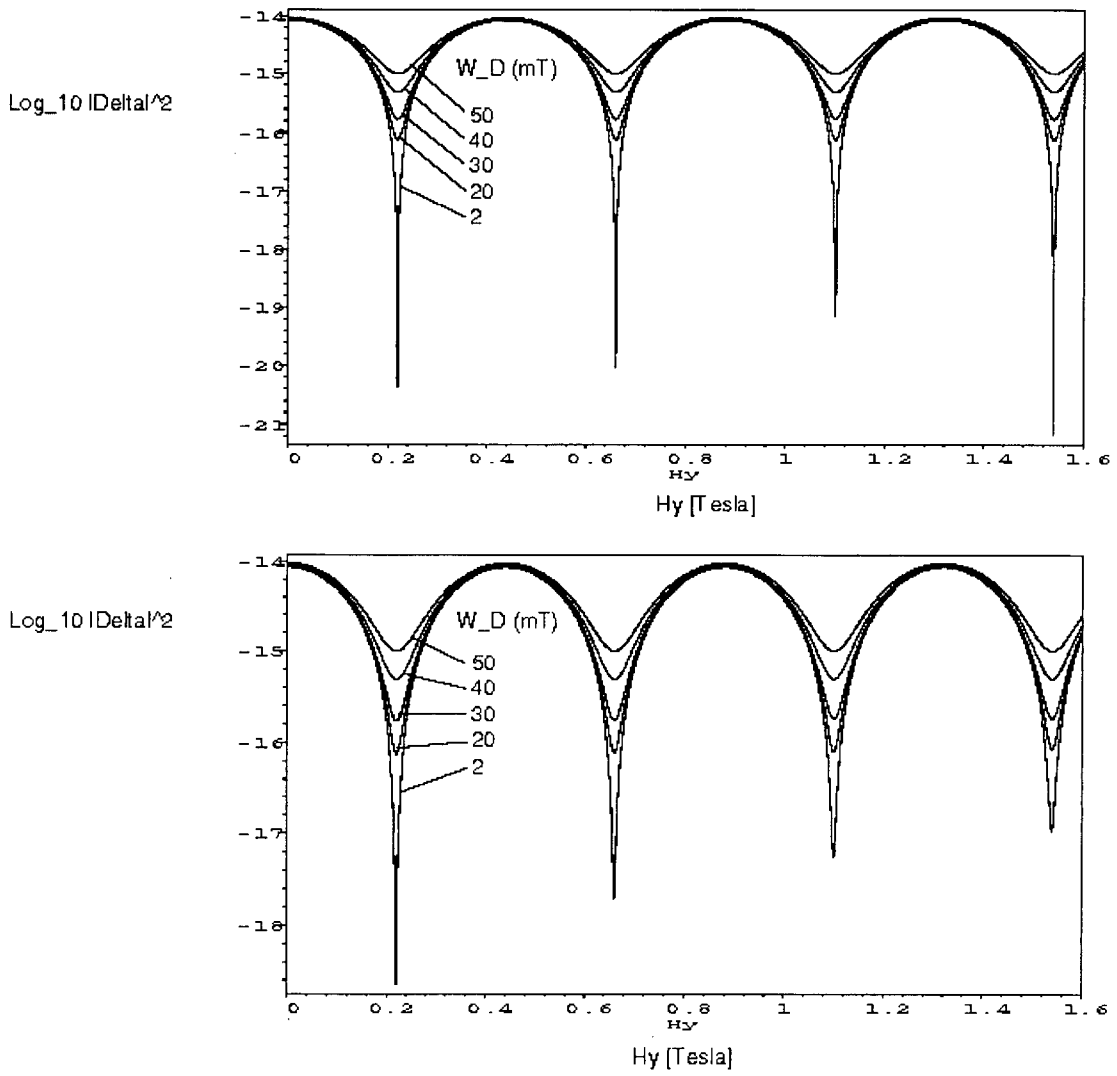

Figure 6.1: Top figure: $Log_{10}\ \Delta^2$ vs. H_y^0, for $\theta = \sin^{-1}(H_x^0/H_y^0) = 0$. Curves are, from bottom to top, $W_D = 0, 10, 20, 30$ and $50\ mT$. Bottom figure: Same, but with $\theta = 1^o$. Note that these results are obtained from our relaxation rate which was derived assuming the instanton approximation for the tunneling amplitude.

ERROR: undefined
OFFENDING COMMAND:

STACK:

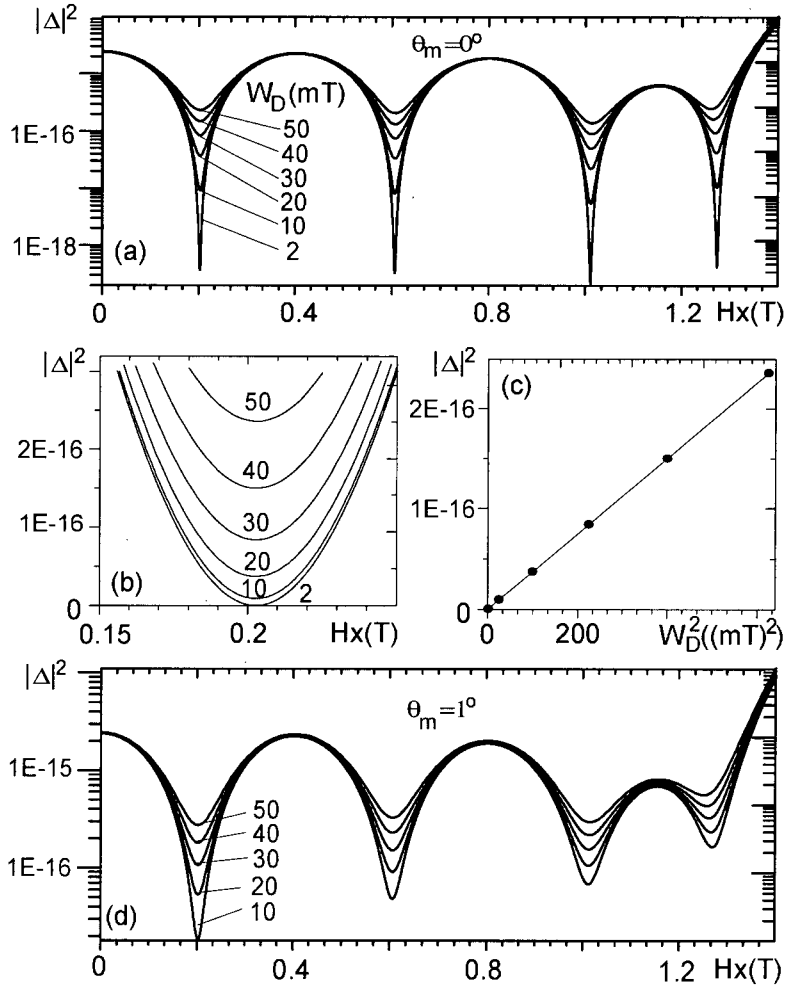

Chapter 7

Summary and Outlook

In this thesis we have presented a quantitative theory of the physics of magnetic relaxation in the presence of time-dependent external fields in crystals of molecular magnets. In so doing we have achieved considerable insight into the effect of spin environments on the quantum dynamics of mesoscale magnetic moments. This research produced several interesting results, which we reproduce here.

We used the standard Prokof'ev and Stamp theory [15, 20, 122], together with the crystallographic structure of the Fe_8 molecular magnet, to extract quantitative values for the topological decoherence $\{\alpha_k^{(1,2)}\}$ and orthogonality blocking $\{\beta_k\}$ parameters for this material. We found that topological decoherence effects were minimal ($|\alpha_k^{(1,2)}| \sim 10^{-3}$) but that orthogonality blocking was significant. We found that the primary source of the orthogonality blocking came from the large number of protons in the organic matter in the Fe_8 molecule. In terms of the value $\kappa = -\ln[\prod_k \cos\beta_k]$ in the Prokof'ev and Stamp theory, we find that κ quickly rises with transverse field, reaching $\kappa \sim 1$ for transverse field magnitude of $|\vec{H}| \sim 110$ gauss in Fe_{8*} (see figures 3.14 and 3.15). All quantities that are functions of the hyperfine couplings were found to exhibit a significant isotope effect. In particular, λ, κ and the nuclear spin linewidth $\mathcal{W}$ all depend on the isotopic concentration in an Fe_8 sample.

Fitting the shape of oscillations in tunneling amplitude to our derived relaxation rate, we found that internal dipolar transverse fields in Fe_8 are on the order of $\sqrt{H_x^2 + H_y^2} \sim 0.03K \sim 30$ gauss. This means that even in the absence of any external transverse fields

$\kappa \sim 0.09$ in Fe_{8*}, which is just large enough to cause significant decoherence [15, 20, 122], erasing any hope of seeing macroscopic quantum coherence in Fe_{8*}.

We derived an expression for the single-molecule relaxation rate in any molecular magnetic substance with an effective Hamiltonian of the form (5.6) being acted upon by a sawtooth AC field, which is given by

$$\tau^{-1} = \frac{\Delta_0^2}{\sqrt{\pi}A} \int_{Z_-}^{Z_+} dZ e^{-Z^2} |\cos \tilde{\Phi}(Z)|^2 \tag{7.1}$$

where

$$Z_\pm = \frac{\pm A - \xi}{2W} \tag{7.2}$$

with ξ the longitudinal bias, W the total energy spread available to the molecule, and A the amplitude of the field. Δ_0 is the bare tunneling matrix element of the spin Hamiltonian part of (5.6) and $\tilde{\Phi}(Z)$ is the Berry phase of the central spin complex, renormalized by the interaction with the nuclear spins.

This expression may be interpreted in the following way. The effect of the nuclear spins is both to broaden the linewidth W of the molecule and to renormalize the Berry phase $\Phi \to \tilde{\Phi}(Z)$. The first of these effects comes about from orthogonality blocking and degeneracy blocking. The second comes about primarily from topological decoherence, although the Z dependence of Φ is due to an interplay between topological decoherence and orthogonality blocking. In the limit where A is much bigger than $|W + \xi|$, the linewidth W becomes irrelevant, and all orthogonality blocking effects disappear, giving

$$\tau^{-1} = \frac{\Delta_0^2 |\cos \tilde{\Phi}|^2}{A} \tag{7.3}$$

In the opposite limit $A \ll |W + \xi|$ we find that

$$\tau^{-1} = \frac{\Delta_0^2}{\sqrt{\pi}W} \exp\left[-\frac{\xi^2}{4W^2}\right] |\cos \tilde{\Phi}(\xi/2W)|^2 \tag{7.4}$$

ie. the relaxation is gaussian, with an unusual bias dependent Berry phase. We showed that in Fe_8, because the topological decoherence effects are so small, this peculiar feature is overpowered by the gaussian and it is permissible to take $\tilde{\Phi}(\xi/2W) \rightarrow \tilde{\Phi}$. This gaussian dependence disagrees with previously quoted results which find the relaxation to be exponential in bias [15, 20, 122]. We believe that the reason for this disparity is that in the calculation leading to the exponential bias dependence the authors added an energy constraint which is unphysical for these systems (see chapter 6 for a discussion of this point).

We used our single molecule relaxation rates as input into a master equation in order to take into account the crystalline nature of the real material [15, 167]. We studied several specific cases and found the following general observations. If the sweeping amplitude of the field is larger than the total longitudinal bias available to the molecules $A > |W + \xi + E_D|$ the relaxation is linear at short times. When the sweeping amplitude $A \ll |W + \xi + E_D|$ the relaxation is initially linear, turning over to square root at later times. This occurs for both Lorentzian and gaussian initial longitudinal bias profiles.

We used these general results in the specific case of AC measurements performed on Fe_8 [39]. In this case we are in the large A limit, giving linear relaxation

$$M(t) \sim M(0)(1 - \frac{\Delta_0^2 |\cos \bar{\Phi}|^2}{A} t) \tag{7.5}$$

where $\bar{\Phi}$ is the renormalized Berry phase, averaged over the transverse internal dipolar fields (7.11). We then fit this relaxation rate to the experimental data. We found the following interesting results.

Our derived expression for the tunneling amplitude produces results which quantitatively match those fund using exact diagonalization techniques for transverse fields less than $\sim$ 0.5 T. This provides evidence that the instanton calculation is valid here. Our expression also qualitatively agrees with experimental results.

In addition to these results, our research produced several new results related to the central problem investigated here. In chapter 2 we showed how the WKB, perturbation theory and instanton methods for calculating tunneling splittings in spin Hamiltonians for selected Bravais lattice symmetries compare to exact results obtained via diagonalization. We found that the standard WKB result's prefactor [25, 26] (corresponding to the first correction $\sim \hbar$ in the WKB expansion) disagrees with the exact result in each case studied.

In chapter 3 we extended the work of Tupitsyn, Prokofiev and Stamp on the effective Hamiltonian of a central spin system [74, 75, 15, 20, 122] to allow for the calculation of the parameters $\{\alpha_k^{(1,2)}\}$ and $\{\beta_k\}$ in real systems. As well, we included in our derivations the effect of electric quadrupolar terms coming from nuclei with spins greater than 1/2.

In chapter 4 we proposed a classification scheme for all exactly solvable time dependent generalized Landau-Zener Hamiltonians. Our proposal is that if the equation for the wavefunction can be mapped to Riemann's equation then the problem is solvable. We presented two such mappings, along with exact results for the transition probabilities in each case.

This concludes the presentation of our results. In conclusion, we would like to point out some avenues for future research related to this work.

It will be quite straightforward at this point to perform investigations on molecular magnets other than the seminal Fe_8, using the methods developed herein. This will give us a new quantitative tool with which to study decoherence and relaxation in these materials.

In terms of the mathematical physics side of this work, there were many tantalizing relations between the theory of special functions and integral and differential equations glimpsed which may be of interest; we have noted these in the text whenever one occured. The problem of how to treat multiple crossings coherently in the presence of a spin bath

(ie. when our coarse graining approximation breaks down), or the related problem of how to go beyond the fast-passage approximation, remain works in progress. The resolution of the conflicting results obtained with the inclusion of an oscillator bath, necessary in the $\mathcal{O}(DS^2)$ effective description, have to be addressed in order to understand the thermal/quantum crossover. The inclusion of the quadrupolar terms in the transition probability may provide many hours of gruesome enjoyment.

Appendix A

Bias Distribution in a Dilute Solution of Dipoles

In this appendix, we derive a general expression for the bias distribution inside a crystal of molecular magnets. The general arguments that we will use have been published previously [123]. It is however worthwhile to understand how the formulae quoted in the text arise, and that shall be the purpose of this exposition.

We begin by presenting the following question. Given an ensemble of dipoles in a crystal of arbitrary shape, what will be the probability that the total dipolar field at some site $\vec{r}$ has the value $\vec{\mathcal{H}}$? Basically we can just write down the general solution to this problem; it is a sum over all possible ways of obtaining this value with the spins we've got,

$$P(\vec{r},\vec{\mathcal{H}}) = \int \frac{d\vec{r}_1}{\Omega}...\frac{d\vec{r}_N}{\Omega}\delta(\vec{\mathcal{H}} - \sum_{\vec{r}_i}\vec{H}(\vec{r}_i - \vec{r})) \tag{A.1}$$

Here each site $\vec{r}_i \neq \vec{r}$ in the crystal can either have a spin pointing "up" or a spin pointing "down", ie. in the $\pm\hat{z}$ directions. The dipolar field is taken to be

$$\vec{H}(\vec{r}_i - \vec{r}) = \frac{E_D v}{|\vec{r} - \vec{r}_i|^3}(\hat{d}_{\vec{r}_i} - 3\hat{r}(\hat{d}_{\vec{r}_i}\cdot\hat{r})) \tag{A.2}$$

where v is a unit cell volume, E_D is the dipolar field scale, and $\hat{d}_{\vec{r}_i}$ is the direction that the i^{th} spin is pointing.

We now specialize our treatment to the case of an ellipsoidal sample. In this case the $\vec{r}$ dependence drops out of $P(\vec{r},\vec{\mathcal{H}})$, and we can write

$$P(\vec{\mathcal{H}}) = \int \frac{d\vec{r}_1}{\Omega}...\frac{d\vec{r}_N}{\Omega}\delta(\vec{\mathcal{H}} - \sum_{\vec{r}_i}\vec{H}(\vec{r}_i)) \tag{A.3}$$

Writing the delta function out as an exponential gives

$$P(\vec{\mathcal{H}}) = \frac{1}{(2\pi)^3}\int d\vec{Y} e^{i\vec{\mathcal{H}}\cdot\vec{Y}} \int \frac{d\vec{r}_1}{\Omega}...\frac{d\vec{r}_N}{\Omega} e^{-\sum_{\vec{r}_i}\vec{H}(\vec{r}_i)\cdot\vec{Y}} \tag{A.4}$$

This can be rewritten as

$$P(\vec{\mathcal{H}}) = \frac{1}{(2\pi)^3}\int d\vec{Y} e^{i\vec{\mathcal{H}}\cdot\vec{Y}} \prod_{i=1}^{N}\int \frac{d\vec{r}_i}{\Omega} e^{-i\vec{H}(\vec{r}_i)\cdot\vec{Y}} \tag{A.5}$$

We note that the contribution from $\vec{H}(\vec{r}_i)$ flips sign depending on the sign of $\hat{d}_{\vec{r}_i}$. Therefore we can write the preceding as

$$P(\vec{\mathcal{H}}) = \frac{1}{(2\pi)^3}\int d\vec{Y} e^{i\vec{\mathcal{H}}\cdot\vec{Y}} \prod_{\{\uparrow\}}\int \frac{d\vec{r}_\uparrow}{\Omega} e^{-i\vec{H}(\vec{r}_\uparrow)\cdot\vec{Y}} \prod_{\{\downarrow\}}\int \frac{d\vec{r}_\downarrow}{\Omega} e^{i\vec{H}(\vec{r}_\downarrow)\cdot\vec{Y}} \tag{A.6}$$

where we have subdivided the total number of spins N into two subsets, those that are up ($\{\uparrow\}$) and those that are down ($\{\downarrow\}$). We now note that because we are only allowing the spins in our solution to point in the $\pm\hat{z}$ directions we have a symmetry here that we can exploit; the solution for $P(\vec{\mathcal{H}})$ has to be of the form

$$P(\vec{\mathcal{H}}) = \delta(H_x = 0)\delta(H_y = 0)P(H_z) \tag{A.7}$$

That is, the final solution in this idealized case has the probability for the transverse fields to be zero. We therefore recast our expression (A.6) into an expression for $P(H_z)$, ie. the probability of being in a longitudinal bias H_z;

$$P(H_z) = \frac{1}{(2\pi)}\int dY e^{iH_zY} \prod_{\{\uparrow\}}\int \frac{d\vec{r}_\uparrow}{\Omega} e^{-iH_z(\vec{r}_\uparrow)Y} \prod_{\{\downarrow\}}\int \frac{d\vec{r}_\downarrow}{\Omega} e^{iH_z(\vec{r}_\downarrow)Y} \tag{A.8}$$

We can perform these integrations;

$$\begin{aligned}\int \frac{d\vec{r}}{\Omega} e^{\pm iH_z(\vec{r})Y} &\equiv 1 - \int \frac{d\vec{r}}{\Omega}\left(1 - e^{\pm iH_z(\vec{r})Y}\right) \\ &= 1 - \frac{2\pi}{\Omega}\int_0^\pi d\theta \sin\theta \int_0^\infty dr r^2 \left(1 - e^{\pm iYE_Dv(1-3\cos^2\theta)/r^3}\right)\end{aligned} \tag{A.9}$$

Changing variables to $x = 1/r^3$ gives

$$1 - \frac{2\pi}{3\Omega}\int_0^\pi d\theta \sin\theta \int_0^\infty \frac{dx}{x^2}\left(1 - e^{\pm iYE_Dv(1-3\cos^2\theta)x}\right) \tag{A.10}$$

This can be broken up into two parts, like this

$$1 - \frac{2\pi}{3\Omega}\int_0^\pi d\theta \sin\theta \int_0^\infty \frac{dx}{x^2}\left(\left(1 - \cos YE_Dv(1-3\cos^2\theta)x\right) \pm i\left(\sin YE_Dv(1-3\cos^2\theta)x\right)\right) \tag{A.11}$$

The leftmost integral is easy to do. We find that

$$\begin{aligned} & \frac{2\pi}{3\Omega}\int_0^\pi d\theta \sin\theta \int_0^\infty \frac{dx}{x^2}\left(1 - \cos YE_Dv(1-3\cos^2\theta)x\right) \\ = & \frac{\pi^2 E_D v|Y|}{3\Omega}\int_0^\pi d\theta \sin\theta |1 - 3\cos^2\theta| \\ = & \frac{8\pi^2 E_D v|Y|}{9\sqrt{3}\Omega} \end{aligned} \tag{A.12}$$

The second one is a little trickier. We write it as follows;

$$\begin{aligned} & \frac{\pm i2\pi}{3\Omega}\int_0^\pi d\theta \sin\theta \int_0^\infty \frac{dx}{x^2} \sin YE_Dv(1-3\cos^2\theta)x \\ = & \frac{\pm i2\pi}{3\Omega}\int_0^\pi d\theta \sin\theta \int_0^\infty \frac{dx}{x^2}\left(\sin\left(YE_Dv(1-3\cos^2\theta)x\right) - YE_Dv(1-3\cos^2\theta)x\right) \end{aligned} \tag{A.13}$$

The reason we can do this is that the term we have added is equal to zero, as

$$\int_0^\pi d\theta \sin\theta(1 - 3\cos^2\theta) = 0 \tag{A.14}$$

and the apparently divergent integral over x contains a cutoff which we've suppressed here (besides, the divergence of this term is only logarithmic). With this new expression we find, defining

$$b \equiv YE_Dv(1 - 3\cos^2\theta) \tag{A.15}$$

that

$$\begin{aligned} & \int_0^\Lambda \frac{dx}{x^2}\left(\sin\left(bx\right) - bx\right) \\ = \; & b\left(Ci(\Lambda b) - \ln(\Lambda) + 1 - \ln(b) - \gamma\right) \end{aligned} \tag{A.16}$$

and the whole expression is

$$\begin{aligned} & \frac{\pm iYE_Dv2\pi}{3\Omega}\int_0^\pi d\theta \sin\theta(1-3\cos^2\theta) \\ & \Big(Ci(\Lambda YE_Dv(1-3\cos^2\theta)) - \ln(\Lambda) + 1 - \ln YE_Dv(1-3\cos^2\theta) - \gamma\Big) \\ = \; & \frac{\pm iYE_Dv2\pi}{3\Omega}\int_0^\pi d\theta \sin\theta(1-3\cos^2\theta) \\ & \Big(Ci(\Lambda YE_Dv(1-3\cos^2\theta)) - \ln\Big(YE_Dv(1-3\cos^2\theta)\Big)\Big) \end{aligned} \tag{A.17}$$

The leftmost term is

$$\begin{aligned} & \frac{\pm iYE_Dv2\pi}{3\Omega}\int_0^\pi d\theta \sin\theta(1-3\cos^2\theta)\left(Ci(\Lambda YE_Dv(1-3\cos^2\theta))\right. \\ = \; & \mp\frac{i|Y|E_Dv\pi^2 8}{9\sqrt{3}\Omega} \end{aligned} \tag{A.18}$$

The rightmost term is

$$\begin{aligned} - \; & \frac{\pm iYE_Dv2\pi}{3\Omega}\int_0^\pi d\theta \sin\theta(1-3\cos^2\theta)\left(\ln(\Lambda YE_Dv(1-3\cos^2\theta))\right. \\ = \; & \frac{\pm iYE_Dv2\pi}{3\Omega}\left(\frac{4}{3} - \frac{8}{9}\sqrt{3}Re(\tanh^{-1}\sqrt{3}) + \frac{4}{9}\sqrt{3}\pi i\right) \end{aligned} \tag{A.19}$$

Collecting our results, we find that

$$\begin{aligned} & \int \frac{d\vec{r}}{\Omega} e^{\pm iH(\vec{r})Y} \\ = \; & 1 - \rho Y\left[1 \pm 1 \pm i \mp iK\right] \quad ,\{Y > 0\} \\ = \; & 1 + \rho Y\left[1 \mp 1 \pm i \pm iK\right] \quad ,\{Y < 0\} \end{aligned} \tag{A.20}$$

where we have defined

$$K \equiv \frac{\pi}{\sqrt{3}} - \frac{2\pi}{3} Re \tanh^{-1}\sqrt{3} \quad , \qquad \rho \equiv \frac{8\pi^2 E_D v}{9\sqrt{3}\Omega} \tag{A.21}$$

Going back to our original expression for $P(\xi)$ we see that

$$\begin{aligned} P(H_z) &= \frac{1}{2\pi}\int_0^\infty dY e^{iH_z Y} \prod_{\{\downarrow\}} [1-\rho Y\,[-i+iK]] \prod_{\{\uparrow\}} [1-\rho Y\,[2+i-iK]] \\ &+ \frac{1}{2\pi}\int_{-\infty}^0 dY e^{iH_z Y} \prod_{\{\downarrow\}} [1+\rho Y\,[2-i-iK]] \prod_{\{\uparrow\}} [1+\rho Y\,[+i+iK]] \end{aligned} \tag{A.22}$$

This can be written

$$\begin{aligned} P(H_z) &= \frac{1}{2\pi}\int_0^\infty dY e^{iY(H_z+\{1-(N_\uparrow-N_\downarrow)\}\rho(K-1)/N)} e^{-2\pi(1-\{N_\uparrow-N_\downarrow\}Y\rho/N} \\ &+ \frac{1}{2\pi}\int_0^\infty dY e^{-iY(H_z+\{1-(N_\uparrow-N_\downarrow)\}\rho(K-1)/N)} e^{-2\pi(1-\{N_\uparrow-N_\downarrow\}Y\rho/N} \end{aligned} \tag{A.23}$$

where $N_\uparrow, N_\downarrow$ are the numbers of up/down spins respectively. As well, we have assumed that Ω is large enough so that we can rewrite the sums as exponentials. Performing the integrals gives

$$P(H_z) = \frac{\Gamma M}{\pi} \frac{1}{(H_z+E)^2+\Gamma^2} \tag{A.24}$$

where we have defined

$$E(t) = \rho(K-1)N(1-M) \quad , \quad \Gamma(t) = 2\pi\rho N(1-M) \tag{A.25}$$

where $M \equiv \frac{\{N_\uparrow - N_\downarrow\}}{N}$ is the magnetization of the sample.

Now in order to write our full $P(\vec{\mathcal{H}})$, we have to include the H_x and H_y dependence which we've seen is in the ideal case very simple. In a real material, the delta functions in this dependence will be spread somewhat. For this reason we are going to replace the

delta functions with gaussians, whose width will be much smaller than the energy scale E_D of the longitudinal distribution. Because we have a $x \leftrightarrow y$ symmetry here, we shall choose the transverse widths to be the same. This gives, for our final result,

$$P(\vec{\mathcal{H}}) = \frac{\Gamma M}{\pi} \frac{1}{(H_z + E)^2 + \Gamma^2} \frac{1}{2\pi W_{dt}^2} \exp\left[-\frac{H_x^2 + H_y^2}{2W_{dt}^2}\right] \tag{A.26}$$

where, as we have mentioned, $W_{dt} \ll E_D$ is the width of the transverse field distribution.

Appendix B

Time Evolution of Nuclear Spin States

In this appendix we shall show how the nuclear spin states evolve over time due to their coupling with the central spin complex in a molecular magnet. We shall assume the same conditions as were presented in chapter 6, and furthermore we shall assume that we are in the large A limit.

We may write down a master equation for the flow of the one-molecule system in the space $|S, M>$ where $|S>$ is the two-level state of the central spin and $|M>$ is the state of the spin environment of the form

$$\dot{P}_{S,M} = -P_{S,M} \sum_{S',M'} \tau^{-1}_{S\to S',M\to M'} + \sum_{S',M'} \tau^{-1}_{S'\to S,M'\to M} P_{S',M'} \tag{B.1}$$

where $P_{S,M}$ is the normalized probability of being in state $|S, M>$ and $\tau^{-1}_{S\to S',M\to M'}$ is the transition rate from state $|S, M>$ to state $|S', M'>$. Now as we explicitly showed in chapter 6, these relaxation rates do not select for any particular state of the central spin system. That is, the rate of flow $|\uparrow>\to|\downarrow>$ is identical to the rate of flow $|\downarrow>\to|\uparrow>$ in the central spin space. This means that we can take

$$\tau^{-1}_{S\to S',M\to M'} = \tau^{-1}_{S'\to S,M\to M'} = \tau^{-1}_{M\to M'} \tag{B.2}$$

and write our master equation in the form

$$\dot{P}_M = -2P_M \sum_{M'} \tau^{-1}_{M\to M'} + 2\sum_{M'} \tau^{-1}_{M'\to M} P_{M'} \tag{B.3}$$

where we have defined

$$P_M = \sum_S P_{S,M} \tag{B.4}$$

We can further simplify this expression by looking closely at the structure of the transition probabilities in chapter 6. We see that these also do not select for specific spin bath states. That is,

$$\tau^{-1}_{M\to M'} = \tau^{-1}_{M'\to M} \tag{B.5}$$

for all $\{M, M'\}$. This means that the master equation simplifies even more. We can write it in the form

$$\dot{P}_M = -2P_M \sum_{M'} \tau^{-1}_{M\to M'} + 2\sum_{M'} \tau^{-1}_{M\to M'} P_{M'} \tag{B.6}$$

Knowing the functional form of $\tau^{-1}_{M\to M'}$ for arbitrary $\{M, M'\}$ allows us to solve this equation numerically (it is simply a system of M linear equations). If we simply assume that $\tau^{-1}_{M\to M'}$ is not a strong function of M' then our master equation becomes

$$\dot{P}_M = -2P_M\tau^{-1}_M + 2\frac{\tau^{-1}_M}{\mathcal{C}} \tag{B.7}$$

where $\tau^{-1}_M = \sum_{M'} \tau^{-1}_{M\to M'}$ and $\mathcal{C}$ is the total number of spin bath states. This is readily solved; in the limit that $\mathcal{C} \gg 1$ the solution is

$$P_M(t) \sim -P_M(0)e^{-2\tau^{-1}_M t} \tag{B.8}$$

together with the constraint that $\sum_M P_M(t) = 1$. What this means is that the different spin bath states will reach a steady state solution where $P_M = P_{M'}$ for all $\{M, M'\}$ in a time on the order of τ_M which is simply the total large A transition rate divided by the average number of nuclear spin flips that occur per sweep.

Shown in figure B.1 is a numerical solution of (B.3) showing the convergence of the spectral weights of the various nuclear spin states for a general system with $\tau^{-1}_{M\to M'} = \tau^{-1}_{M'\to M}$.

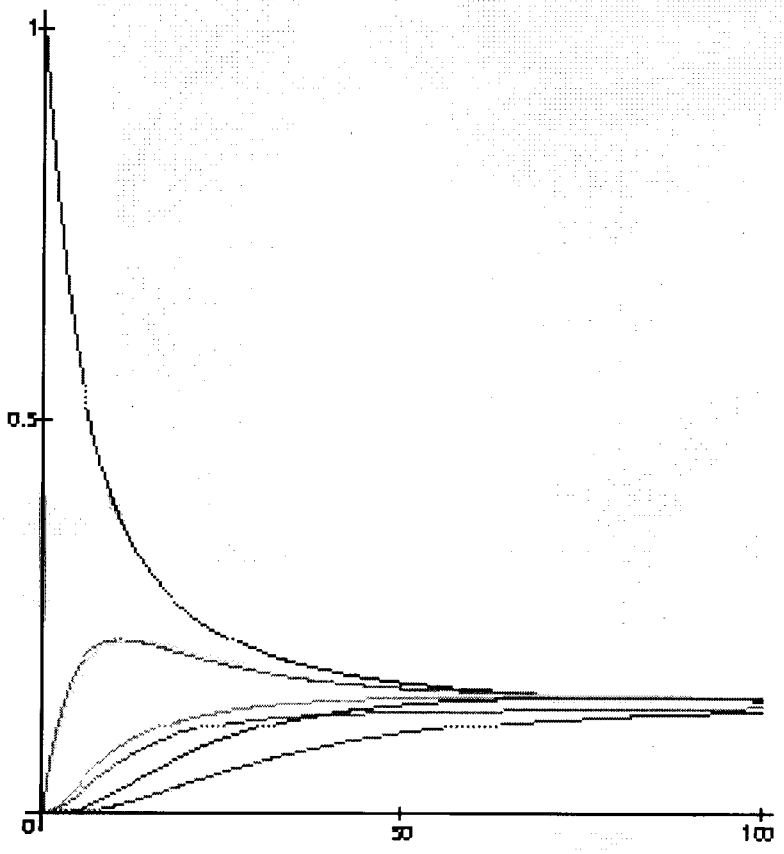

Figure B.1: Here we see a system with seven environmental spin states initially prepared in one of them evolving via (B.3).

Bibliography

[1] Colin P. Williams and Scott H. Clearwater, Explorations in Quantum Computing, Springer-Verlag (1998).

[2] R. W. Keyes, "Miniaturization of Electronics and its Limits", *IBM Journal of Research and Development*, Vol. 32, January (1988) pp. 24-28.

[3] Malone, "The Microprocessor: A Biography", TELOS, Santa Clara, (1995).

[4] R. W. Keyes, "The Future of the Transistor", *Scientific American*, June (1993), pp.70-78.

[5] New Scientist, December (1999).

[6] R.P. Feynman, "There's Plenty of Room at the Bottom", *Engineering and Science*, Vol. 23, pp.22-36 (1960).

[7] C. Bennett, "Logical Reversibility of Computation", *IBM Journal of Research and Development*, Vol. 17, (1973) pp. 525-532.

[8] D. Deutsch, Proc. Roy. Soc. London, Vol. A400, pp.97-117 (1985).

[9] R.P. Feynman, "Quantum Mechanical Computers", *Optics News*, Vol. 11, pp.11-20 (1985)

[10] A. Turing, On Computable Numbers with an Application to the Entscheidungsproblem", *Proc. Lond. Math. Soc.*, Vol.42 (1937), pp.230-265, erratum in 43 (1937), pp.544-546.

[11] S. Jaimungal, M.H.S. Amin and G. Rose, Persistent Currents and Boundary Conformal Field Theory, *Int. J. Mod. Phys. B*, in press; and references therein.

[12] R. Rouse, Siyuan Han, J.E. Lukens, Phys. Rev. Lett. **75** 8 1614 (1995).

[13] Y. Nakamura, Yu. Pashkin and J. S. Tsai, cond-mat/9904003 (1999).

[14] C. Sangregorio et.al., Phys. Rev. Lett. **78** 24 4645-4648 (1997).

[15] N.V. Prokofiev and P.C.E. Stamp, Phys. Rev. Lett. **80** 26 5794-5797 (1998).

[16] D. Gatteschi et.al., *Science* **265** 1054 (1994).

[17] L. Thomas et.al. *Nature* **383** 145-147 (1996).

[18] C. Delfs et.al., Inorg. Chem. **32** 3099-3103 (1993), and references therein.

[19] P. Shor, "Algorithms for Quantum Computation: Discrete Logarithms and Factoring", *Proceedings* 35^{th} *Annual Symposium on Foundations of Computer Science* (1994), pp.124-134.

[20] N. V. Prokofiev and P. C. E. Stamp, Theory of the Spin Bath, cond-mat/0001080, and references therein.

[21] R.P. Feynman, F.L. Vernon, Ann. Phys. **24**, 118 (1963).

[22] A.O. Caldeira, A.J. Leggett, Ann. Phys. **149**, 374 (1983).

[23] K. Wieghardt, Klaus Pohl, Ibrahim Jibril and Gottfried Huttner, Angew. Chem. Int. Ed. Engl. 23, 77-78 (1984). Also see K. Weighardt et.al., Angew. Chem. 95 739 (1983) and Angew. Chem. Int. Ed. Engl. 22 727 (1983) for earlier compounds.

[24] Information from Cambridge Crystallographic Database obtained from Jean Reid, reid@ccdc.cam.ac.uk, and Eugene Cheung of the Chemistry Dept. of UBC. RefCode for Fe_8 is COCNAJ.

[25] J.L. van Hemmen and A. Suto, Europhys. Lett., **1**, 481-490 (1986); J.L. van Hemmen, A. Suto, Physica **141B**, 37-75 (1986).

[26] M Enz, R Schilling, J. Phys **C19**, L711-5; *ibid.*, 1765 (1986).

[27] A.J. Leggett et al., Rev. Mod. Phys. **59**, 1 (1987).

[28] A. Caneschi et.al., J. Am. Chem. Soc. 113, 5873-5874 (1991).

[29] T. Lis, Acta Crystallogr. Sect. B **36** 2042-2046 (1980).

[30] P.D.W. Boyd et.al., J. Am.Chem.Soc. **110** (1988).

[31] R. Sessoli et.al., *Nature* **365** 141 (1993).

[32] W. Low, Paramagnetic Resonance in Solids, p. 113, Academic Press 1960.

[33] Van Vleck, J.H., J, Chem. Phys. **3** 807 (1935).

[34] Pryce, M.H.L., Phys. Rev. **80** 1107 (1950).

[35] C. Paulsen *et al.*, J. Mag. Magn. Mat. **140**, 1891 (1995), and references therein.

[36] J.R. Friedman *et al.*, Phys. Rev. Lett., **76**, 3830-3833 (1996).

[37] A.-L. Barra et.al., Phys. Rev. Lett. **56**, 8192 (1997).

[38] R. Caciuffo et.al., Phys. Rev. Lett. **81** 21 4744-4747 (1998).

[39] D. Loss, D. P. diVincenzo, G. Grinstein, Phys. Rev. Lett. **69**, 3232 (1992).

[40] J. Von Delft, C.L. Henley, Phys. Rev.Lett. **69** 3236 (1992).

[41] P.C.E.Stamp, E.M.Chudnovsky, B.Barbara, Int. J. Mod. Phys. **B6**, 1355 (1992).

[42] E. Chudnovsky, J. Appl. Phys. **73** (10), (1993).

[43] B. Barbara, L.C. Sampaio, J.E. Wegrowe, B.A. Ratnam, A. Marchand, C.Paulsen, M.A. Novak, J.L. Tholence, M. Uehara and D. Fruchart, J. Appl. Phys. **73** (10), (1993).

[44] N.V. Prokof'ev and P.C.E. Stamp, J. Phys. CM **5**, L663-670 (1993).

[45] N.V. Prokofiev and P.C.E. Stamp, JLTP **104** 143-209 (1996).

[46] P.C.E. Stamp, Unconventional Environments, NATO workshop on Tunneling of Magnetization, June-July (1994).

[47] N.V. Prokofiev and P.C.E. Stamp, J. Phys. Cond. Mat. **5** L663-L670 (1993).

[48] H. Kopfermann, Nuclear Moments, Academic Press Inc. 1958.

[49] W. Wernsdorfer et.al. Phys. Rev. Lett. **82** 19 3903-3906 (1999), and references therein.

[50] C. Sangregorio, T. Ohm, C. Paulsen, R. Sessoli, and D. Gatteschi, Phys. Rev. Lett., **78**, 4645 (1997).

[51] W. Wernsdorfer and R. Sessoli, *Science* **284** 133 (1999).

[52] J.M. Hernandez, X.X. Zhang, F. Luis, J. Bartolome, J. Tejada and R. Ziolo, Europhys. Lett. **35** (4), pp.301-306, (1996).

[53] J.F. Fernandez, F. Luis and J. Bartolome, Phys. Rev. Lett. **80**, 25 (1998).

[54] J. R. Friedman, M.P. Sarachik, J. Tejada and R. Ziolo, Phys. Rev. Lett. **76** 20 (1996).

[55] T. Ohm, C. Sangregorio, C. Paulsen, Europhys. J. B **6** 195 (1998).

[56] J. R. Freidman, M.P. Sarachik, R. Ziolo, cond-mat/9807411 (1998).

[57] L. Thomas and B. Barbara, JLTP **113** 1055 (1998).

[58] J. Tejada, X.X. Zhang, Ll. Balcells, J. Appl. Phys. **73** (10), (1993).

[59] J. Tejada et.al., Phys. Rev. Lett. **79** 9 1754 (1997).

[60] W. Wernsdorfer et.al. J. Magn. Mag. Mat. 145 1 (1995).

[61] F. Fominaya et.al., Heat Capacity Anomalies induced by magnetization quantum tunneling in a $Mn_{12}O_{12}$ - acetate single crystal, preprint.

[62] A.M. Gomes et.al., Phys. Rev. B **57** 9 5021 (1998).

[63] W. Wernsdorfer, R. Sessoli and D. Gatteschi, Europhys. Lett. **47** (2), 254 (1999).

[64] A. Abragam, Principles of Nuclear Magnetism, Oxford Science Publications, 1960.

[65] A. Abragam, B. Bleaney, "Electron Paramagnetic Resonance of Transition Ions" (Clarendon, 1970).

[66] W. J. Caspers, "Theory of Spin Relaxation", Interscience Publishers 1964.

[67] A. Abragam and M.H.L. Pryce, *Proc. Roy. Soc. A* 135 (1951).

[68] H. J. Zeiger and G. W. Pratt, Magnetic Interactions in Solids, p.79, Clarendon Press, Oxford 1973.

[69] W. Low, Paramagnetic Resonance in Solids, pp.9-10, Academic Press 1960.

[70] F. Hartmann-Boutron, P. Politi and J. Villain, Int. J. Mod. Phys. B, Vol. 10, No. 21, pp. 2577-2637 (1996).

[71] G. D. Mahan, *Many Particle Physics*, Plenum Press, 1993.

[72] A. Bencini and D. Gatteschi, EPR of Exchange Coupled Systems, Springer-Verlag 1990.

[73] O. Kahn, "Molecular magnetism", VCH publishers (1993).

[74] I.S. Tupitsyn, N.V. Prokof'ev, and P.C.E. Stamp, Int. J. Mod. Phys. B, **11**, 2901 (1997).

[75] I.S. Tupitsyn, JETP Lett., **67**, 28 (1998).

[76] W. Low, Paramagnetic Resonance in Solids, p. 10, Academic Press 1960.

[77] H. J. Zeiger and G. W. Pratt, Magnetic Interactions in Solids, p.155, Clarendon Press, Oxford 1973.

[78] Ashcroft and Mermin, Solid State Physics.

[79] K.W.H. Stevens, Magnetic Ions in Crystals, Princeton University Press 1997.

[80] B. N. Figgis, Introduction to Ligand Fields, Interscience Publishers, 1966.

[81] L. E. Orgel, An Introduction to Transition Metal Chemistry: Ligand-Field Theory, Butler and Tanner Ltd., 1966.

[82] W. Low, Paramagnetic Resonance in Solids, p. 114-115, Academic Press 1960.

[83] L. E. Orgel, An Introduction to Transition Metal Chemistry: Ligand Field Theory, pp. 11-18, Butler and Tanner Ltd., 1966.

[84] H. J. Zeiger and G. W. Pratt, Magnetic Interactions in Solids, p.85, Clarendon Press, Oxford 1973.

[85] H. J. Zeiger and G. W. Pratt, Magnetic Interactions in Solids, p.132, Clarendon Press, Oxford 1973.

[86] H. J. Zeiger and G. W. Pratt, Magnetic Interactions in Solids, p.135, Clarendon Press, Oxford 1973.

[87] W. Low, Paramagnetic Resonance in Solids, p. 45, Academic Press 1960.

[88] H. J. Zeiger and G. W. Pratt, Magnetic Interactions in Solids, p.156, Clarendon Press, Oxford 1973.

[89] W. Low, Paramagnetic Resonance in Solids, p. 119, Academic Press 1960.

[90] B. Barbara et.al., J. Mag. Magn. Mat. 177-181, 1324 (1998).

[91] H. J. Zeiger and G. W. Pratt, Magnetic Interactions in Solids, p.99, Clarendon Press, Oxford 1973.

[92] J. Villain et al., Europhys. Lett. **27**, 159 (1994)

[93] F. Hartmann-Boutron, P. Politi and J. Villain, Int. J. Mod. Phys. B, Vol. 10, No. 21, p. 2630 (1996).

[94] N.V. Prokofiev and P.C.E. Stamp, pp 347-371 in *"Quantum Tunneling of Magnetisation-QTM'94"* (ed. L. Gunther and B. Barbara), Kluwer Publ. (1995)

[95] G. D. Mahan, *Many Particle Physics*, pp. 355-374, Plenum Press, 1993, and references within.

[96] V. A. Kalatsky, E. Muller-Hartmann, V. L. Pokrovski and G.S. Uhrig, Berry's phase for large spins in external fields, preprint, Dec.5th, 1997.

[97] A. Garg, Europhys. Lett. **22** (3), pp. 205-210 (1993), and references therein.

[98] We are pursuing treatments of this technical problem with Igor Tupitsyn from Moscow.

[99] A. J. Freeman and R. E. Watson, Hyperfine Interactions in Magnetic Materials, p.249, in Rado and Suhl, Magnetism II (1963).

[100] A. J. Freeman and R. E. Watson, Hyperfine Interactions in Magnetic Materials, p.291, in Rado and Suhl, Magnetism II (1963).

[101] Personal communication, William Unruh, University of British Columbia.

[102] M. Grifoni and P. Hanggi, Physics Reports **304**, 219 (1998).

[103] L. D. Landau, Phys. Z. Sowjetunion 1, (1932) 89.

[104] C. Zener, Proc. R. Soc. London, Ser. A 137, (1932) 696.

[105] E. G. C. Stuckelberg, Helv. Phys. Acta 5, (1932) 369.

[106] P. Wolynes, J. Chem. Phys. **86**, 1957 (1987).

[107] H. Frauenfelder and P. Wolynes, Science **229**, 337 (1985); A. Garg, J. N. Onuchic, and V. Ambegoakar, J. Chem. Phys. **83** 4491 (1985).

[108] C. P. Slichter, *Principles of Magnetic Resonance*, 2^{nd} ed. (Springer-Verlag, Berlin, 1978).

[109] Y. Kayanuma, Phys. Rev. Lett. **58**, 1934 (1987).

[110] M. Tsukada, J. Phys. Soc. Jpn. **51**, 2927 (1982).

[111] C. Zener, Proc. Roy. Soc. London, Ser. A **145**, 523 (1934).

[112] Y. Gefen and D.J. Thouless, Phys. Rev. Lett. **59**, 1752 (1987).

[113] Abramowitz and Stegun, Handbook of Mathematical Functions, (1968).

[114] L. D. Landau and E.M. Lifshitz, "Quantum Mechanics".

[115] J. M. Lopez-Castillo, A. Filali and J. P. Jay-Gerin, J. Chem. Phys. 97, 1905 (1992).

[116] P. Ao and J. Rammer, Phys. Rev. B **43** 7 (1991).

[117] Y. Gefen, E. Ben-Jacob, A. O. Caldeira, Phys. Rev. B. **36**, 2770 (1987).

[118] G. Floquet, An.. de L'ecole Norm. Sup. 12 (1883) 47. Also see [102] for a list of references for Floquet theory.

[119] S. Coleman, *Aspects of Symmetry*, Cambridge University Press (1989).

[120] C. H. Henry and D. V. Lang, Phys. Rev. B **15** 989 (1977).

[121] M. A. Kmetic and W. J. Meath, Phys. Lett. A **108**, 340 (1985).

[122] N.V. Prokof'ev and P.C.E. Stamp, J. Low Temp. Phys., **104**, 143 (1996).

[123] The reference usually given here is P. W. Anderson, Phys. Rev. **82** 342 (1951). However, this reference is nothing but a cryptic paragraph. Therefore we felt it best to rederive this expression for ourselves (see Appendix A).

[124] J. Von Delft, C.L. Henley, Phys. Rev. B **48** , 965 (1993).

[125] A.K. Zvezdin, V.V.Dobrovitski, B.N.Harmon, M.I. Katsnelson, cond-mat/9807096 (1998).

[126] Personal communication of unpublished data on tunneling quenching via transverse field application in Fe_8, W. Wernsdorfer, Nov. 16th, 1998.

[127] S. Hill, J. Perenboom, N.S.Dalal, T. Hathaway, T. Stalcup and J.S. Brooks, Phys. Rev. Lett. **80** 11 (1998).

[128] W.T.Coffey, D.S.F. Crothers, J.L. Dormann, Yu. Kalmykov, E.C. Kennedy, W. Wernsdorfer, Phys. Rev. Lett. **80** 25 (1998).

[129] N.V. Prokofiev and P.C.E. Stamp, Decoherence in the Quantum Dynamics of a "Central Spin" Coupled to a Spin Environment, preprint, April 12th, (1999).

[130] A. Chiolero, D. Loss, Phys. Rev. B **56** 2 (1997).

[131] E.N. Bogachek and I.V. Krive, Phs. Rev. B **46** 22 (1992).

[132] R. Sessoli, H-L Tsai, A.R. Schake, et.al. J. Am. Chem. Soc. 115, pp.1804-1816, (1993).

[133] P.C.E. Stamp, Physica B **197**, 133 (1994) [Proc. LT-20, Aug. 1993]. See also P.C.E. Stamp, Nature **359**, 365 (1992).

[134] N.V. Prokofiev, B. Svistunov and I. Tupitsyn, Tunneling Problems by Monte Carlo, preprint, (1999).

[135] Yunbo Zhang et.al., cond-mat/9901325 (1999).

[136] M. N. Leuenberger and D. Loss, cond-mat/9810156 (1998).

[137] Jiushu Shao and P. Hanggi, Phys. Rev. Lett. **81**, 26 (1998).

[138] A. Shimshoni, Y. Gefen, Ann. Phys. **210**, 16 (1991).

[139] M. Murao, C. Uchiyama, F. Shibata, Physica A **209** pp.444-456 (1994).

[140] V. Yu. Golyshev and A.F.PopKov, Europhys. Lett. **29** (4). pp.327-332 (1995).

[141] David Awschalom, David P. DiVincenzo, Joseph F. Symth, *Science* **258** p.414 (1992).

[142] S. Gider et.al., *Science* **268** 77 (1995); replies by J. Tejada and A. Garg with counter from S. Gider and D. Awschalom *Science* **272** 424-426 (1996).

[143] E. Dan Dahlberg and Jian-Gang Zhu, Physics Today p.34 April (1995).

[144] John L. Simonds, Physics Today p.26 April (1995).

[145] Jacques Villain, From Perturbation Theory to Instantons, preprint February 2nd (1998).

[146] Seiji Miyashita, J. Phys. Soc. Japan **65** 8 pp.2734-2735 (1996).

[147] S.L. Heath and A. Powell, Angew. Chem. Int. Engl. **31** 191 (1992).

[148] K.L. Taft and S.J. Lippard, J. Am. Chem. Soc. 9629 (1990).

[149] K.L. Taft et.al., J.Am.Chem.Soc. **116** 823 (1990).

[150] A. Caneschi et.al. J.Am.Chem.Soc. **113** 5873-5874 (1991).

[151] R. Sessoli et.al. J. Am.Chem.Soc. **115** 1804-1816 (1993).

[152] A. Fort et.al., Phys. Rev. Lett. **80** 612 (1998).

[153] E. M. Chudnovsky and L. Gunther, Phys. Rev. Lett. **60** 661 (1988).

[154] Yicheng Zhong et.al., Inelastic Neutron Scattering Study of Mn_{12} Acetate, cond-mat/9809133 (1998).

[155] B. Bleaney and K. W. H. Stevens, Proc. Phys. Soc. **61** 108 (1950).

[156] V.V. Dobrovitski, M.I. Katsnelson and B.N. Harmon, Mechanisms of decoherence in weakly anisotropic molecular magnets, cond-mat/9906375, June 24th (1999).

[157] S.E. Barnes, Manifestation of intermediate spin for Fe_8, cond-mat/9907257, July 19th (1999); A. Garg, Large transverse field tunnel splittings in the Fe_8 spin Hamiltonian, cond-mat/9906203, June 14th (1999).

[158] J. Villain et.al., Europhys. Lett. **27** 159 (1994).

[159] H. J. Zeiger and G. W. Pratt, Magnetic Interactions in Solids, p.136, Clarendon Press, Oxford 1973.

[160] M. A. Novak and R. Sessoli, in *Quantum Tunneling of the Magnetization*, Vol.301 of *Nato Adavnced Study Institute, Series E: Applied Science*, ed. L. Gunther and B. Barbara (Kluwer, Dordrecht, 1995), p. 171.

[161] See A. Garg, Phys. Rev Lett. **70**, C2198 (1993), and reply of D. D. Awschalom et al., *ibid.*, C2199 (1993); or A. Garg, Phys. Rev. Lett. **71**, 4241 (1993), and the associated Comment of D. D. Awschalom et al., *ibid.*, C4276 (1993); or A. Garg, Science **272**, 425 (1996), with the reply of D. D. Awschalom et al., *ibid.*, 425 (1996).

[162] D.D. Awschalom et al., Phys. Rev. Lett. **68**, 3092 (1992).

[163] This derivation is in the spirit of [74] and [75].

[164] I.S. Tupitsyn and B. Barbara, Quantum Tunneling of the Magnetization in Molecular Complexes with Large Spins. Effect of the Environment, preprint, p.12 .

[165] L. E. Orgel, "An Introduction to Transition Metal Chemistry: Ligand Field Theory", p. 92, Butler and Tanner Ltd., 1966.

[166] W. Gordy, W. Smith and R. Trambarulo, "Microwave Spectroscopy", John Wiley and Sons, 1953.

[167] G. Rose, P.C.E. Stamp, J. Low Temp. Phys. **113** 1054 (1998).

[168] P.C.E. Stamp, Phys. Rev. Lett., **66**, 2802 (1991).

[169] G. Tatara and H. Fukuyama, Phys. Rev. Lett., **72**, 772 (1994); J. Phys. Soc. Jap., **63**, 2538 (1994).

[170] M. Dube′ and P.C.E. Stamp, J. Low Temp. Phys., **110**, 779 (1998).

[171] K.Hong, N. Giordano, Europhys. Lett. **36**, 147 (1996); W. Wernsdorfer et al., Phys. Rev. **B55**, 11552 (1997); and refs. therein.

[172] P.C.E. Stamp, Phys. Rev. Lett., **61**, 2905 (1988).

[173] A. Garg, Phys. Rev. Lett., **74**, 1458 (1995).

[174] For Quantum Spin Glasses, see M.J. Thill, D.A. Huse, Physica **A214**, 321 (1995), and refs. therein.

[175] N. Nagaosa, A. Furusaki, M. Sigrist, H. Fukuyama, J. Phys. Soc. Jap. **65**, 3724 (1996).

[176] G.Scharf, W.F.Wreszinski, J.L. van Hemmen, J. Phys. **A20**, 4309 (1987).

[177] I.Y. Korenblit, E.F. Shender, JETP **48**, 937 (1978).

[178] A. J. Leggett, pp 396-507 in "Matter and Chance: Proc. 1986 les Houches Summer School", ed. J. Souletie, J. Vannimenus, R. Stora, North-Holland, Amsterdam (1987); and A. J. Leggett, in "Frontiers and Borderlines in Many-Particle Physics", ed. R.A. Broglia, J.R. Schrieffer, North-Holland, Amsterdam (1988).

[179] P.C.E.Stamp, Phys. Rev. Lett. **66**, 2802 (1991).

[180] G. Tatara, H. Fukuyama, J. Phys. Soc. Jap. **63**, 2538 (1994); G. Tatara, H. Fukuyama, Phys. Rev. Lett. **72**, 772 (1994).

[181] References on bosonic oscillator models of quantum environments; F. Bloch, Zeit. fur Physik **81**, 363 (1933), for a bosonic representation of spin waves; S. Tomonaga, Prog. Theor. Phys. **5**, 349 (1950), and D. Bohm and E.P. Gross, Phys. Rev. **75**, 1851 (1949), for a representation of the low-energy excitation of Fermi systems by "collective mode" oscillators (the beginning of "bosonization"); and other similar models for phonons, photons, etc. Important early discussions of the effect of such environments on the quantum dynamics of a system coupled to them are in G.W. Ford, M. Kac, P. Mazur, J. Math. Phys. **6**, 504 (1965); J. Schwinger, J. Math. Phys. **2**, 407 (1961); and I.R. Senitzky, Phys. Rev. **119**, 670 (1960).

[182] For response function theory, see eg., L.D. Landau and E.M. Lifshitz, "Statistical Physics" (Pergamon); or D.Pines, P. Nozières, "Theory of Quantum Liquids", Ch. 2 and Ch. 5 (Benjamin, 1965).

[183] R.P. Feynman, A.R. Hibbs, "Quantum Mechanics and Path Integrals" (McGraw-Hill, 1965).

[184] U. Eckern, G. Schon, V. Ambegaokar, Phys. Rev. **B30**, 6419 (1984); G. Schon, Phys. Rev. **B32**, 4469 (1985).

[185] Y. Kagan, N.V. Prokof'ev, JETP **69**, 1250 (1989).

[186] "Magnetostriction: Theory and Applications of Magnetoelasticity", by E. du Tremolet de Laicheisserie (CRC Press, 1993).

[187] L.D. Landau, E.M. Lifshitz, "Electrodynamics of Continuous Media", (Pergamon).

[188] P. Politi et al., Phys. Rev. Lett. **75**, 537 (1995); and Int. J. Mod. Phys. **10**, 2577 (1996). See also A. Burin et al., Phys. Rev. Lett. **76**, 3040 (1996), for a Comment on this paper; and the reply of Politi et al., immediately following.

[189] Y. Kagan, N.V. Prokof'ev, Ch. 2 in ref. [190].

[190] *Quantum Tunneling in Condensed Matter*, Elsevier Science Publishers B.V., eds. Yu. Kagan and A.J. Leggett (1992).

[191] A. Schmid, Ann. Phys. **170**, 336 (1986).

[192] U. Weiss, "Quantum Dissipative Systems", (World Sci., 1993).

[193] A.J. Leggett, Phys. Rev. **B30**, 1208 (1984).

[194] B.A. Jones, C.M.Varma, J.W. Wilkins, Phys. Rev. Lett. **61**, 125 (1988), and refs. therein.

[195] P. Hanggi, P. Talkner, M. Borkovec, Rev. Mod. Phys. **62**, 251 (1990).

[196] V. Hakim, V. Ambegaokar, Phys. Rev. Phys. Rev. **A32**, 423 (1985).

[197] A.J. Leggett, Prog. Th. Phys. Supp. **69**, 80 (1980).

[198] Personal communication, Philip Stamp, University of British Columbia and Spinoza Institute, Utrecht.

[199] I. Tupitsyn and B. Barbara, Quantum Tunneling of the Magnetization in Molecular Complexes with Large Spins. Effect of the Environment; to be published in "Magnetoscience – From Molecules to Materials", Miller, Drillon (Eds.) WILEY VCH Verlag GmbH, 2000.

[200] G. Rose, I. Tupitsyn and P.C.E. Stamp, submitted to PRL.